DEVELOPMENT AND APPLICATION OF AN ADAPTIVE SWITCHING CONTROLLER

A Thesis presented to the

VICTORIA UNIVERSITY OF MANCHESTER

BY

J. O. GRAY M.Sc.

for the degree of

DOCTOR OF PHILOSOPHY

Manchester May 1967.

ProQuest LLC.
789 East Eisenhower Parkway
P.O. Box 1346
Ann Arbor, MI 48106 – 1346

G 16417

The author obtained a B.Sc. degree in Electrical Engineering at Queens University, Belfast in 1959 and subsequently took up an appointment as a Senior Development Engineer at Short Brothers and Harlands Ltd., Belfast where he worked on the development of solid state electronic control equipment for the S.C1 V.T.O.L. aircraft. In 1961 the author received a Masters degree in Electrical Engineering from the Light Electrical Engineering Department of Queens University Belfast. In 1963 he was appointed as Lecturer in the Department of Electrical Engineering in the Faculty of Technology of Manchester University and at the present time he holds an appointment as Lecturer in the Control Systems Centre of the University of Manchester Institute of Science and Technology.

SUMMARY

This thesis is concerned with the solution of the actuation and identification problem in a particular model adaptive control system and with the structure of a suitable decision computer for the generation of a sub optimal bang bang switching function. The control strategy is one of feed forward prediction where emphasis is placed on minimizing the time required for the processes of identification and actuation. The behaviour of a proposed new type of fast actuating or adaptive mechanism based on photo electric principles is investigated for adjusting the parameters of the plant model which is formulated in electronic analogue terms. By the use of a semiconductor crystal lamp and photo diode detector the performance of the adaptive element is subsequently improved to produce a linear adaptive mechanism which has a settling time of approximately 160 micro seconds.

A plant parameter identification system based on iterative computation techniques has also been devised, for the particular model structure chosen, which minimizes estimation time and whose output is compatible with the adaptive mechanism.

The fuel supply pressure loop of a pulverised coal fired power station boiler model was taken as an example of the possible application of the model adaptive and identification schemes. It is shown that though boiler dynamics are governed by complex thermodynamic and

hydrodynamic phenomena the overall plant characteristics, while being time varying, are relatively simple in form and can be closely represented by the type of generalized model chosen for the control scheme. A discussion of the physical behaviour of the boiler plant isolates the time varying parameters.

An accurate sub optimal control function is subsequently generated for the derived boiler model by a relatively simple iterative procedure. Electronic analogue equipment [redacted] is used throughout and emphasis is placed on achieving a reduction in computation complexity where possible.

ACKNOWLEDGEMENTS

The author wishes to thank Professor Colin Adamson, D.Sc. for accepting him as a research student in the Electrical Engineering Department of the University of Manchester Institute of Science and Technology. He also wishes to express appreciation to his late supervisor, colleague and friend Professor Frederick Walker with whom he had the privilege of working for three short years, and whose constant help and encouragement has inspired much of the work herein.

A special acknowledgement is due to Dr. Alistair MacFarlane for his encouragement and assistance during the latter stages of the work and the author also wishes to thank the many engineers both in industry and the Institute who have contributed in any way.

CONTENTS

page

CHAPTER 1

INTRODUCTION

1.1. Adaptive Control.

A conventional automatic control system can be described as completely structured in the sense that system and controller parameters are so chosen to achieve a desired optimum performance for a given class of input signal. Large changes in either system parameters, external environmental conditions or class of input signal could rapidly degrade the system performance despite the normalizing influence of negative feed back especially if the forward loop gain of the process is low. The term adaptive control is normally applied to the system which has the facility of adjusting or adapting its control parameters automatically to maintain system performance at some desired optimum level.

The concepts of optimality and adaptivity are interlinked and indeed the first adaptive control system was referred to as an optimal control system by Draper and Li in 1951 (1)(2). These authors were concerned with achieving the optimum static operating point for an aero engine to obtain maximum efficiency in the presence of varying environmental and engine parameters. The correct operating point was achieved by peak holding techniques where an input perturbation signal was superimposed on the control signal. Subsequent examples of adaptive control systems were closely related to the aero space field in which

the benefits of adaptation were immediately obvious. Aerodynamic parameters undergo wide variations with vehicle altitude and velocity and some form of automatic control compensation is essential. An early example of automatic compensation has been given by Gregory (3) where the parameters of an automatic flight control system are continually adjusted to maintain correct damping over the complete flight trajectory. A more recent example is the glide path control of a V.T.O.L. aircraft (4) in which an adaptive loop automatically compensates for changing aircraft parameters to provide correct pilot "feel" at all stages in the final approach.

No general theory of adaptive control has yet emerged and adaptive systems still tend to be classified by their mode of operation (5). One class of adaptive system continually monitors its own performance either by a train of input pulses or by cross correlation techniques and adjusts the parameters of the controller for optimum response. Due to the time lag associated with the identification process it is assumed that parameter rate of change is small in comparison with the dominant time constant of the system. Another approach, which is sometimes referred to as non linear adaptive control, is to cause the system to undergo a radical change in its operation as a function of the input signal. An example of this form of system is the dual mode servo which acts as a bang-bang servo for large signals but for small signals is switched to linear operation (6). Taylor and Flugge-Lotz(7) have developed this

principle and produced a control system which switches between one of eight compensating networks depending upon the character of the input.

The term computer controlled adaptation is generally attributed to those systems which incorporate an electronic computer for the purposes of process identification and optimization. One of the earliest works on computer optimization was published by Kirchmayer (8) and was related to the problem of optimum energy distribution in interconnected power system generators. Recently Kalman (9) has demonstrated that for a linear complex system with a quadratic performance index an optimal control law can be determined analytically in terms of linear recurrence functions using Bellmans (10) concept of dynamic programming. If the optimal forcing function is derived on the basis of updated system information the control law is adaptive and a powerful technique thus exists of applying the principle of adaptation to extremely complex systems. Examples of the application of this technique have been limited to date but at least two have been published by Kalman (11) and Nicholson (12). Kalmans method has several severe limitations in that the system must be linear and, for mathematical tractability, the performance index must be quadratic. This latter constraint could well result in a totally unrealistic performance index in a practical application (13).

Though the advance in computer technology and mathematical techniques has rendered the attainment of multidimensional adaptation possible several formidable computation problems still exist (14). The presence of local maxima or minima and discontinuities in the performance index contours can lead to erroneous results unless extensive preprogramming is undertaken. Likewise if the performance index contours are open ended no meaningful results will be obtained unless strict bounds are set to the search region in the N space.

Direct optimization is thus exploratory or heuristic in nature; the results of each parameter adjustment being assessed and used as a basis for further control manipulation. Though simple in concept, if the performance index is directly measurable, direct optimization has several limitations in application including those due to noise, irregular performance index contours and the complexities associated with multiple inputs.

Model Adaptation (15)(16) provides an alternative approach to optimizing control where the model may be a physical analogue of the system or a mathematical abstraction such as a set of equations describing the system behaviour. Using the system model as a basis for deriving optimal control equations has several advantages.

(1) The model can be scaled to run much faster than the system so that the time required for complete exploration of the system performance contours is negligible relative to the dominant time constant

of the system. A complete fast time exploration of the performance contours eliminates problems due to local maxima or minima or other irregularities in the contour shape and the noise free model output can be used as an accurate prediction signal for further control strategy.

(2) System perturbation signals are not required and thus losses due to system transients and hunting are removed.

The system model can be used in two ways. Firstly if the ideal plant characteristics are known then the plant performance can be compared directly with an ideal model reference system, any difference signal being used as a basis for adapting the plant control parameters. This so called model reference adaptive control technique has found particular application in the aero space field (17),(18) where vehicle control characteristics must be held within rigid limits over a wide range of aerodynamic conditions. Secondly and more commonly the model may be used as a basis for generating predictively the correct system forcing functions when the plant is subject to a series of arbitrary inputs.

The correct generation of the optimal forcing function depends directly on the validity of the plant model chosen. In practical application to a complex plant the model structure will usually deviate from the actual plant structure for several reasons.

(a) Insufficient knowledge available of the actual process dynamics and actual plant design may be largely empirical.

(b) Many of the variables which affect system behaviour cannot be accurately determined with existing instrumentation and thus are not available for model formulation.

(c) Even if the process dynamics were completely known their complexity may well be such as to render detailed model formulation prohibitively expensive in computer capacity.

In general the model only represents the dominant factors of the system equations and therefore some error will exist between model and system response. Compensation is afforded by a self checking or model adaptation technique whereby the model is adjusted to force a best fit between the model response and the system response in the vicinity of the current operating point. Model adaptation is normally accomplished by parameter variation within a rigid model structure, the updated model being subsequently used as a basis for accurate generation of the correct forcing function.. The automatic self checking inherent in the model adaptation philosophy allows the adaptive model to be regarded as an elementary learning machine.

The basic adaptive control concept has beem summarised by Truxal (19) whose general representation is shown in the block diagram of figure 1. Here the input signal is identified either to determine its characteristics for mode switching or to obtain information for ultimate system performance estimation. The decision computer uses information from both signal and process identifiers to determine the required controller characteristics or to generate the necessary system forcing function. Performance criteria are programmed into this computer which must also be fed with environmental data if relevant.

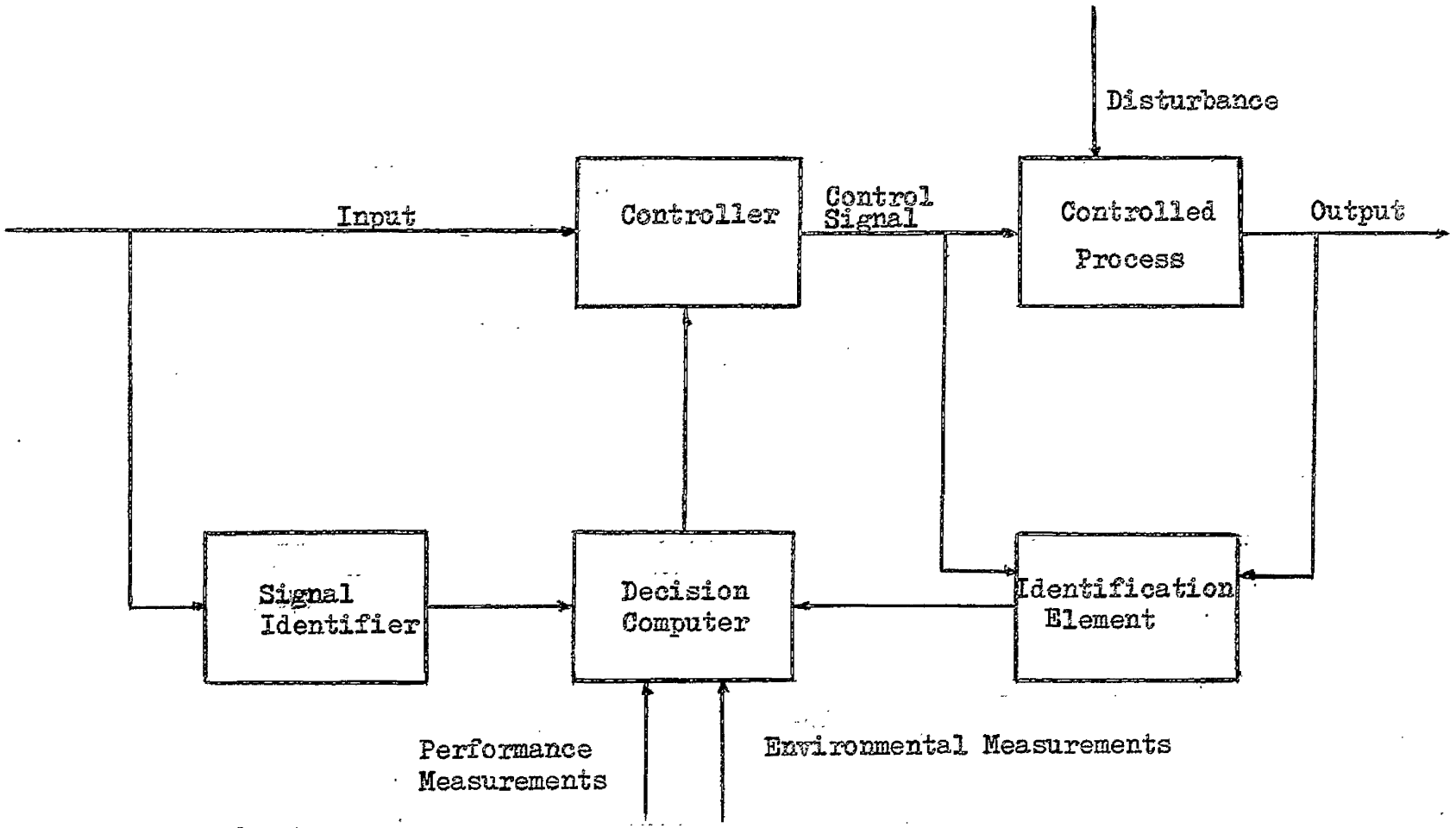

Figure 1.1. The General Adaptive Control System.

The output from the decision computer may either be an optimal control forcing function or a signal to alter controller characteristics in order to obtain optimum plant response. In the former case adaptation is performed within the computer configuration either by physically changing a parameter or by an abstract adjustment of the coefficients of some implied analytical function. In the latter case adaptation takes place within the controller system and the computer output can be regarded as a signal which actuates the physical adjustment.

An adaptive control system has therefore the following two characteristics,

(a) identification

(b) actuation

where identification refers to the measurement of the system to be optimized and actuation refers to the generation of a command signal which varies some parameter to achieve optimization. For effect the processes of identification and actuation must take a shorter time than the time required for any dominant system parameter to vary by a significant amount.

1.2. Object of thesis.

This thesis deals with the solution of the actuation and identification problem in a particular model adaptive control system and with the structure of a suitable decision computer for the generation

of a sub optimal bang-bang switching function. The control strategy is one of feed forward prediction where emphasis is placed on minimizing the time required for the processes of identification and actuation. The behaviour of a proposed new type of fast actuating or adaptive mechanism is investigated for adjusting the parameter of the plant model which is formulated in electronic analogue terms. A plant parameter identification system based on iterative computer techniques has also been devised for the particular model structure chosen which minimizes estimation time and whose output is compatible with the adaptive mechanism.

The fuel supply pressure loop of a power station boiler model was taken as an example of the possible application of the model adaptive and identification schemes and it is shown how an accurate sub optimal control function can be generated for the derived boiler model by a relatively simple iterative procedure. Electronic analogue formulation is used throughout and emphasis has been placed on achieving a reduction in computation complexity where possible.

1.3.1. The Adaptive Mechanism.

The new mechanism is based on photo resistor principlesand its performance has proved to be fast, accurate and reliable. It is thought that this device could eventually replace servo potentiometers in the adaptive role for all control systems. Recent efforts to increase further the speed of adaptation led to an investigation of the performance of

of Gallium Arsenide crystal lamps when used in conjunction with Silicon photo duo diodes. This combination has resulted in an adaptive device with a time response of the order of microseconds.

The photo resistor system has a time response which is about an order better than the conventional servo system and an improvement of several orders is achieved with the photo diode combination. Though the response of the latter is much faster than required for most adaptive systems it should find a wide application in the field of high speed hybrid computation by ensuring compatability between adaptation and computation periods.

Due to the parallel nature of its operation the computation period of an analogue computer can be measured in microseconds and a compute period of one millisecond for complete trajectory computation is quite feasible. By reducing model adaptation time to a small fraction of a millisecond many hundred performance contours can be explored in one second and a search in N-fold optimizing space completed in a few seconds.

1.3.2. The Control Scheme.

If the dynamic equations governing the behaviour of a system are accurately known it is possible in theory to calculate the conditions necessary for optimum performance. A particular case is shown in figure 1.2. where a full knowledge of the process dynamics enables the control laws of the feed forward computer to be determined and hence the optimum control functions generated. An exact mathematical knowledge

of the process is, however, seldom available due either to lack of precise information of the system dynamics or to the magnitude of the computer facilities required to derive it.

Model adaptation schemes have thus been proposed by several authors (15) (16) as a practical method of controlling complex systems. The basic philosophy of this approach is that the process model, structured within the control computer, is continually adjusted to force a best fit of the model to the observed system behaviour in the vicinity of the current operating point. Control functions are then derived on the basis of the updated dynamic model.

The synthesis of this adaptive system presents formidable problems unless radical simplifications are made. Consequently the model only represents the dominant characteristics of the system equations. Errors due to system reduction are however small because of the self checking or learning abilities of the model. The general approach used in this study is that of Lefkowitz (16) who represents a complex process by a simplified model of rigid structure the parameters of which are updated by direct comparison with the process outputs.

The following assumptions are made.

(1) The process operates normally in the steady state with, however, frequent step changes in load variable.

(2) The process dynamics are significant relative to the frequency of load variations and thus the overall performance is influenced by the system behaviour during the transients.

(3) The process exhibits an open loop monotonic response.

1.3.3. Dynamic Optimization.

If we concern outselves with an industrial process a common problem encountered is that of quickly restoring equilibrium after a large input disturbance. The problem is usually complicated by the presence of long thermal and distance velocity lags. A realistic suboptimal control criterion therefore would be to drive the process from one steady state condition to another in minimum time in response to an input disturbance.

This criterion will result, for a linear system, in a bang-bang control law (20)(21) and if a linear model of the system is used then a bang bang control function will be developed by the control computer. A simple generalised model of the form

$$G(s) = \frac{K E^{-SD}}{1 + ST}$$

will yield a control switching function of the form shown in figure 1.3. where due to an input disturbance of magnitude $(U_2 - U_1)$ the process output must change from P_1 to P_2 in the minimum possible time. If due to system constraints the maximum control effort available at this operating point is M then

$$P(s) = \frac{M}{s} \frac{K E^{-DS}}{1 + Ts}$$

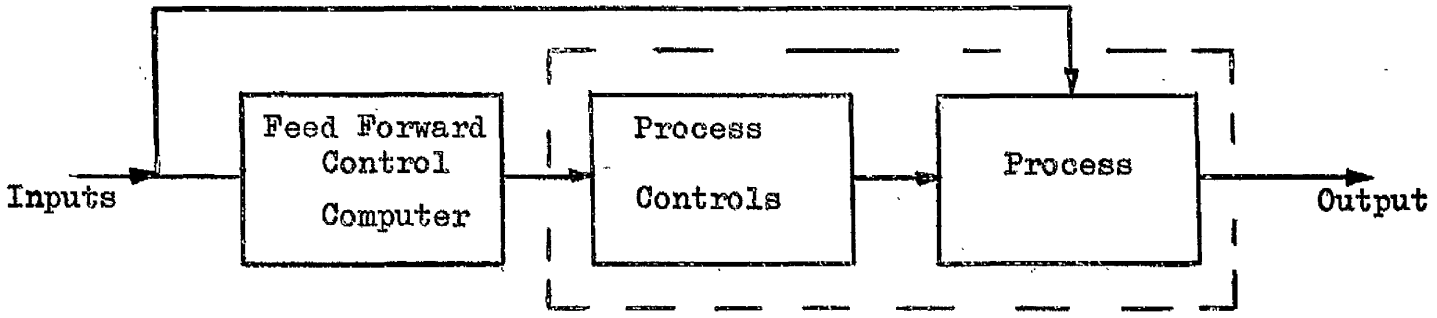

Feed Forward Control

Figure 1.2.

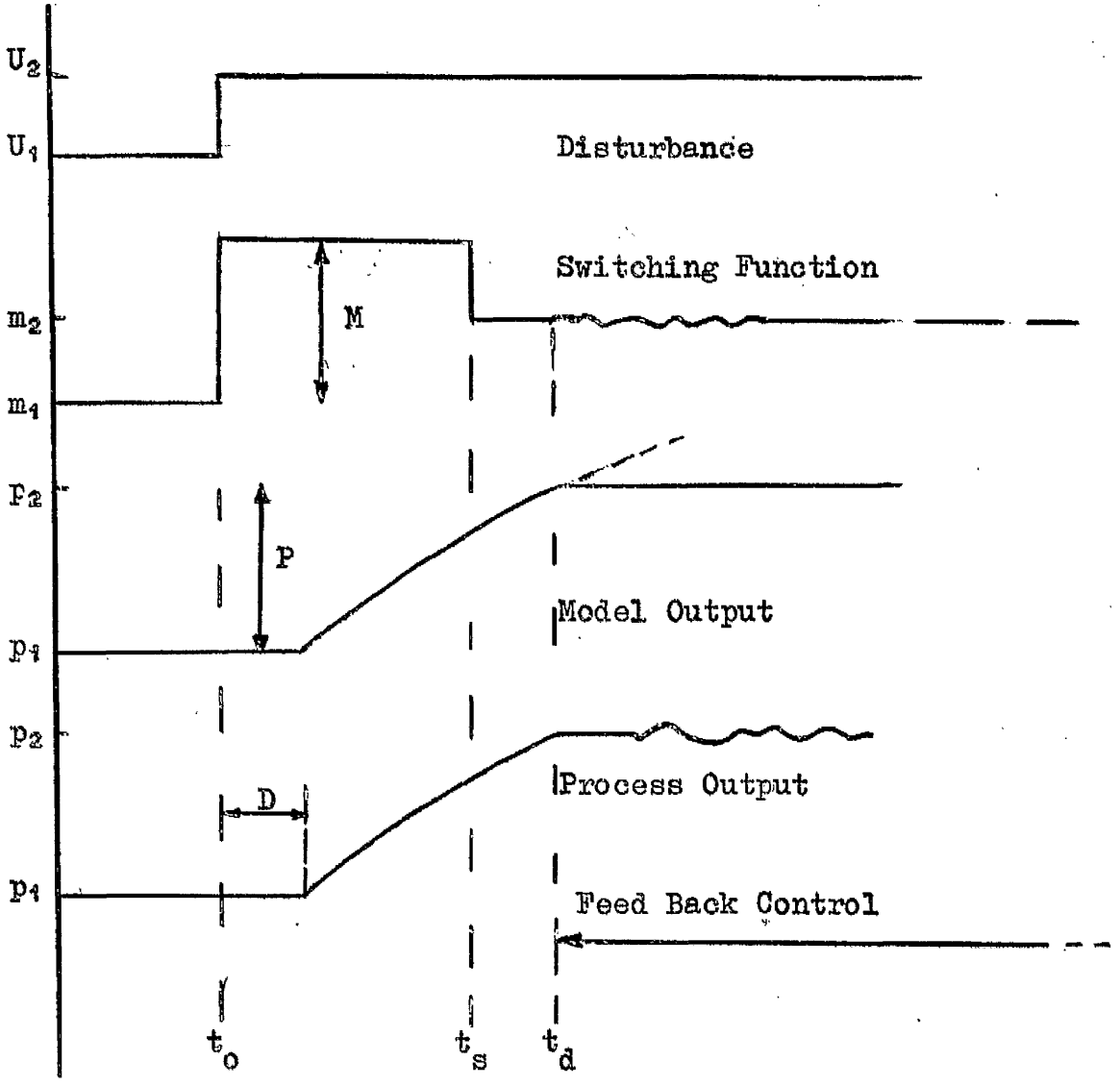

Control Computer Response Curves for Step Change in Disturbance

Figure 1.3.

$$P(t) = \begin{cases} MK\ (1 - \varepsilon^{-\frac{(t-D)}{T}}) & \text{for } t \geqslant D \\ 0 & \text{for } t < D \end{cases}$$

$$t_d = D - T\ \text{Log}\left(1 - \frac{P}{MK}\right)$$

$$t_s = -T\ \text{Log}\left(1 - \frac{P}{MK}\right)$$

where $P = P_2 - P_1$.

The value of t_s and t_d can be computed on a fast time basis from the generalised model and used to control the exact switching time of the process. As the switching function need only be generated at the onset of a large transient the process can remain under its normal analogue controls during quiescent operation. The complete dual mode control scheme is shown in figure 1.4.

The dynamic control computer, which incorporates the fast time adaptive model, monitors the output and input variables, determines when the input deviation reaches the preprogrammed switching boundary and subsequently develops the correct switching function. Information from the output variablesis used to estimate the process parameters and update the generalised plant model for correct computation. Four distinct functions are thus performed by the control computer, viz: mode switching, switching function generation, parameter estimation and model adaptation.

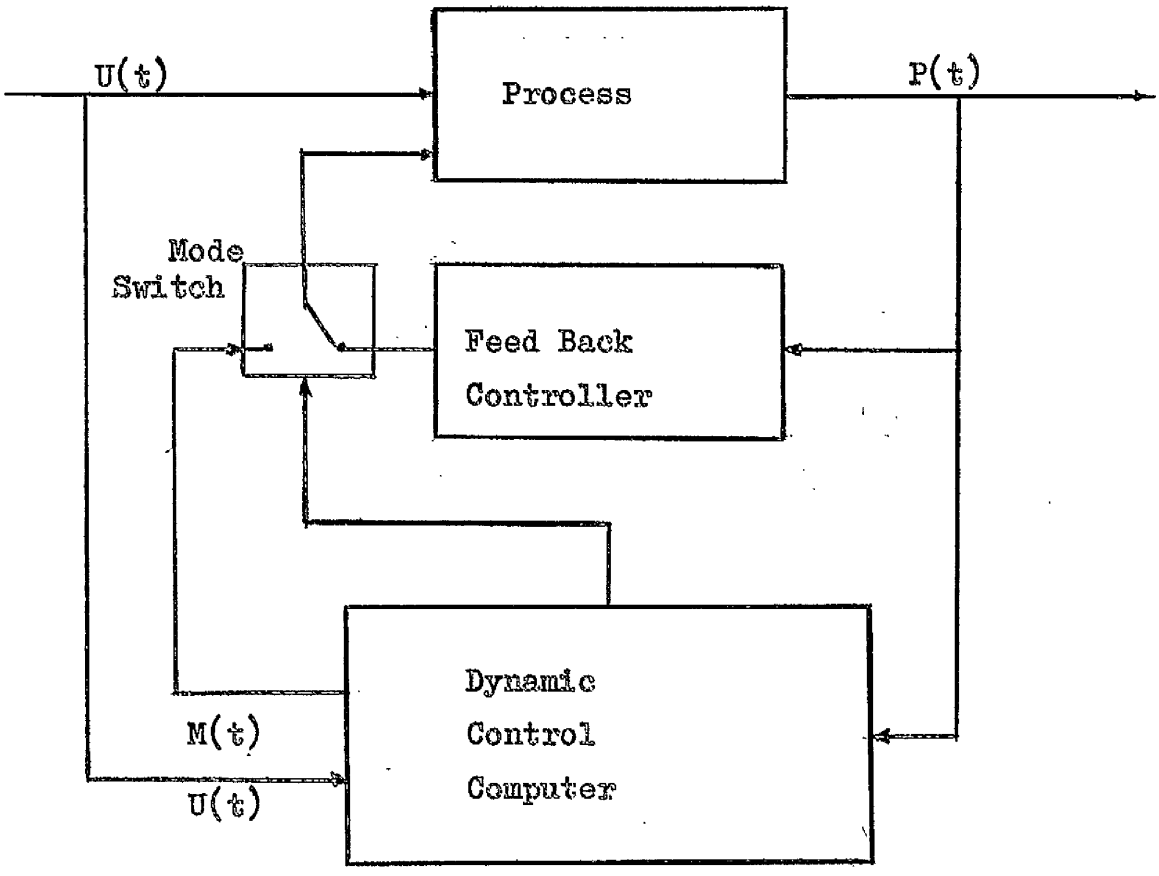

Dual Mode Control.

Figure 1.4.

1.3.4. Parameter Estimation.

Estimation of the process parameters is one of the key realization problems in any adaptive control scheme and the advantage obtained from using a simplified linear plant model could be lost if the designer were forced to use a complex identification system. One of the objects of this study therefore was to realize parameter estimation equipment which would be compatible with the chosen model structure.

The parameter estimators which were developed consists of electronic analogue elements controlled by external transistor logic circuits programmed to identify completely an exponential time function. Identification of this form appears to have been achieved previously only by the use of relatively complex digital computer techniques.

1.3.5. Controller Application.

A study was undertaken of the application of the control scheme to a specific industrial process. The process chosen, the fuel supply pressure loop of a pulverized coal fired power station boiler, can be approximated by a simple generalized model and is thus representative of the type of application envisaged.

As electric supply networks become increasingly complex to fulfil the demands of an expanding industrial economy the problems of electric power systems stability grow increasingly critical. An important factor in the overall stability of a power supply network is the transient performance of fossil fired high pressure boilers, which equip the vast bulk of our generating stations, where the time delay associated

with pulverized coal fired units accentuates the normal control problem.

The boiler model developed in chapter 4 demonstrates that though boiler physical processes are governed by extremely complex laws of thermodynamics and hydrodynamics the overall plant characteristics, whilst time variant, are of relatively simple form and closely represented by the type of generalized model described in paragraph 1.3.3. From the practical aspect plant parameter estimation has been greatly facilitated by the recent development at C.E.G.B. Leatherhead of a device which measures the direct heat flux passing into the boiler tubes from the furnace. It is thought that this is the first time that this particular device has been proposed as an element in a boiler control loop. Excellent dynamic characteristics combined with very low noise signal levels ensures good compatability with modern data processing equipment.

The boiler model was simulated on an analogue computer and its behaviour studied under the influence of the derived switching function. A successful iterative computation procedure has been developed which yields accurate results with the minimum of added computer complexity.

The behaviour of drum water level under transient load conditions constitutes a major constraint on the controlled performance of the boiler. The nature of this phenomenon has thus been investigated and the results of earlier workers emphasised to show how they can be used to improve water level control by correct boiler design. Finally a method has been outlined of extending optimum switching techniques to water level control to make the best use of installed plant capacity.

CHAPTER 2

THE ADAPTIVE MECHANISM

2.1. Introduction.

If a complex plant is represented by a simplified model of rigid structure the parameters of which are variable, actual model formulation obviously will be influenced by the model structure chosen. For a plant which can be structured into a series of elemental transfer functions of the form

$$G(s) = \frac{K}{1 + LS}$$

where K and L are variables, model formulation by electronic analogue techniques can readily be achieved.

In such a formulation, the gain parameter K can be adjusted by using either a servo-potentiometer or electronic multiplier. Though the latter is preferable due to its wide bandwidth and consequent short response time the former has found application in practical adaptive systems (1), (2). Normally adjustment of the time constant L can only be achieved by servo potentiometric methods and if this parameter is a variable then the system designer is constrained to use such a device.

Servo potentiometers possess the usual disadvantages of mechanical systems, a relative slowness of operation due to component inertias, wear on moving parts, and sensitivity to environmental conditions (especially shock and vibration). The associated low torque potentiometers are expensive and noisy during variation of resistor value. It is the

intention here to outline the development of an adaptive mechanism which while capable of the dual adaptive function of the servo potentiometer possesses none of its inherent limitations.

The use of photo conductive devices rather than potentiometers to produce variable resistive elements yields several advantages including faster response time, virtual noise-free resistance variation, absence of moving parts, and a low sensitivity to environmental conditions. The unit can be small, light weight, inexpensive with complete electrical isolation between the variable resistive element and the controlling light source. This latter property is essential to avoid circuit complexity in the analogue simulation. Figure 2.1 illustrates the method of parameter variation.

In the initial development work a cadmium sulphide photo conductor slab was used as the variable resistive element, the ohmic value being controlled by light emission from a filament lamp. A control circuit was designed which achieved a high degree of static linearity between an incremental input voltage and the incremental value of the variable resistance, together with a transient settling time of the order of 300 milliseconds. Although this transient performance represents a six fold improvement over presently available servo systems it is still not compatible with the computation time of the electronic analogue system which, because of the parallel nature of the computation, is of the order of microseconds.

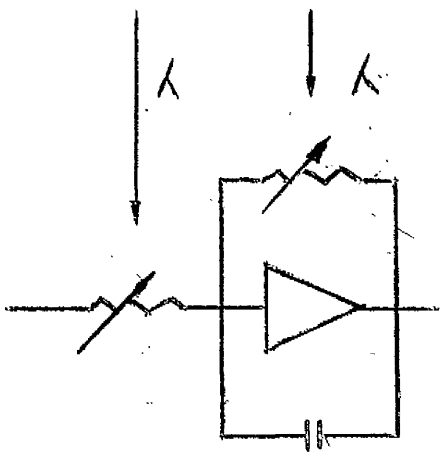

(a) Variation of time constant

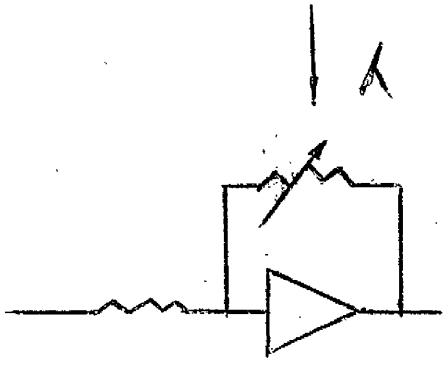

(b) Variation of gain.

Figure 2.1. The Photo conductor used as a variable operational element.

An attempt was therefore made to eliminate the two dominant lags in the photo conductor control system, namely the lag associated with the filament lamp response and the lag associated with the photo conductor response. The reduction or complete removal of these lags, both of which are of the order of 100 milliseconds, would greatly enhance the overall system performance. Replacing the filament lamp by a semiconductor crystal lamp which has a light rise time of 15 nano seconds is an obvious improvement provided that a suitable light detector with the correct degree of spectral compatability is available. A satisfactory choice for the latter would be a silicon photo diode - a device which also has a very short photo current rise time of the order of 2 microseconds.

A control circuit was subsequently developed incorporating this new lamp detector unit which, at the cost of a small degree of increased complexity due to the nature of the diode detector characteristics, reduced the settling time of the resistor control system to the order of 160 microseconds and thus improved the transient response by a factor of 1500.

2.2.1. <u>The Photoconductive Process</u>.

The absorption by a semiconductor material of a photon of energy hv which is greater than the energy gap δE will raise an electron from the valence band to the conduction band where this excess carrier will increase the electrical conductivity of the material. This process

is illustrated in figure 2.2. where, as the threshold energy hVo is exceeded, the photo conductive response rapidly increases for a constant photo flux. The threshold wave length for this effect is given by the relationship (3).

$$\lambda_o = \frac{c}{v} = \frac{hc}{\delta E}$$

where c is the velocity of light. If the incident phonol energy is below the threshold level light is largely transmitted through the material or reflected from the surface.

The time response of the photo conductive process depends on a complex interaction of several variables: incident light flux density, trapping and doping concentrations within the crystal structure and the life time of the excess majority carriers present. In general due to the relationship existing between doping level and carrier life time there is an inverse relationship between the sensitivity of the photo conductor and its speed of response to a change in incident light energy. For a given light source, therefore, the doping level chosen will depend on the compromise reached between speed and sensitivity.

2.2.2. The Photo Conductor Element.

The photo conductor element used in this work was the Mullard O.R.P. 39 LUXISTOR which consisted of a cadmium sulphide photo conductor and a filament lamp encapsulated in an opaque epoxy resin.

The device is fitted with terminal pins suitable for standard printed circuit boards and is illustrated in figure 2.3. and figure 2.4. the main electrical characteristics being as follows (4).

Maximum input voltage	12V
Nominal input current (V_{in} = 12v)	65mA
Maximum output (photo resistor) voltage	70V
Maximum photo resistor dissipation	15mW.
Operating temperature Maximum +	60°C
Minimum -	20°C.

The small dimensions of the O.R.P. 39 together with a maximum input potential of 12 volts and current level of 65mA suggest that the device may be used without difficulty in transistorised circuits. Measured output input characteristics are shown in figures 2.5. and 2.6.

It will be seen that the relationship between the input lamp voltage and the resistance of the photo conductor element is highly non linear. This non linearity, which is mainly due to the complex relationship between applied filament voltage and light intensity, can be removed by a suitable feedback system.

An essential property of any material constituting the conductive element is the linearity of the current through the material with respect to the voltage applied to the ohmic terminals of the material block.

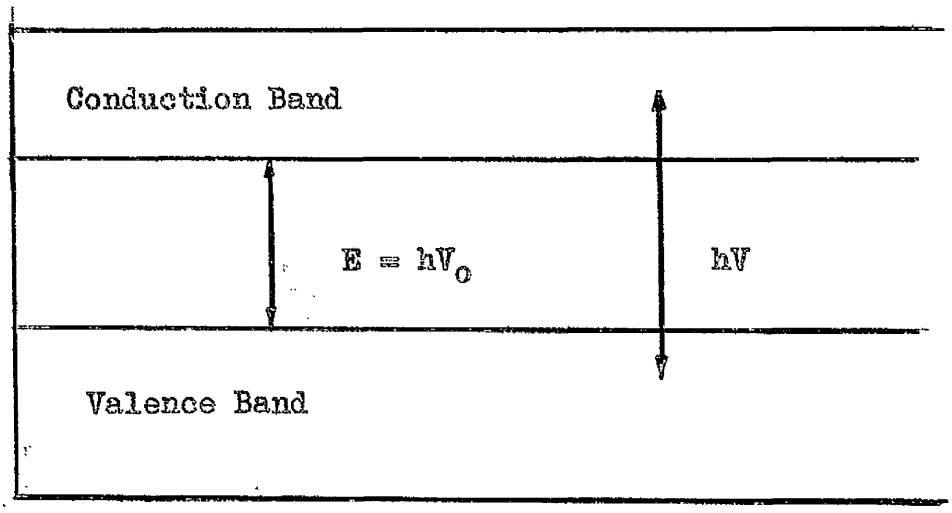

h = Plancks constant

V = Frequency.

Figure 2.2. Photo electric excitation.

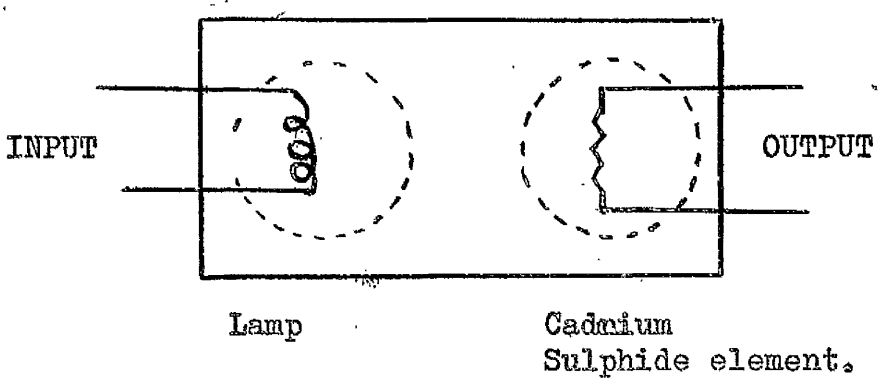

The Luxistor Schematic Diagram.

Figure 2.3.

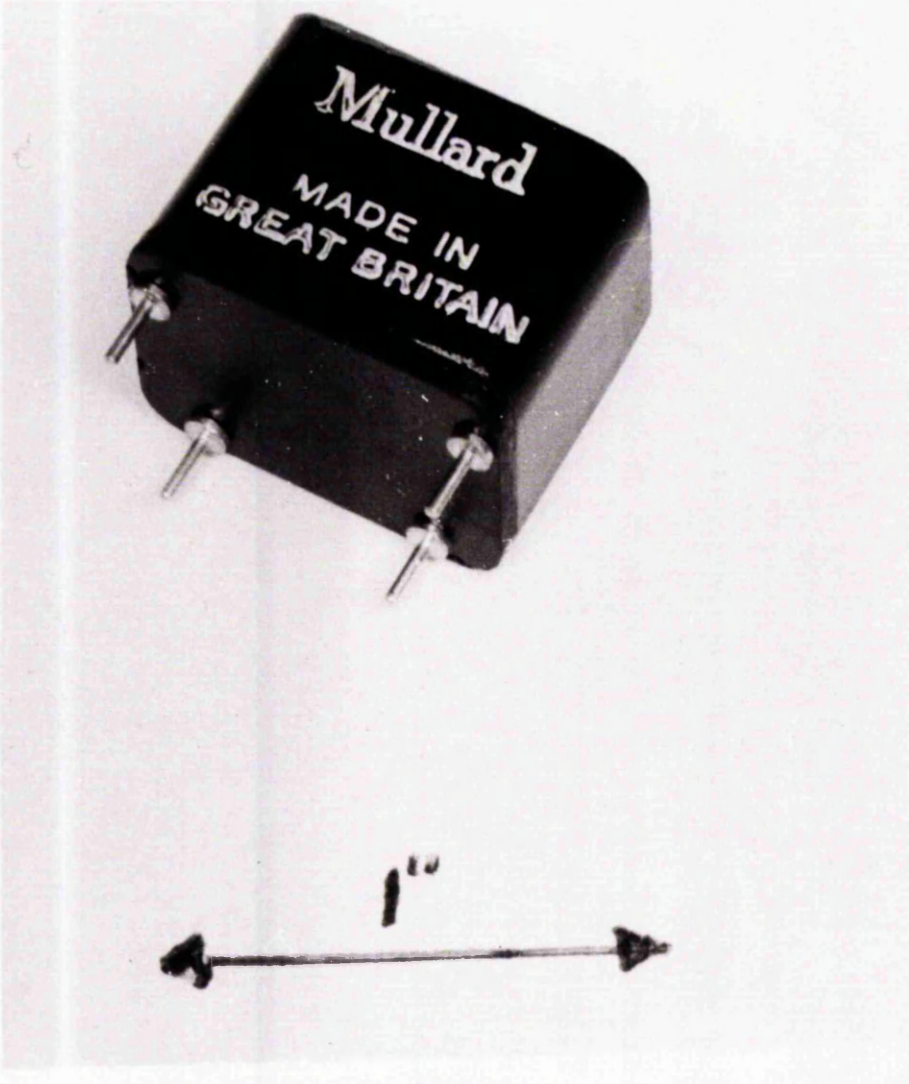

THE O.R.P. 39 LUXISTOR

Figure 2.4.

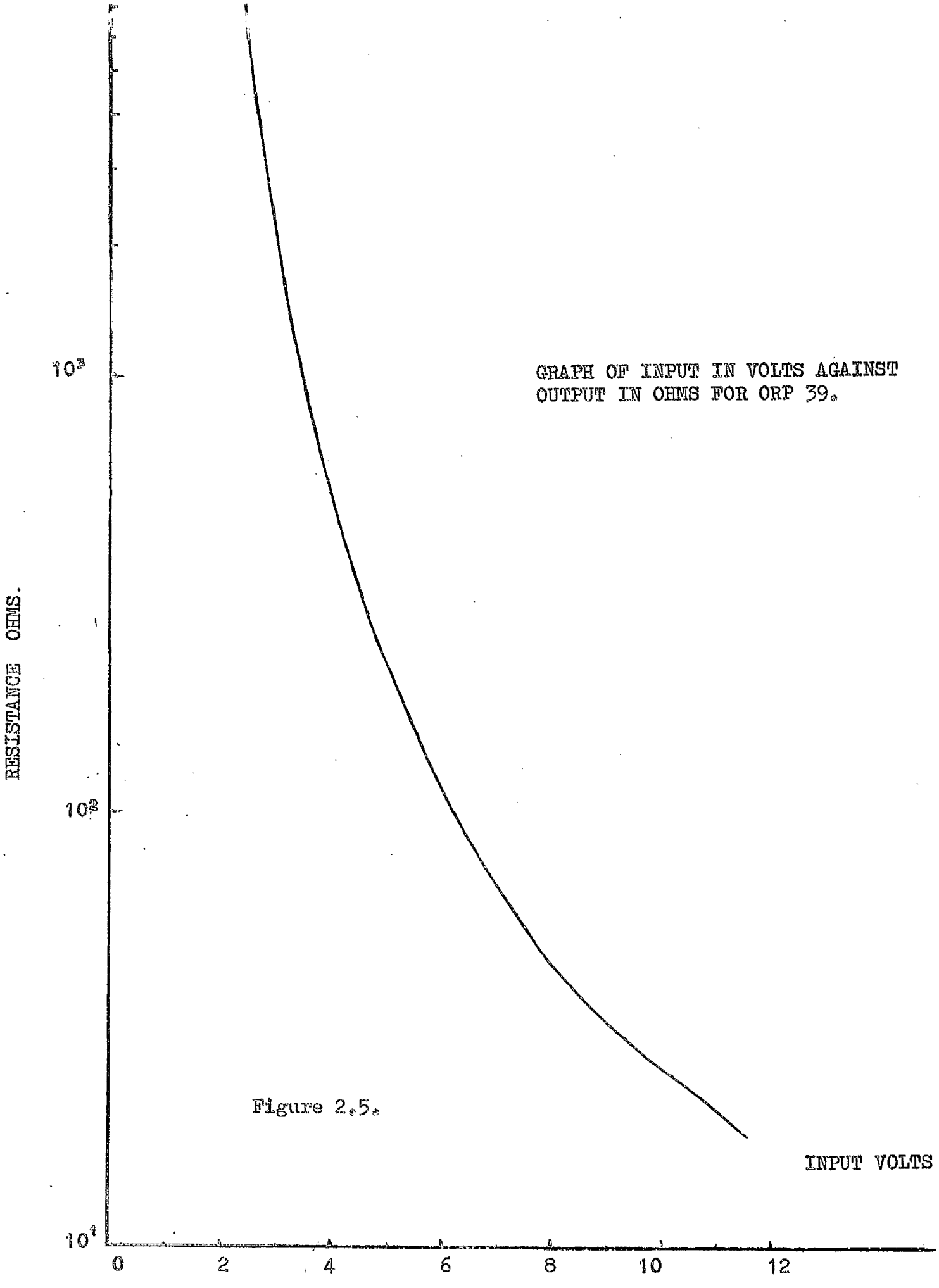

GRAPH OF INPUT IN VOLTS AGAINST OUTPUT IN OHMS FOR ORP 39.

Figure 2.5.

This linearity was checked for the O.R.P. 39 with the cadmium sulphide element set at a nominal resistance value of 10KΩ when connected in series with a 3.3KΩ resistor. The measured linear voltage current relationship is shown in figure 2.7.

2.2.3. The Adaptive Control System.

Variations in the plant parameters will be represented at the output of the parameter estimators by variations about a nominal d.c. bias voltage. To update the model these voltages are used to vary the appropriate resistor value in the model about its nominal value. This adjustment takes place when the model is switched to the adaptive mode. When the model is subsequently switched to the compute mode the variable resistors are connected as operational elements in a computer configuration to formulate an updated dynamic model. As it is proposed to use photo resistors rather than servo potentiometers in this role two factors must be considered.

Firstly as the LUXISTOR characteristics are non linear a feedback loop must be incorporated to achieve linearity and secondly to avoid circuit difficulties in the computer system whilst the model is in the compute mode, the variable resistors must behave as completely electrically isolated elements with respect to the control circuit. As it is essential that the elements, though isolated, retain their updated value accurately for a period of time at least equal to one computation cycle

Current Voltage Relationship of Combined Cadmium Sulphide Element and External 3.3KΩ Resistor

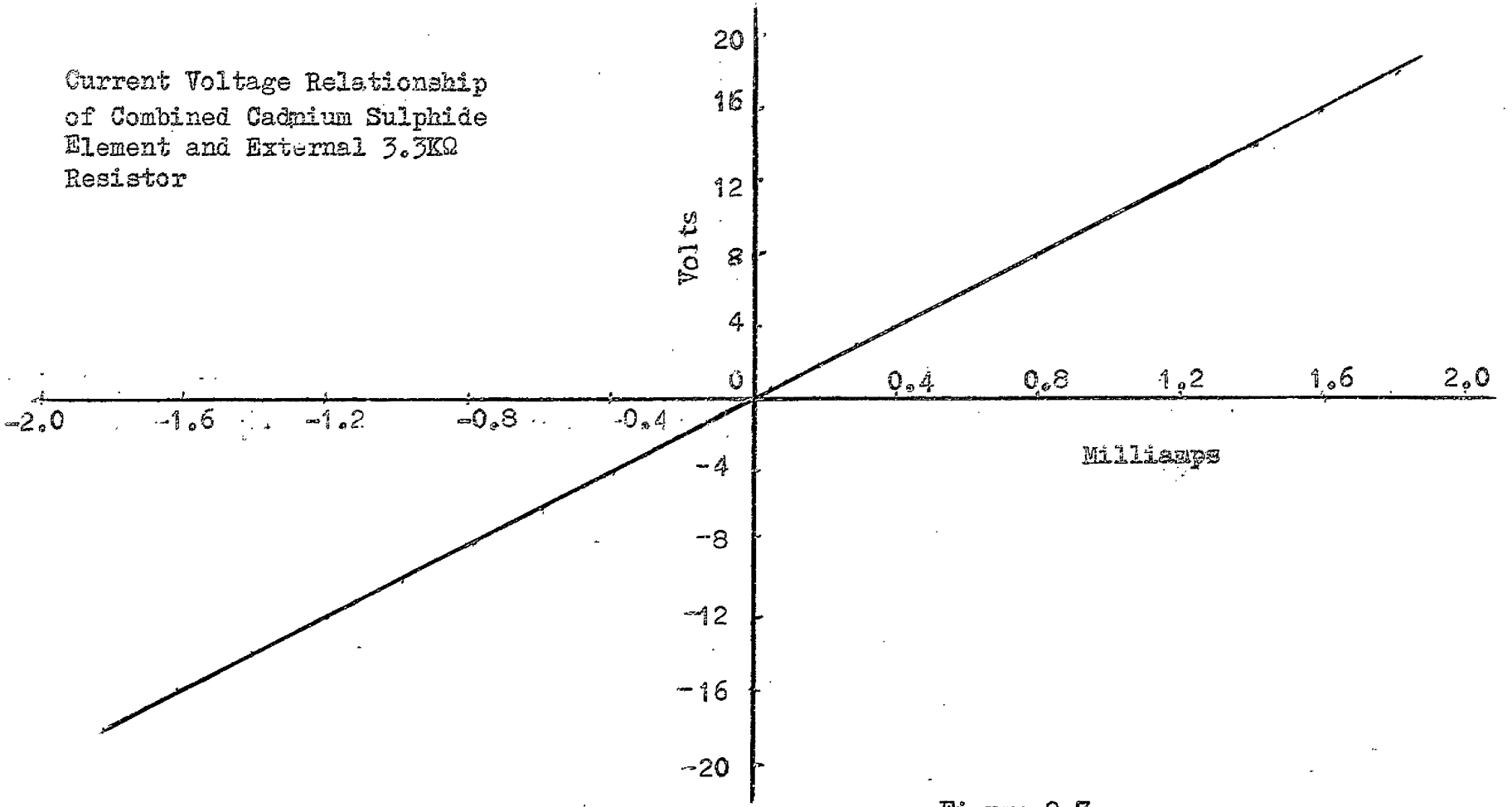

Figure 2.7.

some form of memory is essential in the control circuit.

A possible arrangement for a LUXISTOR control circuit is shown in figure 2.8. In the adaptive mode switch S.W.1. is closed and switches S.W.2. and S.W.3 are in position 1. If a constant current is supplied to the resistor chain then the voltage at A is proportional to the resistance R of the cadmium sulphide element. Any change in the input voltage about a nominal d.c. level causes the integrator output voltage to change altering the value of R and the voltage level at A. If the resulting incremental change in level at A is negative with respect to the input variation the output of the integrator will reach a new steady state value corresponding to the required change in R.

Switch S.W.1 can now be opened and the integrator will maintain this new output voltage and hence the new value of R for a finite period enabling the isolating switches S.W.2 and S.W.3 to be switched to position 2, thus connecting R as an isolated element into the computer system. The adaptive model is now in the computation mode. It is clear that for satisfactory operation S.W.1 must open before S.W.2 or S.W.3 and that the integrator should exhibit an excellent drift performance in the hold mode. While behaving as a memory unit the integrator also ensures a high degree of steady state accuracy in the adaptive mode due to its integral action on the system.

Graph of input volts against input current for ORP 39

Figure 2.6.

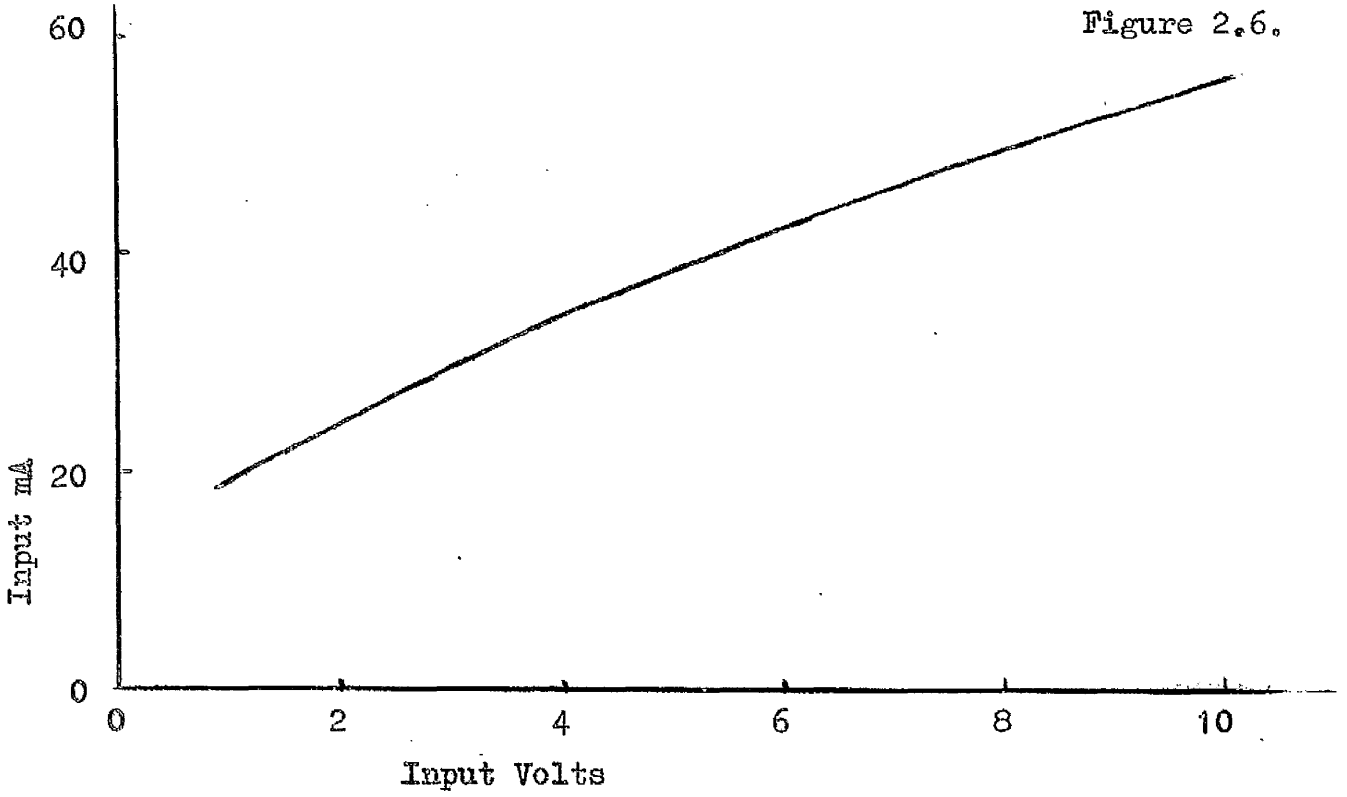

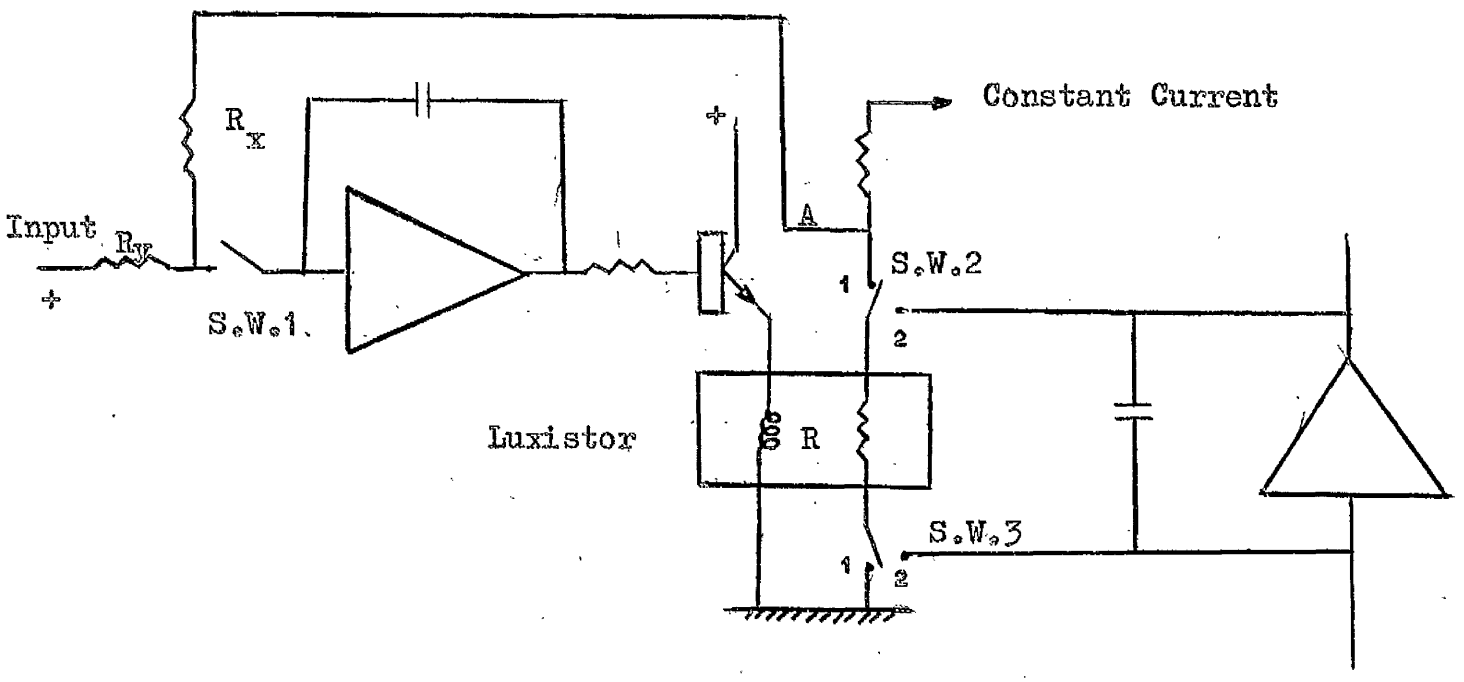

Fig. 2.8. Adaptive Controller Schematic

The initial design specifications were taken as follows.

(a) A variation of ± 20% in the resistive element about a nominal input voltage level.

(b) A linearity of better than 1%.

(c) A satisfactory dynamic performance with adequate damping.

(d) The adaptive mechanism memory should possess satisfactory drift characteristics when the adaptive model is switched to the compute mode.

2.2.4. The Electronic Circuit.

A study of the LUXISTOR static and dynamic characteristicsis an essential prerequisite of the detailed design of the schematic circuit shown in figure 2.8. The most convenient operating point in the characteristic shown in figure 2.5. must first be decided and this will determine the input bias level of the LUXISTOR. This characteristic is quite linear in the region 5→9K and, if the silicon element is used in combination with a 3KΩ resistor, 7K will be a suitable operating point on the curve with a corresponding input voltage bias level of Ω2.5 volts and variation of ±0.1 volts. Other suitable operating points are clearly possible.

The combination of the standing current in R and the value of R_x determines the feedback ratio of the circuit. R_y determines the input bias level and the slope of the input volts versus output ohms

characteristic obtained. At the bias level of 2.5 volts the lamp draws approximately 30.mA and in order to minimise integrator drift in the HOLD condition an additional buffer stage was deemed necessary to supply the emitter follower base current.

As the dynamic performance of the circuit will be a function of the LUXISTOR dynamic characteristics some knowledge of these must first be obtained in order to design adequate circuit compensation. It was thought that the LUXISTOR could be considered as a combination of two lags, one associated with the lamp and the other with the time response of the cadmium sulphide element. Data available indicated that the former was of the order of 100 milliseconds.

Due to the physical nature of the material the dynamic response of cadmium sulphide is a compromise between speed and sensitivity. Suitable doping can produce a fast acting device but the resulting sensitivity is poor. Likewise if sensitivity is required a slow response will result. Some typical response curves which have been given by Bube (5) and shown in figure 2.9. [redacted] indicate an equivalent time constant of the order of 100 milliseconds. For the LUXISTOR this latter figure would obviously depend on the type of doping used.

The measured frequency response of the device is shown in figure 2.10. A steady bias current was established in the cadmium

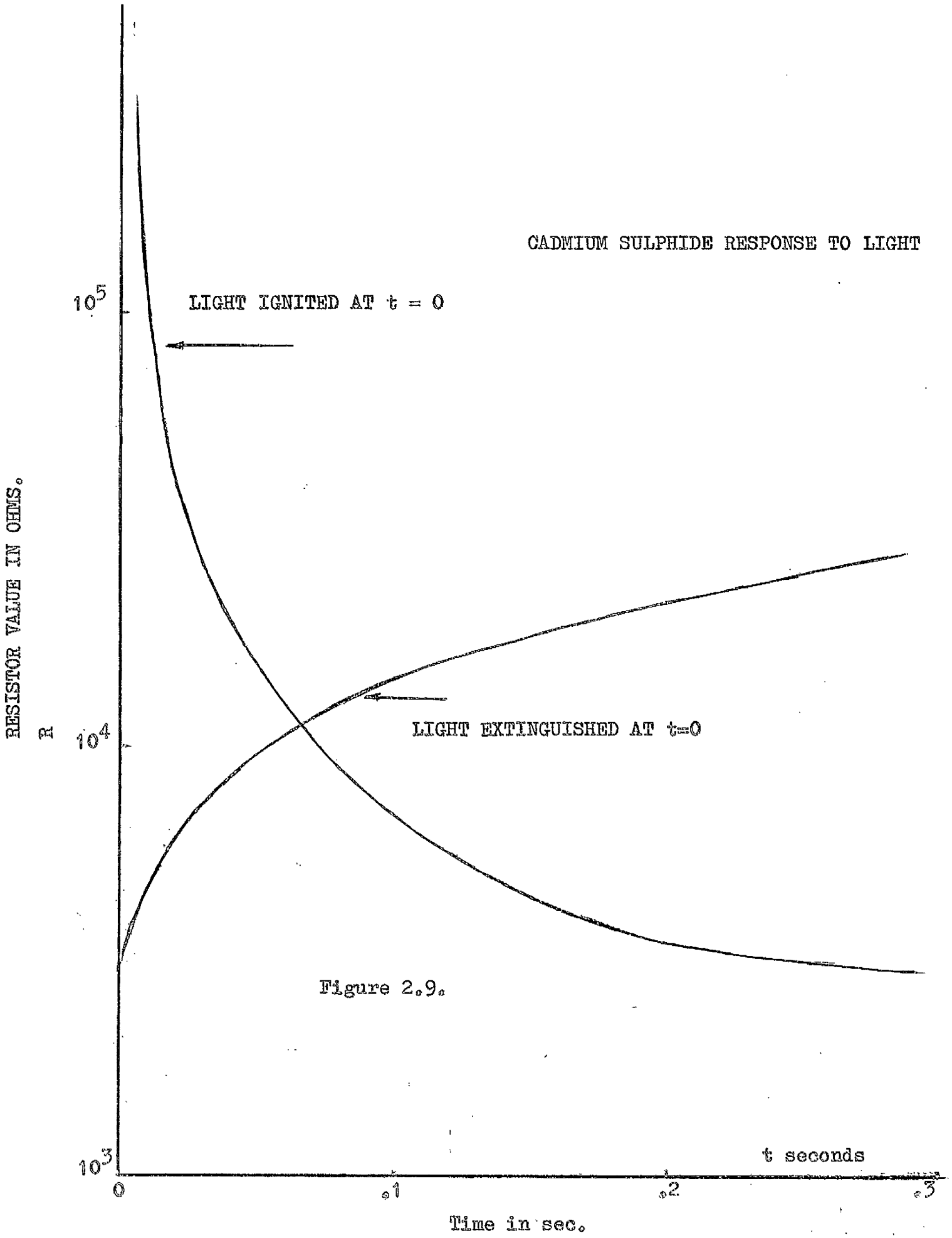
CADMIUM SULPHIDE RESPONSE TO LIGHT
LIGHT IGNITED AT t = 0
LIGHT EXTINGUISHED AT t=0
RESISTOR VALUE IN OHMS.
R
10^5
10^4
10^3
0
.1
.2
.3
t seconds
Time in sec.

Figure 2.9.

sulphide element and the terminal voltage measured for a varying frequency 0.5 volt peak to peak input voltage superimposed upon a 2 volt bias level. The second order characteristic of the device is clearly evident, maximum gain occurring at a frequency of 0.33 c/s. Gain value will be a function of the bias current level in the element and the chosen operating point.

The open loop transfer function of the integrator and LUXISTOR system will be of the form

$$\frac{1}{s} \quad \frac{K_A}{(1+sT_A)(1+sT_B)}$$

where T_A = time constant of lamp $\underline{\Omega}$ 0.1 seconds

T_B = time constant of sulphide element $\underline{\Omega}$ 0.1 seconds

K_A = steady state gain of the LUXISTOR.

The value shown for T_B is based on <u>figure 2.9</u>. and is to be regarded as an assumption only.

To enhance stability in the closed loop the system order can be reduced by cancellation of one of the poles associated with the LUXISTOR. Hence as a proportional factor is included in the integrator circuit the open loop transfer function will now be

$$\frac{1+sT_P}{sT_P} \cdot \frac{K_A}{(1+sT_A)(1+sT_B)} \underline{\Omega} \frac{K_A}{sT_P(1+sT_B)}$$

if T_P = 0.1 sec. $\underline{\Omega}$ T_A

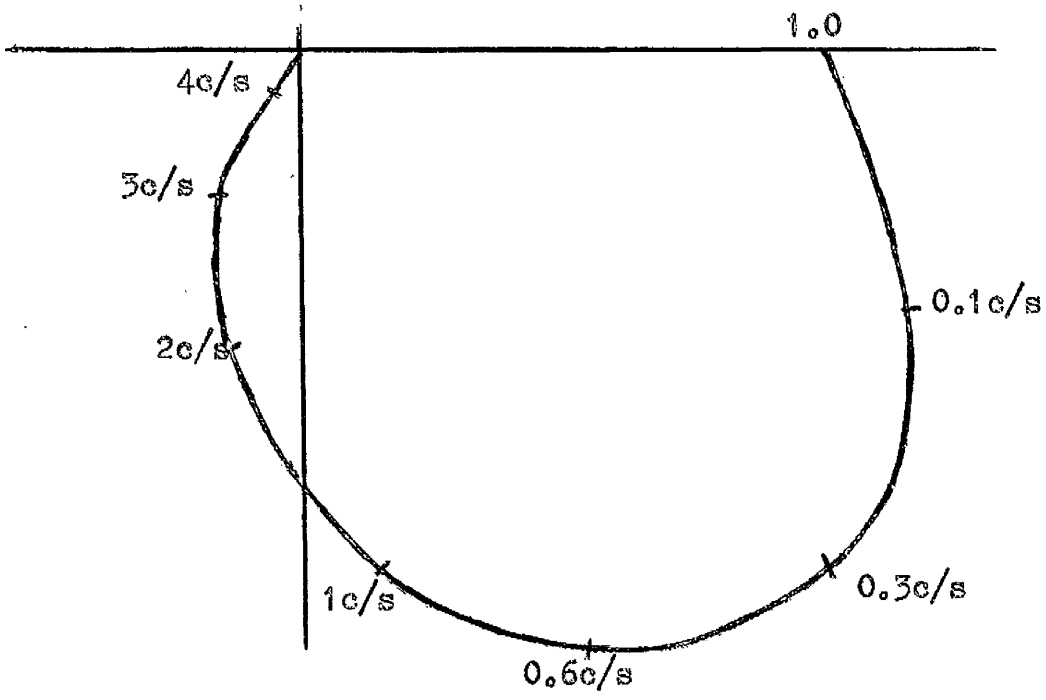

Figure 2.10 Luxistor Frequency Reponse.

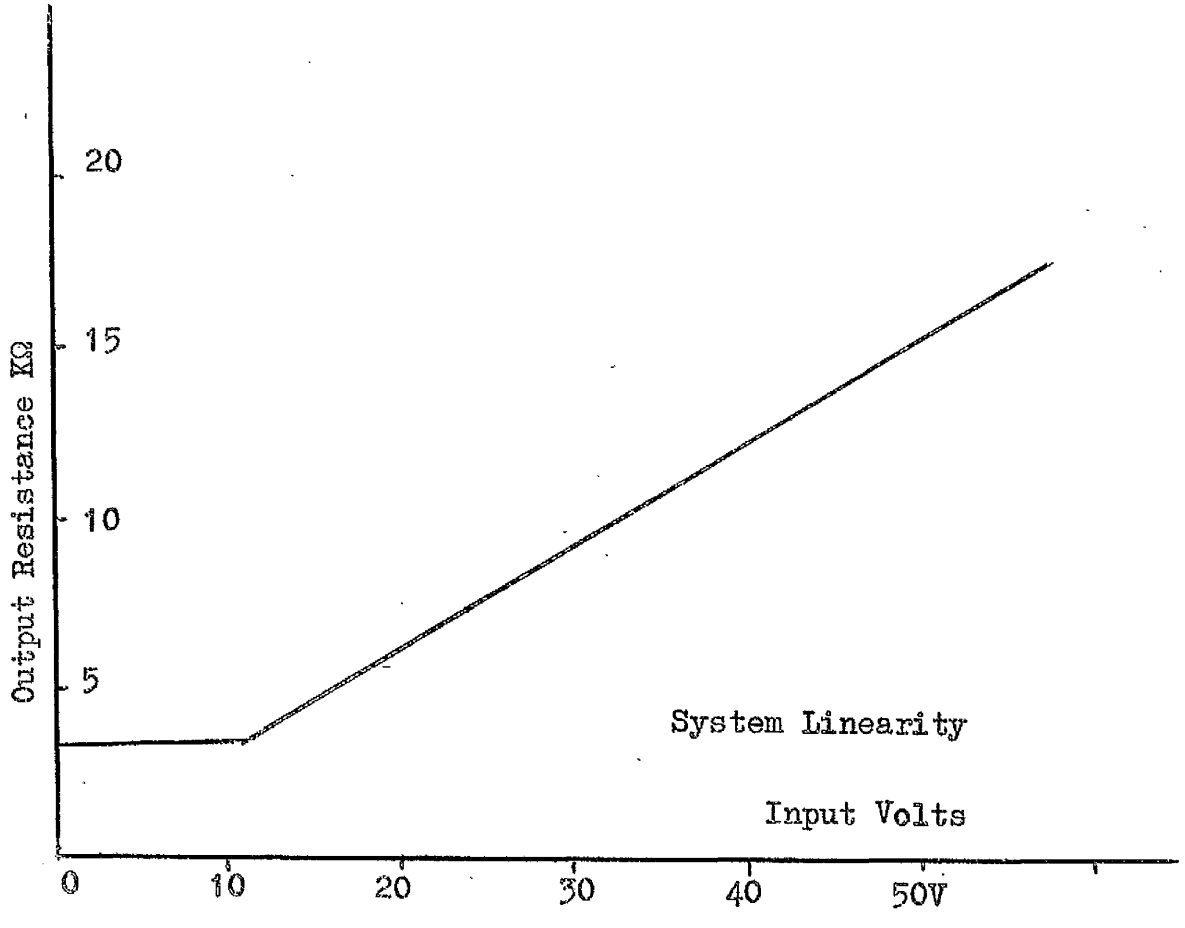

Figure 2.11

T_P is the time constant of the combined proportional plus integral factor in the integrator circuit. This form of compensation proved very satisfactory, resulting in a stable closed loop system with an excellent transient response.

The final circuit is shown in figure 2.12. Two Solartron 100 volt operational amplifiers were available and used, for convenience, in this experimental circuit, as integrator and buffer stages. With suitable scaling a ± 10 volts operational amplifier would be equally applicable. To obtain a reasonable volt swing at the integrator input the buffer stage gain was made equal to 0.1.

2.2.5. Experimental Results

A steady bias current for the cadmium sulphide element was established in the emitter circuit of a ZT 82 transistor operating from an isolated ± 20 volt supply. The resulting emitter degeneration ensures a high degree of bias stabilisation without the use of additional compensating elements. R_x was made equal to 0.1 MΩ, R_y equal to 1.0 MΩ and the integrator capacitor equal to 0.1μF. For a bias current level of 0.32 mA the quiescent input voltage was thus 32 volts. The graph of input voltage versus output resistance is shown in figure 2.11. the minimum output resistance being limited by the series 3.3 KΩ. Percentage changes of input voltage versus percentage change in output voltage about a bias level of 10 KΩ is shown in figure 2.13 the linearity being better than 0.5%.

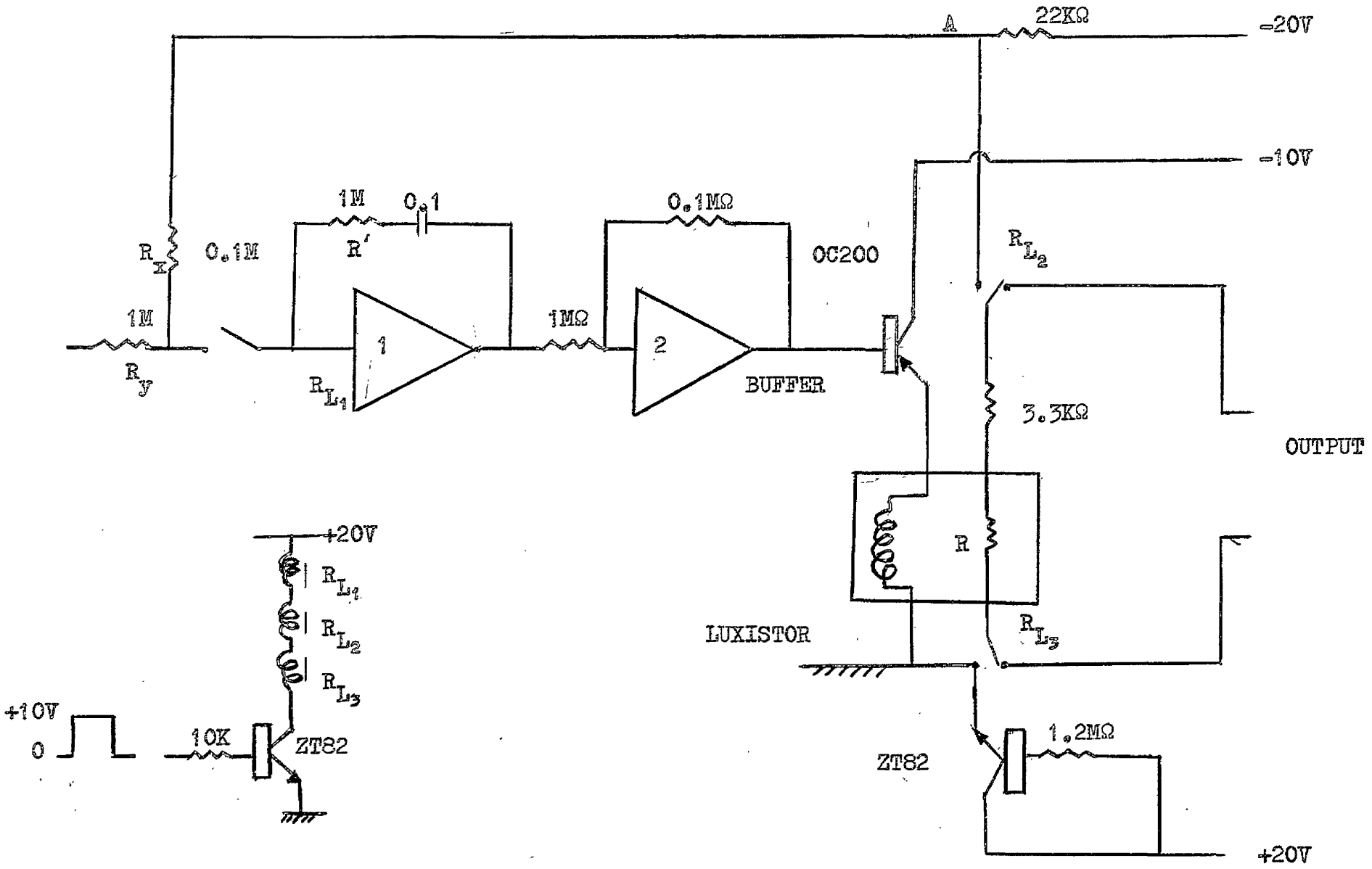

Figure 2.12. Luxistor Control Circuit.

The closed loop frequency response of the circuit is shown in figure 2.14 and 2.15. Measurement was carried out at an input bias level of 32 volts and a perturbation voltage of 3.2 volts R.M.S. Resonance occurs at 0.85 cycles per second and the gain at this frequency indicates a closed loop damping factor of approximately 0.6 (6). The second order nature of the system is clearly demonstrated in figure 2.15. The transient response characteristics of the circuit are shown in figure 2.16. for a 10% change in input voltage about a bias level of 32 volts. The effect of variation of the input integrator proportional resistor is indicated. Curve (e) gives an excellent response with a measured damping factor of approximately 0.6 (6), and a settling time of the order of 240 milliseconds. The damping factor obtained from the transient response corresponds with the damping factor obtained from the closed loop frequency measurements of figure 2.15.

When the adaptive model is switched to the compute mode the feedback loop in the adaptive circuit is broken and the long term accuracy of the variable resistive element depends directly on the drift characteristics of the circuit integrator in the HOLD mode. The sensitivity of this accuracy to integrator drift voltage is a function of the quiescent operating point chosen for the cadmium sulphide element and the percentage ohmic value that this element contributes to the total resistor magnitude.

It was found that with correct adjustment the integrator

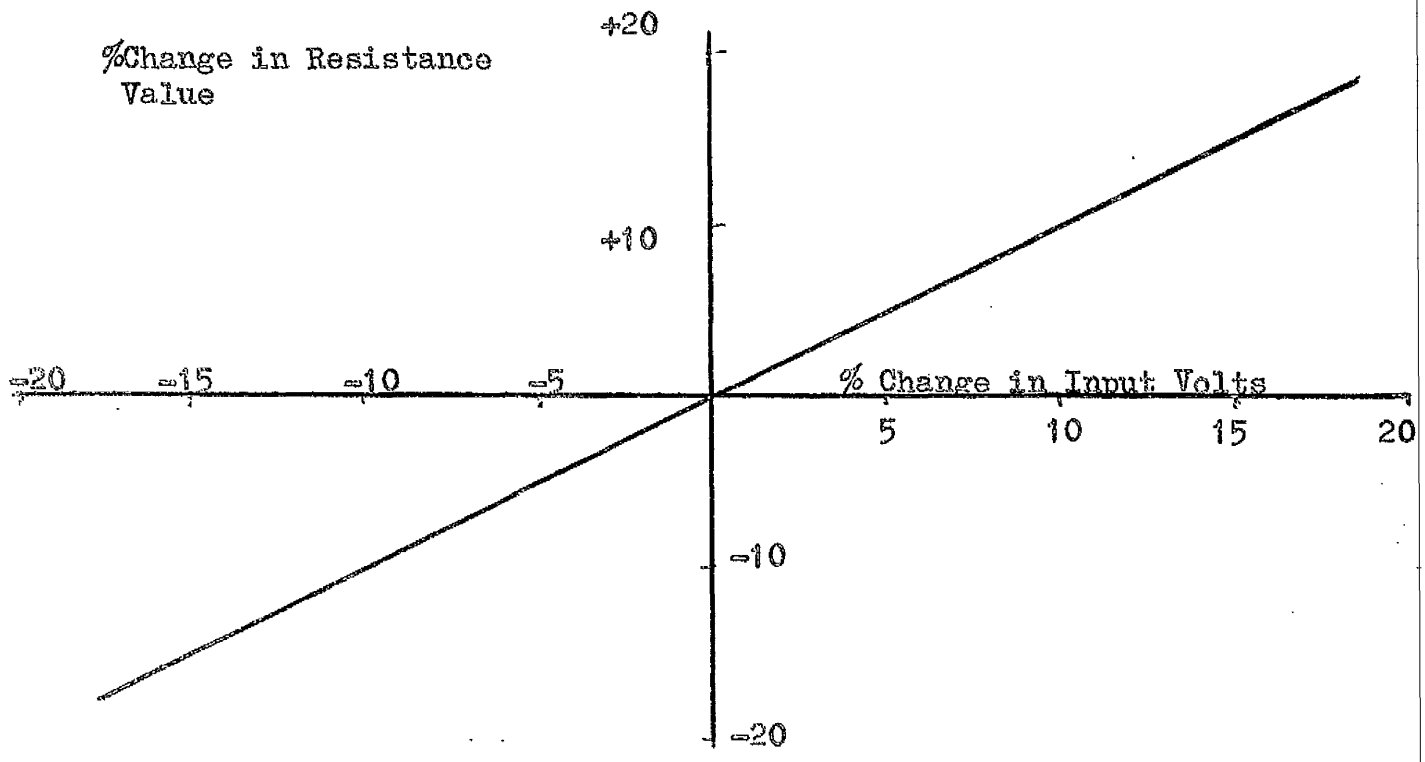

Fig. 2.13. Operation about a bias level of 10KΩ.

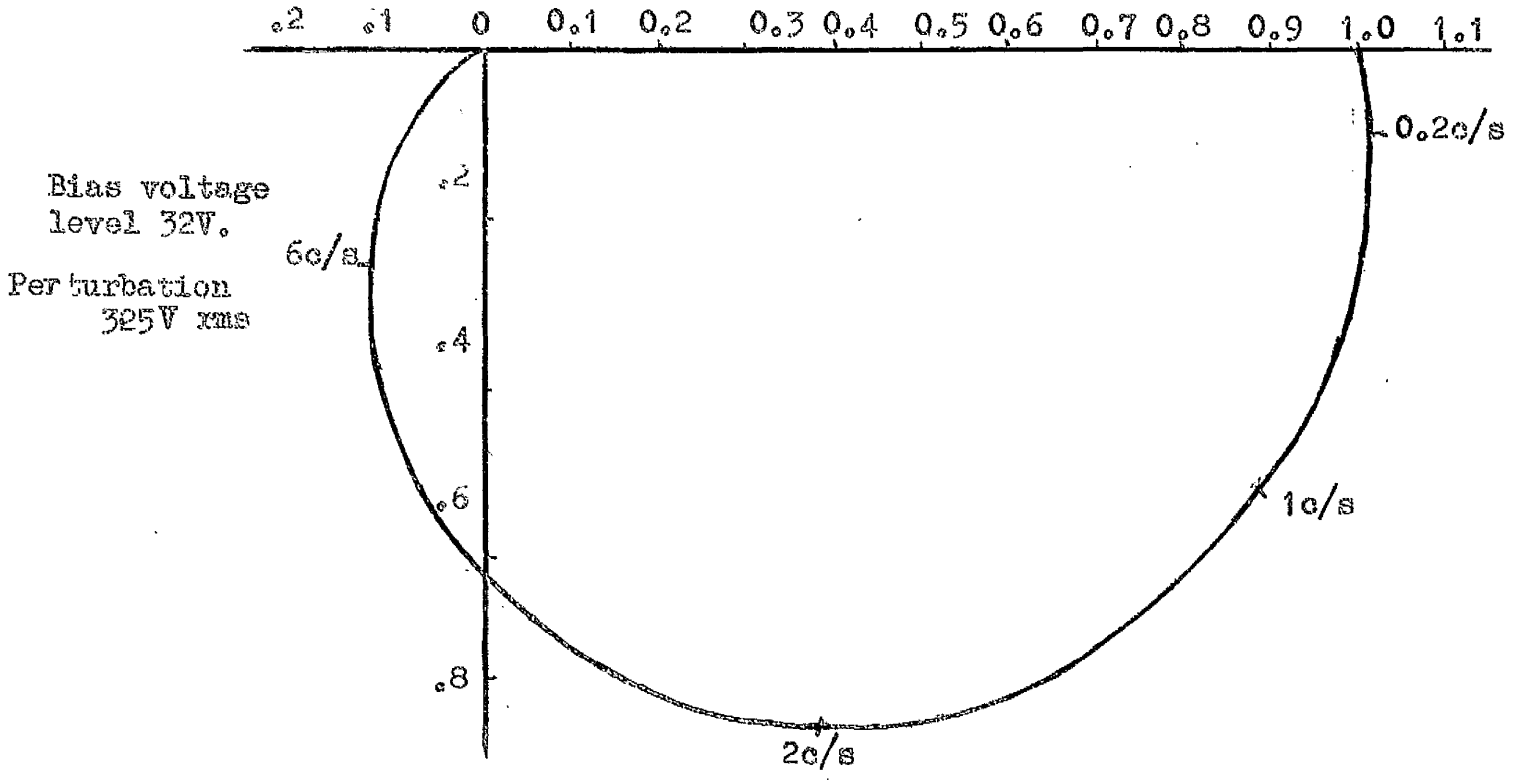

Closed loop frequency response for complete system Polar Diagram.

Fig. 2.14.

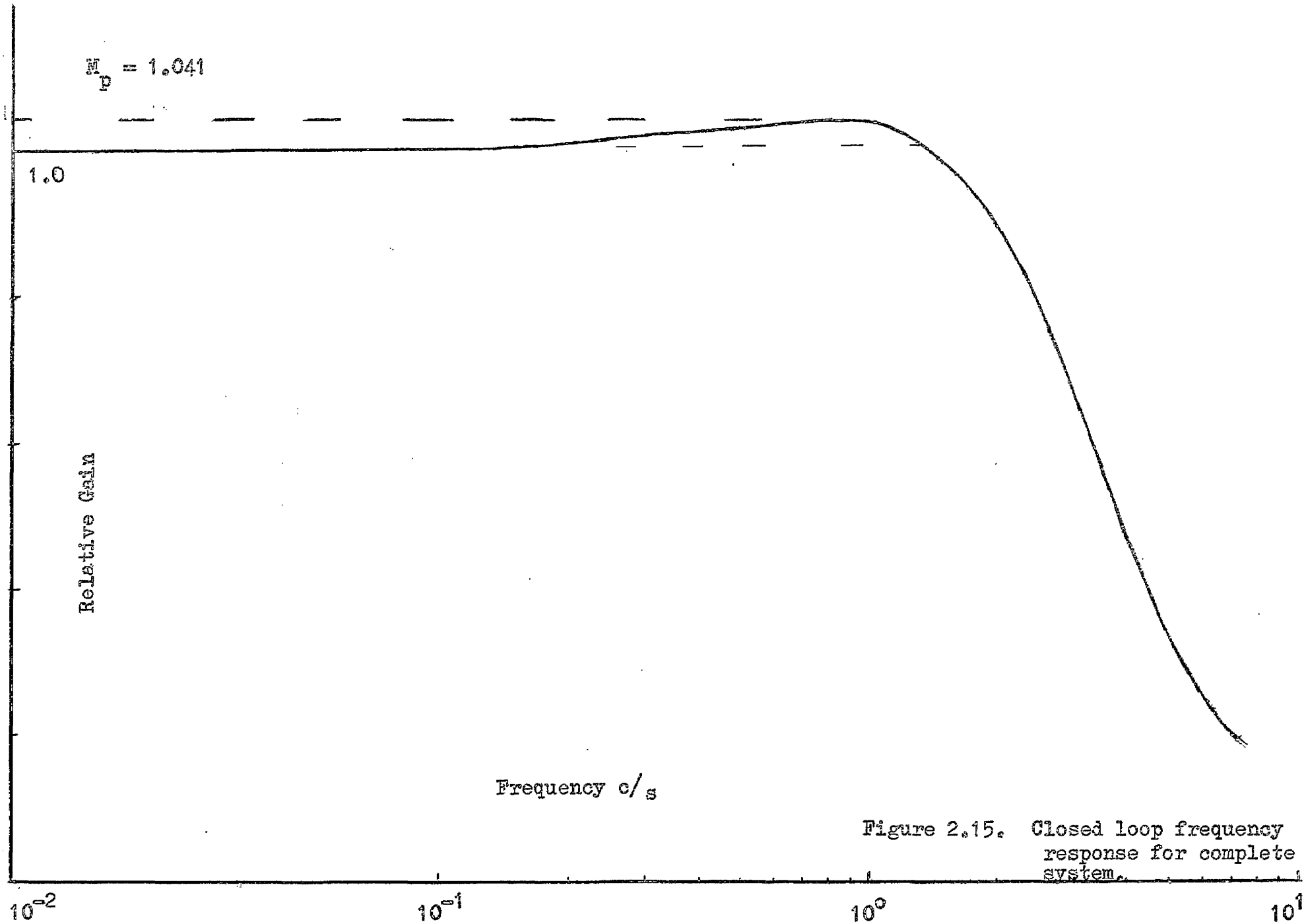

Figure 2.15. Closed loop frequency response for complete system.

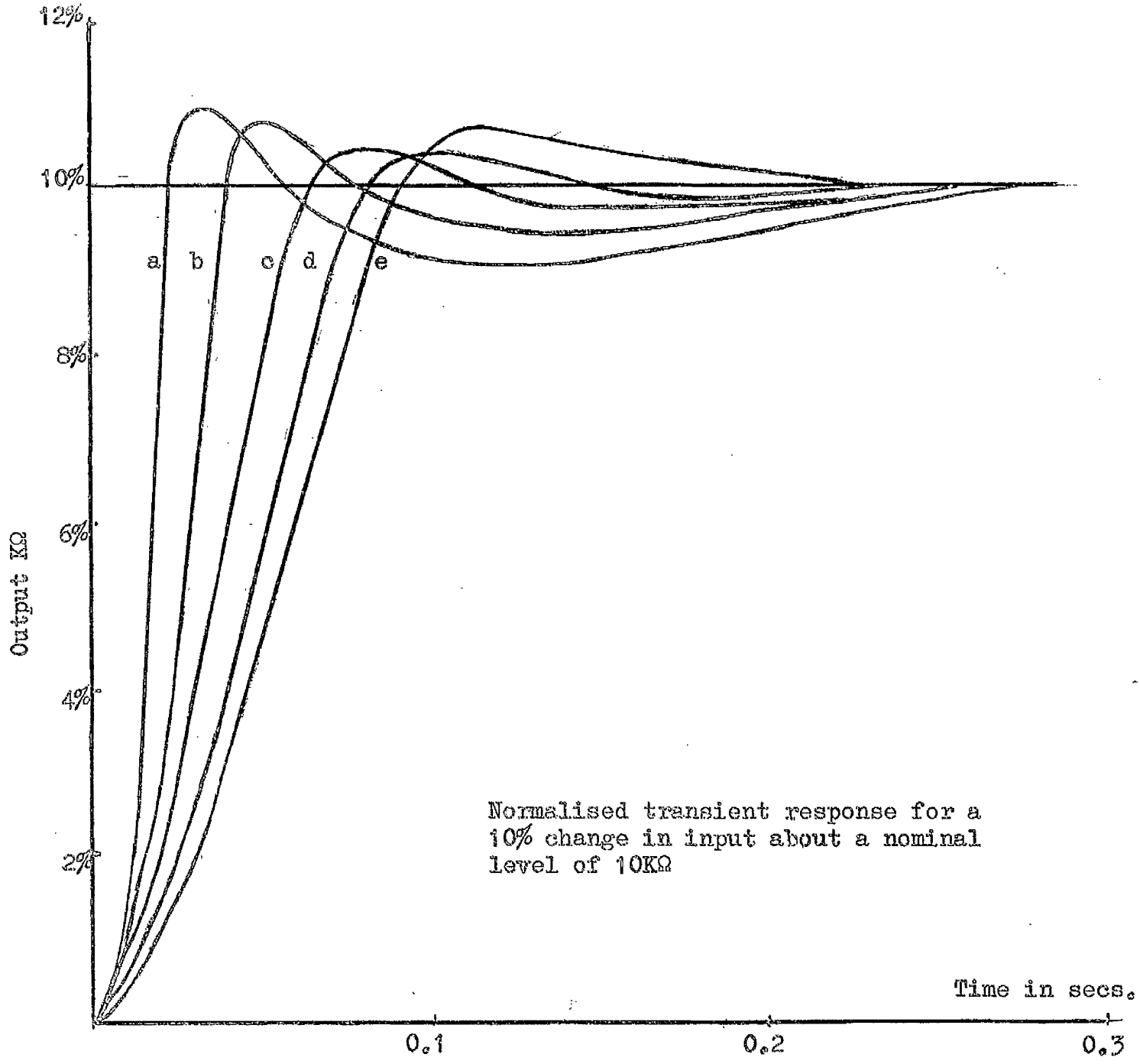

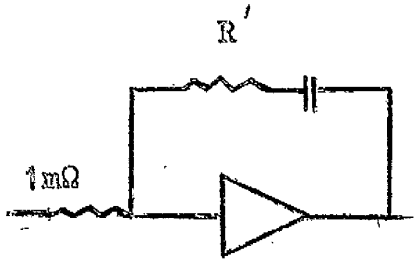

a - R'=3mΩ
b - R'=2.5mΩ
c - R'=2mΩ
d - R'=1.5mΩ
e - R'=1mΩ

Figure 2.16.

could maintain a voltage in the HOLD mode to an accuracy of 0.05% for a period in excess of 30 seconds. Thus for a total resistor value of 10KΩ with the cadmium sulphide element biassed at approximately 7KΩ the error in resistance value at the end of a computation period of 30 seconds will not be greater than 0.45%. It will be seen from figure 2.5. that a bias point in the region of 5KΩ will reduce this total error by a factor of two. For fast repetitive operation computation periods of the order of one second are envizaged and, if we assume linear integrator drift characteristics, the total resistor error at the end of the computation period will thus be less than 0.015%.

Relays RL1, RL2 and RL3 are operated from a ZT 82 transistor trigger. RL1 is a 3 volt reed relay with a much faster response than the six volt moving armature device used for the other two relays thus ensuring that RL1 opens before R is isolated from the circuit.

Figure 2.17 illustrates the general layout of a printed circuit board containing two full control circuits designed for operation with four operational amplifiers.

2.2.6. Environmental Considerations.

(a) Temperature.

Steady state accuracy is dependent on the accuracy of the bias current level setting and hence sensitive to variations in the ± 20 volt power supply and the parameter values of the output ZT 82 transistor. Assuming that temperature compensated power supplies and associated high stability resistors are available only the latter variations need be

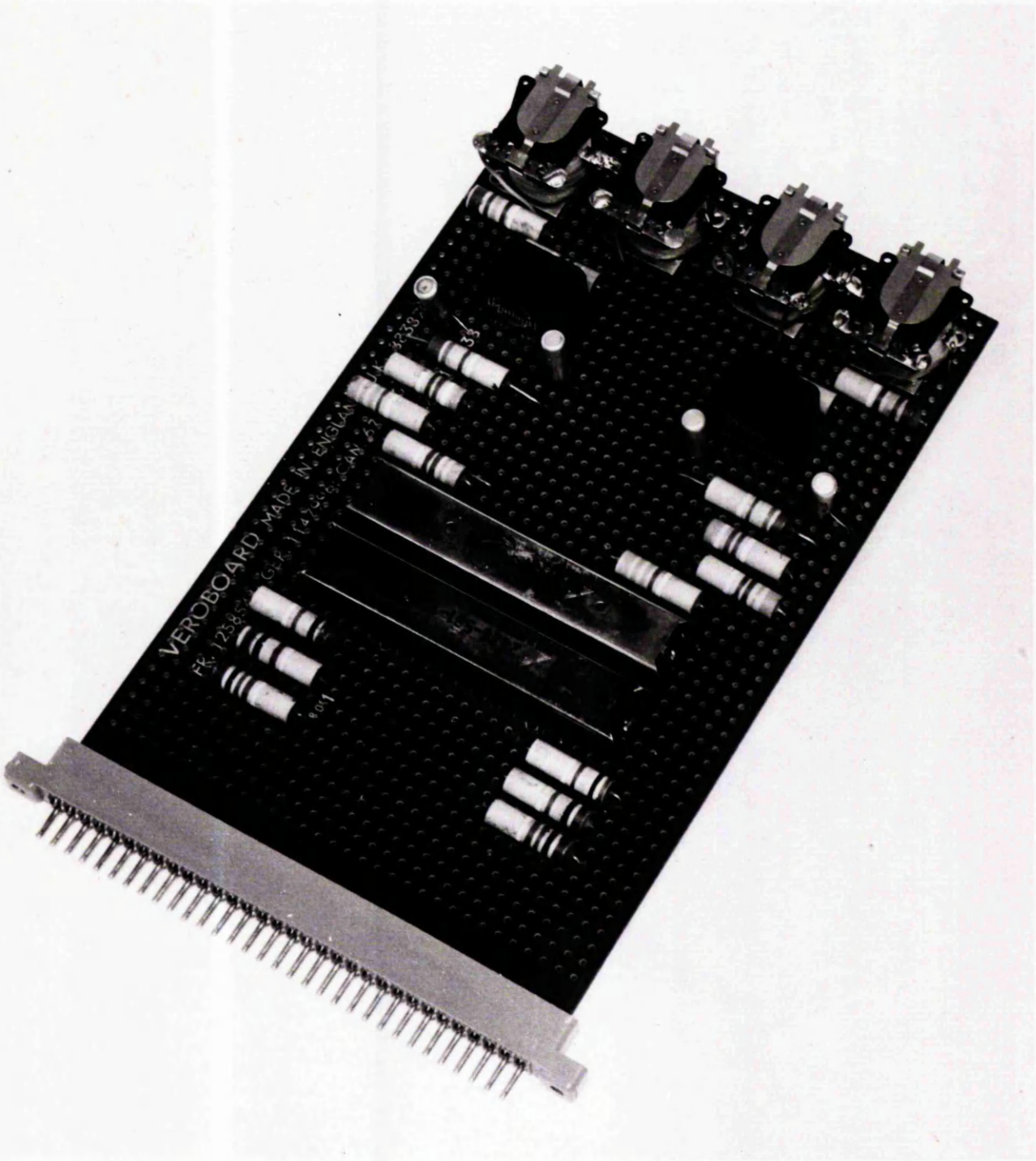

Adaptive Control Circuit Assembly

Figure 2.17.

discussed here. The three transistor parameters which must be considered are (7): the reverse saturation current I_{co}, the emitter base voltage and the transistor current gain. A variation in any one of these values will result in a queiscent current change in the ZT 82 and hence in a control system static error.

A high degree of bias stabilisation can be accomplished by emitter current degeneration alone as used in figure 2.12 without the addition of temperature compensating elements such as thermistors. This can be seen by referring to the emitter follower circuit of figure 2.18.

(a) As I_{co} varies V_E varies changing V_B and thus I_B which results in a change in I_c counteracting initial change in I_{co}.

(b) If V_{BE} changes, say a reduction, then I_B increases increasing I_c and hence V_E. V_B is thus increased and I_B again decreases.

(c) If the current gain alters, say an increase, then, for a given I_B, I_C will increase forcing V_E and hence V_B up. I_B will thus decrease counteracting the initial change in the current gain.

A current of 0.3200 mA was established in a ZT 82 transistor

connected as shown in figure 2.19 and the variation of this current monitored as the transistor temperature was raised through 30^{o}F. The results were as follows.

Temperature	I_E mA
70^{o} F	0.3200
100^{o} F	0.3205

Percentage change in current /^{o}F $= \frac{0.0005}{.32} \times \frac{100}{30} = .0052\%$.

It was thus considered that for moderate temperature changes emitter degeneration alone would provide sufficient bias stabilisation without the added complexity of thermistor units.

Temperature variation not only affects the conductivity of the cadmium sulphide element but also the emission spectrum of the filament lamp. The resistance of the cadmium sulphide element is thus a complex function of temperature. An indication of the nature of this function was obtained by placing a Luxistor alone in an oven and connecting the cadmium sulphide element to an external 3.3KΩ resistor. The input bias voltage to the filament lamp was adjusted to achieve a total resistance value of approximately 10KΩ. The oven temperature was increased and the resulting variation in total resistance value was monitored. The results are shown in figure 2.20.

The Luxistor was now connected as an element in the complete external feedback circuit of figure 2.12 and the voltage at point A

V_{BE} = emitter base voltage
I_{CO} = Reverse saturation current
I_C = Total collector current.

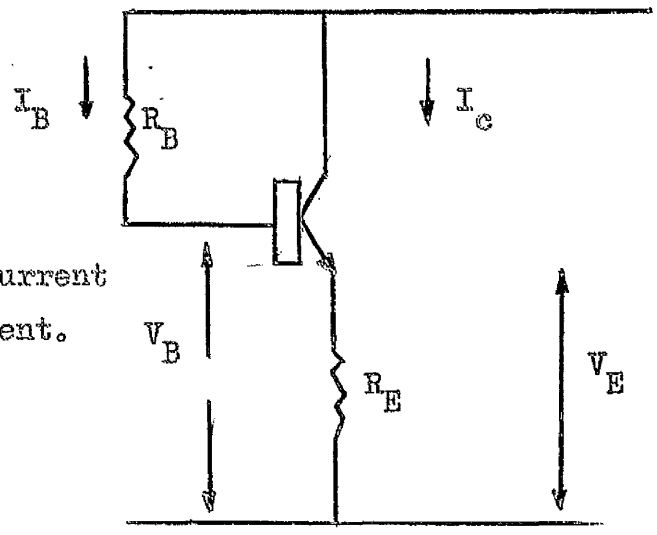

Emitter Follower. Figure 2.18.

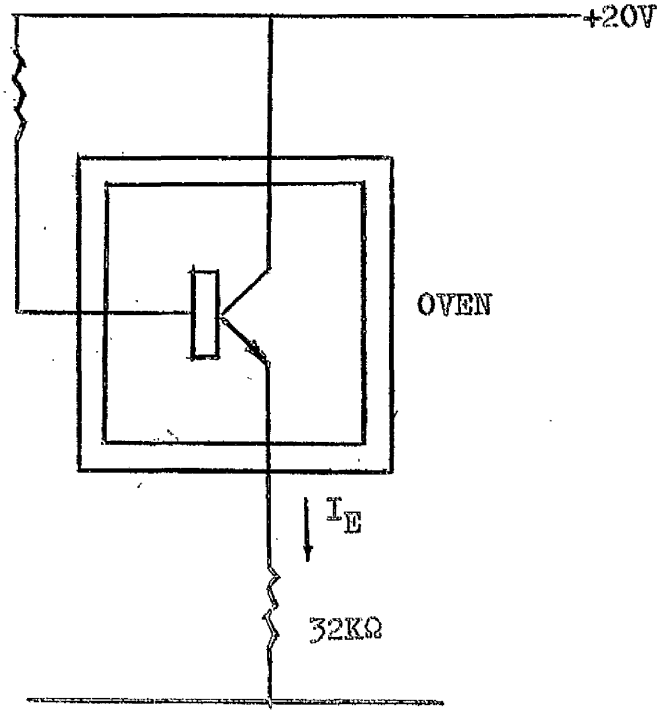

Temperature Testing Figure 2.19.

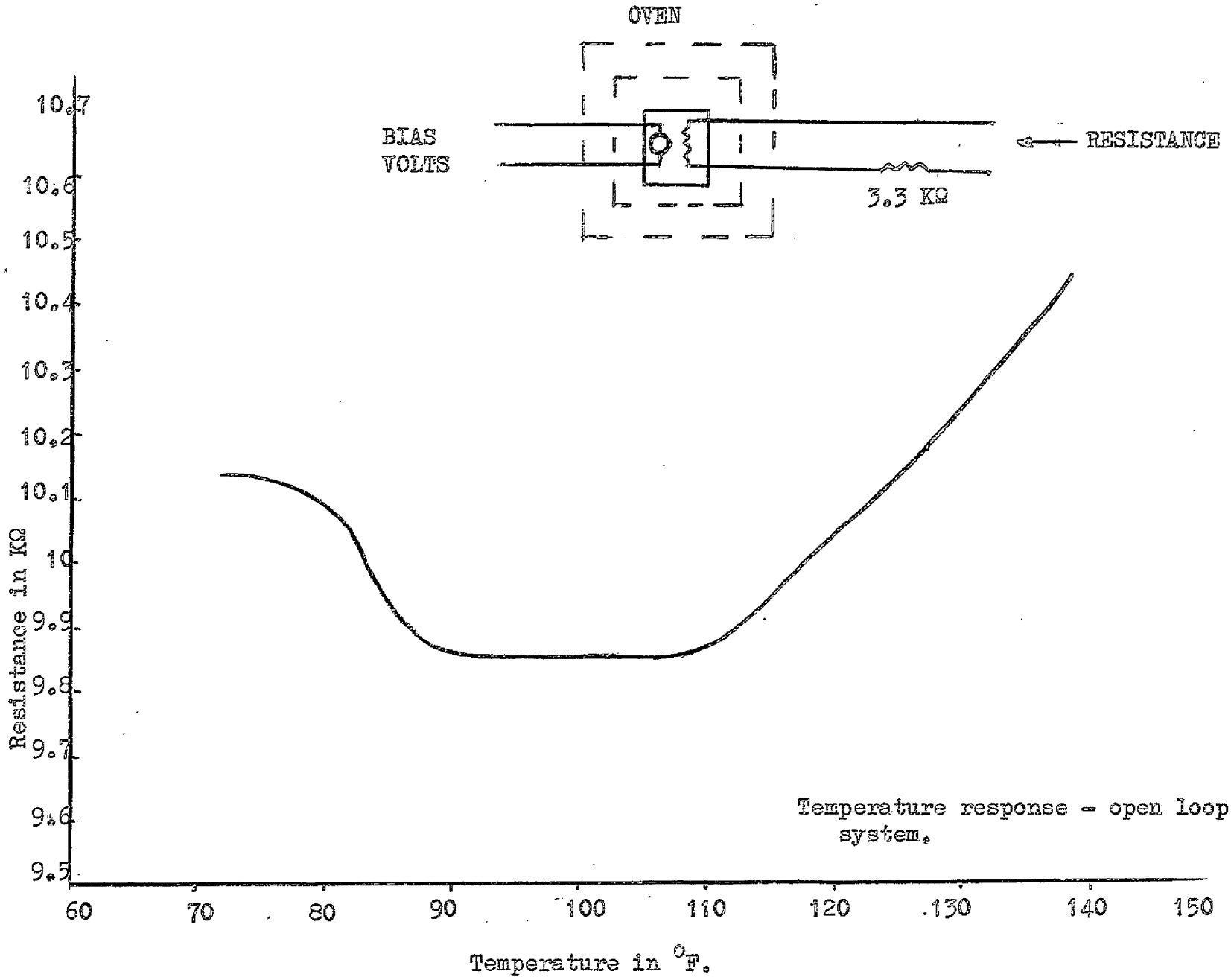

Temperature response - open loop system.

Figure 2.20.

monitored as the Luxistor was again subjected to the heating cycle. For a Luxistor temperature change of approximately 70°F the voltage at point A remained constant to within 0.05% which was the limit of accuracy of the digital voltmeter.

Due to the high static gain of the integrator the system accuracy can thus be considered independent of parameter change within the feedback loop.

(b) Vibration and Shock.

The behaviour of the solid state electronic unit under conditions of vibration and shock will depend entirely on the type of packaging used and, assuming that solid state integrated amplifiers are eventually incorporated, extremely high "g" forces can be tolerated. The vibration performance of armature relays is poor and, if mechanical switches are specified, reed relays should be used throughout. Typical shock resistance of a reed relay switch is 100g with a pulse duration of up to 10 milliseconds and typical vibration resistance is 20 g up to 20Kc/s (8).

At the time of writing no figures are available on the allowable "g" forces for the Luxistor element though its complete encapsulation affords a high degree of shock resistance. A possible weak point however would be the dynamic characteristics of the lamp filament.

2.2.7. Summary.

The control circuit of figure 2.12 exhibits excellent static and dynamic characteristics and more than fulfills the initial limited design specifications of paragraph 2.2.3. Apart from the two operational amplifiers which can be regarded as standard components this performance has been realized by an extremely simple and hence inexpensive circuit configuration.

Due to the high forward static gain of the integrator the relationship between input voltage and output resistance value is linear to within 0.5% and noise free resistance changes are accomplished with a settling time of less than 300 milliseconds. This latter time corresponds very favourably with the settling time of a modern servo multiplier which is of the order of 2 seconds. The circuit is insensitive to moderate temperature changes and, provided the power dissipation of the cadmium sulphide element is not exceeded, relatively fool proof in operation.

Proposed further development work here would involve replacing the computer operational amplifiers by solid state integrated amplifiers such as the UA709 (9) and the relays by field effect transistor switching circuits, with a view to producing a compact, completely solid state adaptive mechanism compatible with modern solid state analogue or hybrid computing systems.

2.3.1. Semiconductor Electroluminescence.

Light emission from a semiconductor crystal was first observed by H.J. Round in 1901 when studying the passage of electric current through silicon carbide and the phenomenon, the direct conversion of electrical energy into light without the intervention of heat, was termed electroluminescence. Subsequently sharp line spectra emission due to recombination of holes and electrons has been observed from many semiconductor materials including silicon (10) germanium (11) and silicon carbide (12). In 1962 the discovery by Keys (13) of highly efficeint electroluminescence at forward biassed P.N. junctions in gallium arsenide crystals led to intensive research work in this field (14) with particular reference to the development of an efficient solid state laser.

To understand the concept of recombination light emission it is necessary to study the semiconductor energy band structures. In figure 2.21 δE represents the energy required to raise an electron from the valance band to the conduction band. The magnitude of the quantum energy involved in this process is a fundamental property of the specific semiconductor material. The lifetime of the free electron in the conduction band is relatively short and it quickly recombines liberating energy equivalent to δE. Light emission is involved in this energy release, the wavelength being a function of δE,

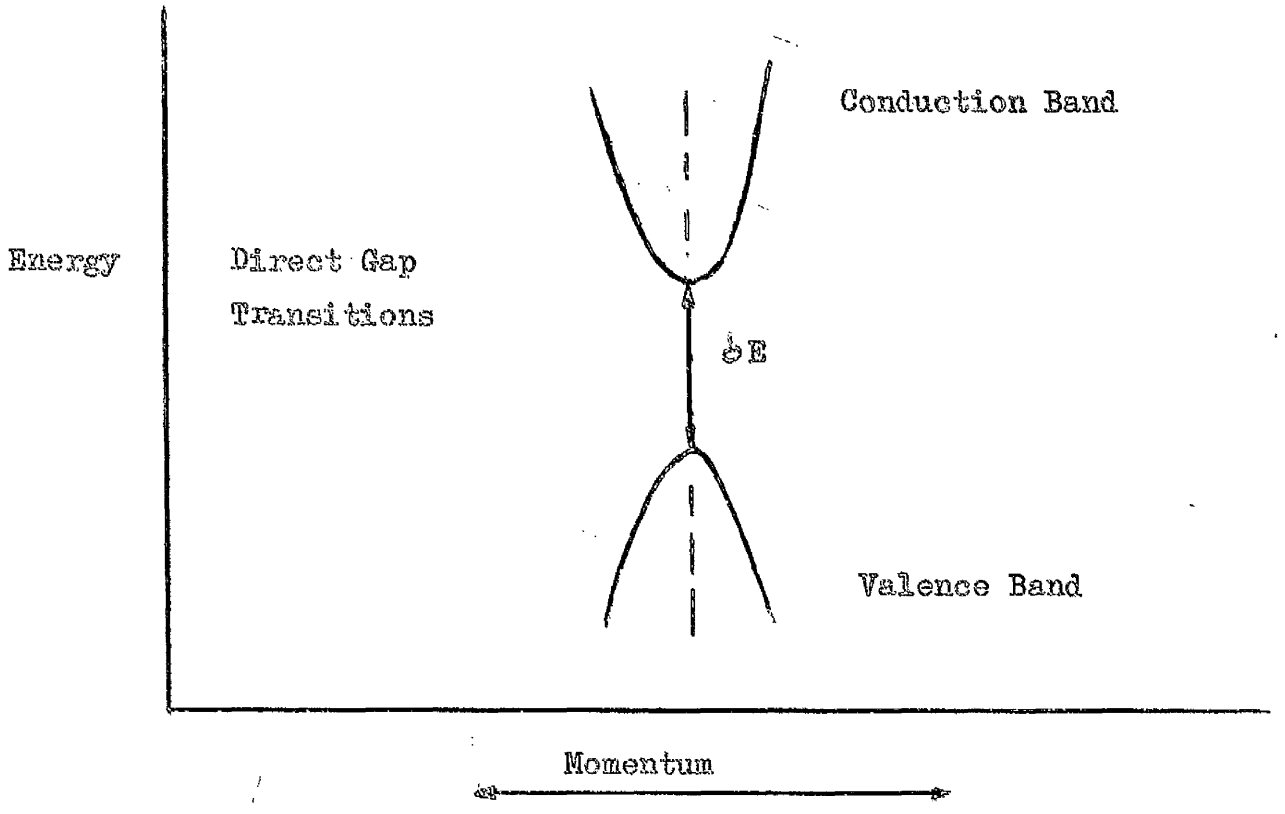

Figure 2.21 Probable band structure for Ga.As.

and, when the gap energy if of sufficient magnitude, visible radiation is observed.

Figure 2.21 shows the probable band structure of gallium arsenide crystal where the horizontal axis represents particle momentum. In semiconductor crystals transitions take place between the minimum conduction band energy level and the maximum valance band energy level and it will be seen that, for this material, such transitions are accomplished without any change in particle momentum and thus no heat is involved in the transformation, light energy only being released. This latter effect accounts for the unusually high efficiency associated with light emission in gallium arsenide which is termed a direct gap semiconductor. In the case of indirect gap semiconductors such as silicon and germanium momentum changes occurring during particle recombination result in a proportion of the energy release being converted into crystal lattice vibrations and thus being dissipated as heat with subsequently low light generating efficiency. Normal gallium arsenide lamp emission is obtained from a P.N. junction formed in the crystal by diffusion or alloying techniques. When forward biassing is applied to this junction recombination takes place in both the P and N regions, the amount of light emitted from each depending on the degree of absorption present. A typical spectral emission characteristic has been given by Effer (15) and is shown in figure 2.22.

The lamp used in this work was the Ferranti XS32L device, the main characteristics being as follows (16).

Max continuous forward current	100 mA.
Forward voltage at this current	1.3 volts
Rise time (Light)	15 n Sec.
Fall time (Light)	15 n Sec.
Spectral Peak	9000 A^{o}.

It will be seen that the device has extremely short rise and fall timesand an exceptionallly fast system response time should thus be possible. The forward input characteristic which is illustrated in figure 2.23 shows a forward breakdown voltage of 1.2 volts and light emission commences at this point, the emission being roughly proportional to the current passing (15). The maximum current that may be passed depends mainly on the power dissipation allowable at the junction diode and improved performance can be obtained by encasing the diode in a suitable heat sink. Low device operating temperatures are desirable because as the junction temperature increases the quantum efficiency of the recombination emission falls.

As the overall quantum efficiency of the radiation is low (of the order of 0.1%) an attempt has been made with the XS32L to improve light output by adding a focussing lens with a non reflecting coating. The resulting light flux is thus focussed in the manner shown in the polar diagram figure 2.24.

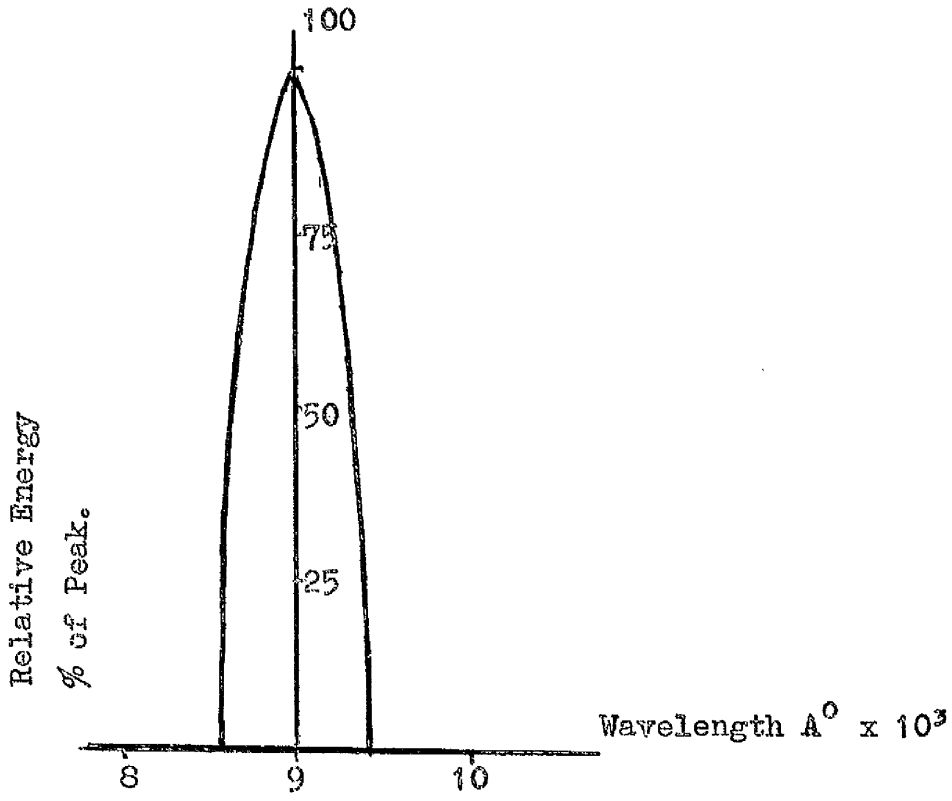

Figure 2.22. Spectral Emission of Ga.As at 25°C.

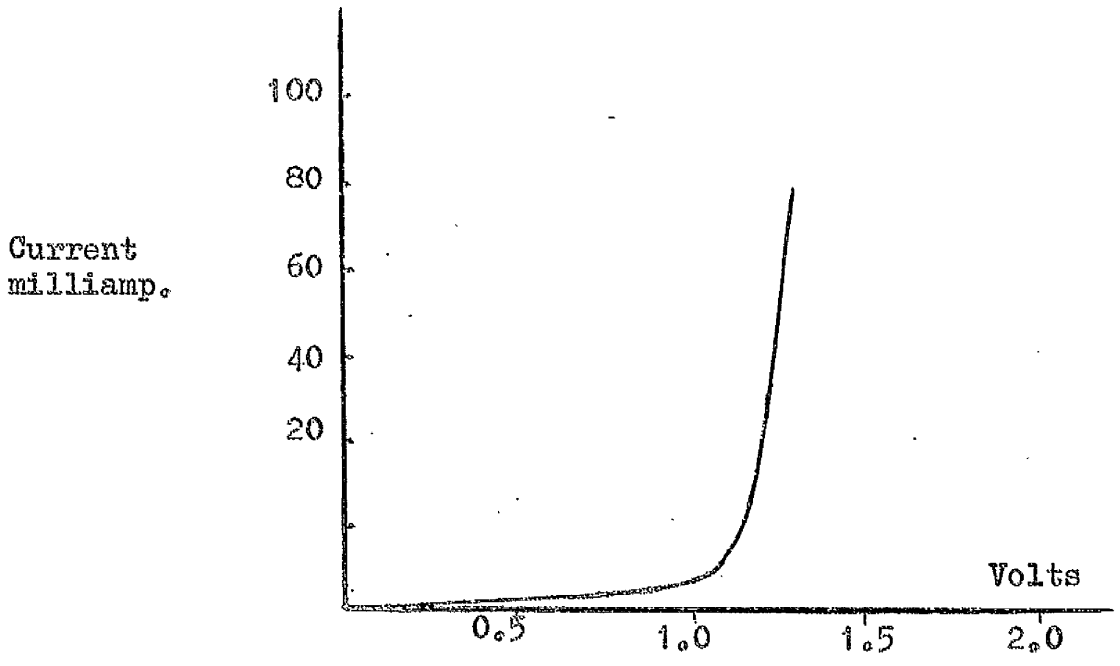

Figure 2.23. Forward Characteristic of XS32L.

2.3.2. The Photodetector.

In conjunction with the crystal lamp it is essential to use a photodetector which is compatible with the light source in both spectral sensitivity and speed of response. The silicon photo diode meets both these requirements with a peak spectral response in the region of 10^4 Å and a photo current rise time of 2 microseconds.

If uniform illumination is applied through the volume of a reverse biassed P.N. junction and its adjacent P and N regions for a distance of several diffusion lengths we may write the photo current as (3)

$$I = q\,An\,I_L\,(L_N+L_P) + I_0$$

where

n = efficiency light in electron hole pairs per second per cubic centimetre per unit of light intensity.

q = electronic charge.

I_L = light intensity.

A = c.s. a. of junction

L_N, L_P = electron, hole lifetimes respectively.

I_0 = reverse saturation current.

If I_0 is small then the photo current is approximately proportional to the incident light intensity. From the above equation it is clear that the best sensitivity is found for very long lifetime

materials where L_N and L_P are high. However, as before, this sensitivity is achieved at the expense of photo current transient response time.

The detector used in this work is the Texas Instruments N.P.N. photo duo diode type 1N 2175. In this device two symmetrical P.N. junctions are diffused in the silicon substrata so that either terminal can be biassed positively or negatively. This latter property while in no way altering the basic philosophy of the approach, greatly increases the flexibility of the device in its ultimate application as an adaptive element.

The 1N 2175 has the following characteristics. (17).

Maximum bias voltage	= $\pm$ 50 volts
Power dissipation	= 250 milliwatts
Dark current at 25°C $\pm$ 50V bias	= 0.5 µA
Light current at 25°C + 10V bias	= 100 µA
Photocurrent rise time	= 2 µsec
Photocurrent fall time	= 45 µsec
Sensitivity	= 22.3 µA/mW/cm^2
Spectral peak	= 10,000 Å.

Typical forward characteristics of the 1N 2175 are shown in figure 2.25. the reverse characteristics being completely symmetrical. The dynamic impedance here ranges from about 2MΩ at an irradiance of 2mW/cm^2 to about 250KΩ at an irradiance of 16mW/cm^2. The maximum

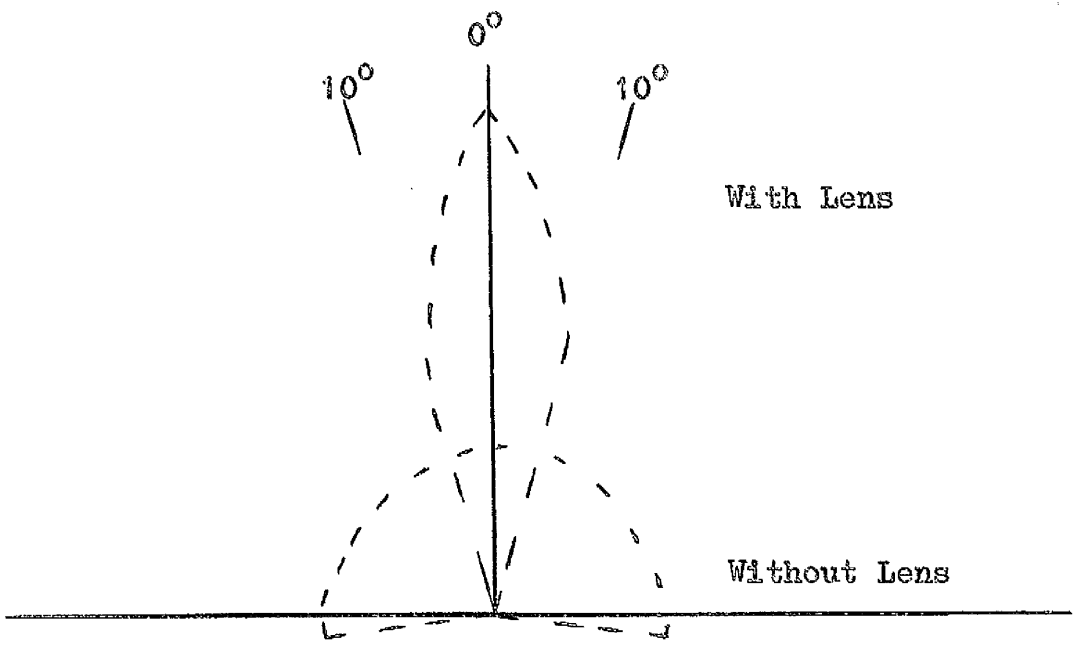

Figure 2.24. Polar Diagram of XS32.

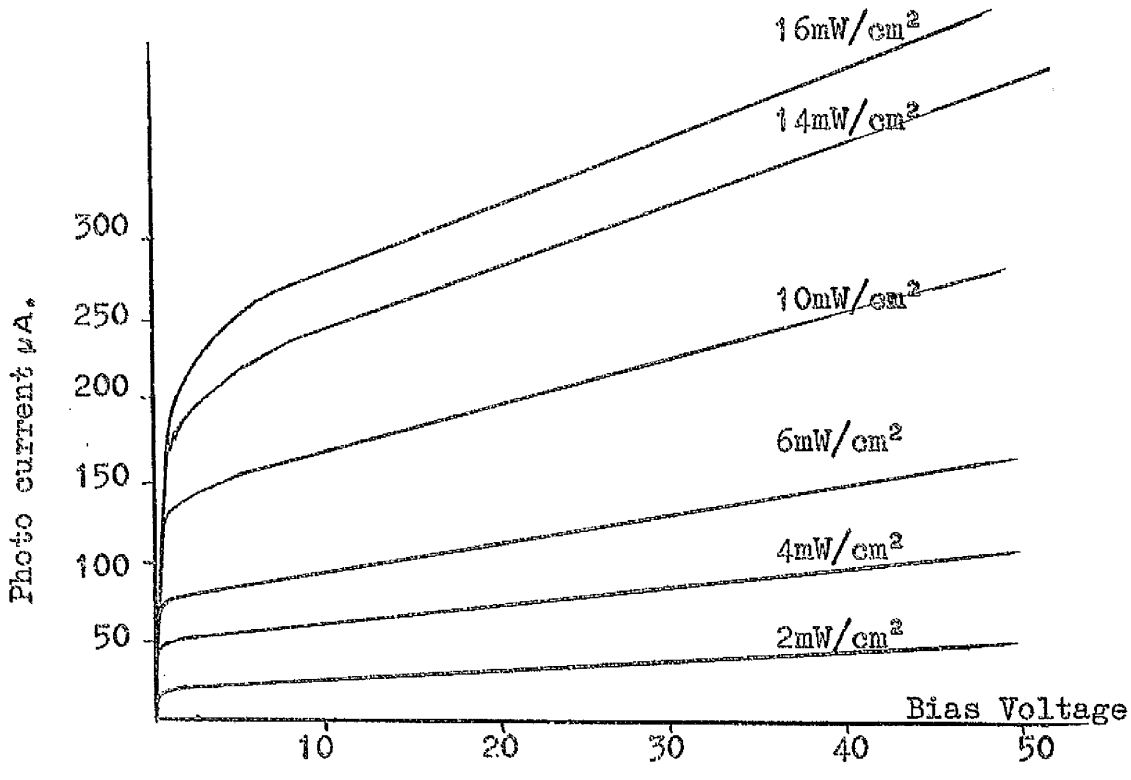

Figure 2.25. 1N2175 Characteristic

dynamic impedance possible is the impedance at zero light flux which is of the order of 100MΩ. It will be seen that above 10 volts bias the curves are perfectly linear. The diode spectral response is illustrated in figure 2.26 with the response of the Ga.As crystal lamp superimposed for comparison. The closeness of the spectral peaks indicates a good degree of spectral compatability. The dark current I_o is small and above an irradiance of $2mW/cm^2$ a linear relationship exists between the applied irradiance and the photo current. The sensitivity of the device is increased by the use of a focussing lens system which produces a directional characteristic as shown in figure 2.27.

2.3.3. Combined Characteristics.

The mechanical arrangement of the lamp detector combination is shown in figure 2.28. The XS321 crystal lamp is inserted at the end of a thick walled brass tube the inner surface of which is threaded and the IN 2175 duo diode is located in the drilled out centre of a threaded bolt. This configuration besides establishing a fixed positional relationship between lamp and detector offers three additional advantages.

(a) Full advantage is taken of the axial directional sensitivity of both devices.

(b) Fine focussing is possible to adjust for maximum diode sensitivity.

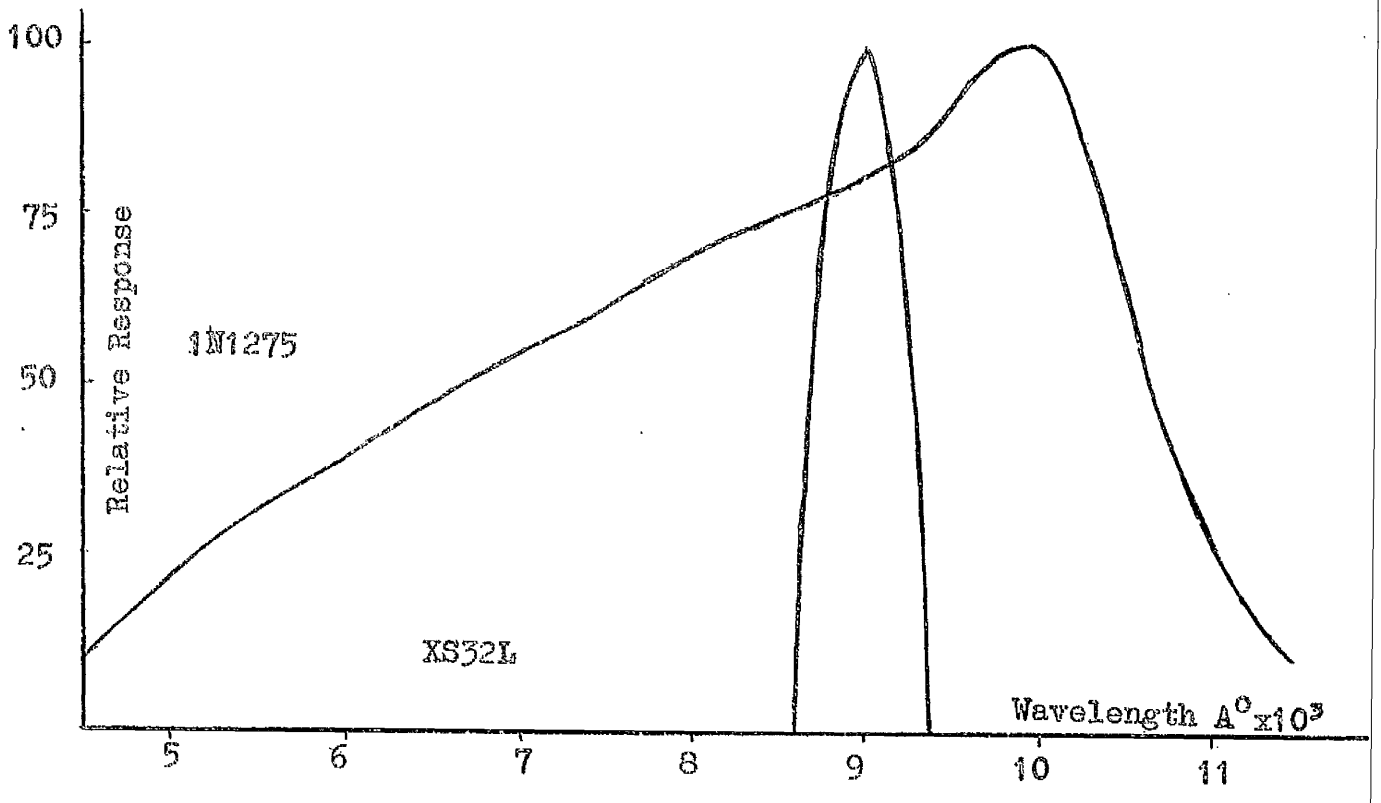

Figure 2.26. Spectral Compatability

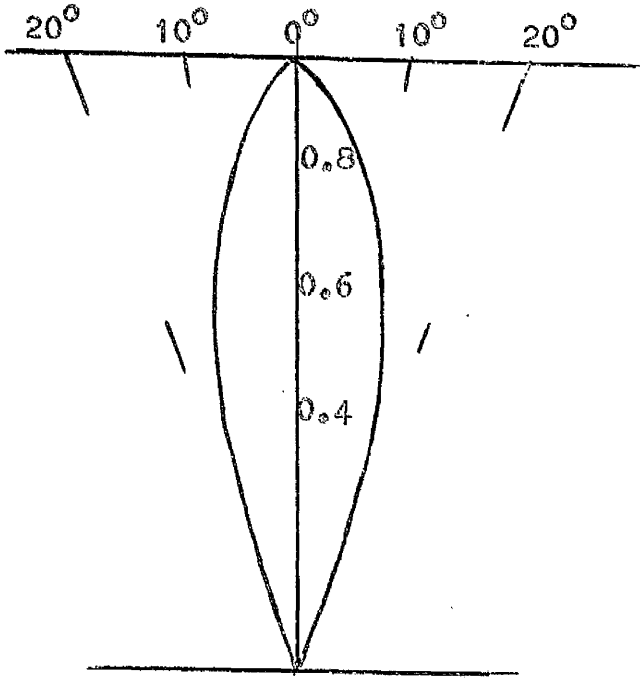

Figure 2.27. Directional Sensitivity of 1N1275.

(c) The thick brass surround, acting as an efficient heat sink, lowers the Ga.As junction temperature at any current rating and thus improves light output by increasing diode efficiency. The maximum power dissipation of both devices is also obviously improved.

The combined characteristics relating Ga.As input diode current with the voltage current relationship of the duo diode are shown in figure 2.29. The minimum duo diode dynamic impedance possible at full rated Ga As input diode current is of the order of 3MΩ which, from figure 2.25, represents an irradiance of about 2mW/cm^2. It is thus obvious that the maximum light power available from the XS321 restricts experimental investigation to a region of high duo diode dynamic impedance. When placed across the terminals of an operational amplifier the duo diode gave a linear output swing of ± 20 volts about a bias level of 30 volts, positive or negative bias being possible due to the symmetry of the junction structure.

2.3.4. The Control Circuit.

The object here was to develop a control circuit using the same design philosophy as the Luxistor system which would achieve a linear relationship between an incremental input voltage and an incremental output resistance value. As before when the linearising feed back loop is broken an integrator can perform the function of system memory and

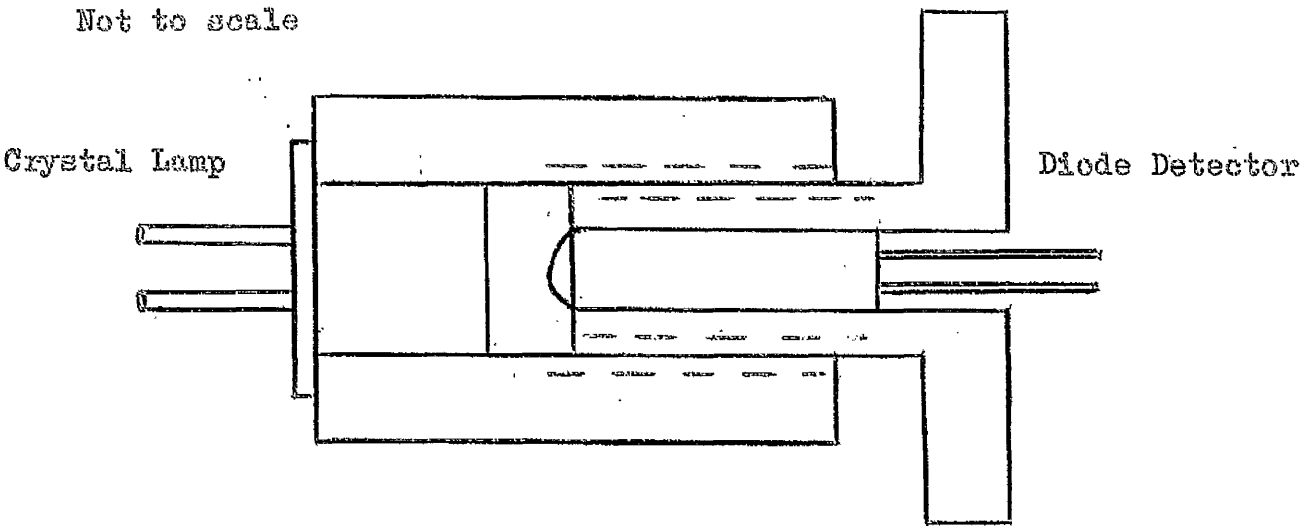

Lamp Detector Mechanical Layout.

Figure 2.28.

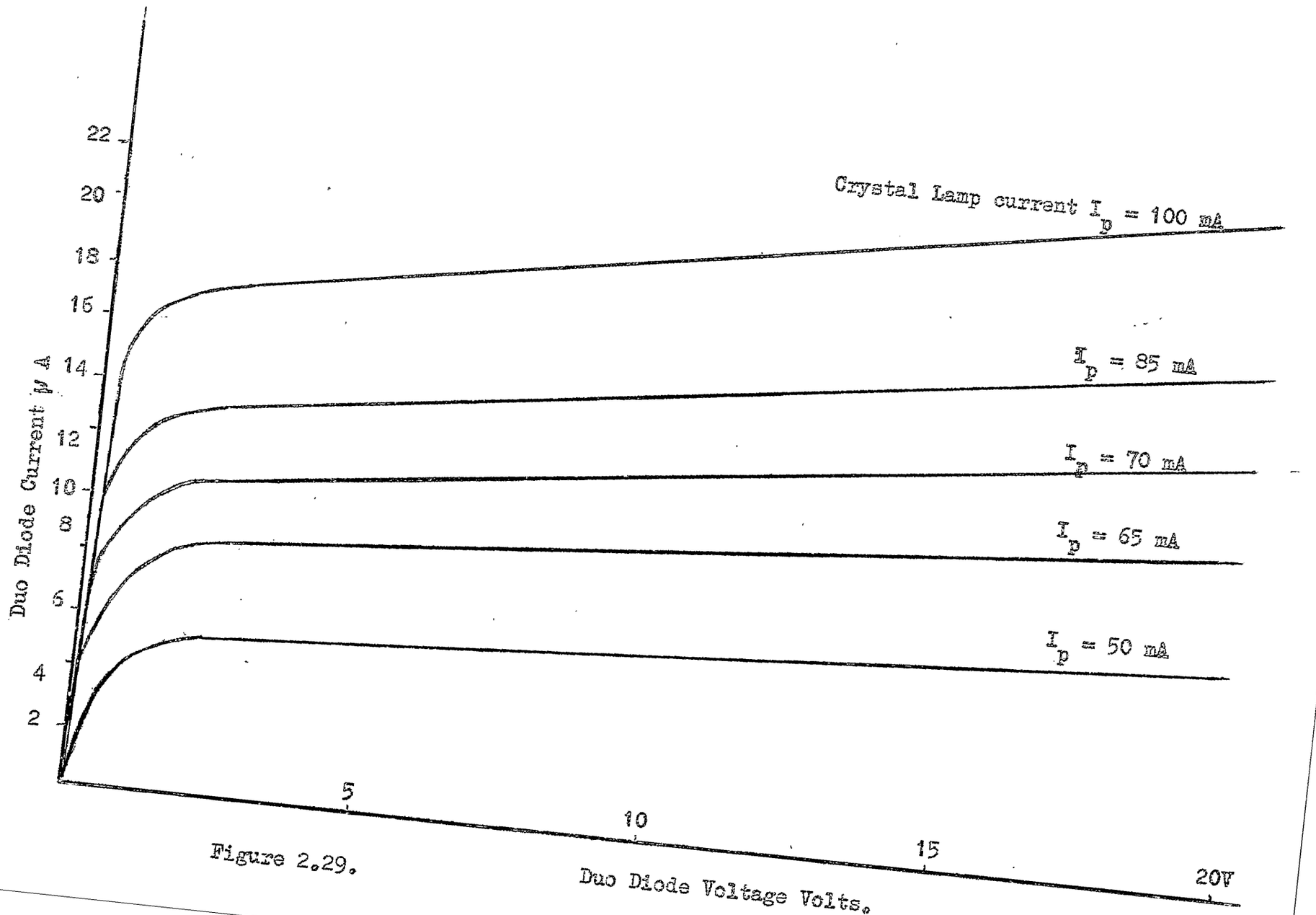
Crystal Lamp current I_p = 100 mA
I_p = 85 mA
I_p = 70 mA
I_p = 65 mA
I_p = 50 mA
Duo Diode Current μA
22
20
18
16
14
12
10
8
6
4
2
5
10
15
20V
Duo Diode Voltage Volts.

Figure 2.29.

the radiation link can achieve absolute electrical isolation between the resistive element and its controlling circuitry. Some circuit modifications will however be necessary due to the difference which exists between diode static and dynamic impedance.

In figure 2.12 a linear relationship is imposed between incremental input voltage and the incremental voltage across the resistive element which, for a constant current drive, establishes a linear change in resistor static value. For a device, such as a cadmium sulphide block, having equal static and dynamic resistance values a linear relationship is thus established between incremental input voltage and dynamic resistance value. To ensure correct operation of a diode as a linear incremental operational element it must be biassed into the linear regime where the effective operational resistance value is determined by the appropriate dynamic slope. Hence what is required now is a scheme to achieve a linear relationship between incremental input voltage and diode dynamic slope.

In figure 2.30 if δ represents the fractional change in the input bias voltage to the control circuit then the voltage change across the diode for a fixed current I must be δMK where M is the characteristic asymtotic point and K the quiescent diode voltage.

Voltage change across diode

$$= \delta MK$$

$$= \delta(MO + OK) = \delta MO + \delta OK$$

$$= \delta \times \text{constant} + \delta OK.$$

For a feedback system similar to that illustrated in figure 2.12. a fractional change δ in the input voltage results in a voltage change δ OK across the diode. If the voltage across the diode is now constrained to vary by an additional δMO volts where MO is a constant then the correct change in diode dynamic impedance is accomplished.

A possible schematic circuit is outlined in figure 2.31. where the resistance P is so scaled that for a fractional increase δ in the bias voltage the change in the voltage at point A in the circuit is

$$\delta \text{ OK } + \delta \text{MO}.$$

where OK is the quiescent voltage at A and MO the characteristic asymtotic voltage.

A practical circuit suitable for the implementation of the control scheme is illustrated in figure 2.32. where a fixed bias current is established in the 1N 2175 from an external current source. To avoid excessive loading feed back voltage from point A to the integrator input is accomplished via a T.I. 2N3820 source follower with an input impedance of approximately 150MΩ. The XS32L constitutes the load of a ZT 82 emitter follower which is current fed directly from the integrator. A current limiting 200Ω resistor is included in series with this diode to prevent excessive diode dissipation in the event of a circuit fault.

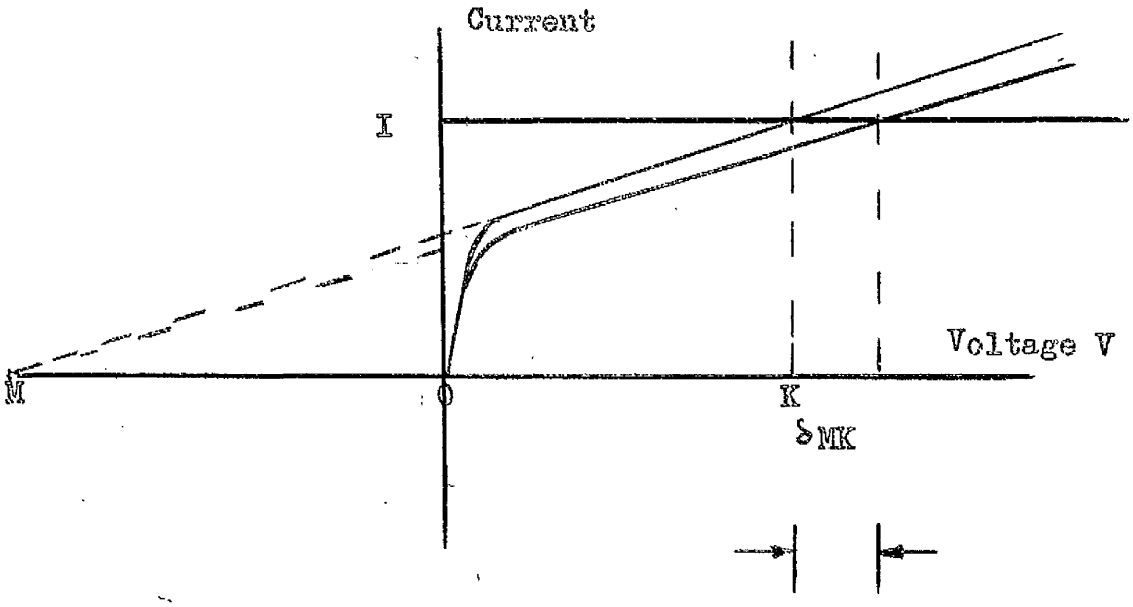

Figure 2.30.

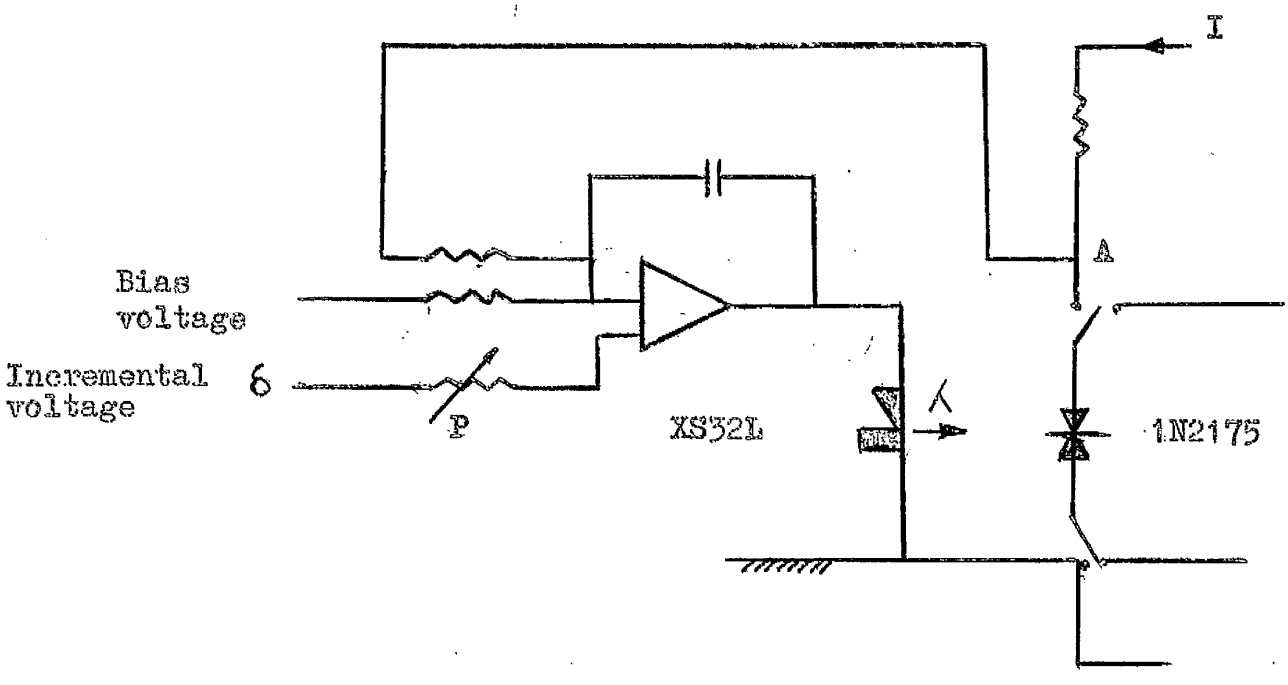

Schematic Circuit Diagram Figure 2.31

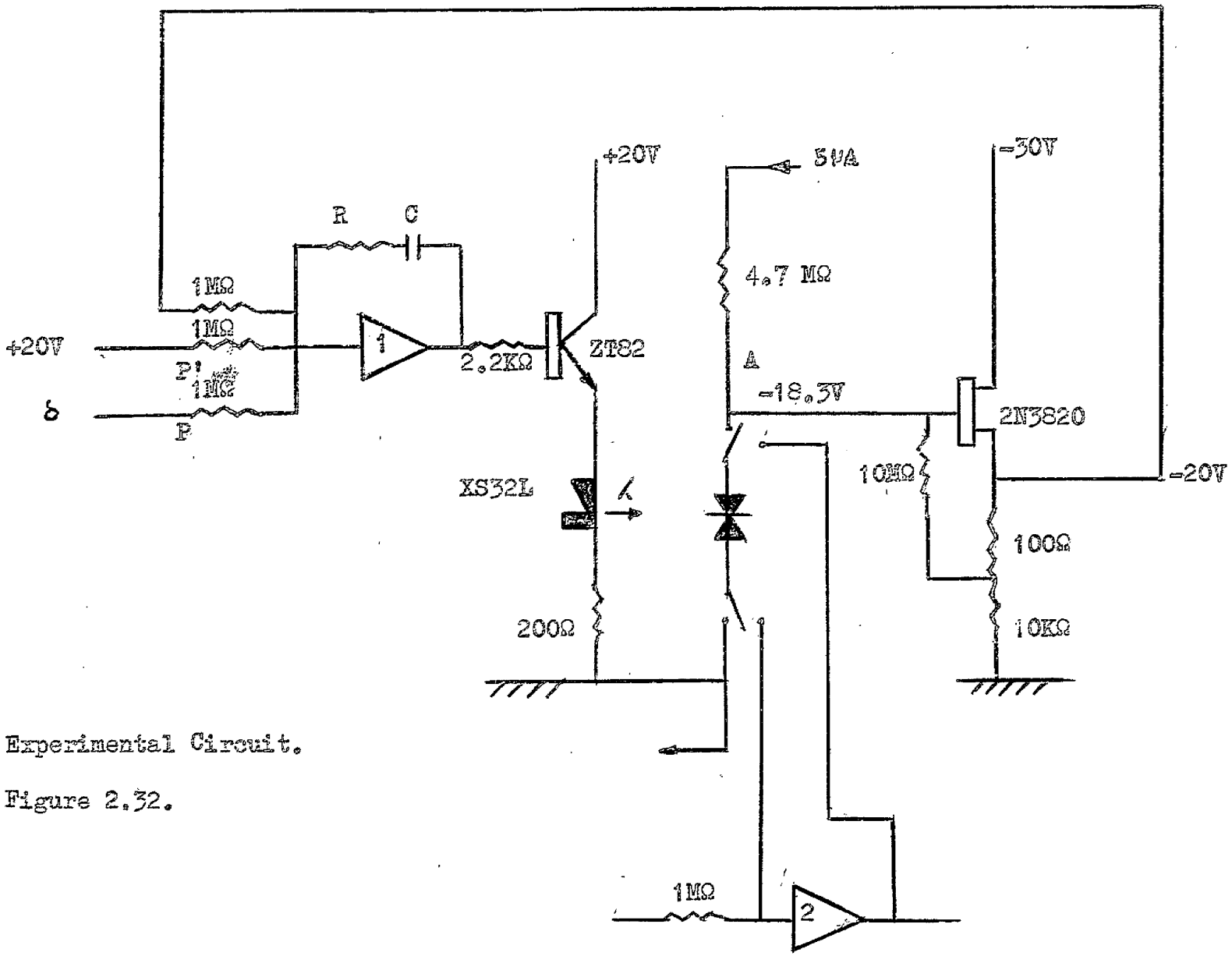

Experimental Circuit.

Figure 2.32.

As the exact magnitude of the asymtotic voltage at the working point is critical to the overall system accuracy its value is best determined from a closed loop linearity test on the system rather than from extrapolation of the combined characteristics which can only be approximate. Evaluation of the asymtotic voltage will enable the integrator resistor P to be correctly scaled.

2.3.5. Experimental Results.

The circuit bias voltage levels were set as shown in figure 2.32 where the P channel source follower has a positive offset voltage of 1.70 volts and a measured gain of 0.922. A constant current of 5μA was established in the duo diode and the resistor P was made equal to 1MΩ. The input voltage was varied in steps, and after each step change the diode was switched across operational amplifier 2. A series of points were then plotted relating the input and output voltage of amplifier 2 the feed back loop being briefly closed before each plot to compensate for integrator drift and re-establish the correct operating light flux. In this experiment capacitor C was fixed at 1μF to minimize integrator drift and R was 1MΩ. The dynamic impedance of the diode at each step change in incremental input voltage was obtained from the input output voltage plot of amplifier 2, and the relationship thus established between diode dynamic impedance and incremental input voltage is shown in figure 2.33. It will be seen that this relationship is

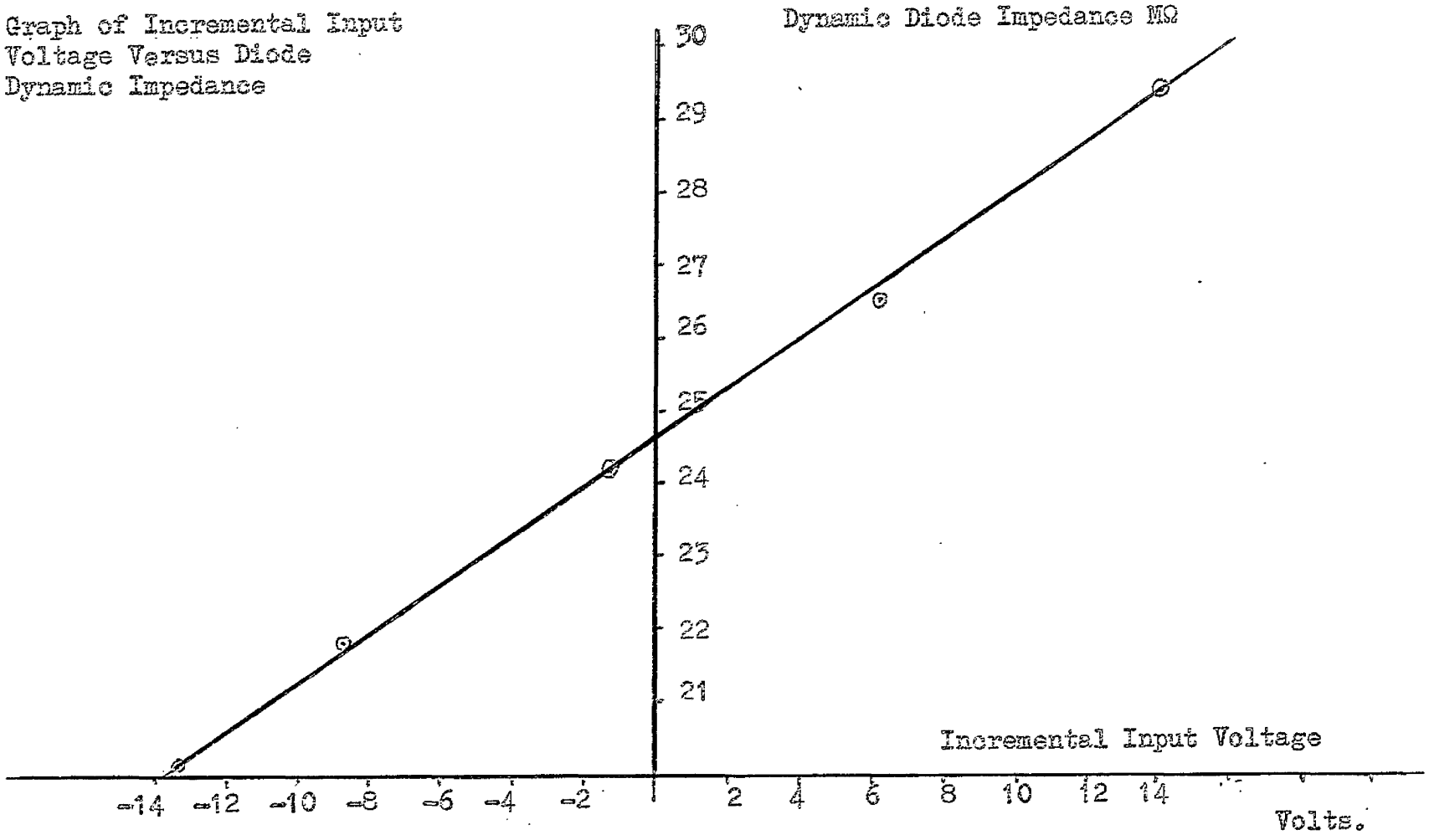
Graph of Incremental Input Voltage Versus Diode Dynamic Impedance
Dynamic Diode Impedance MΩ
30
29
28
27
26
25
24
23
22
21
Incremental Input Voltage
-14
-12
-10
-8
-6
-4
-2
2
4
6
8
10
12
14
Volts.

Figure 2.33.

quite linear with some slight scatter due to measurement errors inherent in the rather cumbersome derivation technique. The maximum scatter error is of the order of 1% and the actual circuit linearity is at least better than 0.5%.

From the graph of figure 2.33. and knowledge of the circuit bias levels and parameter values we can determine the value of the resistor P to establish a linear relationship between percentage incremental input voltage and percentage change in diode dynamic impedance.

From figure 2.33

% change in dynamic impedance equals 18.7% for an input voltage increment of 13.6 volts. Corresponding change in diode voltage is

$$\frac{13.6}{0.922} = 14.75 \text{ volts.}$$

$$\therefore \frac{18.3 \times 18.7}{100} + \frac{18.7}{100} \times OM = 14.75 \text{ volts}$$

$$3.42 + 0.187\ OM = 14.75 \text{ volts}$$

where the diode voltage is 18.3 volts at an input bias level of 20 volts

$$\therefore OM = 60.6 \text{ volts.}$$

If the resistor P' in figure 2.32 is made equal to 0.915 MΩ then the input bias voltage can be considered as 18.3 volts rather than 20 volts. An increase of 18.7% in this bias level represents an incremental signal of 3.42 volts.

Thus

$$3.42/P = \left\{ 3.42 + \frac{60.6 \times 18.7}{100} \right\} \times 0.922$$

$$\therefore \quad P = 0.398$$

Thus to achieve a linear relationship with unity slope between percentage incremental input voltage and percentage change in diode dynamic impedance resistor P' must be so scaled to achieve equality between diode and input bias voltages and, for this particular range, the resistor P must be made equal to 0.398 MΩ.

The light output power of the Ga.As diode ultimately sets a lower limit to the duo diode dynamic impedance available and the voltage rating of the duo diode itself will set a limit on the possible upper impedance level. Assuming that the minimum duo diode voltage is one volt and that the maximum allowable diode voltage is 50 volts, then for the particular bias level indicated in figure 2.32 the maximum theoretical diode dynamic impedance swing about a quiescent level of 24.6 MΩ is -22% to + 62.7%, a total impedance variation of 84.7%.

To achieve a fast response the integrator capacitor value must be of the order of pico farads and figure 2.34 shows the effect of varying capacitor value on the circuit transient behaviour. A step change of 5 volts was applied to the circuit which was biassed at 20 volts and, in the absence of any proportional resistance, an oscillatory

response was obtained. The magnitude of the overshoot decreased with increasing capacitor value and the settling time was of the order of 700 μ seconds. The addition of a low value proportional resistor greatly reduced both overshoot and settling time for any capacitor value and a minimum settling time of 160 μ seconds was obtained with R equal to 300KΩ and a capacitance value of 200 pico farads. This response is shown in curve (b) of figure 2.35 where the maximum overshoot is 8%. The settling time here compares very favourably with the settling time achieved for the Luxistor (curve (e) of figure 2.16) and represents a reduction of settling time by a factor of 1500.

Figure 2.35 illustrates the response of the circuit to a negative step demand in resistance value. Due to the relatively long photo current fall time of the 1N2175 the settling time of the system to a positive step demand in resistance value is about 50% longer than the time indicated by curve (b) of figure 2.35.

The closed loop frequency response of the complete circuit is shown in figure 2.36 and it will be seen that for the values of R and C indicated the system has a closed loop band width of 2.4 Kc/s figure 2.36 and a roll off slope of 8 dB per octave. The indicated damping factor is of the order of 0.7

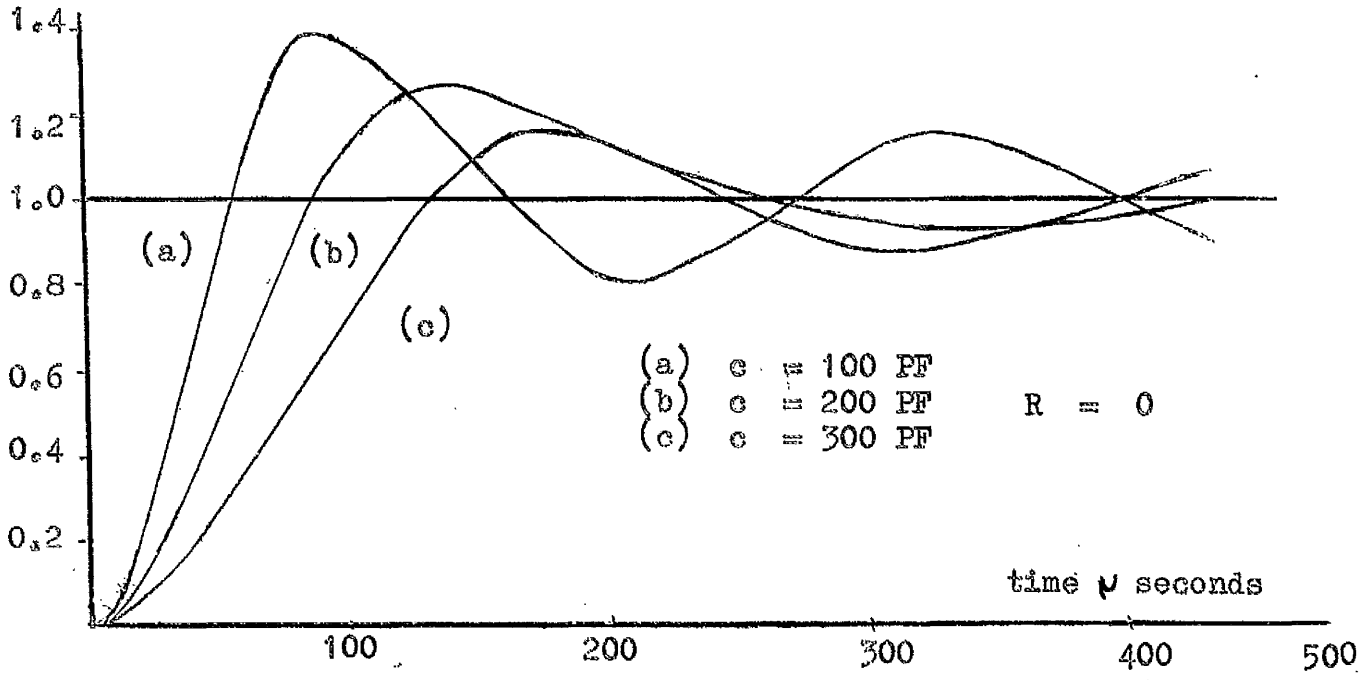

Circuit Transient Response Figure 2.34.

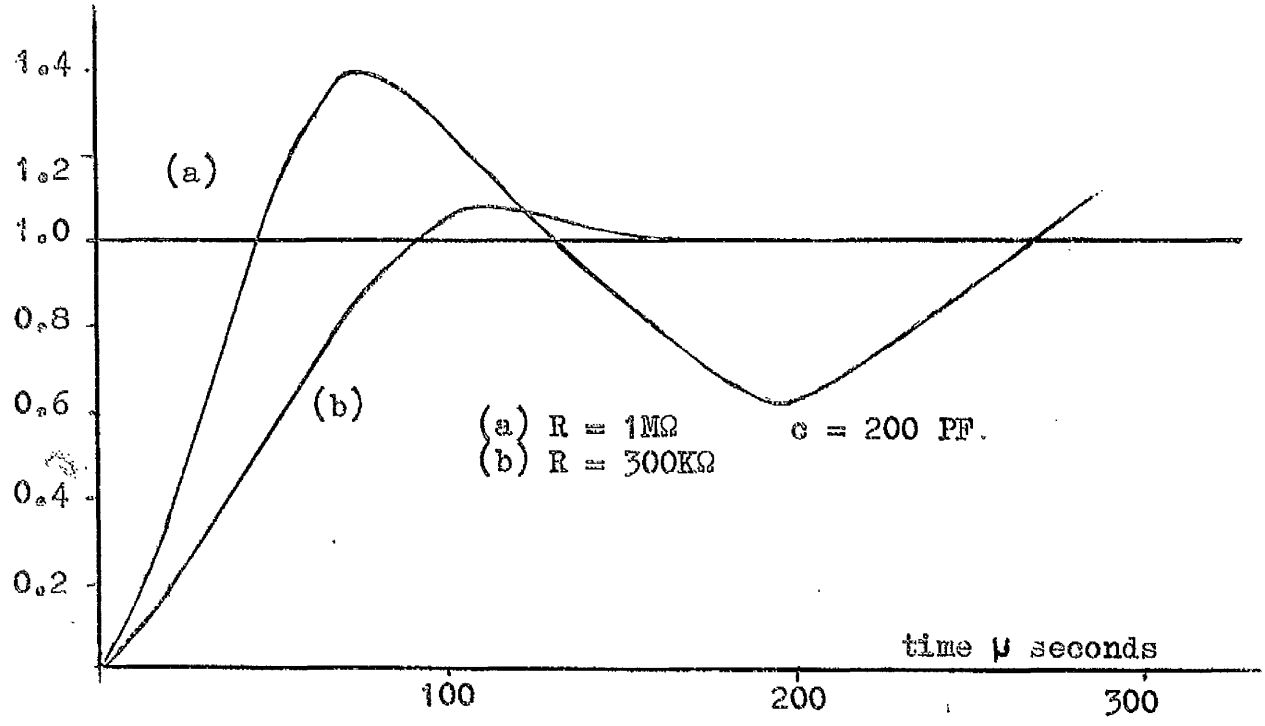

Circuit Transient Response Figure 2.35.

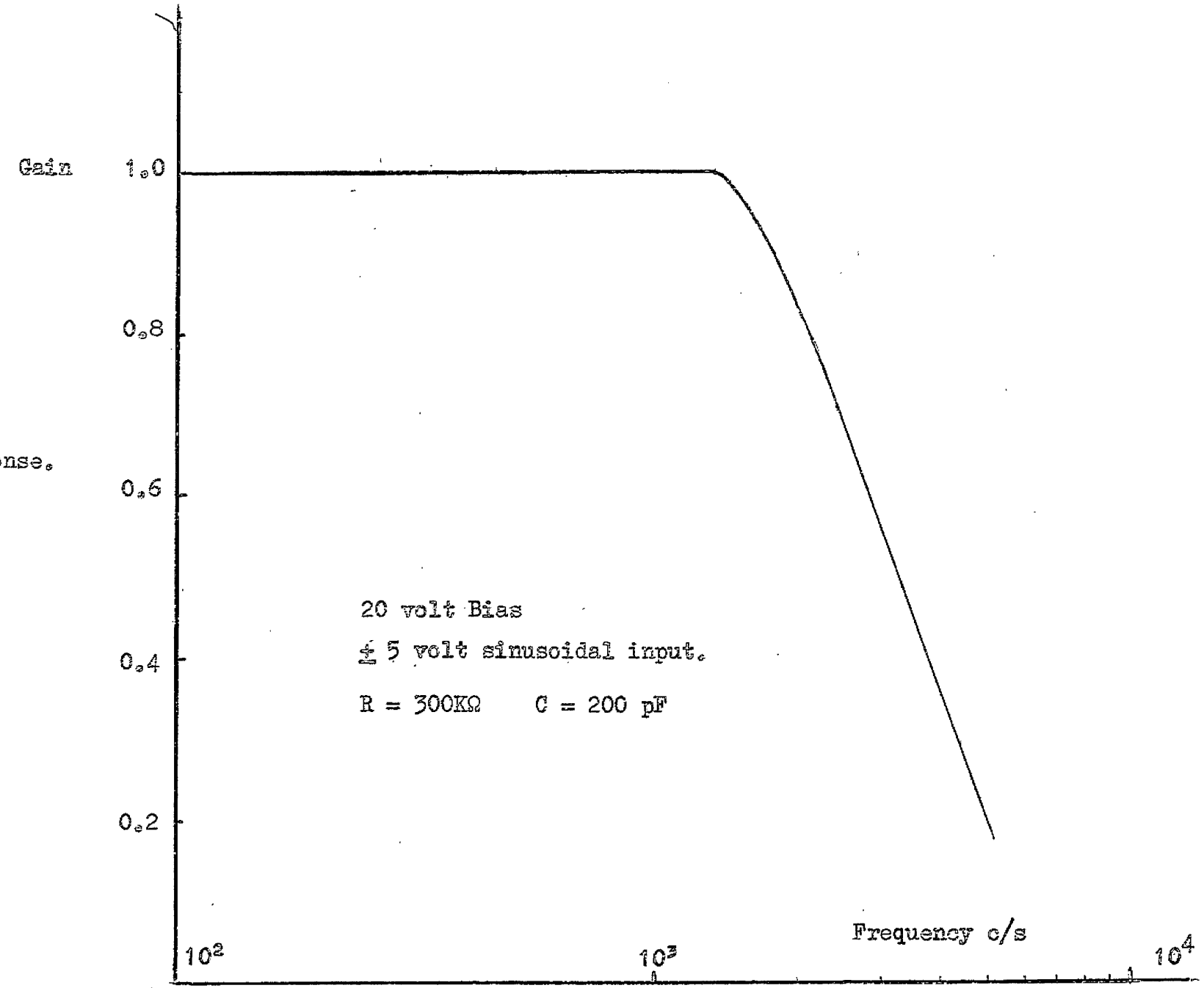

Closed Loop
Frequency Response.

Figure 2.36.

2.3.6. Bias Considerations.

For correct performance as an operational element the quiescent operating point of the duo diode must be biassed into the linear regime, a bias voltage of, say, 30 volts allowing a linear excursion of ± 20 volts. The bias voltage, which for the 1N2175 can be positive or negative, is easily removed by subsequent operational techniques. Variation of the diode dynamic impedance also varies the diode static impedance and hence, for a given bias level, compensation must be provided in the operational circuit which removes the bias voltage. A suitable circuit utilizing a second adaptive element which is operated in parallel with the first is shown in figure 2.37 where E_B represents the bias voltage applied to the duo diode when it is switched as an operational element. The two adaptive elements are operated from the same voltage source.

2.3.7. Summary.

By the utilization of a novel lamp-detector combination the performance of the voltage controlled variable resistance circuit has been improved, with a linear adaptive mechanism being produced which has a settling time of 160 μ seconds and a band width of 2.4 Kilocycles. With this circuit the variation of adaptive model lag parameters can be achieved in a fraction of a millisecond compared with the several seconds required by conventional techniques. Provided that the

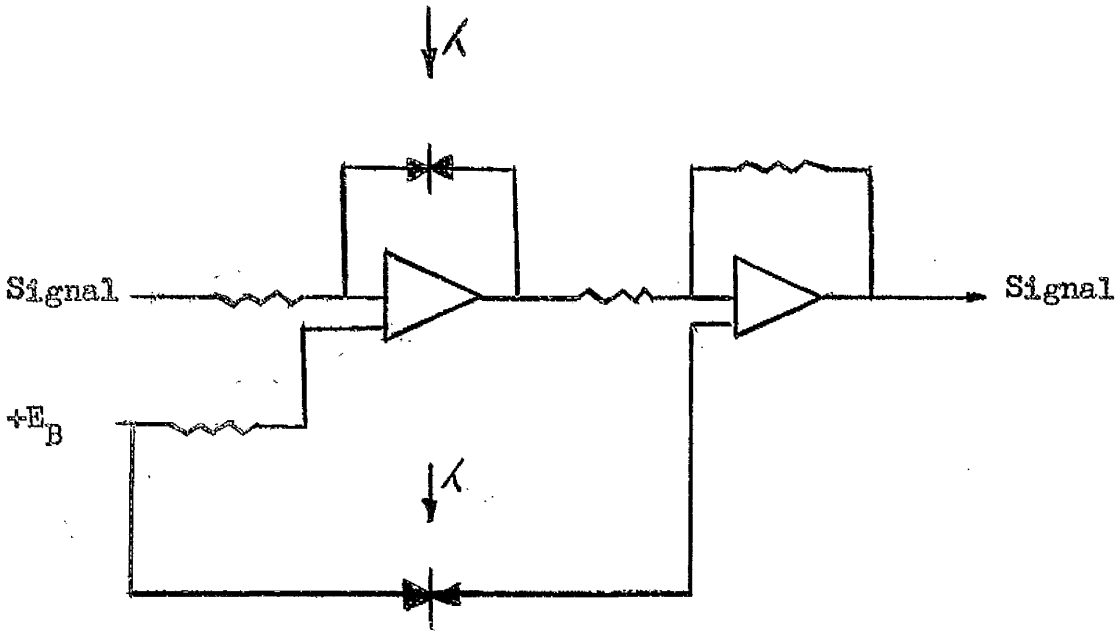

Diode Bias Voltage Removal

Figure 2.37.

parameter variation is less than one order the adaptive mechamism can also be used for adjusting adaptive model gain parameters. It has a bandwidth which is compatible with the best available electronic multipliers and, besides constructional simplicity it has the additional property of being able to adjust both types of parameter value.

Due to the low light output power of the XS32L crystal lamp the present circuit operates in a region of high diode dynamic impedance and for some applications this could be inconvenient. Improvement here will be sought in two directions. Firstly in the application of more powerful crystal lamps and secondly in the utilization of more sensitive detector diodes such as the photo avalanche diode (18).

As with the Luxistor circuit future development work will also be devoted to producing a completely solid state adaptive mechamism combining integrated operational amplifiers and field effect transistor switching circuits, the final unit being completely compatible with solid state hybrid computing systems.

CHAPTER 3

PARAMETER ESTIMATION

3.1. Introduction.

Plant identification is important in its own right as a fundamental part of overall control system design. Identification in adaptive control, however, differs from the normal problem found in control systems because of the importance of minimizing the time required to complete the determination of significant process characteristics. Complete identification without a priori knowledge can normally be accomplished by cross correlation techniques (1), (2) though success here is only possible for a stationary plant or, at most, for a plant with slowly varying parameters.

Some a priori knowledge of plant structure is nearly always available and although no general method of approach has yet been formulated three distinct techniques of utilizing such knowledge have been advanced by Kalman (3), Margolis (4) and Corbin (5). Kalman's method which uses sampled values of the plant input and output variables together with a plant model requires digital computer facilities and is relevant to sampled data control systems. The philosophy underlying the learning model technique of Margolis is closely akin to the approach of Lefkowitz (6) on which the control strategy of this thesis is based and Corbin's method is used directly in the latter section of this chapter.

This study is limited to the investigation of systems in which the dominant plant tranfer function is of the form.

$$G(s) \doteq \frac{K_c \, e^{-Ts}}{1 + sT_m}$$

where T is assumed in variant and either one or both the remaining parameters time variant. If we assume that the input signal to the system is a step function, plant identification in the former case is comparatively easy and can be performed by an analogue computer configuration in the method of Corbin. In the latter case however the presence of two unknowns renders on line identification less tractable, and recourse to digital computer solution has been suggested by several authors (6), (7). In order to maintain an essential control system simplicity which is compatible with the form of plant model chosen, it is the intention here to realize parameter estimation with a relatively simple hybrid computing system.

The majority of this chapter will thus be devoted to describing a parameter estimation scheme which has been developed to perform the identification of plant with two unknowns. Finally we will deal briefly with the identification problem posed by the presence of only one unknown in the transfer function.

As the general nature of this work will be related ultimately to a simple boiler model some reference will be found below to boiler transfer functions and time constants, a full description of which is to be found in Chapter 4.

3.2. Parameter estimation in the presence of two unknowns.

If the plant in figure 3.1. is subjected to a step input of magnitude C_f the time function of the output after a time interval T is of the form

$$V(t) = K_c C_f (1 - e^{-t/T_m})$$
$$= V_m (1 - e^{-t/T_m}). \qquad \ldots\ldots\ldots\ldots\ldots\ldots (1)$$

where $V_m = K_c C_f$

The problem is thus to obtain the on line solution of V_m and T_m from the measured values of $V(t)$. Arranging the analysis in a form suitable for analogue computer solution we have

$$V(t) = V_m (1 - e^{-t/T_m}).$$

$$\frac{dV(t)}{dt} = \frac{V_m}{T_m} e^{-t/T_m}.$$

$$\left.\frac{dV(t)}{dt}\right|_{t=t_1} = \frac{V_m}{T_m} e^{-t_1/T_m} = \delta_1$$

$$\left.\frac{dV(t)}{dt}\right|_{t=t_2} = \frac{V_m}{T_m} e^{-t_2/T_m} = \delta_2 \qquad \ldots\ldots\ldots(2)$$

$$\frac{\delta_1}{\delta_2} = \frac{e^{-t_1/T_m}}{e^{-t_2/T_m}}$$

$$\text{Log} \frac{\delta_1}{\delta_2} = \text{Log} \frac{e^{-t_1/T_m}}{e^{-t_2/T_m}} = \frac{t_2 - t_1}{T_m} = \frac{t_d}{T_m}$$

where $t_d = t_2 - t_1$

so $$\text{Log} \frac{\delta_1}{\delta_2} = \frac{t_d}{T_m} \qquad \ldots\ldots\ldots(3)$$

or in general, we have recursive relation.

$$\text{Log} \frac{\delta n}{\delta n+1} = \frac{t_d}{T_m} \qquad \ldots\ldots\ldots(4)$$

Hence

$$T_m = t_d \text{ Log} \frac{\delta_{n+1}}{\delta_n} \qquad \ldots\ldots\ldots(5)$$

From (2)

$$V_m = T_m \delta_1 . e^{+t_1/T_m}$$

$$\text{Log } V_m = \text{Log } T_m + \text{Log } \delta_1 + t_1/T_m$$

$$V_m = \text{Anti Log } [\text{Log } T_m + \text{Log} \delta_1 + t_1/T_m] \qquad \ldots\ldots\ldots(6)$$

Though solutions of equations (3) and (6) will yield the correct values of V_m and T_m both equations involve a derivative of the time function. Differentiation even at low noise levels can induce large errors and it is essential that a method of obtaining the various slopes of the function V(t) without direct analogue differentiation be found.

One such method of approach is shown in Figure 3.2. The slope of the function at t_m is equal to

$$\frac{V_2 - V_1}{t_2 - t_1}$$

where $V_1 \Omega \dfrac{\int_{t_{10}}^{t_{11}} V(t)\, dt}{t_{11} - t_{10}}$ and $V_2 \Omega \dfrac{\int_{t_{20}}^{t_{21}} V(t)\, dt}{t_{21} - t_{20}}$

This method has the advantage of using integration rather than differentiation to obtain slope values and thus tends to suppress rather than accentuate noise errors.

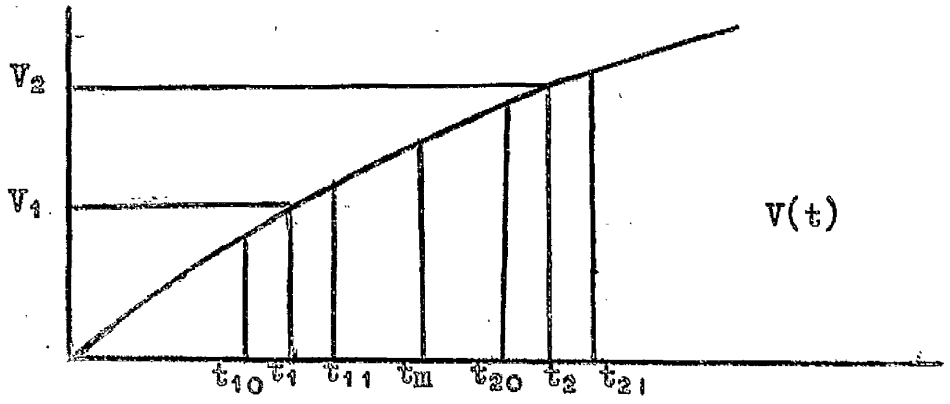

Figure 3.2. Slope Estimation.

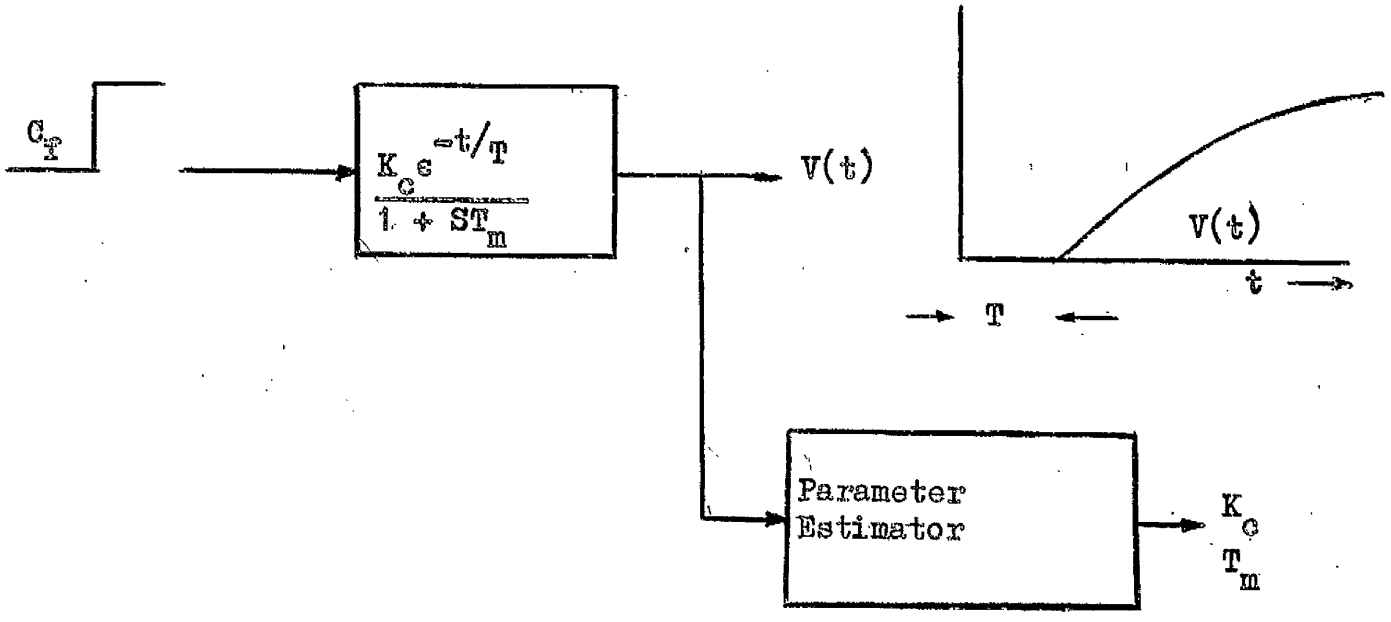

Figure 3.1. Parameter Estimation

The validity of the approximations involved in the functions above will be discussed later.

Two further conditions were thought necessary for satisfactory operation. Firstly that any solution be made on a repetitive basis to reduce the overall effect of any one spurious reading and secondly that the computer configuration be such as to render any spurious reading self cancelling when the repetitive readings are averaged. An excellent introduction to Hybrid computing techniques has been given by Paul (8) and Korn (9).

3.2.1. Computer Configurations for the determination of T_m.

A suitable computer configuration for the repetitive solution of equation (3) is shown in Figure 3.3. The operation of the various amplifiers is controlled by relays activated by external transistor logic and the method of computation is illustrated in Figure 3.4. The value of the function V(t) can be estimated at times $t_0, t_1, \ldots t_n$ by integrating the function for a finite interval of time t_s at times $t_{10}, t_{20} \cdots t_{no}$. The slope of the function at times $t_1, \cdots t_n$ can then be estimated as

$$\delta_1 = \frac{V_2 - V_0}{t_2 - t_0} \; ; \qquad \delta_2 = \frac{V_3 - V_1}{t_3 - t_1} \; ; \qquad \delta_n = \frac{V_{n+1} - V_{n-1}}{t_{n+1} - t_{n-1}}$$

For a repetitive solution we require the formation of the function $\frac{\delta_r}{\delta_{r+1}}$ with r taking the sequential values 1 to n. For any one value of $\frac{\delta_r}{\delta_{r+1}}$ four values of the function V(t) are required and hence a minimum number of four integrators is necessary in the computer configuration.

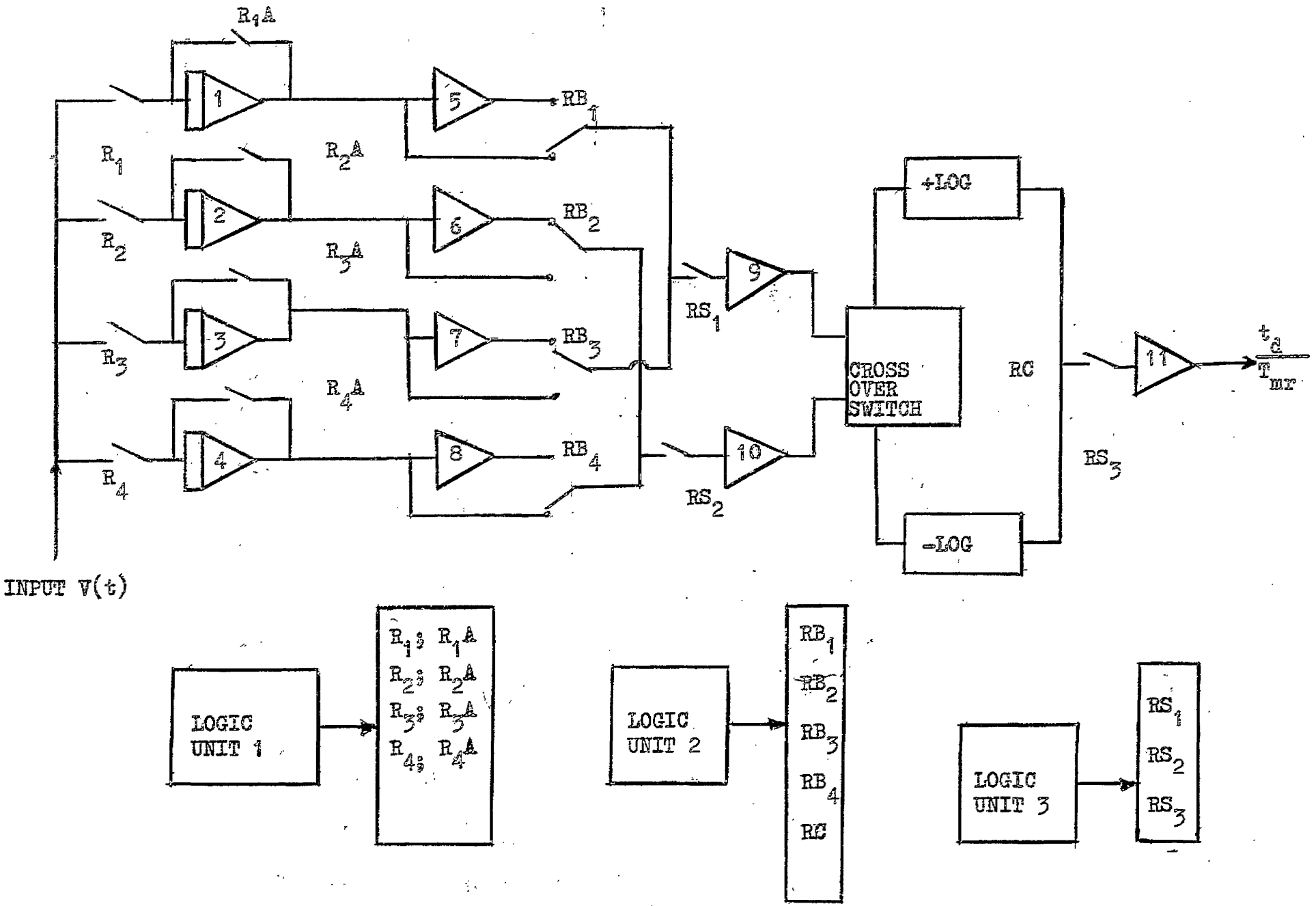

Figure 3.3. Generation of t_d/T_{mr}

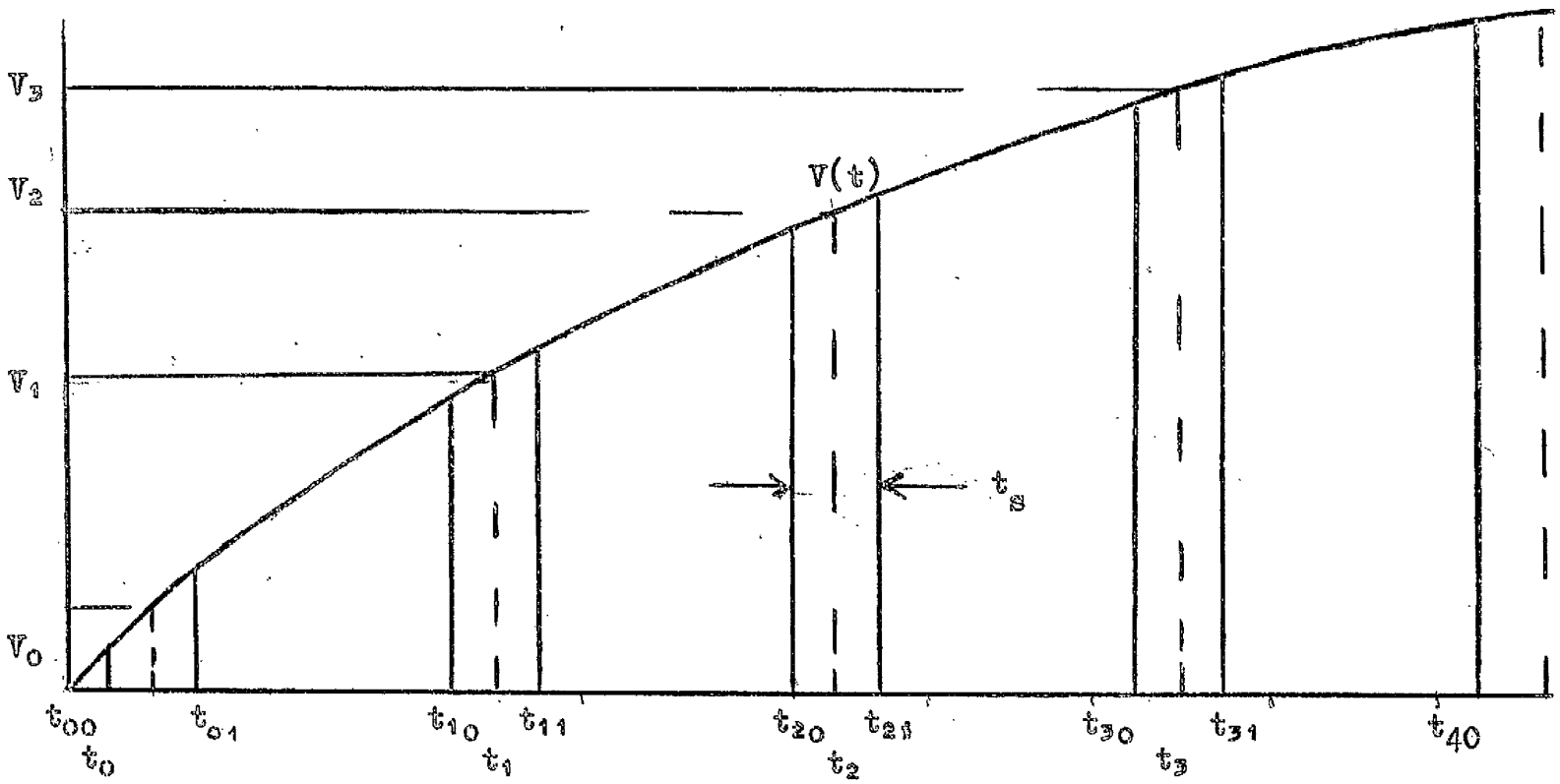

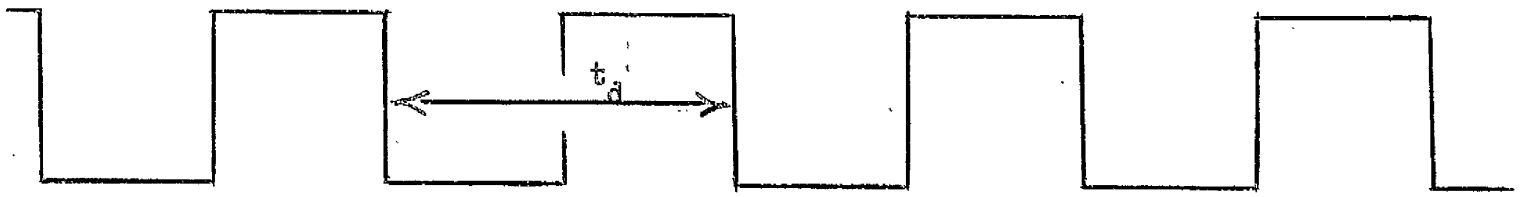

Master Oscillator

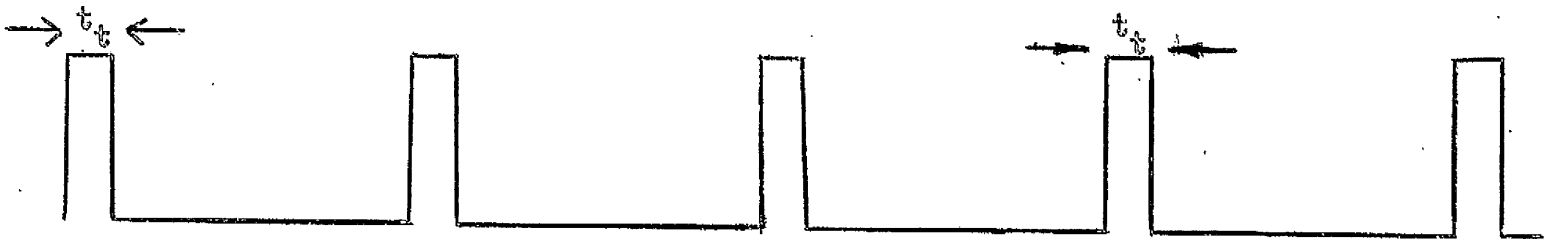

Reset Relay R_A

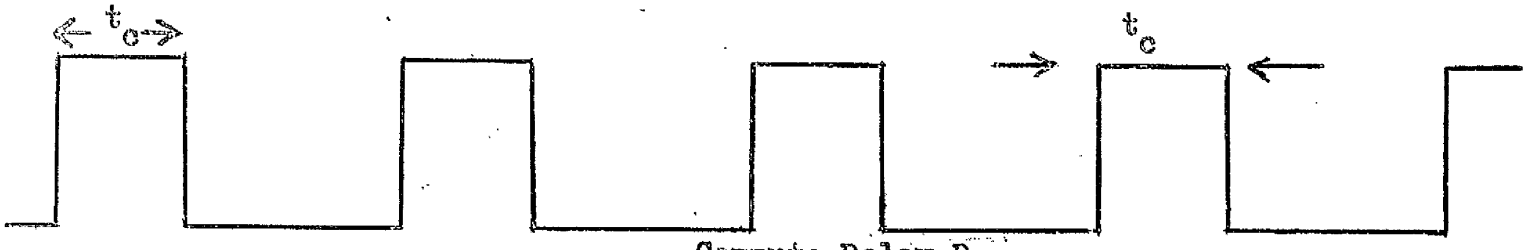

Compute Relay R

Figure 3.4.

A square wave from a master oscillator is fed to the transistor logic unit 1 Figure 3.5 where the first negative going edge opens AND gate AG1 and triggers monostables MNA1 and MNB1 whose outputs close relays R1 and R1A for periods t_c and t_t respectively. Hence the computation time is given by

$$t_s = t_c - t_t$$

The negative going edge which triggers the monostables also triggers the bistable BS1, which changes state thereby closing AG1 again, and the bistable BS2 which on changing state so alters the condition of AND gate AG2 that the arrival of the next negative going edge from the master oscillator opens this gate, triggering monostables MNA2, MNB2 and bistables BS2 and BS3.

AND gates AG3 and AG4 are now opened in sequence, the output of the latter triggering BS1 thus allowing AG1 to open on the arrival of the next negative going edge from the master oscillator and the sequence repeats.

After a time t_c from the first opening of AG4, four voltages V_0, V_1, V_2 and V_3 are established on integrators 1, 2, 3 and 4 respectively and the first solution of equation (3) is possible.

At a period of time t_d later amplifier 1 has completed the computation of V_4 and a second solution is now possible with subsequent solutions being available at intervals of t_d seconds.

While logic unit 1 controls the integrators to obtain sequential values of the function V(t) at times, t_1, t_2 ---- etc. logic unit 2

PARAMETER ESTIMATION
LOGIC UNIT 1

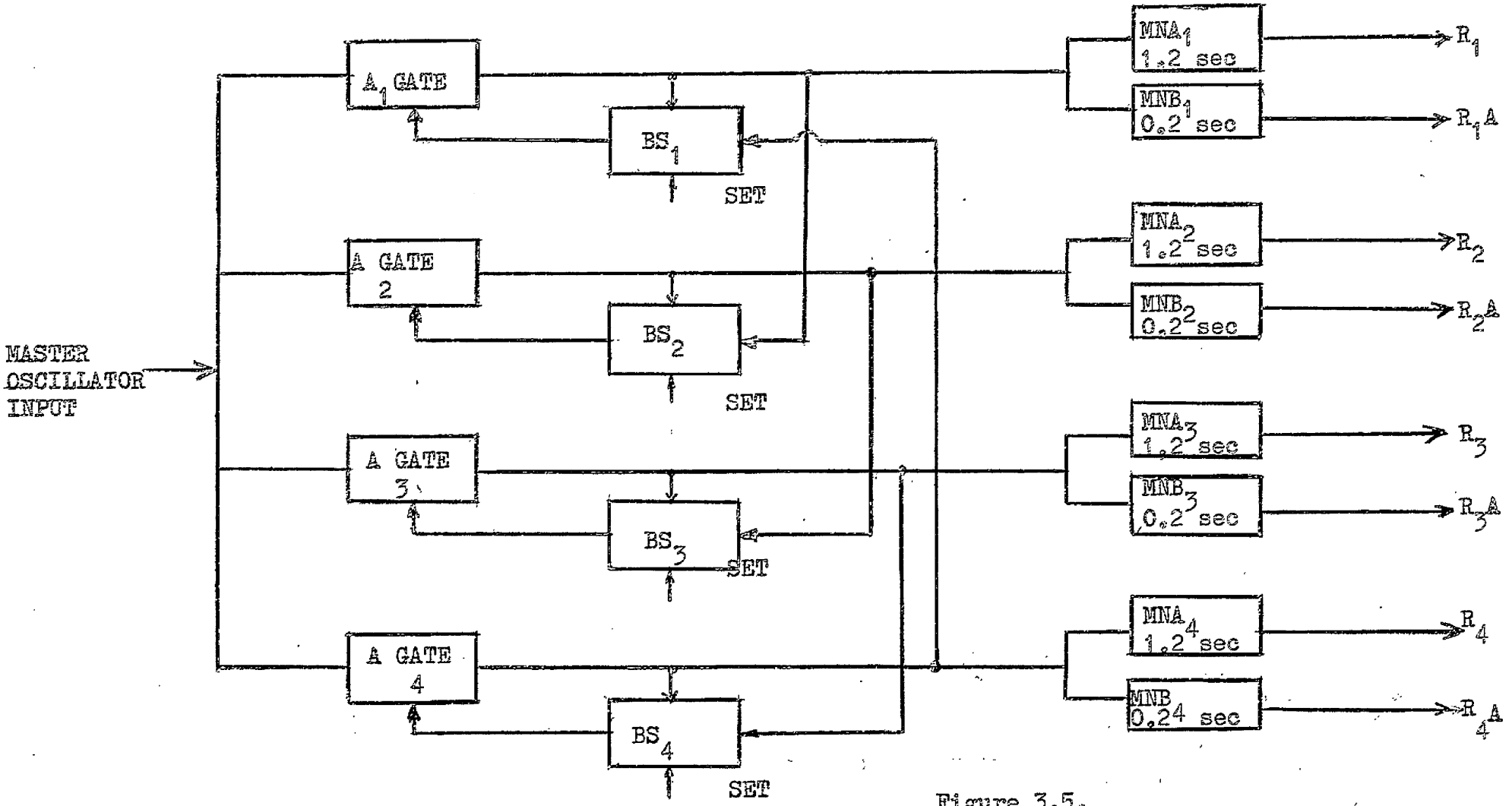

Figure 3.5.

processes these values to generate the appropriate function $\frac{\delta_r}{\delta_{r+1}}$ as shown below.

Integrator 1	V_0	V_4	V_4	V_4	V_4
Integrator 2	V_1	V_1	V_5	V_5	V_5
Integrator 3	V_2	V_2	V_2	V_6	V_6
Integrator 4	V_3	V_3	V_3	V_3	V_7

giving $\frac{\delta_r}{\delta_{r+1}} = \frac{V_2-V_0}{V_3-V_1}\ ;\ \frac{V_3-V_1}{V_4-V_2}\ ;\ \frac{V_4-V_2}{V_5-V_3}$ .....

It will be seen that the outputs of integrators 1 and 3 are always associated as are the outputs of integrators 2 and 4. Hence the former are summed by amplifier 9 and the latter by amplifier 10. For a function of the form

$$V(t) = V_m(1-\epsilon^{-t/T_m})$$

$V(t_{r+1}) > V(t_r)$ and thus to maintain the sign of the function $\frac{\delta_r}{\delta_{r+1}}$ constant the signs of the output voltages of the integrators must be adjusted appropriately.

Integrator 1	+	+	-	-	+
Integrator 2	-	+	+	-	-
Integrator 3	-	-	+	+	-
Integrator 4	+	-	-	+	+

It will be seen with this sign sequence that the numerator will always be positive (after summing) and the denominator always negative resulting in a constant sign of the output function $\text{Log}\frac{\delta_r}{\delta_{r+1}}$ as $\delta_r > \delta_{r+1}$.

Sign control of the integrator output voltages is exercised by relays RB1, RB2, RB3 and RB4 acting in conjunction with amplifiers 5, 6, 7 and 8 respectively. Correct signal direction to the + log unit and the - log unit is performed by the double change-over relay RC.

The RB set of relays and RC are controlled by logic unit 2. (Figure 3.6) which consists of three bistables and only three relay trigger circuits as it is possible to pair relays RB1 and RB3 and relays RB2 and RB4. The bistable BS6 is operated by a positive going edge and bistable BS7 by a negative going edge, both units being triggered directly from bistable BS5. It is assumed that the relay trigger circuits are activated by positive going edges from the bistable outputs. The change-over relay RC is operated directly from bistable B.S.5. The initial set conditions for the bistables are shown in Figure 3.6. and the initial positions of the relay contacts in Figure 3.7.

The operation of the reset relays RA causes momentary overload of the amplifiers 9, 10 and 11 until new steady voltages are established on the integrators. Relays RS1, RS2 and RS3 are included in the configurations to isolate these amplifiers during transient conditions and thus ensure satisfactory operation of the computer. These relays are controlled by logic unit 3 Figure 3.8.

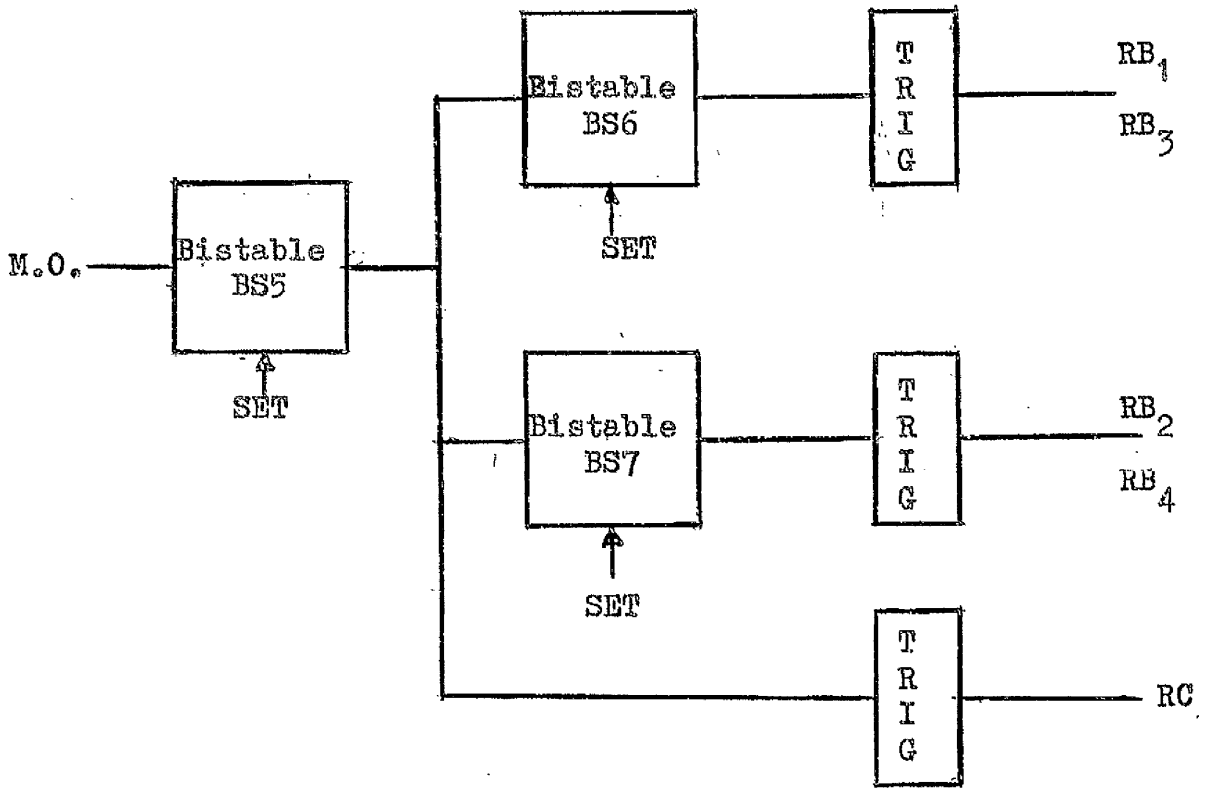

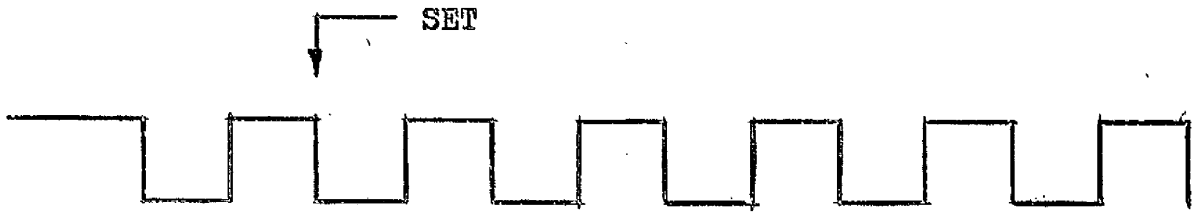

Master Oscillator Signal

Output of Bistable No. 5.

Output of Bistable No. 6

Output of Bistable No. 7

Figure 3.6. Logic Unit No. 2.

Initially AND gate AG6 is held closed and the trigger circuit inactivated leaving RS1, RS2 and RS3 open circuited. The first output from AG4 opens AG5 triggering bistable BS8 the output of which again closes AG5 enabling BS8 to remain in this new state for the duration of the system operation.

AND gate AG6 can now open and the relays close after a period of time equal to the duration of the output pulse from monostable M.N C which is of sufficient length to allow Integrator 4 to complete its computation.

Subsequent negative going edges from the master oscillator again isolate the amplifiers for the required period of time and satisfactory computer operation is thus possible. RS3 was found necessary to eliminate high voltage spikes on the output voltage level caused by a finite difference in switching times between RS1 and RS2.

3.2.2. Computer Configuration for the determination of V_m.

Rearranging equation (6) for repetitive solution we have

$$V_{mr} = \text{ANTILOG} \left\{ \log \frac{V_{r+1}-V_{r-1}}{2t_d} + \log T_{mr} + \frac{t_r}{T_{mr}} \right\}$$

$$= \text{ANTILOG} \left\{ \log (V_{r+1}-V_{r-1}) - \log \frac{2t_d}{T_{mr}} + \frac{t_r}{T_{mr}} \right\} \qquad (7)$$

where t_r is the time interval between t=0 and the mid point of the rth sampling period and T_{mr} is the value of T_m which has been derived from

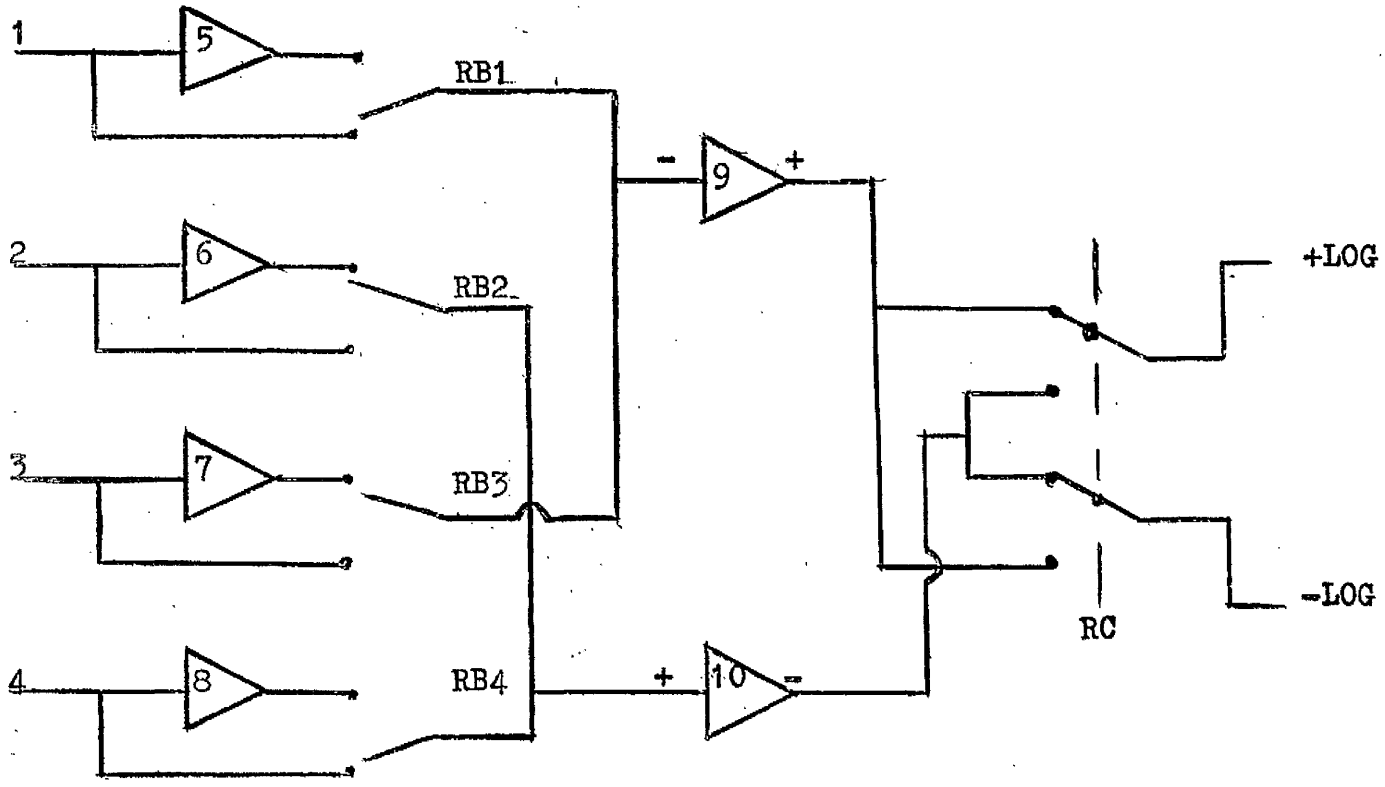

Figure 3.7. Initial Positions of Relays RB and RC

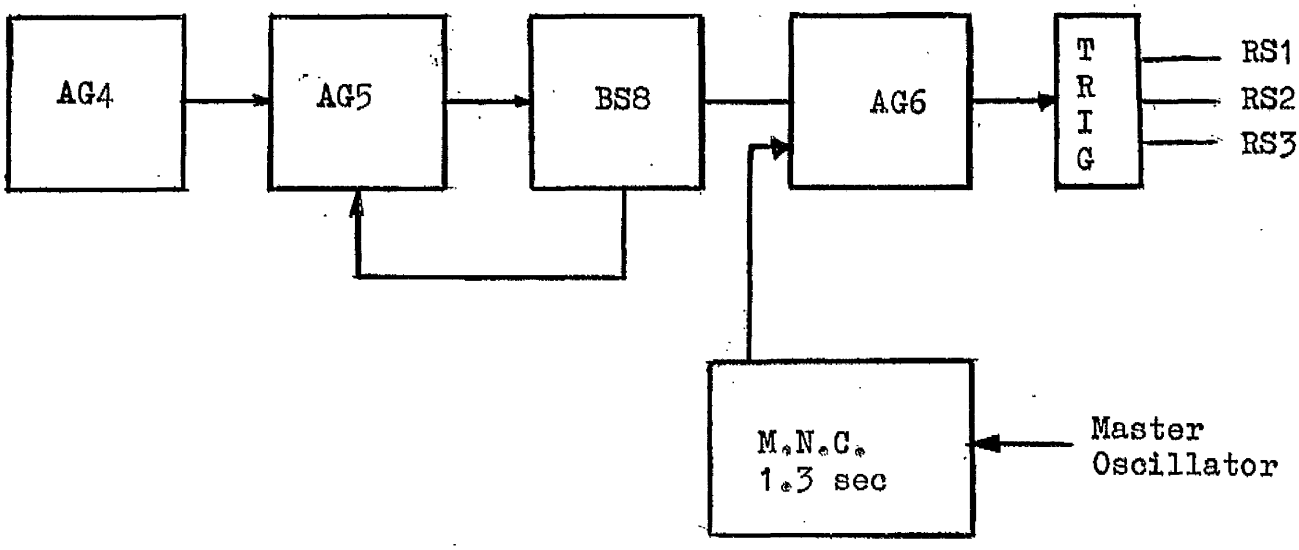

Figure 3.8. Logic Unit 3

the sampled values of V_{r-1}, V_r, V_{r+1} and V_{r+2}.

$$t_r = rt_d + \left(\frac{t_s}{2} + t_t\right)$$

$$= Pt_d + (r-1)t_d \text{ where } Pt_d = t_d + \frac{t_s}{2} + t_t.$$

$$\text{giving } P = \frac{t_d + \frac{t_s}{2} + t_t}{t_d}$$

For any value of r, $1/T_{mr}$ is easily found and using a multiplier the function $\frac{t_r}{T_{mr}}$ can be evaluated, summed with the other components of V_m and averaged. An averaged value of $\frac{t_r}{T_{mr}}$ can be achieved, however, without the use of a multiplier by writing

$$\frac{t_r}{T_{mr}} = \frac{Pt_d}{T_{m1}} + t_d \sum_{k=2}^{k=r} \frac{1}{T_{mk}}$$

The latter function can be formulated by using logic elements from logic unit 1 and logic unit 3 as shown in Figure 3.9. Approximately 1.3 seconds after AND gate AG4 is opened for the first time by the arrival of a negative going edge from the master oscillator the output pulse from monostable M N C terminates opening AND gate AG6 and closing relays RS1, RS2 and RS3, thus producing a voltage proportional to $\frac{t_d}{T_{m1}}$ at the output of the computer. If monostable MND is also triggered at this instant closing RLB for a period of, say, 0.2 seconds, then at the end of this interval the output voltage of the integrator is proportional to $\frac{t_d P}{T_{m1}}$ when the contact

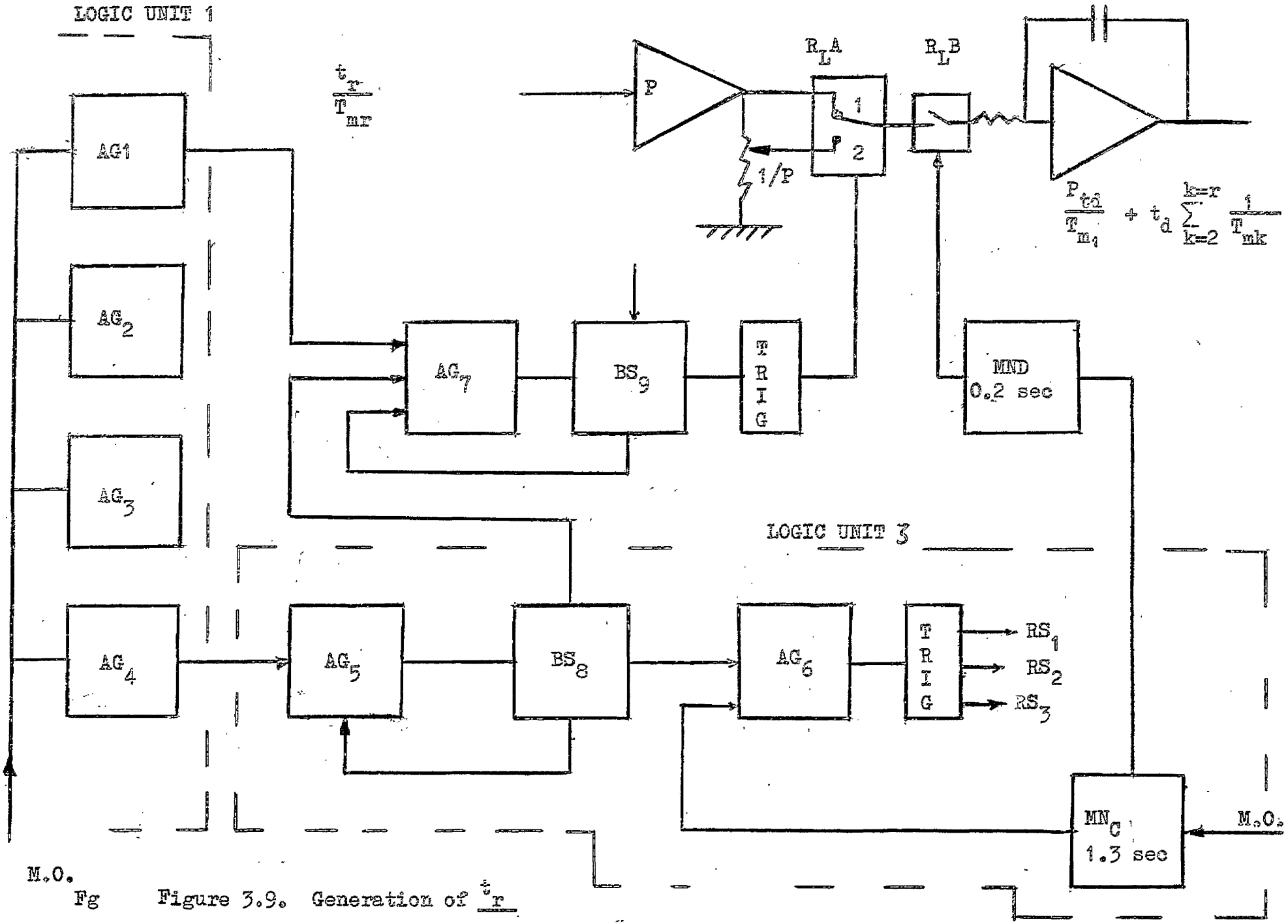

Fg Figure 3.9. Generation of $\frac{t_r}{T_{mr}}$

of relay RLA is at Position 1 as shown in Figure 3.9.

As mentioned previously the output from AG4 alters the state of bistable BS8 which is also connected to the input of AND gate AG7. BS9 is so set that the next negative going edge from the master oscillator which opens AG1 and passes through also opens AG7 operating BS9 and triggering relay RLA into Position 2.

This negative going edge also triggers monostable MND after a delay of 1.3 seconds and hence after a further period of 0.2 seconds the integrator output voltage is proportional to

$$\frac{Pt_d}{T_{m1}} + \frac{t_d}{T_{m2}}$$

The operation of BS9 closes AG7 locking RLA in Position 2, and the subsequent integrator output is given by the function

$$\frac{P_{td}}{T_{m1}} + t_d \sum_{k=2}^{k=r} \frac{1}{T_{mk}}$$

The function $\log (V_{r+1}-V_{r-1})$ can be obtained most economically via a log unit from the input terminal of the positive log unit of Figure 3.3. and $\frac{t_d}{T_{mr}}$ is available at the output of the computer. The computer configuration for repetitive solution of V_m is shown in Figure 3.10.

3.2.3. Time scaling.

The nature of the time scaling used will depend on the magnitude

of the time constants associated with the plant transfer function and hence on the specific application envisaged. In this study we will consider the application to a power station boiler where V(t) represents the measured value of the heat flux time function and T_m the grinding mill time constant.

As T_m is of the order of 40 seconds for a large boiler installation computation can easily be performed in real time. The upper limit of the sampling frequency is determined by the settling time of the adaptive mechanism which adjusts the plant model, a settling time of less than 300 milliseconds being possible with the type of cadmium sulphide element discussed in chapter 2.

It was found that a ratio t_d/T_m approximately equal to 0.1 resulted in an easily controlled system which was ideal for experimental purposes.

To minimise any error due to relay contact bounce the integration period t_s was chosen to be 1 second. The reset period t_t is a function of the maximum integrator voltage and the maximum deviation from zero tolerable after the reset period. A value of t_t of the order 0.2 seconds was found to give an accuracy compatible with the overall system accuracy. The pulse duration of monostable M N B is determined by the sum of t_s and t_t and is thus approximately 1.2 seconds fixing the duration of M N C. at a slightly higher value say 1.3 seconds.

3.2.4. Amplitude Scaling.

The amplifiers used have a rated maximum swing of $\pm$ 10 volts and as 10% over-voltage was possible a full excursion of $\pm$ 10 volts could

be used. The input signal to the computer was of the form

$$V(t) = V_m(1-\varepsilon^{-t/T_m})$$

where V_m is 10 volts and T_m is of the order of 40 seconds.

Thus an integrator time constant of one second gave maximum integrator output volts with no possibility of overload. The maximum slope of an exponential function occurs at the origin and thus the maximum differential voltage will appear at the output of amplifier 9 after the computation of V_2 (Figure 3.4.) for a V_m of 10 volts and t_d/T_m equal to 0.1. This maximum voltage can easily be calculated and is of the order of 2 volts. In order to limit the input to the log units to 10 volts the maximum gain possible on summing amplifiers 9 and 10 was thus 5. Amplifier 11 was arranged to give a gain of 4 in association with the log units resulting in an output voltage of the order of 0.4 volts. This gain can be increased if required.

As the gain of amplifiers 9 and 10 was made equal to 5 equation (7) can be written as

$$V_m = \text{Antilog}\left\{ \log 5(V_{r+1}-V_{r-1}) - \log \frac{2t_d}{T_{mr}} + \frac{t_r}{T_{mr}} - \log 5 \right\}$$

$$V_m = \text{Antilog}\left\{ \log 5(V_{r+1}-V_{r-1}) - \log \frac{10t_d}{T_{mr}} + \frac{t_r}{T_{mr}} \right\}$$

Maximum value for gain of log units in this expression is again 4.

The pulse duration of monostable MND was chosen to be 0.2 seconds yielding a time constant for the integrator determining $\frac{t_r}{T_{mr}}$ as 0.2 to

produce the required output value of $\frac{4t_r}{T_{mr}}$.

3.3. Electronic Circuit Techniques.

3.3.1. Amplifiers.

The configuration was simulated on a PACE TRIO machine, the amplifiers being chopper stabilised solid state devices. The ability of the integrator amplifiers to maintain their voltages accurately in the HOLD mode for a period of the order of $3 \rightarrow 4\, t_d$ is of prime importance to ensure system accuracy. It was found that, by correct adjustment of the amplifier balance potentiometers, the integrators could maintain a voltage in the HOLD mode to an accuracy of 0.05% for a period in excess of 30 seconds. This performance was more than sufficient to meet the required specifications. Full details of the amplifier specifications are given in Reference (10).

3.3.2. Relays.

Glass encapsulated reed relays were used throughout. The setting time of these relays is of the order of 1 millisecond, their operation being controlled by high speed transistor trigger circuits. The glass envelope provides a high resistance leakage path and the figure obtained above for the integrator drift rate was measured with both integrator relays in circuit.

3.3.3. Trigger Circuit.

The relay coils are 3 volt operation requiring 50 mA for the single pole and 100 mA for the double pole switches. A typical trigger circuit operated by a bistable is shown in Figure 3.11. Amplification of the bistable output is necessary for satisfactory operation of the ZT82 trigger

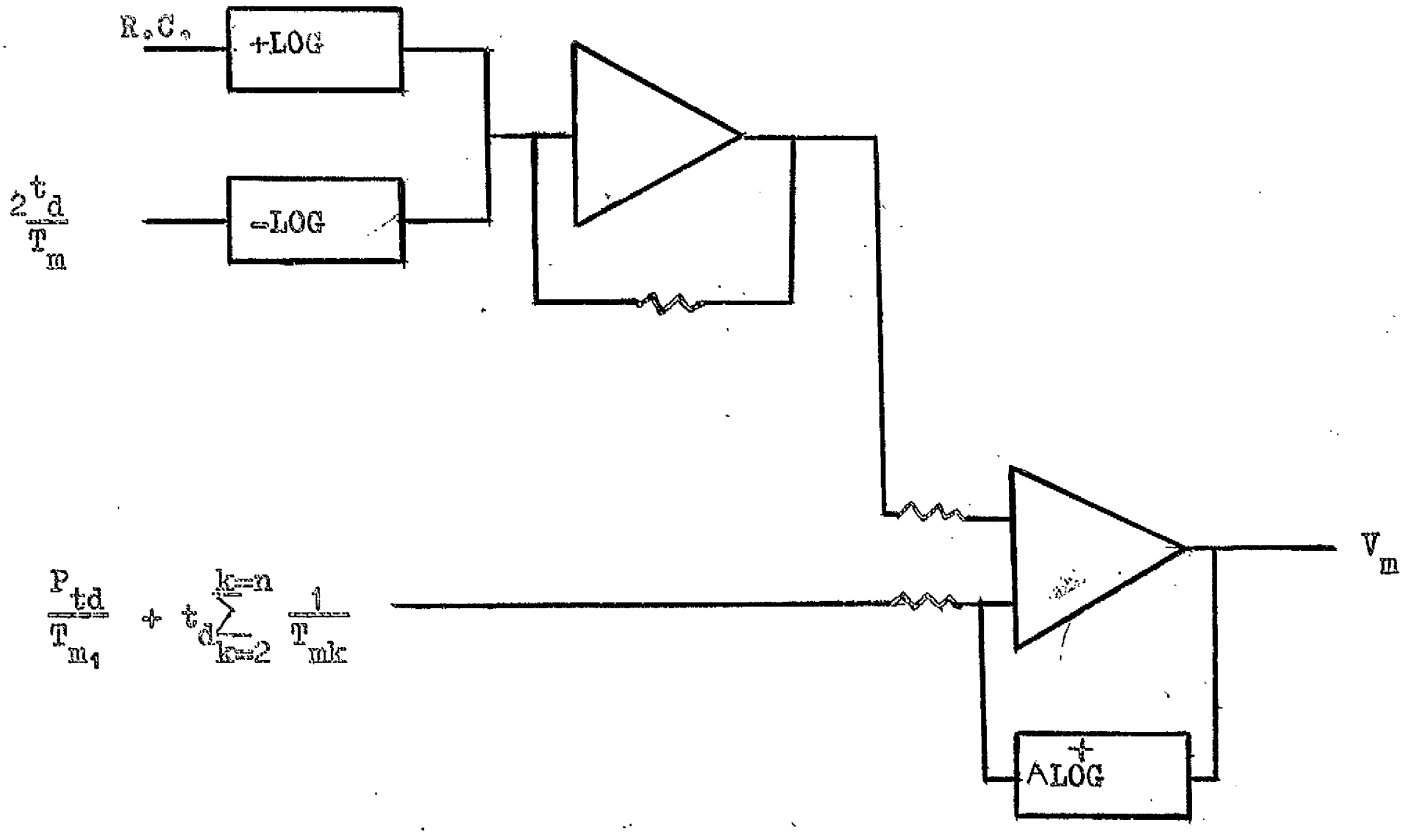

Figure 3.10. Determination of V_m

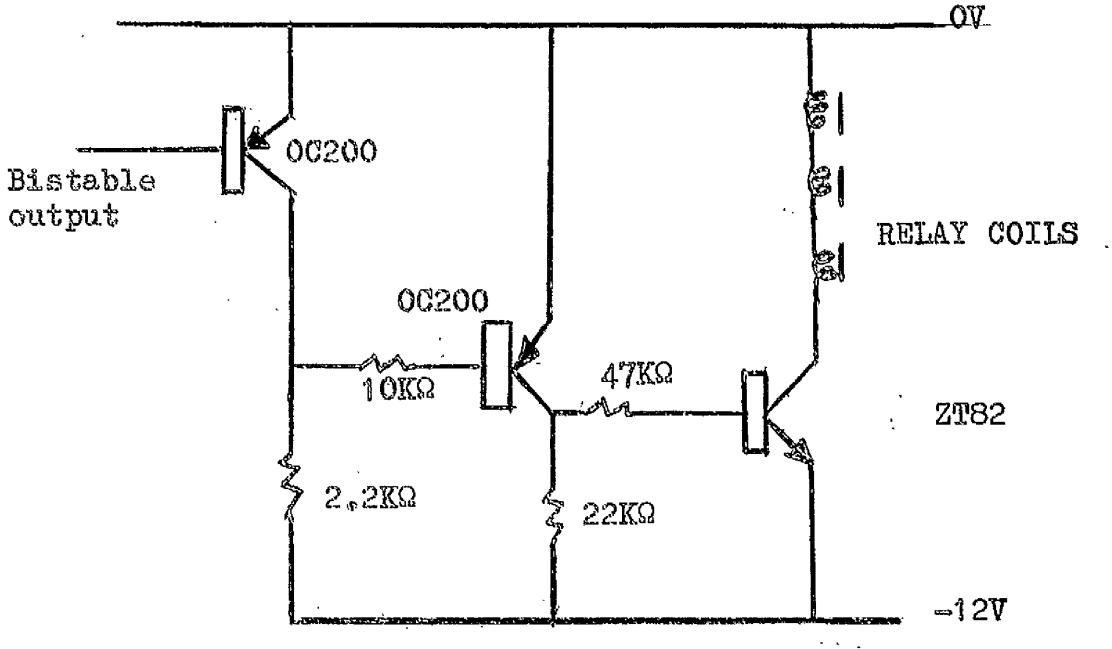

Figure 3.11. Trigger circuit

transistor and the additional OC 200 provides the necessary sign reversal to operate the relays from a positive going input step.

3.3.4. Bistable Circuit.

A typical bistable circuit is shown in Figure 3.12, and it is of the standard form outlined by Hurley (11). The output varies between 0 and -12 volts state transition being initiated by a positive going edge with steering diodes guiding the pulse to the appropriate OFF transistor. Two sets of steering diodes are provided to enable the bistable to be triggered from two isolated sources. Additional diodes can be included to perform SET and RESET functions.

3.3.5. Monostable Circuit

Two types of monostable circuit are used, one with a pulse duration of the order of 1.2 seconds and the other with a pulse duration of 0.2 seconds. The circuit diagram of the former, together with its trigger circuit is shown in Figure 3.13 and of the latter in Figure 3.14. The principle of operation is similar in both circuits and is described by Hurley (11) P.423. For a given value of t_t the integration interval and hence the integration accuracy is dependent on the pulse width of monostable A and its correct adjustment is thus vital. In Figure 3.13 the potentiometer VR is used to adjust the width of the output pulse. The set up procedure is as follows.

t_t is first determined by adjusting monostables MNB Figure 3.14 by adjustment of VR. The pulse duration of the four monostables compared

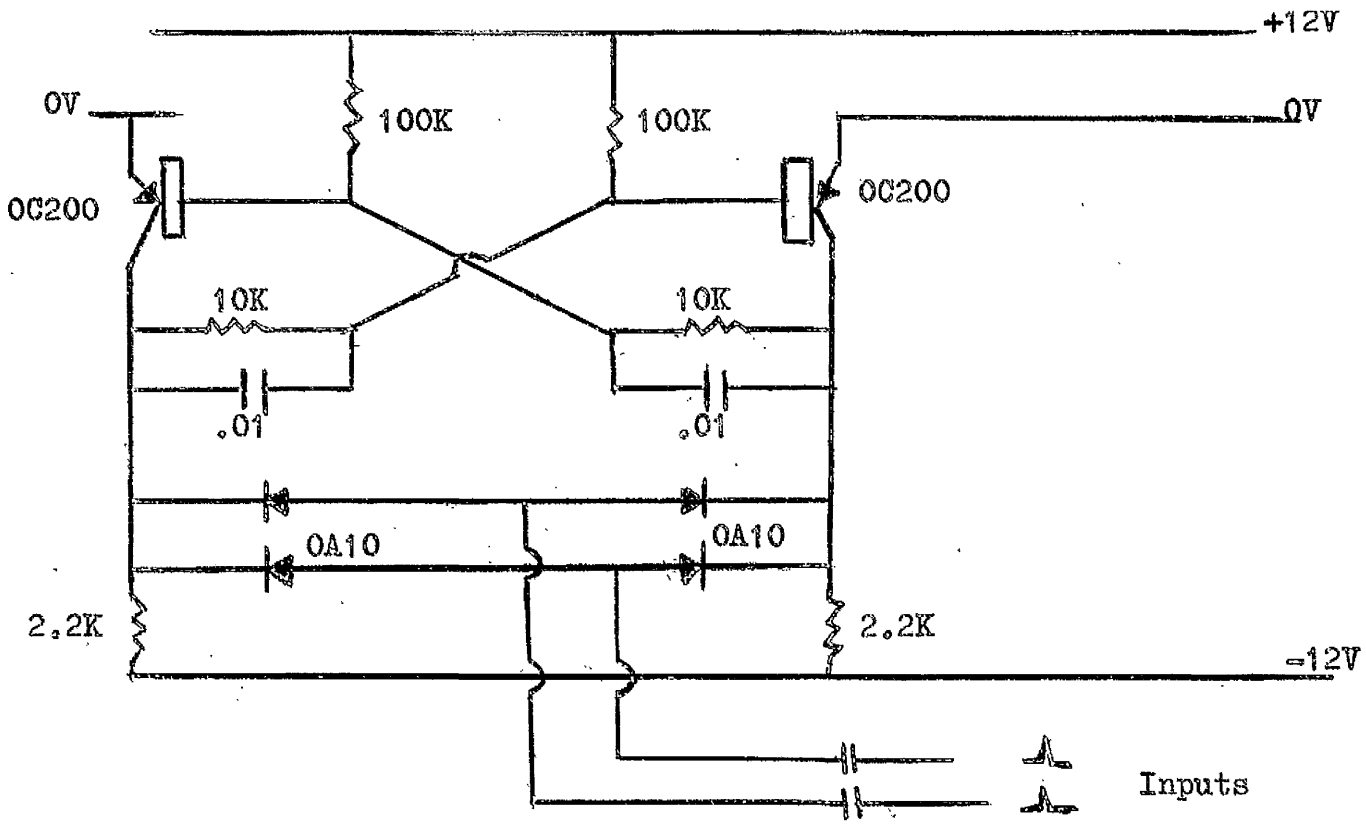

Figure 3.12 Bistable Circuit.

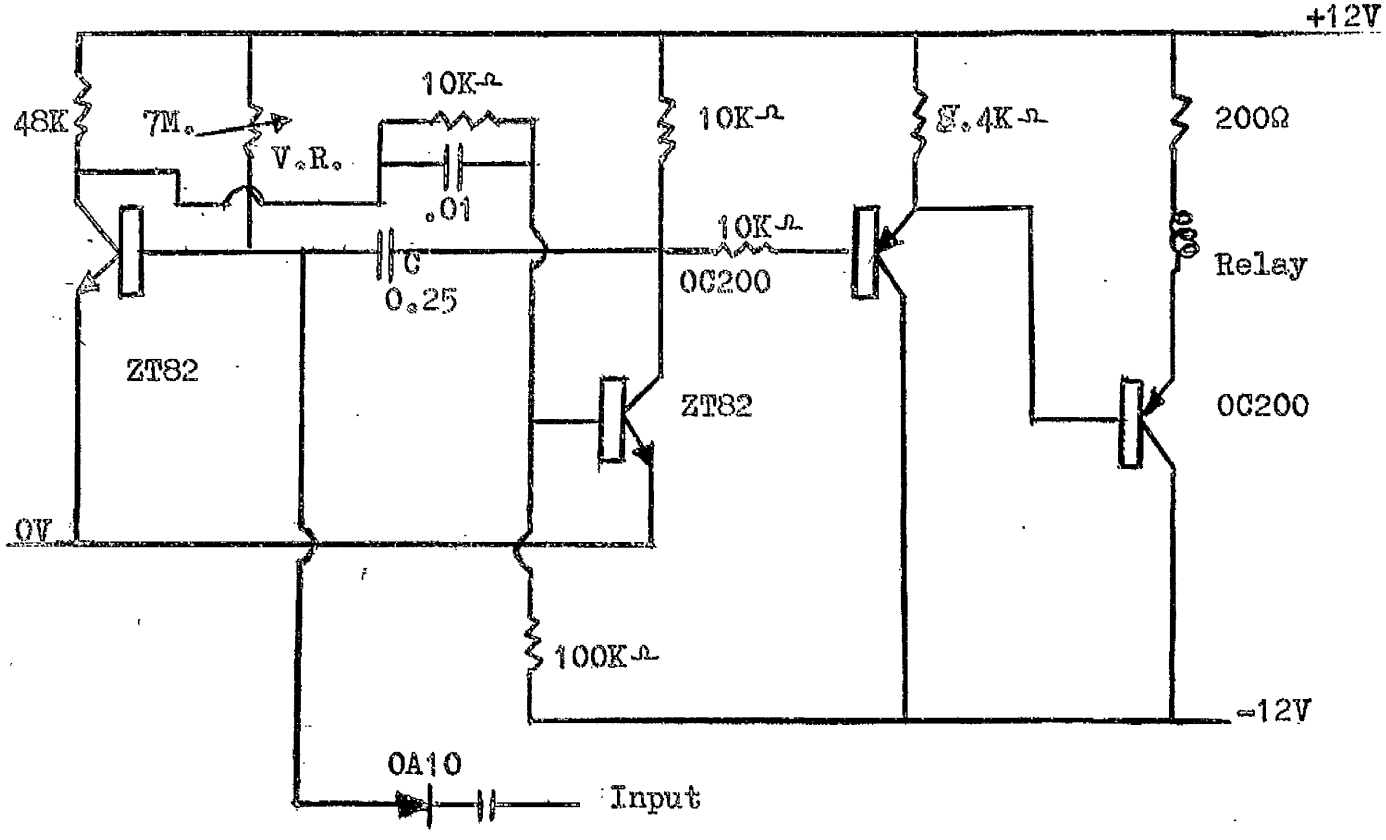

Figure 3.13. Monostable 1.2 seconds and trigger circuit.

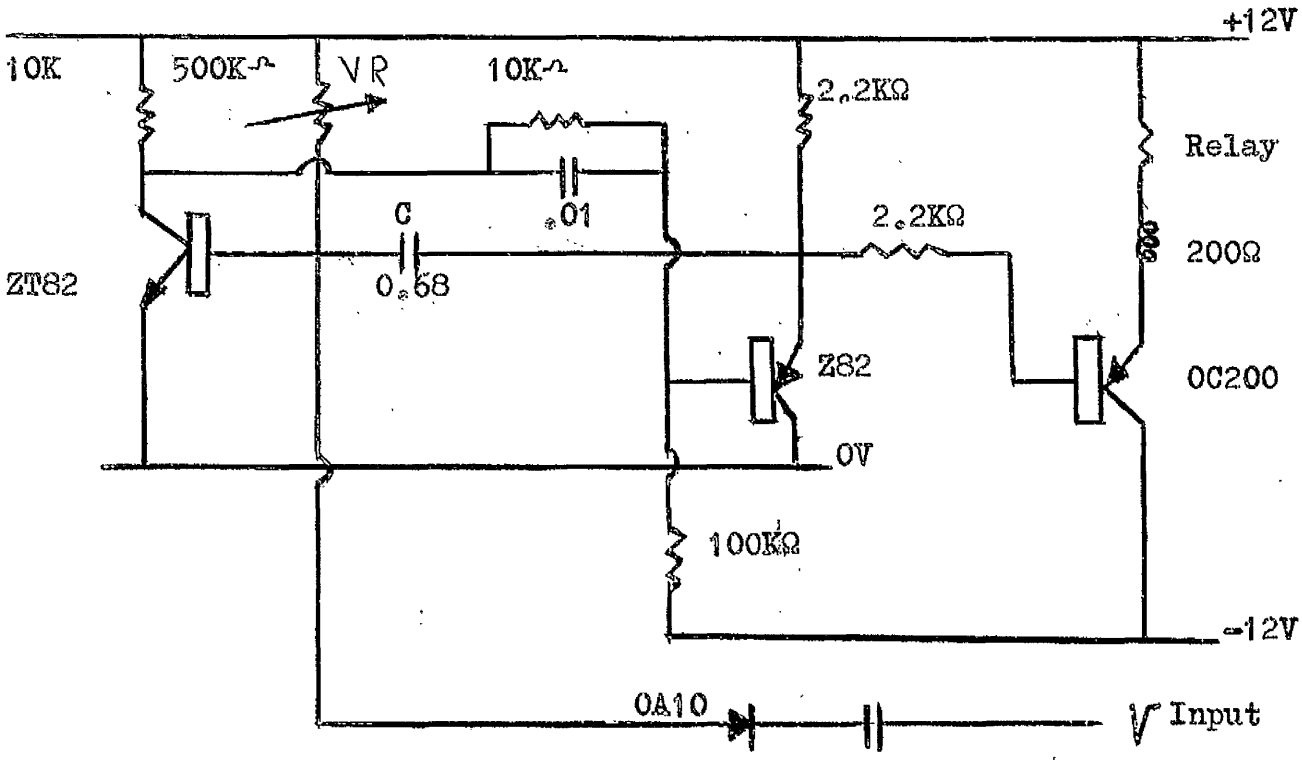

Figure 3.14 0.2 Second Monostable and Trigger Circuit

within an accuracy of 0.5%. A known voltage is now applied to the input contact of relay R and both monostables MNA and MNB are triggered, the final voltage of the integrator being measured. The operation is repeated with adjustment of VR until the output voltage of the integrator equals the applied voltage. The voltages were measured on a Solartron 1420 digital voltmeter to an accuracy of 0.05%. This set up procedure tends to compensate for (a) Variations in the set up value of t_t (b) Errors in the amplifier operational components which are a nominal 0.1% and (c) Errors due to the finite switching time of the relay.

Once set up both monostables are liable to be affected by temperature variations. If the base emitter junction voltage of the left hand transistor in both circuits is considered constant, the pulse width duration is determined by the product of VR and C and it is essential that high stability components be used if constant adjustment is to be avoided. Wire wound resistors have a temperature stability of the order of $\pm$.002% per degree centigrade and high grade polystyrene capacitors can be obtained with temperature coefficients of the order - .015 $\pm$ .006% per degree centigrade. The emitter base junction of a silicon transistor has a negative temperature coefficient of 2.5 mV/^{o}C which varies little at different currents and from one device to another. (Griffin (12)). The latter effect can usually be negated by suitable circuit compensation. The temperature coefficient of the capacitor will thus limit the temperature variation possible to maintain a given pulse width accuracy.

Both monostables are triggered by a negative going edge applied to the base of the left hand transistor turning it off and dropping the level of the right hand collector from +12 volts to approximately zero volts. To obtain adequate pulse width an additional emitter follower buffer element was included in the circuit of MNA Figure 3.13.

3.3.6. AND Gates.

A two input AND gateis shown in Figure 3.15(a). The gate is opened by the simultaneous application of a -10 volt level to both input terminals turning both transistors on and turning off the right hand OC 200, the collector of which drops to -12 volts. The gate will close on the removal of one of the negative inputs. The three input AND gate AG7 is shown in Figure 3.15(b). AND gate 6 and its trigger circuit have been combined in a single circuit the ZT 82 transistors performing a dual function as shown in Figure 3.15c.

3.3.7. Log Units.

The general layout of the log units is shown in Figure 3.16. diode break points and segment number being determined by the analytical methods of Hamer (13). As the solution is obtained as a difference between the outputs of two log units the individual accuracy of each unit must be high to ensure a reasonable accuracy in the differential result. The maximum output from each log unit will be of the order of 2 volts and the differential voltage of the order of 0.1 volts. Thus to obtain an accuracy of 1% in the output an individual unit accuracy

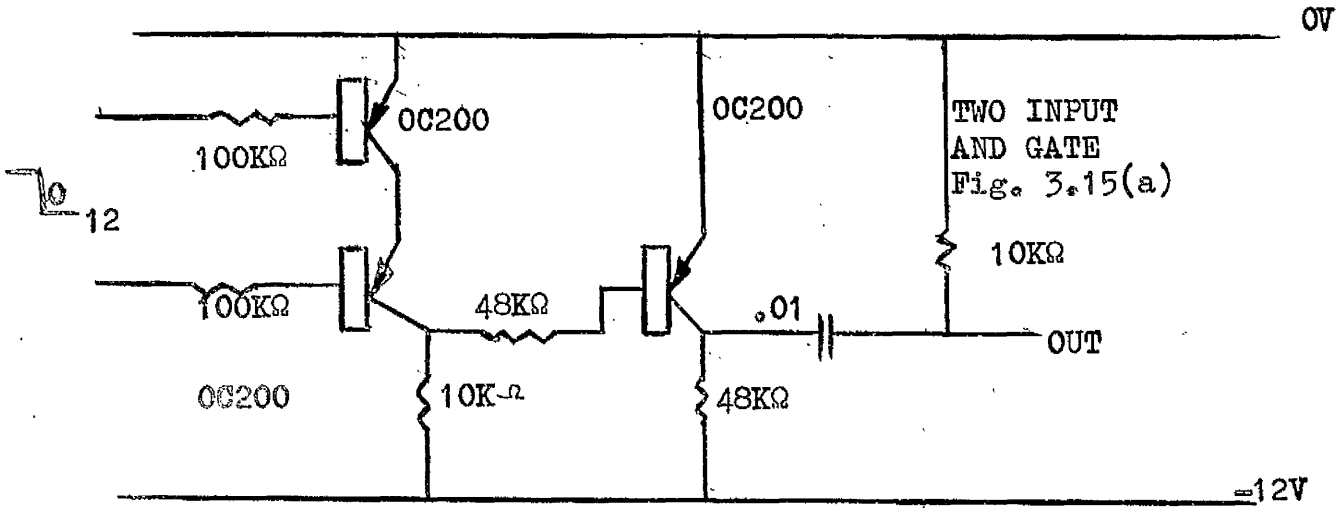

TWO INPUT AND GATE
Fig. 3.15(a)

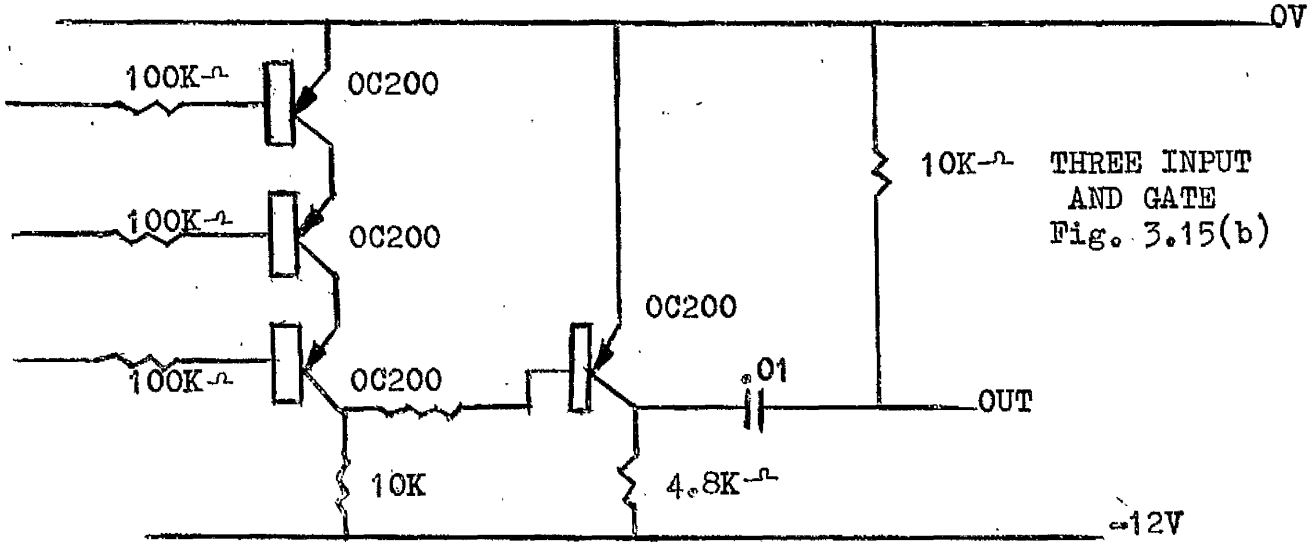

THREE INPUT AND GATE
Fig. 3.15(b)

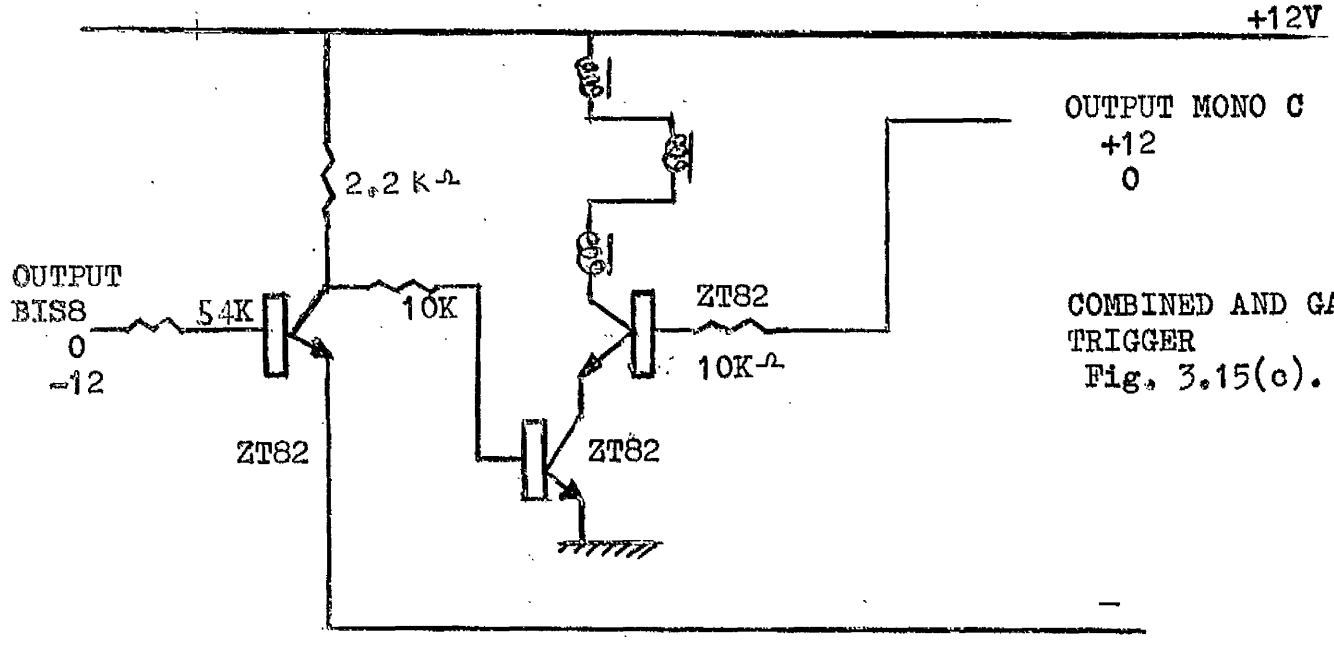

COMBINED AND GATE AND TRIGGER
Fig. 3.15(c).

of .05% is theoretically required.

The log units were initially designed to an accuracy of 0.1% as it was reasoned that if each unit is built to an identical specification some compensation must result and the differential error at least halved. This in fact proved to be the case and a final differential accuracy of better than 1% was easily achieved.

The relationship between error and the number of segments for an optimum linear approximation to an arbitrary function has been given by Hamer as

$$EN^2 = 1/2\left\{\sum_{k=1}^{k=n}\sqrt{|\delta K_2|}\right\}^2$$

where E is the greatest difference between the function and the straight line sgement and is called the error.

δ_{K_2} is the second difference of the function in the kth region.

For the function y = Log x the RHS of the above equation can be obtained from tabulation as

EN^2 = 0.106 when x lies between 4 and 10.

For any given number of segments the theoretical error can be halved by a method known as error splitting where the approximating linear segment is moved vertically by half the theoretical error. Thus to achieve a theoretical accuracy of $\underline{\Omega}$ 0.1% we can use seven segments.

$$\%E = \frac{.106}{49} \times 100 = 0.216$$

with error splitting

$$\%E = \frac{0.216}{2} = 0.108.$$

The various break points and slopes are now determined and the resulting setting voltages are shown in Figure 3.17. Thus set up of the log units were theoretically accurate to within 0.1% for input values in the range 4 volts to 10 volts. With minor adjustments the final accuracy was greatly improved yielding a differentical output voltage correct to within 0.05%.

3.4. System Accuracy.

Due to the sensitivity of the final log function it was imperative that the preceding computer stages be as accurate as possible and the accuracies of the individual stages will now be considered.

3.4.1. Accuracy of Integration.

Using high gain amplifiers the integration accuracy will be determined by the accuracy of the pulse width of MNA, which has already been discussed. We will now investigate the accuracy of the approximation made in paragraph 4.2. Namely that the V_1 of Figure 4.2. is given by

$$V_1 \Omega \frac{\int_{t_{10}}^{t_{11}} V(t)\, dt}{t_{11}-t_{10}}$$

$$\text{area under the segment} = \int_{t_{10}}^{t_{11}} V_m \left(1-\varepsilon^{-t/T_m}\right) dt$$

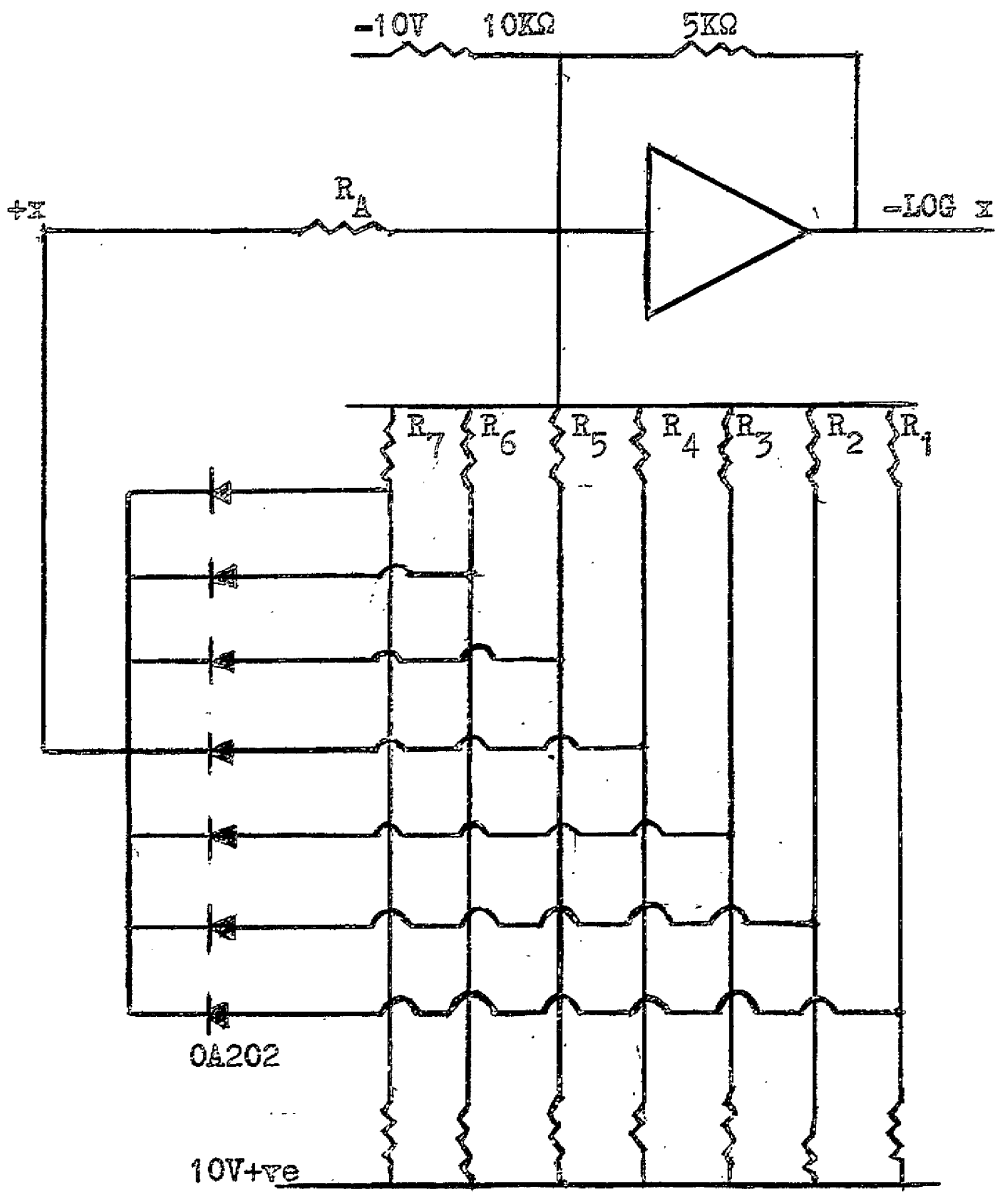

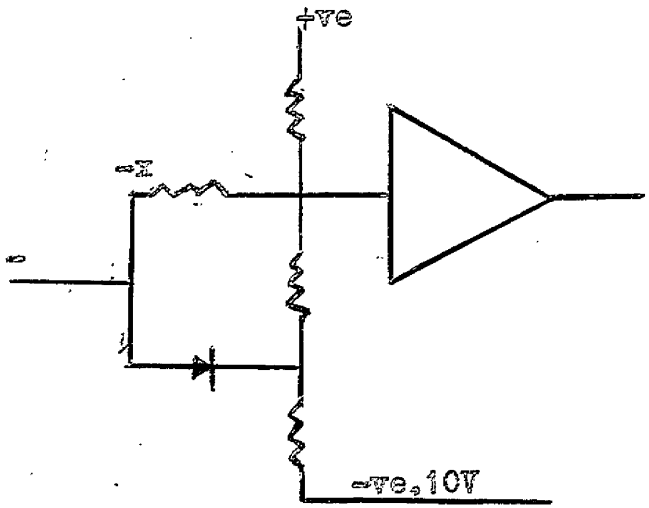

The log unit for negative x is similar to log unit for positive x with the differences shown above.

Figure 3.16 Log Units Circuit Diagrams

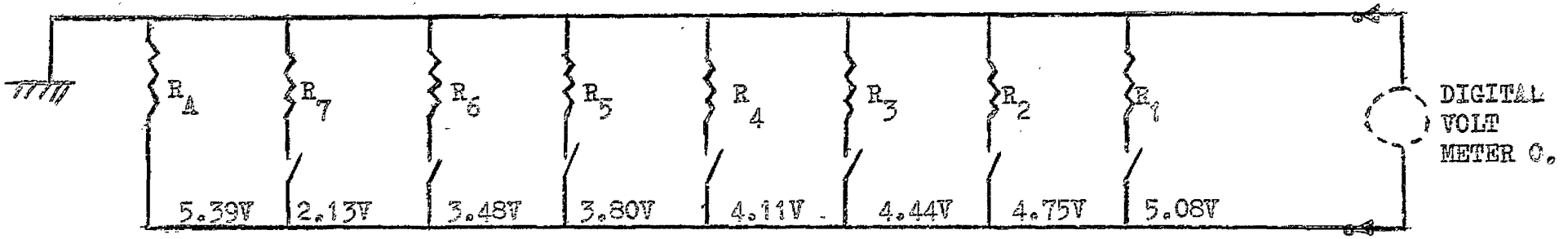

(a) SLOPE DETERMINATION

10KΩ±0.1%

+10 VOLTS ± 0.1%

PROCEDURE

(a) All switches OPEN adjust R_A to obtain 5.39V

(b) Close S_1 and adjust R_1 to yield 5.08V

(c) Repeat for remaining six resistors

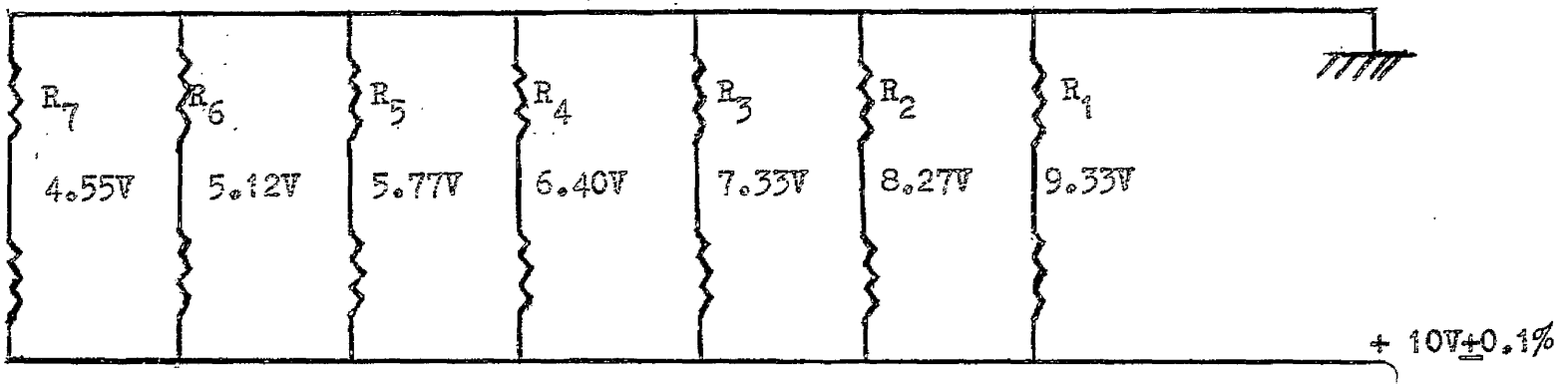

(b) Determination of Diode Break Point Voltages

Figure 3.17 Setting up Voltages for LOG D.F.G.

$$= V_m \left[t + T_m \varepsilon^{-t/T_m} \right]_{t_{10}}^{t_{11}}$$

$$= V_m \left\{ t_{11} + T_m \varepsilon^{-t_{11}/T_m} \right\} - \left\{ t_{10} + T_m \varepsilon^{-t_{10}/T_m} \right\}$$

$$= (t_{11} - t_{10}) + T_m \left\{ \varepsilon^{-t_{11}/T_m} - \varepsilon^{-t_{10}/T_m} \right\}$$

$$\therefore V_1 \simeq V_m \left(1 + \frac{T_m}{t_s} \left\{ \varepsilon^{-t_{11}/T_m} - \varepsilon^{-t_{10}/T_m} \right\} \right)$$

where $t_s = (t_{11} - t_{10})$.

Exact value of V_1 is given by

$$V_1 = V_m (1 - \varepsilon^{-t_1/T_m}) = V_m (1 - \varepsilon^{-(t_{11} - \frac{t_{11} - t_{10}}{2})/T_m})$$

error in the approximation

$$= -V_m \left\{ \varepsilon^{-(t_{11} - \frac{t_{11} - t_{10}}{2})/T_m} + \frac{T_m}{t_s} (\varepsilon^{-t_{11}/T_m} - \varepsilon^{-t_{10}/T_m}) \right\}$$

$$\text{error} = -V_m \varepsilon^{\frac{-t_{11}}{T_m}} \left\{ \varepsilon^{\frac{-t_s}{2T_m}} - \frac{T_m}{t_s} (1 - \varepsilon^{-t_s/T_m}) \right\}$$

for a given ratio of $\frac{t_s}{T_m}$

$$\text{error} = e \cdot V_m \cdot \varepsilon^{-t/T_m}$$

where

$$e = \left\{ \varepsilon^{\frac{-t_s}{T_m}} - \frac{T_m}{t_s} (1 - \varepsilon^{-t_s/T_m}) \right\}$$

The ratio $\frac{\delta_1}{\delta_2}$ is given by

$$\frac{\delta_1}{\delta_2} = \frac{V_2-V_o}{V_3-V_1} = \frac{\left\{\varepsilon^{-\frac{t_o}{T_m}} - e^{-t_2/T_m}\right\} - e\left\{\varepsilon^{-\frac{t_{21}}{T_m}} - e^{-t_{o1}/T_m}\right\}}{(e^{-t_1/T_m} - e^{-t_3/T_m}) - e(\varepsilon^{-\frac{t_{31}}{T_m}} - e^{-t_{11}/T_m})}$$

For $\frac{t_s}{2} << 2t_d$

$$\frac{\delta_1}{\delta_2} \Omega \left\{\frac{e^{-t_o/T_m} - e^{-t_2/T_m}}{e^{-t_1/T_m} - e^{-t_3/T_m}}\right\}\frac{(1+e)}{(1+e)}$$

Hence any error tends to cancel out in the calculation of the function t_d/T_m.

For t_s = 1 second and T_m = 40 seconds e can be determined from tables (14) as

$$e = -.0000262.$$

The error in the first reading V_o is given by

$$\text{error} = V_m e^{-\frac{t_{o1}}{T_m}} \times .0000262 \text{ where } t_{o1} \text{ is } 1.2 \text{ seconds}$$

$$= V_m \times .0000254$$

$$\% \text{ error} = 0.1470\%$$

% error in first differential voltage $V_2 - V_o$

= 00.00256% assuming a t_d of 4 seconds.

This theoretical error is more than one order less than any measurable

system error and thus the original approximation can be taken as valid.

3.4.2. Sign Changers.

The gain of the sign changing amplifiers 5,6,7 and 8 and of the summing amplifiers 9 and 10 has been closely defined by using 0.01% high stability resistors as operational elements.

3.5. Experimental Results.

3.5.1. Measurement of t_d/T_m.

A lag of 35 seconds was simulated to an accuracy of better than one percent on a Solartron SCD 10 analogue computer. The output of the lag was connected to the parameter estimator. A step waveform of 10 volts was applied to the input of the lag and simultaneously the estimator's oscillator was triggered. The oscillator used was a Servomex low frequency oscillator; the period of the output waveform being used was 3.6 seconds. After a period of 12.1 seconds a reading was obtained from the estimator output which was monitored on a digital voltmeter. Subsequent readings appeared at the end of every 3.6 seconds interval. Each reading varied by approximately $\pm$ 1% around a mean value of 0.410 volts to give an output value of $\frac{t_d}{T_m} = 0.1205$ giving a value of $T_m =$ 35.1 seconds.

After a time approximately equal to the time constant T_m large deviations occurred in the output readings due to the limitations of the log units, the accuracy of which deteriorated rapidly below inputs of the

order of 4 volts.

The ratio $\frac{t_d}{T_m}$ was varied in the range ± 20% and the resulting response of the estimator output voltage is shown in Figure 3.18.

3.5.2. Measurement of V_m.

For a step voltage of magnitude ± 10 volts ± .05% into the lag unit which had a gain of unity within an accuracy of ± 0.1% the sequential parameter estimator output voltages were within ± 2% of 10 volts for a period of time approximately equal to the time constant T_m. Variations in the estimator average output voltage were then monitored for a ± 20% swing in the input step voltage around a level of 8 volts. The results are shown in Figure 3.19. Variation of the step voltage magnitude had no significant effect on the measured value of T_m and likewise the variation of the ratio t_d/T_m had no significant effect on the measured V_m.

3.5.3. Noise Measurements.

The noise error in any sampled value of the input will be equivalent to the noise signal on the output of an integrator of unity time constant after a computation period of one second. A Solartron Random Signal generator was available with a specified spectral density (15).

$$G(x) = G(0)\left(\frac{\sin x}{x}\right)^2 \quad \text{where } x = \frac{\pi f}{f_c}$$

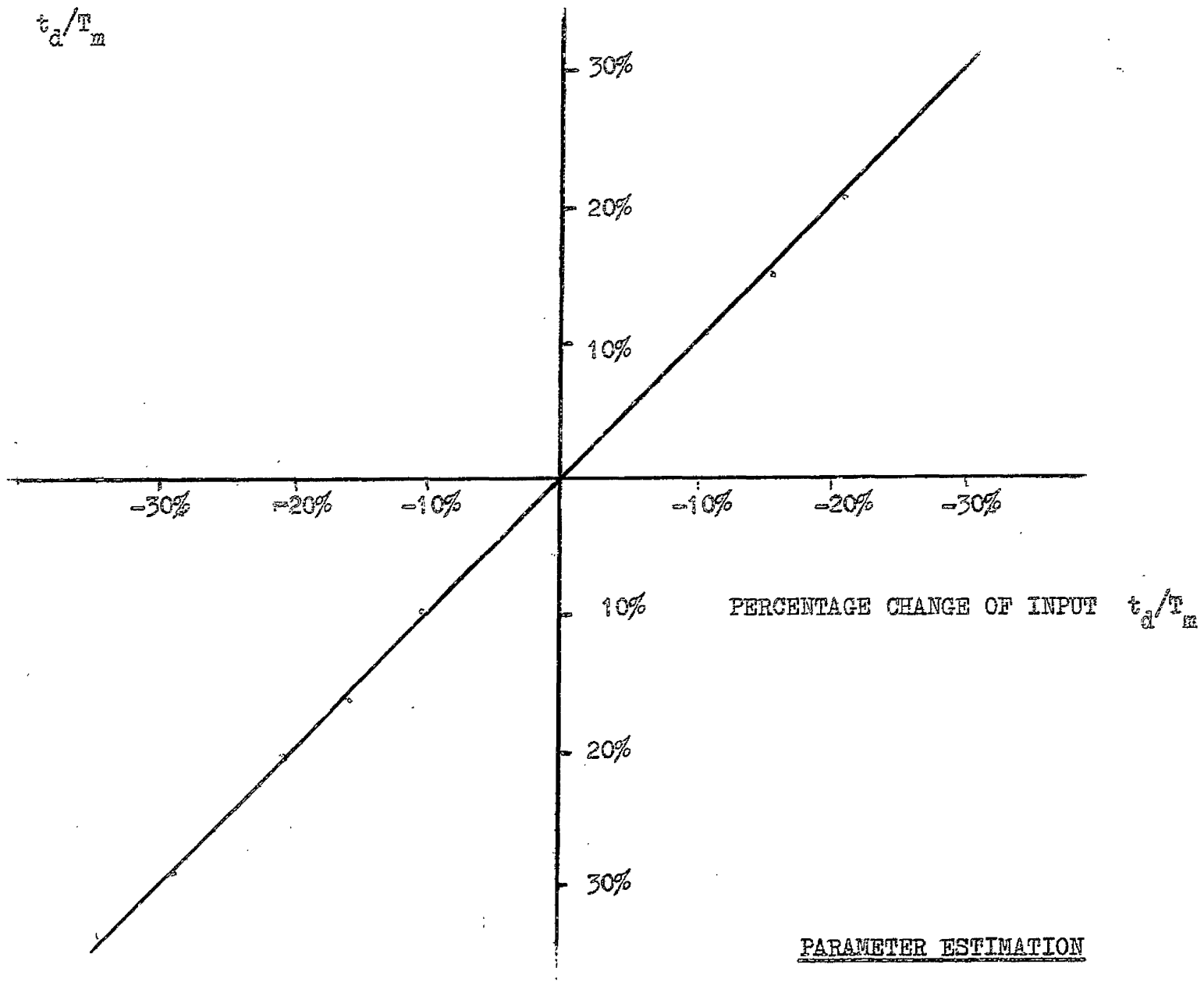

PARAMETER ESTIMATION

$\frac{t_d}{T_m}$

Figure 3.18.

Graph of % increase in Vm Measured

$$V_m = \text{Antilog} \left\{ \text{LOG } 5(V_{r+1} - V_{r-1}) + \frac{t_r}{T_{mr}} - \text{LOG } \frac{10t_d}{T_{mr}} \right\}$$

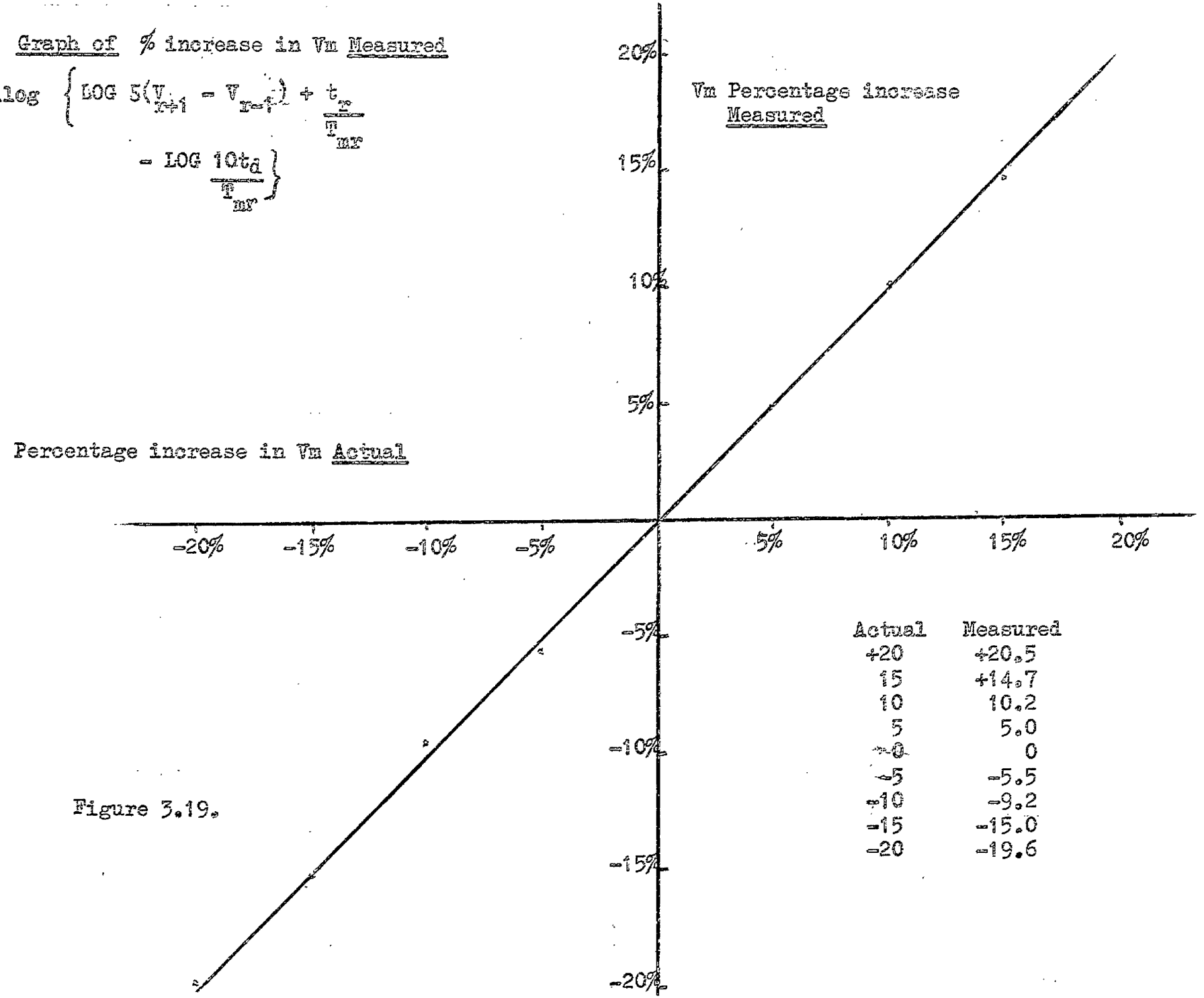

Actual	Measured
+20	+20.5
15	+14.7
10	10.2
5	5.0
0	0
-5	-5.5
-10	-9.2
-15	-15.0
-20	-19.6

Figure 3.19.

where G(0) is a constant set by the instrument controls and the cut off frequency f_c is adjustable in semidecade steps from 0.032 c/s to 10 Kc/s. A crest factor (Peak to R.M.S. Ratio) of 9.8 was used to give near gaussian distribution. The peak level was set at 1 volt, the resulting R.M.S. output being approximately 100 mV. Care was taken to avoid the presence of any D.C. signal bais level.

An integrator was switched to repetitive operation with a compute period of one second. The signal from the noise generator was fed to the integrator and the value of the integrator voltage measured at the end of each computation for about 30 computations. The maximum value of this series of readings was then tabulated and the operation repeated for various values of f_c. The tabulation is shown below.

F_c	Max. Integrator Output Voltage	F_c	Max. Integrator Output Voltage
10 Kc/s	0.004	32 c/s	0.30
3.2 Kc/s	0.005	10 c/s	0.50
1.0 Kc/s	0.07	3.2 c/s	0.80
320 c/s	0.10	1.0 c/s	1.0
100 c/s	0.20		

Though this test was not rigorous the results do indicate that above an f_c of 320 c/s the maximum noise error is less than 1%, assuming a signal level of 10 volts, for a peak noise voltage of 10%. From the point of view of boiler application it should be noted here that the maximum noise content of the output signal from the heat flux meter described in chapter 4 is of the order of 1% and confined to the high end of the frequency spectrum. It is thus reasonable to suppose that the resulting noise error using this technique will be insignificant.

Further protection against the effect of spurious noise signals is afforded by the nature of the system switching logic which will cancel out any large deviation from the average output value.

The general layout of the parameter estimation switching logic, control computers and model adaptation networks is shown in Figure 3.20.

3.6. Parameter Estimation of Second Order System.

If the transfer function of the plant is of the form

$$G(s) = \frac{1}{1 + T_f s} \quad \frac{K_c \; e^{-Ts}}{(1 + T_m s)}.$$

where T and T_f are known, parameter estimation can proceed in the manner outlined above if the proper compensation network is used. Figure 3.21(a) shows the relationship between fuel flow signal and heat flux of a boiler where the heat flux time function H(t) is second order. If a processor of the form

$$P(s) = (1 + T_f s)$$

is used

then a first order time function H'(t) can be developed Figure 3.21(b) where H'(t) is of a form suitable for parameter estimation.

Processor realisation depends on the magnitude of the constant T_f and in the particular case of boiler application, where T_f is of the order of 4 to 5 seconds, it is easily accomplished in electronic analogue form.

3.7. Parameter Estimation in the Presence of One Unknown.

If G(s) in the equation

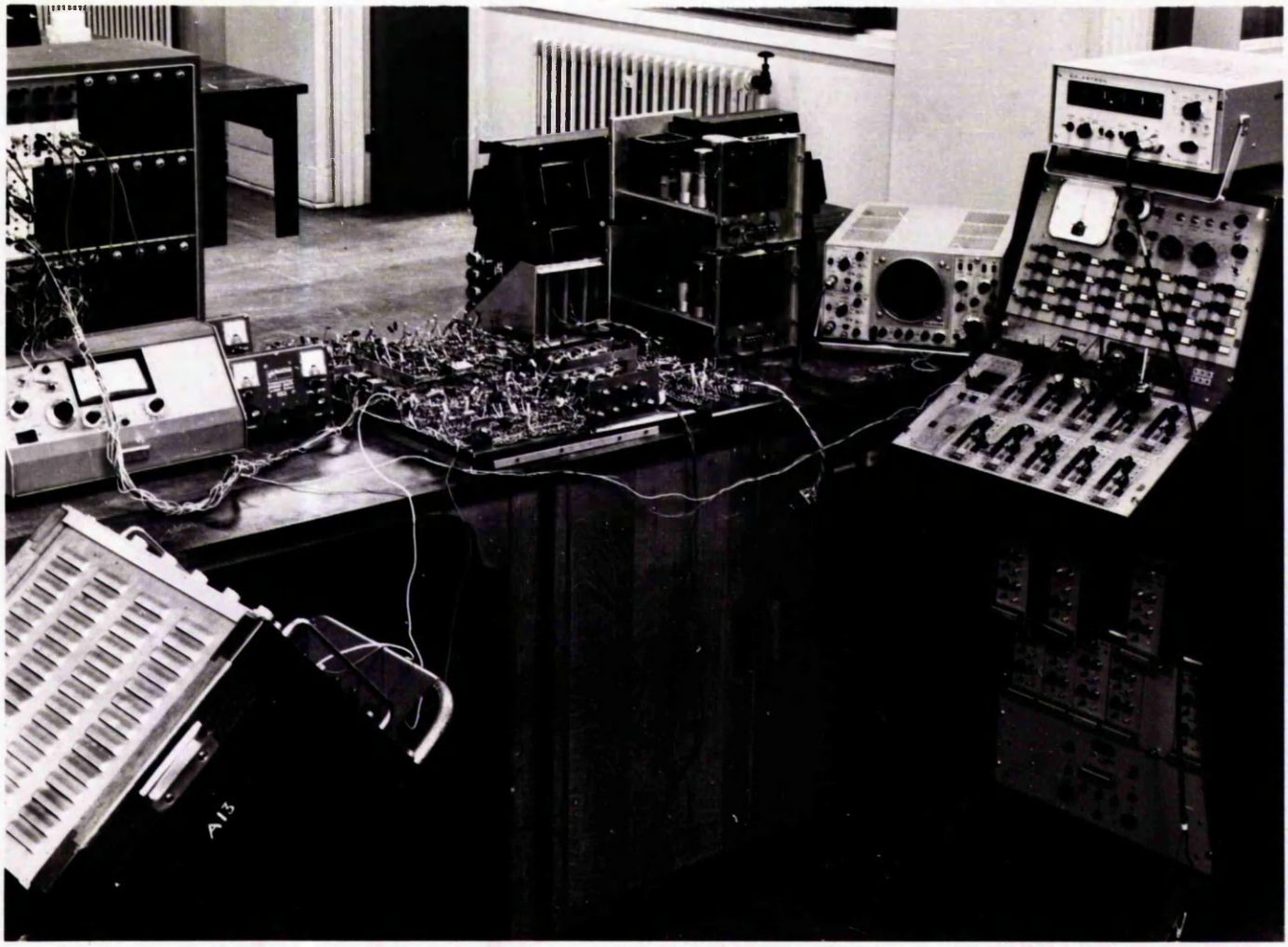

GENERAL LAYOUT OF PARAMETER ESTIMATION AND MODEL ADAPTIVE SYSTEM

Figure 3.20.

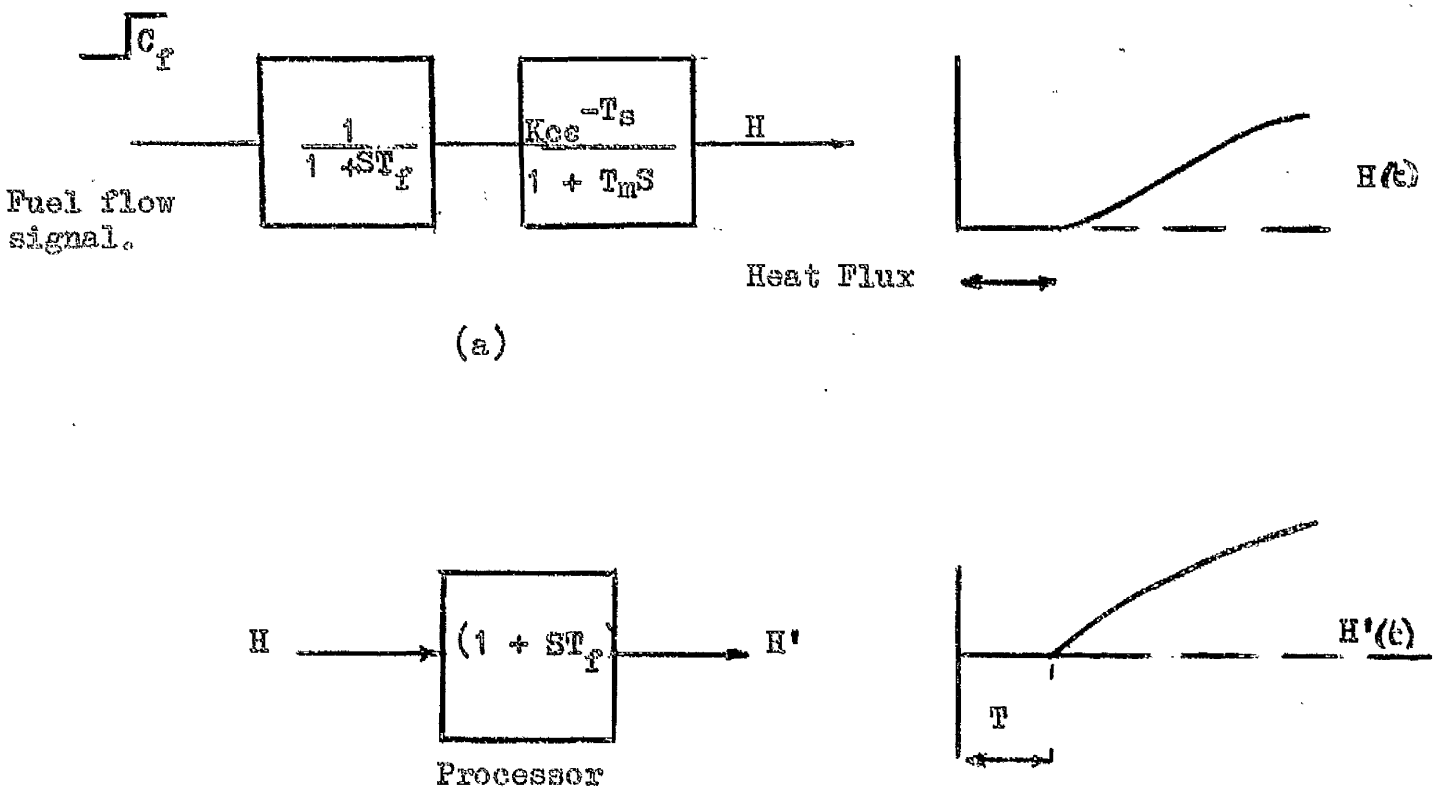

Figure 3.21. Signal Processing.

$$C(s) = M(s)\, G(s)$$

is of the form $\frac{A}{1 + sB}$ and if $M(t)$ and $C(t)$ are continuous functions of time Corbin has shown that A can be determined by simple analogue methods.

$$C(s) = M(s) \frac{A}{1 + sB}$$

$$AM(s) = C(s) + sB\ C(s)$$

$$M(t)\, A = C(t) + \frac{d}{dt} B\ C(t).$$

$$A \int_o^t M(t) = \int_o^t C(t) + B\ C(t) + C(o).$$

For $C(o) = 0$.

$$A = \frac{\int_o^t C(t) + B\ C(t)}{\int_o^t M(t)}$$

$$B = A \frac{\int_o^t M(t) - \int_o^t C(t)}{C(t).}$$

3.7.1. Experimental Procedure.

(a)

In the particular case of a boiler, incremental heat flux and boiler pressure are related by the transfer function

$$P(s) = \frac{K_1}{(1 + sT_1)(1 + sT_2)} H(s)$$

where K_1 is a variable and T_1 and T_2 are known, T_2 being equal to $10T_1$. It is required to estimate K_1 from the measured values of $P(t)$ and $H(t)$.

K_1 can be derived by the method shown in Figure 3.22. The simple boiler model of Figure 4.11 with the exception of the distance velocity lag was simulated on an analogue computer with δH, the incremental heat flux, and δP, the incremental pressure signals, being processed as shown, computation being performed in real time. The inclusion of the lag T_1 in the δH circuit compensates for the second order nature of the steam generation response. Using this approach K_1 was determined within 1% of its known value. The computer output was also monitored as K_1 was varied within $\pm$ 20% of its median value. The resulting linear response of the computer output is shown in Figure 3.23.

(b).

To illustrate the general use of the method in determining an unknown plant time constant the above experiment was repeated with the computer configuration arranged to estimate T_2, K_1 now being assumed invariant for the purpose of this experiment only. The appropriate computer configuration is shown in Figure 3.24. and the corresponding results in Figure 3.25.

3.8. Summary.

If the dominant plant transfer function is of the form assumed

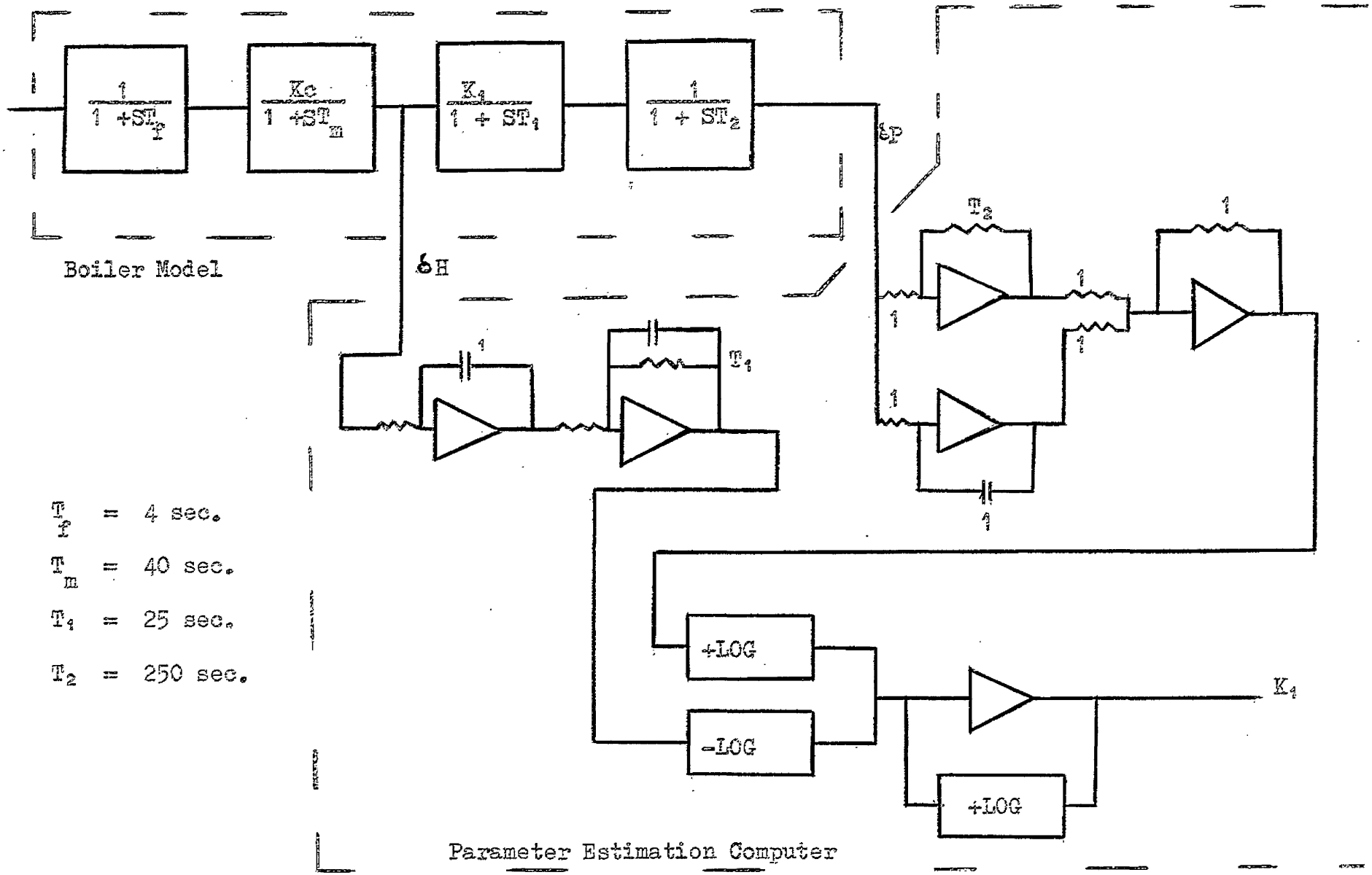

Figure 3.22. Determination of K_1.

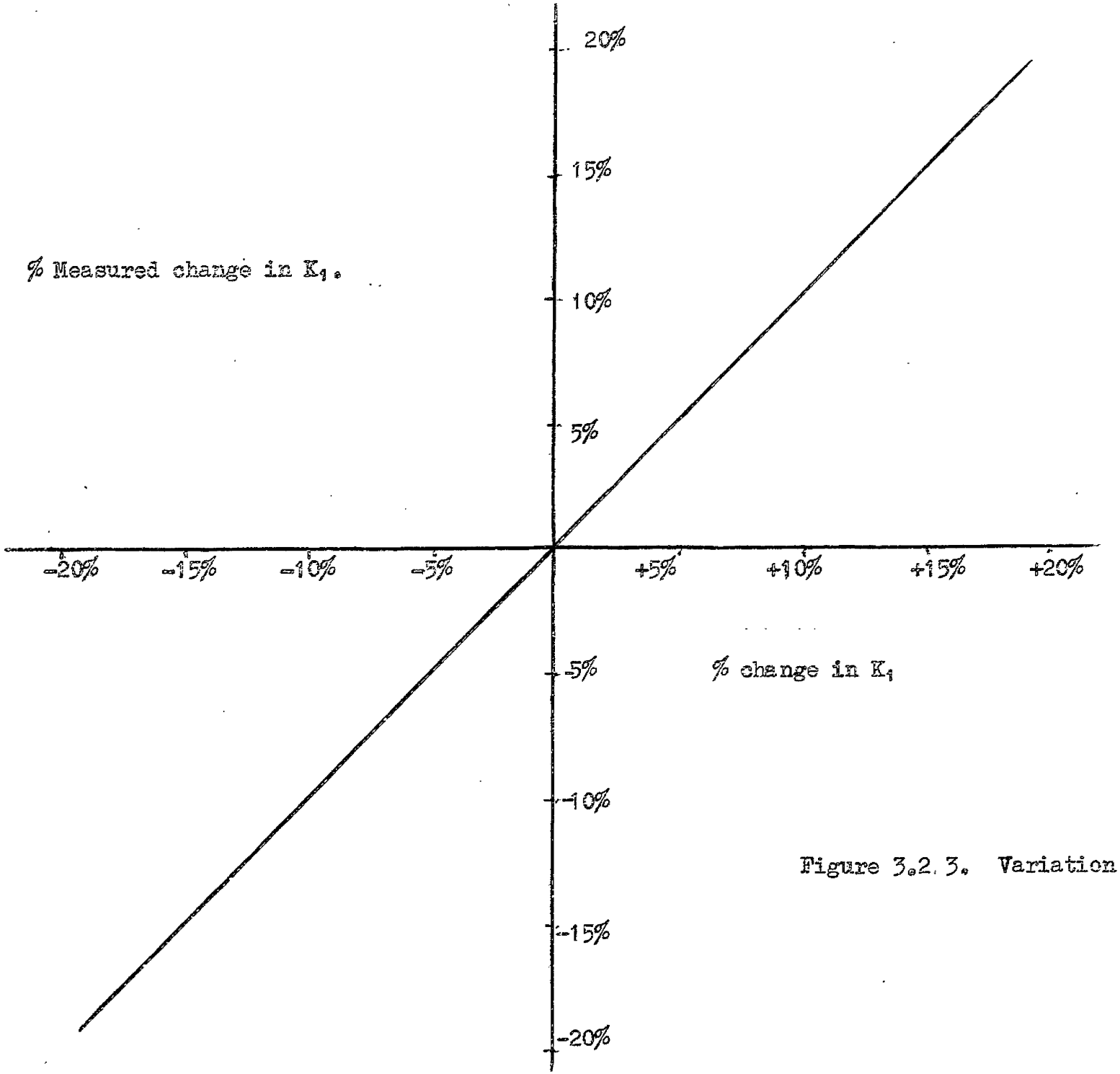

Figure 3.2.3. Variation in K_p

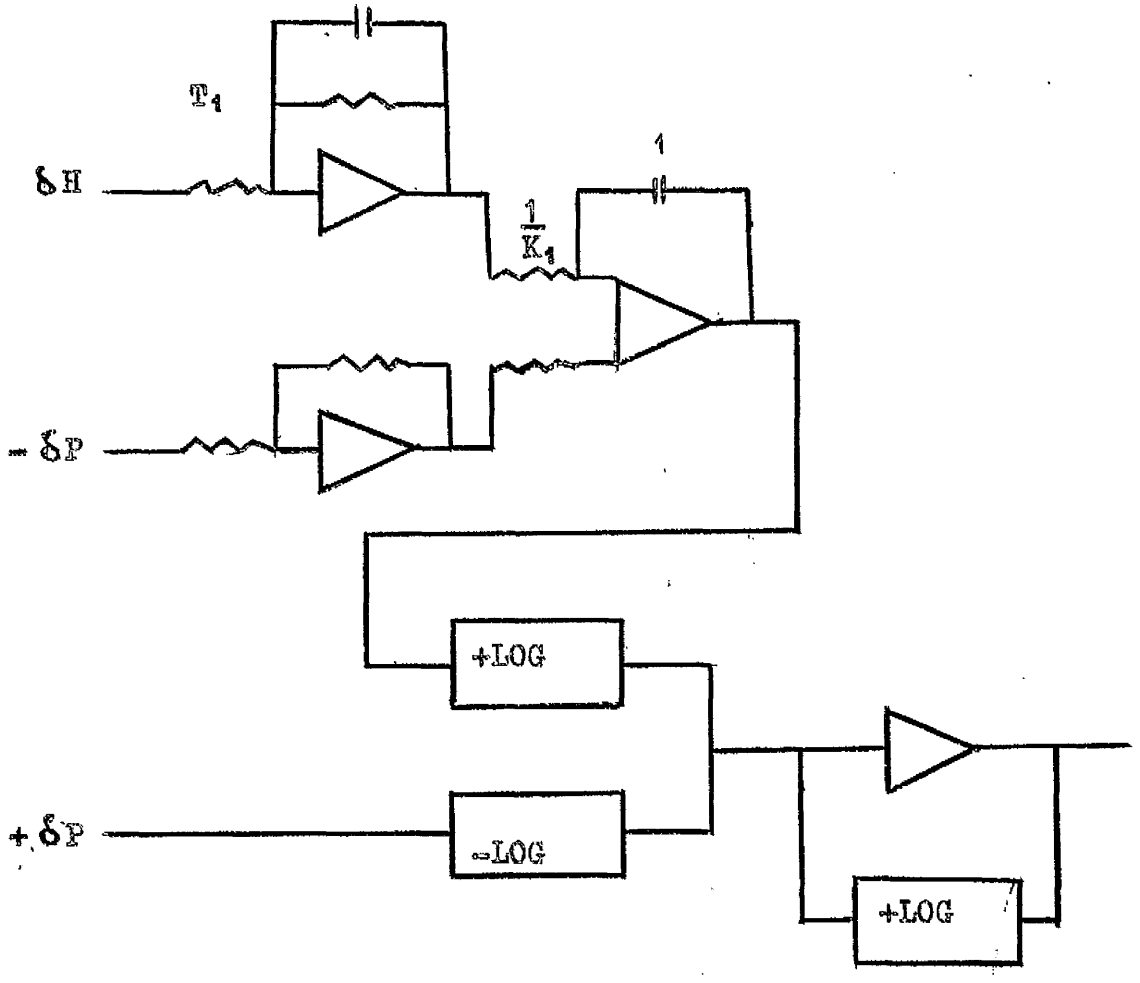

Figure 3.24. Computer configuration for the line estimation of plant time constant.

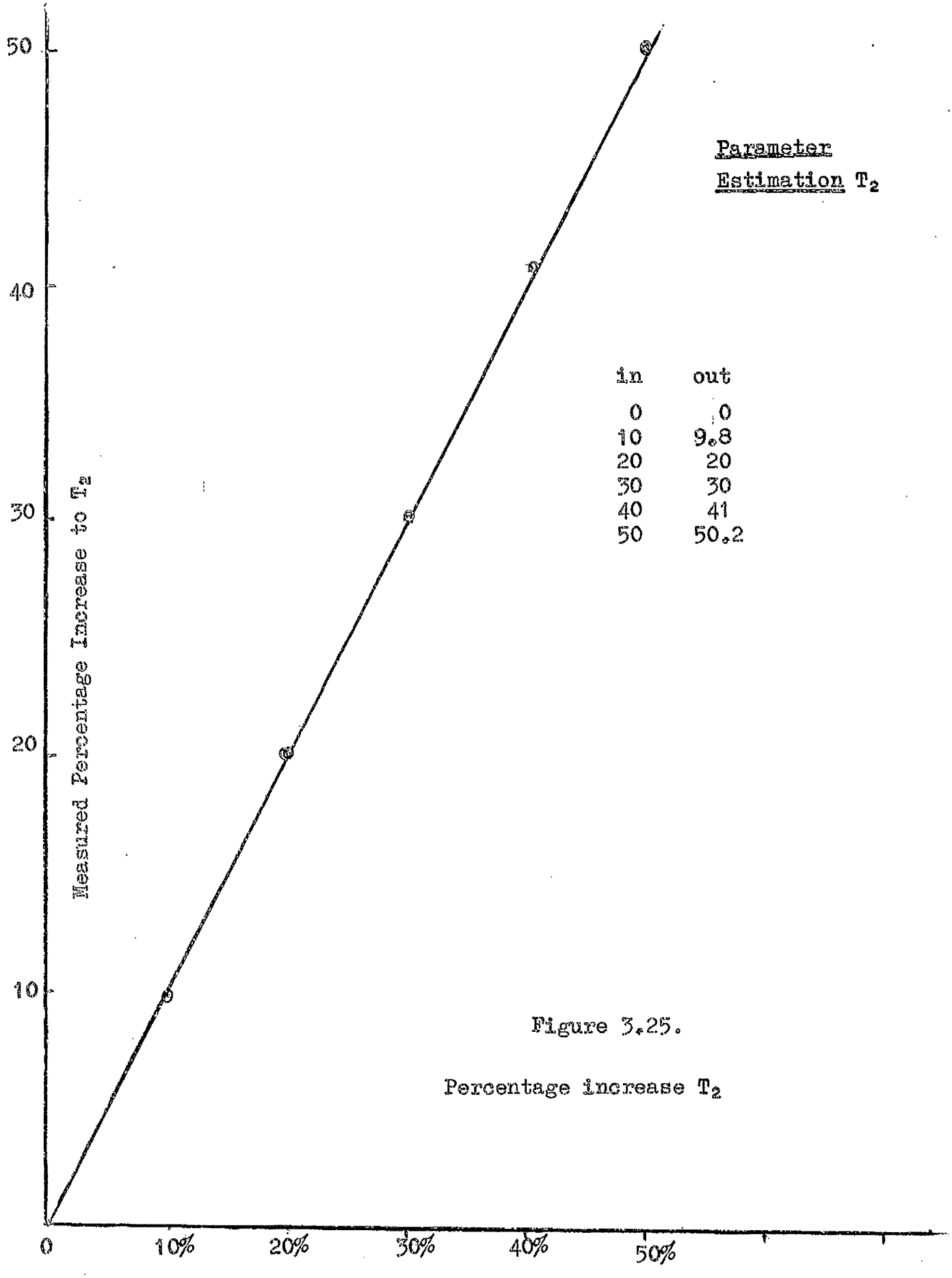

Parameter Estimation T_2

in	out
0	0
10	9.8
20	20
30	30
40	41
50	50.2

Figure 3.25.

Percentage increase T_2

in paragraph 1.3.3. then it has been shown that on line derivation of the unknown transfer function parameters can be achieved by the methods outlined above in a manner which is both accurate and linear. Variations in the parameter values have been transformed into variations about fixed bias voltage levels which are fed directly, or in the case of T_m, via an inverse function generator to the adaptive mechanism which them formulates the plant model and any other variables within the dynamic control computer.

CHAPTER 4

BOILER DYNAMICS

4.1. Introduction.

A steam generator is basically a heat exchanger where an input feed water flow is converted by heat energy into output steam flow at a determined pressure and temperature. Heat is supplied by the burning of fuel - oil, gas or coal - in a furnace and transferred by a process of radiation, conduction and convection first to the water walls, where the complex mechanism of nucleate boiling produces steam at saturation temperature, and thence to the superheater banks where the steam is raised to the desired degree of superheat.

Steam generation is a dynamic process both the steady state and transient behaviour of a particular plant configuration being determined by the laws of thermodynamics and hydrodynamics. Because of the difficulty inherent in the rigorous application of these disciplines to a dynamic polyphase system, plant design has been, until quite recently, largely an empirical exercise and plant control purely empirical. However two valid simpliciations can be made.

Firstly though a wide diversity in design of steam generators exist, in any steam plant there are two main flow paths, one being the path associated with heat generation comprising fuel, combustion air and combustion products and the other the steam generation path comprising the water and steam circuit. Thus we have a firing and combustion stage and a steam generation stage. This division is

generally accepted by authors and though simple in concept its effect is far reaching, enabling, for example, the knowledge obtained of water - steam dynamics in nuclear and experimental electric boilers to be directly applied to fossil fired industrial units.

Secondly to a large extent the use of superheaters enables the steam pressure and temperature to be regarded as two separate parameters over which independent control can be exercised. For a constant pressure the degree of superheat can be altered by variation of the gas damper angle or of the desuperheater spray water mass flow with a minimum of system interaction.

4.2. Firing and Combustion Stage.

4.2.1. Gas and Oil.

Due to the absence of fuel transport or combustion lags the response of a gas fired furnace is practically instantaneous. The ignition time of atomised oil particles though longer than that of coal gas still constitutes no meaningful delay and the heat release in an oil fired furnace is dominated by the fuel pump response. Ergin (1) has characterised the oil pump response by a single lag, a result subsequently confirmed experimentally by Ferrier (2).

4.2.2. Pulverised Coal.

In the United Kingdom the majority of steam plants above 300,000 lbs per hour are fired with pulverised fuel. A typical layout of the fuel feed system is shown in Figure 4.1. Raw coal-fed

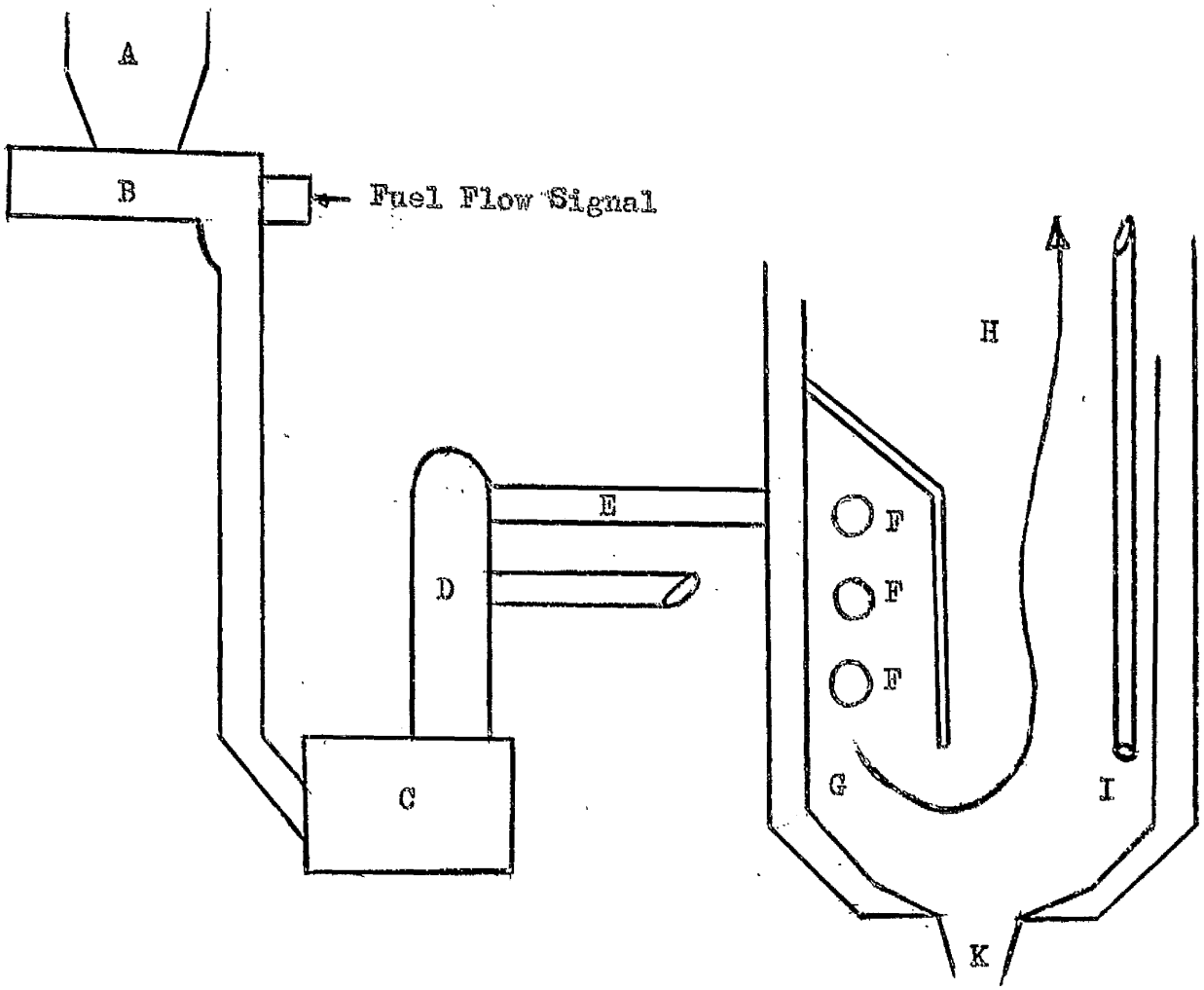

A. Coal Bunker

B. Coal Feeder

C. Grinder

K. Slag Exit

F. Burners

G. Flame Space

H. Main Furnace

I. Water Walls

Fig. 4.1. Pulverised Coal. Firing and Combustion Stage.

from a bunker-passes through the feeder to the grinding mill where a stream of hot air blows the finely ground particles through a sieve to regulate fineness and thence via pipework to the burners in the furnace. The coal dust is ignited in the flame space and the hot products of combustion pass up the furnace, transmitting heat to the water-steam circuit. What is required is a relationship between a signal input to the coal feeder and the consequent heat release in the furnace.

Various dynamic phenomena are involved in the link between these two factors: free fall of coal from feeder to mill, mill grinding characteristics, separation of coarse and fine grained material in the sifter, pneumatic transport to the burners and final mixing and combustion in the furnace. The last two phenomena are most easily dealt with. Hazard (3) has shown that the mechanism of mixing and combustion can be represented by a single lag of the order of 40 milliseconds and, as a reasonable approximation, the mechanism of pneumatic transport is analogous to a simple dead time.

Little is known theoretically about the dynamics of the grinding mill which dominates the fuel response. Some static characteristics have been given by Hiorns (10) and Frensch (4) and Schneider (5) have undertaken some theoretical analysis but their work is unobtainable at the time of writing. Profos (6) established empirical relationships for three different types of firing system.

(a) $F = \frac{e^{-T_s s}}{1+T_1 s} \quad C_F$. Direct injection slow regulation

(b) $F = \frac{1}{(1+T_2 s)(1+T_3 s)} \cdot C_F$. Direct injection fast regulation

(c) $F = \frac{1}{(1+T_4 s)} \quad C_F$. Bunker feed system.

where F is defined as the intensity of the furnace fire and C_F is the signal for adjusting the firing rate. The relationships were developed for a Sulzer monotube boiler where:

$$T_1 \ \underline{\Omega} \ . \ 50 \text{ seconds}$$

$$T_2 = T_1 \ \underline{\Omega} \ . \ 60 \text{ seconds}$$

$$T_3 << T_2 \ .$$

$$T_4 \ \underline{\Omega} \quad 20 \text{ seconds.}$$

The results for a bunker system were subsequently confirmed by Frensch in 1961 (Loveridge (7)). Bunker firing is usually associated with smaller units where preground coal is stored in a bunker close to the furnace and fed via a pneumatic pump to the burners. The time response of such a system is dependent only on the pump dynamics and is thus quite fast.

The physical difference between the terms slow regulation and fast regulation is not immediately obvious and Profos does not elaborate. However an explanation must lie in the type of control exercised over the components of the firing system. Loveridge (7) has suggested that one of the lags in expression (b) may be due to the fuel distribution network

and flame/furnace geometry effects. The lack of transit delay in this expression is interesting and a partial explanation may lie in the quasi fluid characteristics of the turbulent air dust mixture.

A detailed account of the measurement of a pulverized fuel system transfer function has been given by Quack (8). A constant flow of water was pumped through a tube projecting about 6 feet into the furnace gas stream, heat input to the tube being estimated by measurement of entry and exit water temperature. The initial transfer function obtained was of the form

$$\frac{e^{-sT}}{(1+T_1 s)(1+T_2 s)} \qquad \text{where } T = 25 \text{ seconds.}$$

$$T_2 \gg T_1$$

$$T_2 = 60 \text{ seconds.}$$

As the time response of both the coal feeder and the heat measuring system were known the transfer function of the mill could be derived and was found to be of the form

$$\frac{e^{-sT'}}{1+T_3} \qquad \text{where } T' \underline{\Omega} \text{ 5 seconds}$$

$$T_3 \underline{\Omega} \text{ 60 seconds}$$

Using radio active tracer elements Bishop (11) conducted tests on the firing system of a 100,000 lb per hour unit in the U.K. and his results confirm those of other workers. The measured dead time was of the order of 35 seconds and the mill time lag 45 seconds.

4.2.3. Variation in Calorific Value.

Unlike oil or gas which have fairly constant calorific values the calorific value of coal varies widely. Results published by Stafford (9) show the variation in calorific value of coal supplied to a typical power station. The values of consecutive 8 cwt lots of coal, corresponding to a 1 minute supply for a 120 mw unit, were measured and a variation of between 4070 to 10,000 Bthu/lb obtained.

4.2.4. Furnace Efficiency.

The efficiency of any furnace configuration is dependent on the mass flow of combustibles and tends to fall as the mass flow increases. A detailed description of the process is given in Appendix 1.

4.2.5. Heat Flux Measurement.

Direct measurement of heat flux in boiler tubes can now be accomplished accurately by a thermo-couple method developed by Northover (12). The thermocouple meter shown in Figure 4.2. consists of a hollow cylinder, one end of which is closed by a disc of thermo electrically dissimilar material. The walls of the cylinder are welded to the boiler tube.

Heat flowing into the disc distributes radially to the cylinder walls, the thermal resistance of the disc creating a radial temperature gradient. The emf developed between the centre of the disc and the cylinder wall is proportional to the magnitude of the disc radial

temperature difference and therefore to the heat flux. The device is simple, robust and inexpensive and the average output of a matrix of such meters will yield the average value of the heat flux into the riser tubes.

Northover has stated (42) that the time response of the meter is of the order of one second and that the noise content of the output signal is approximately one percent. If short term variations in the flame shape are averaged out by a matrix of meters the remaining noise consists of very high frequency components which can be easily filtered.

An instrument which can measure boiler heat flux quickly and directly obviously provides the boiler control engineer with a new approach to boiler control philosophy.

4.2.6. Summary.

It is apparent that the transfer function of the firing and combustion stage of a pulverised coal unit is of the form

$$F = \frac{K_c e^{-Ts}}{(1+T_f s)(1+T_m s)} \quad C_f$$

where F is heat released in the furnace and C_f is the signal adjusting the fuel rate. T is a dead time associated with the mill and pipework configuration and is hence constant. K_c is dependent on fuel calorific value, dryness and furnace efficiency and is a variable. T_m is the

grinding mill time lag and is a function of coal hardness and dampness and will be assumed to be a variable. T_f is the lag associated with the coal feeder which can be considered constant, and is of the order of 4 to 5 seconds for a large unit.

4.3. Steam Generation.

4.3.1. The Boiling Process.

The advent of nuclear reactors as heat sources in steam generators has led to intensive research into the dynamics of boiling steam water mixtures. Much experimental work has been undertaken and several theories advanced. It is relevant to review this work briefly before proceeding to study the dynamics of large boiling water systems.

4.3.2. Regimes in Boiling.

If the wall temperature of a submerged heating element is raised above saturation temperature convection currents circulate the superheated liquid and steam is evaporated from the free liquid surface. When the wall temperature is increased bubbles of vapour form on the metal surface at favoured spots, grow, and finally rise from the wall but condense before reaching the free liquid surface. A further rise in wall temperature produces larger and more numerous bubbles which transmit steam directly to the free surface.

With the onset of vapour bubble formation the rate of heat transfer to the liquid increases. Accelerated boiling causes the heating element to become covered with a thin layer of vapour which has a poor

coefficient of heat transfer and for a given dissipation in the element high wall temperatures result.

The exact mechanism of nucleation or bubble formation is unknown though Rohsenow (13) has shown quantitatively that only a small fraction of the heat is transferred to the vapour in the bubble and that the rise in heat transfer rate associated with nucleate boiling occurs due to the local agitation or mixing in the liquid caused by bubble motion. Bubbles tend to form at special points on the heated surface and the boiling process is greatly influenced by surface conditions. Quantitative results have been given by Jackobs (14). A high degree of local superheat is essential - of the order of one to two hundred degrees - before bubble formation can occur, the exact degree of superheat being dependent on surface conditions. The liquid agitation caused by subsequent bubble motion immediately reduces local superheat to the order of a few degrees.

Boiling in Vertical Tubes.

Of particular interest to the boiler engineer is the study of boiling in vertical heated tubes. Subcooled water enters the bottom of the tube and a mixture of steam and water exits from the top. The various regimes of boiling exist along the length of the pipe, some idea of their relative position being possible by local measurement of heat transfer coefficients.

Rohsenow (15) has shown that the heat transfer rate in the non-boiling and subcooled (i.e. no net generation of vapour) boiling regimes

is determined by t_x where

$$t_x = (t_w - t_L)$$

t_w = tube wall temperature

t_L = liquid temperature

There is some dependence on liquid velocity in the non-boiling zone but at the onset of nucleate boiling bubble agitation largely determines the heat transfer rate and the effect of fluid velocity is not great.

Empirical correlations by Jens (16) for surface boiling of upward flowing water in electrically heated stainless steel tubes produced an equation for heat transfer in the boiling zone which has been used, in a modified form, by subsequent workers in the study of boiler dynamics

$$\text{Heat flow} = C(t_x)^4 \quad \text{where } C = \left\{ \frac{e}{1.9}^{P/900} \right\}^4$$

P is the absolute pressure and e the exponential function.

Recent research work into the behaviour of boiling fluids in heated tubes has been carried out by several groups of workers. The apparatus usually consists of a vertical tube heated uniformly by electrical means, or in the case of Dengler (17) by external steam jackets, through which is forced water at high pressure. Exit qualities of up to 100% have been obtained for the correct simulation of once through boilers. Facilities were available to measure steam quality and wall fluid temperatures and the steam void fraction at various positions in the

pipe has been monitored by several authors. Dengler used soluble radioactive tracer elements with counter units on the tube wall. Laird (18) and Haywood (19) have proposed systems whereby the attenuation suffered by gamma rays passing through the two phase fuild gives an indication of the water content of the mixture.

Detailed photographic evidence of the two phase flow patterns has been provided by Gunther (20) for horizontal channels, by Tippets (21) for vertical pipes and Zahn (22) for horizontal tubes.

The general flow pattern experienced is summarised by Becker (23) and shown in Figure 4.3. The pipe can be divided into several regions.

1. Subcooled Region.

Cool water enters the bottom of the pipe and the upward flowing liquid is brought to saturation condition by two mechanisms.
(a) temperature of the liquid increases due to heat transfer from the walls
(b) the local saturation temperature decreases because of pressure decrease owing to wall friction effects and reduction in static head.

2. Subcooled Boiling.

Bubbles form on the tube wall detach themselves but later condense in the main fluid stream. No net vapour is generated though the resulting bubble agitation results in increased heat transfer rate.

3. Bulk Nucleate Boiling.

In this region there is a rapid increase in the number and size of the bubbles generated and hydrodynamic effects tend to concentrate

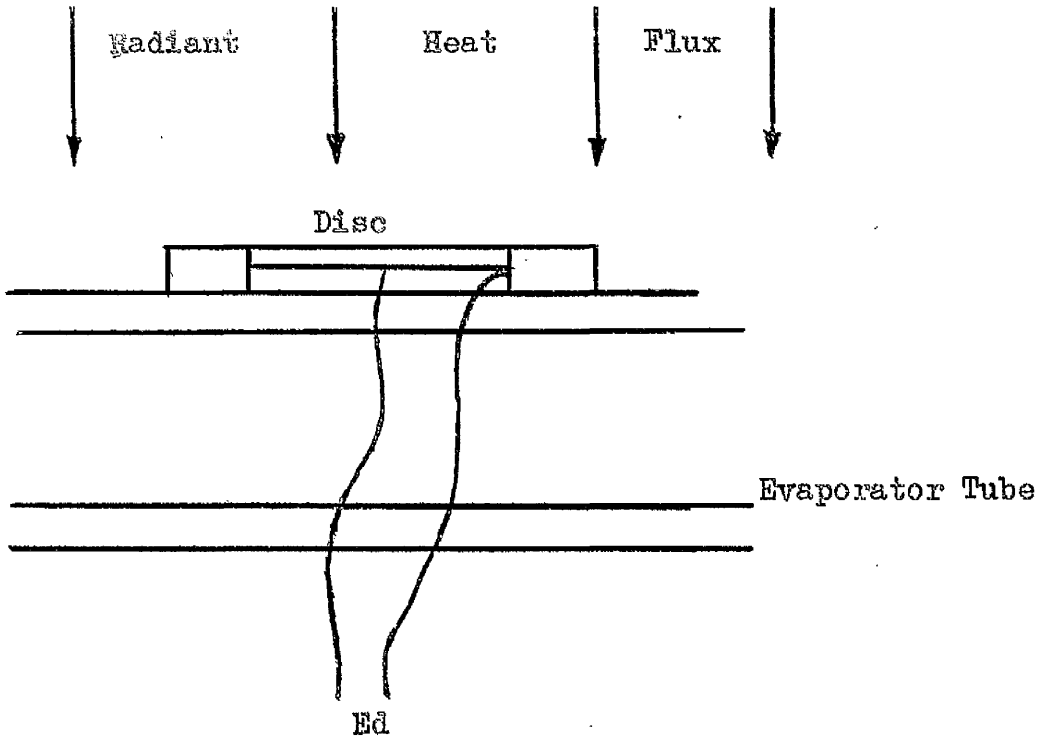

Figure 4.2. Heat Flux Measurement.

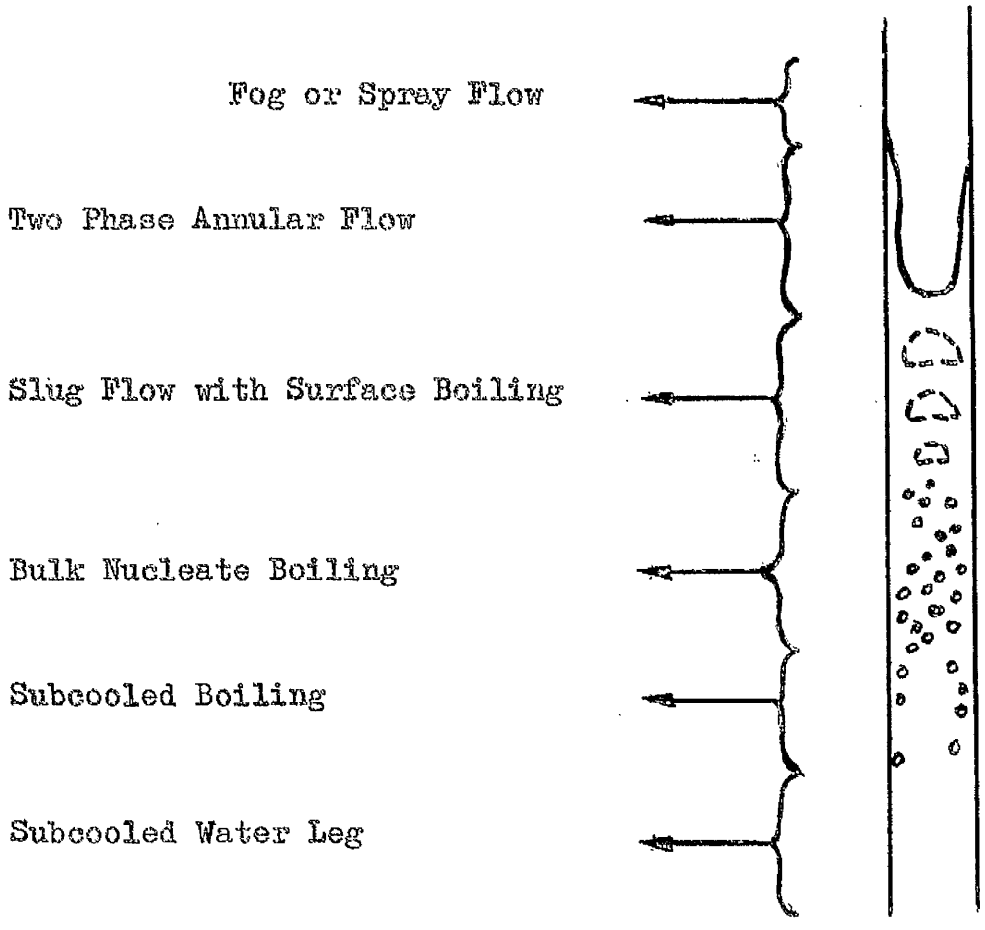

Figure 4.3. Boiling Regimes in a Vertical Tube.

the upward flowing vapour in the centre of the fluid stream.

4. Slug Flow.

Slugs of a finely divided froth of vapour and liquid alternate periodically with a configuration which consists of a thick calm layer of liquid against the wall face and a central zone of high vapour concentration. The periodicity of alteration has been measured by Tippets and found to be of the order of 0.1 seconds for one configuration.

According to Dengler heat transfer in this zone is largely convective the nucleate boiling processes being suppressed by increased liquid velocity caused by the increased kinetic energy of the vapour phase. Departure from nucleate boiling is indicated by a rapidly rising wall/fluid temperature differential. Heat transfer rate is largely dependent on bulk fluid velocity.

5. Two Phase Annular Flow.

In this region the walls of the tube are covered with a fine layer of boiling liquid and the bulk of the tube volume being occupied at low mass velocities and high steam qualities by a dispersion of droplets in a continuous vapour phase and at high mass velocities and low steam quality by an emulsion of liquid and vapour. Vigorous boiling takes place in the thin water layer and water evaporates into the vapour core, there being a simultaneous diffusion of droplets to the water film.

The net effect is a decrease in the water layer thickness in the direction of flow. The increasing velocity of the vapour causes a

shear stress to occur at the phase boundary, the resulting ripple formation tending to destroy the water layer continuity and leading at high steam velocities to dry wall conditions with associated burn out dangers above critical heat flux levels.

A thin film of vapour effectively exists between the wall and liquid layer resulting in poor heat transfer and very high wall temperatures. Swenson (24) has derived empirical heat transfer relationships for this region where the evaporation process is sometimes termed film boiling.

6. Fog or Spray Flow.

With the final collapse of the wall liquid layer the flow resembles a low density mist or spray. Surface boiling no longer exists and heat transfer rate is influenced mainly by the vapour velocity.

4.3.3. The effect of flow rate, heat input and pressure variations.

The observed effect of increasing the entry liquid velocity or increasing entry liquid subcooling is to suppress the initiation of boiling, lengthen the liquid leg and move the various boiling regimes further upstream. The resulting loss of hydrostatic head in the nucleate boiling zone adversely effects vapour velocity and subsequent heat transfer rates in the upstream regions which more than counteracts the slight increase of heat transferred in the subcooled zone. The net result is a decrease in the exit fluid dryness for a given heat input.

A rise in heat input for a given liquid velocity has the reverse effect while a pressure increase, by raising saturation temperature, again

suppresses nucleate boiling and lengthens the tube water leg.

4.3.4. Theoretical Studies.

The difficulty of estimating a Reynolds number to determine the frictional pressure drop of a two phase fluid is one of the factors hindering the theoretical solution of the annular boiling problem. Tentative empirical relationships advanced by Martinelli (25), which were based on a comparison of single and two phase flow pressure drops, are quite widely used and have had a fair measure of success. Several recent theoretical models have been published, the two limiting cases of homogenuous flow (completely mixed) and annular flow (completely separated) being normally considered.

The homogeneous model is relatively easy to analyse as the two phase mixture is considered as a single fluid with zero steam/water slip velocity. The study of annular flow systems has been undertaken by Hillier (27) and Chisholm (28). The latters' theoretical model being subsequently supported experimentally by Laird.

The dynamics of the intermediate bubble flow regime (partially mixed) which dominate a large portion of the boiling volume have proved difficult to analyse. Levy (26) has proposed a momentum exchange model which assumes that the liquid and vapour phases have equal friction and head losses. Such an assumption implies a differing flow structure between vertical and horizontal flow which has little support from the literature. However fair correlation has been obtained by this model

with the earlier empirical results of Martinelli.

A variable density single fluid model with zero phase slip has been proposed by Bankoff (29) in which he assumes that the vapour bubbles have a fixed distribution across the tube diameter, the distribution being a maximum at the tube centre. Though fair correlation has been obtained with earlier workers the model appears unrealistic because, as zero void friction is assumed at the tube walls, additional friction due to wall bubble formation has been neglected.

4.4. Boiling Water Systems.

Some early work by Haywood (30) on the dynamics of a simple natural circulation down comer riser drum loop demonstrated the theoretical equivalence of the hydrodynamic and thermodynamic circulation theories. A homogeneous riser fluid was assumed and thus poor correlation was obtained between practical and theoretical results due to the neglect of the steam slip effect.

When steam slip exists the steam velocity is greater and the water velocity less than under corresponding conditions in homogeneous flow and since the water forms the main mass of the mixture under normal conditions the increase of momentum of the riser mixture is less in slip flow. The effect of slip is consequently to reduce the acceleration pressure drop below that produced by the homogeneous theory. Also, since the water velocity is reduced by slip flow, the water occupies a greater percentage of the tube volume in slip flow than under corresponding conditions in homogeneous flow, so that the effect of slip is to increase

the gravitational pressure drop above that predicted by the homogeneous theory.

Later experimental work incorporating this effect was undertaken by Laird and Anderson (31).

Both used an electrically heated riser section, investigated the relationship between flow rate and input power and the conditions which led to circuit instability. Though the results of Laird are by far the more comprehensive, Anderson's work is interesting because a computer simulation of the theoretical model was made and direct comparison obtained between the model and the physical system.

As expected the model was sensitive to the value chosen for the steam slip. Experimental work was carried out using a variety of pipe diameters.

The effect of pressure variations on steady state down comer and hence riser mass flow rates has been highlighted by Laird and his results are summarised in Figure 4.4. It is obvious that for pressure changes of the order of 200 lbs/sq.in. the operating region of 1000 lbs/sq.in. mass flow changes are small, the largest being approximately 5% for a 1 1/4" diameter pipe at 100% of maximum heat input.

Instability or circuit breakdown was investigated by both sets of authors. Parameter perturbation on Anderson's computer model showed that the riser time delay was a key factor and its removal enhanced stability at all power levels. This result is in keeping with the

assumption that pressure change resulting from incremental riser steam flow is the dominant factor in the system stability.

Tests performed by Laird show that:

(a) At any pressure, for each tube diameter there is a limiting rate of pressure fall beyond which natural circulation fails.

(b) There exists for any boiler pressure a circulation velocity beyond which circulation failure cannot be produced by pressure drop. This result is illustrated in Figure 4.5.

Result (a) is well known and is a consequence of down-comer ebullition which leads to a loss of hydrostatic head, circuit failure and possible tube burn out. The ramifications of result (b) appear to have been overlooked by some later workers (33) and (34), in the field of boiler water level control. Drum pressure fall due to increased steam load is accompanied by a rapid increase in evaporation rate with consequent drop in the length of the water leg and surge in drum water level.

Drum level can be restored by a reduction in feed-water flow rate. However the decrease in flow of the relatively low enthalpy feed-water increases average drum and down-comer enthalpy which for a given rate of pressure fall hastens the onset of down-comer ebullition. If by correct boiler design the danger of ebullition can be removed or at least minimised a wider turn down of feed flow is obviously possible and greater control can thus be exercised over boiler water level transients. Clearly this is a case where controllability can be designed into the boiler system.

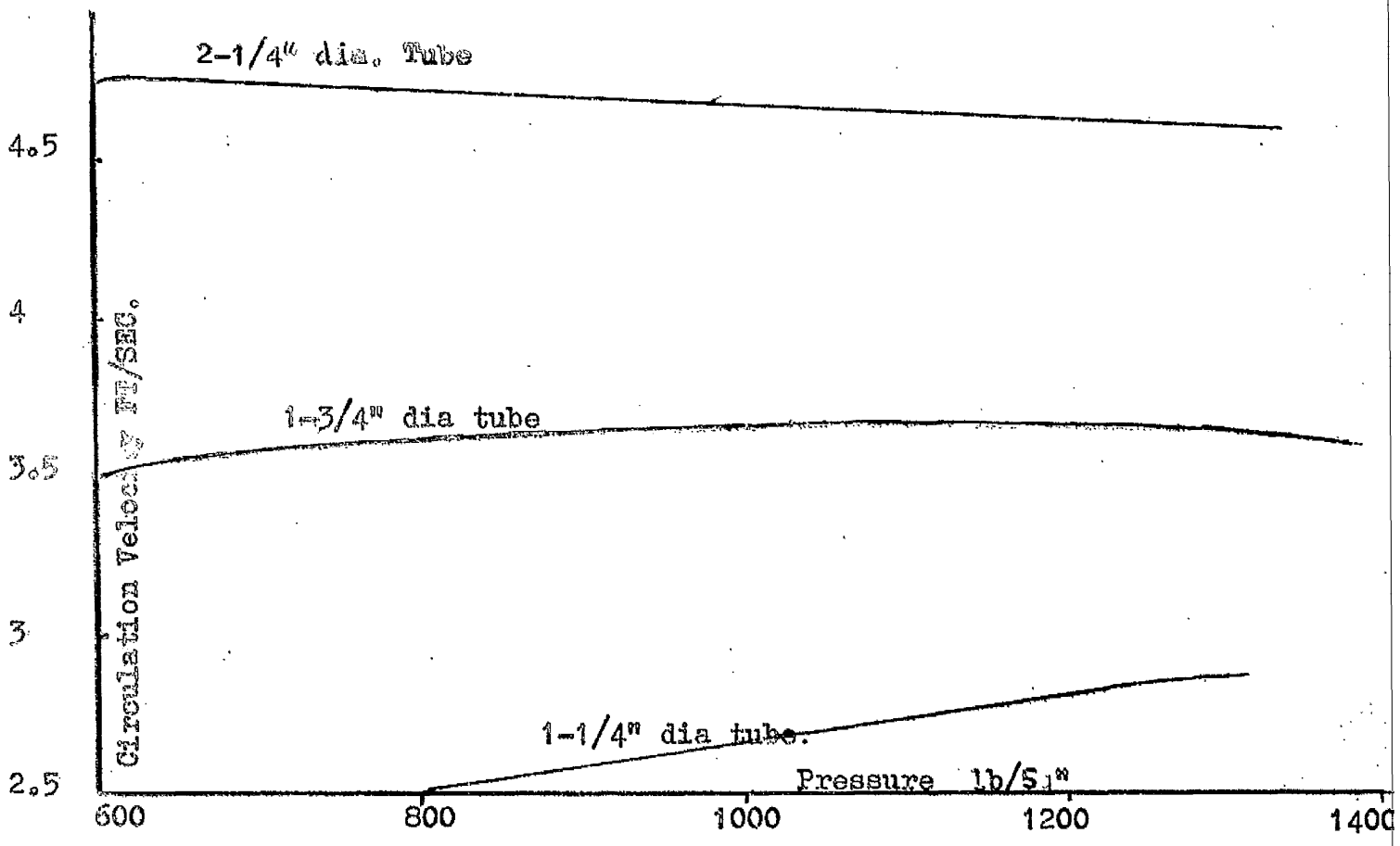

Figure 4.4. Effect of Pressure on Circulation Velocity.

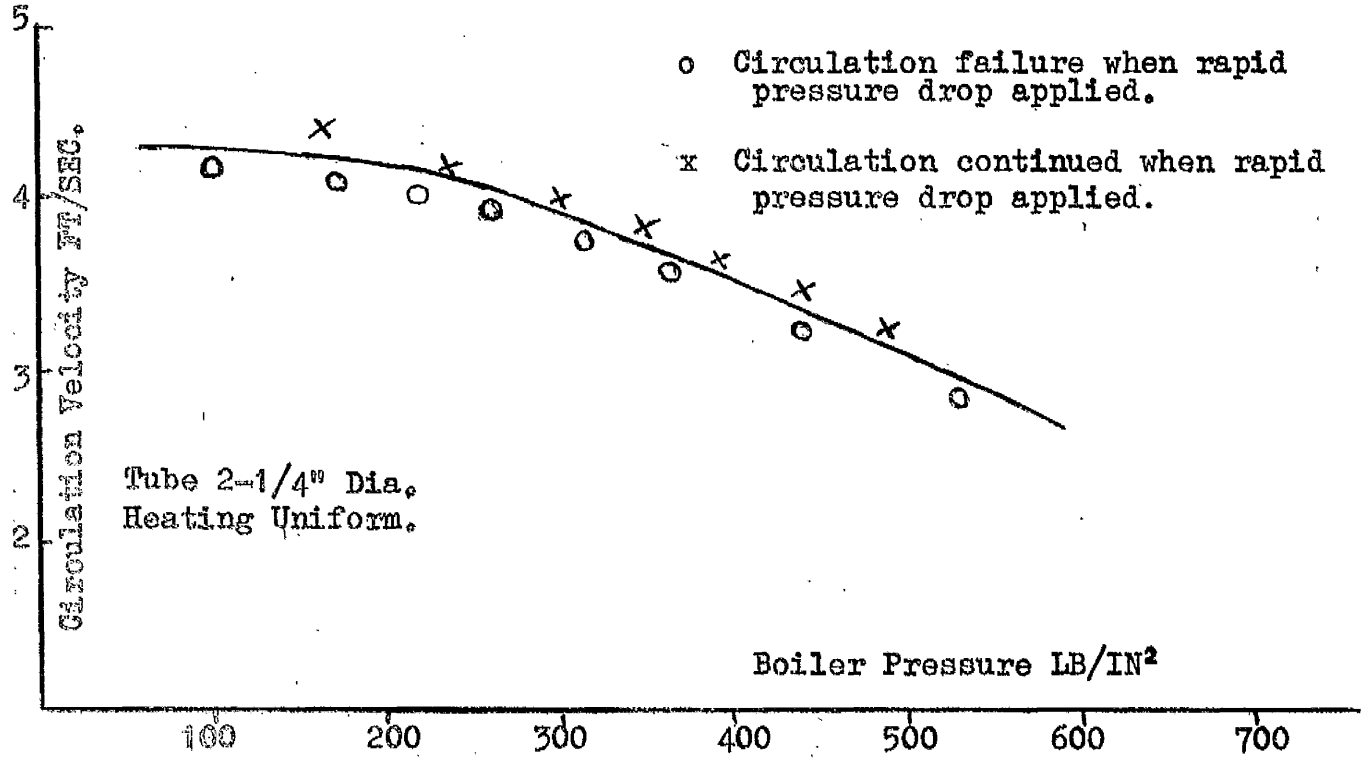

Figure 4.5. Initial Circulation Velocity - Boiler Pressure

The direct relevance of the results outlined from uniformly heated systems, such as those used by Laird and Anderson, to furnace fired waterwalls with non-uniform heating was demonstrated by Laird, who showed experimentally that the system behaviour was dependent only on the heat input and not on the manner of its distribution around the tube.

4.5. Theoretical Boiler Models.

Some elementary work on boiler modelling has been undertaken by Profos (6) for a once through boiler and by Thomas (35) for a shell type boiler. Although these boilers differ widely in structure both authors related the dynamic response of the heat output (steam section) to changes in the heat input (combustion) by a simple first order lag.

The first comprehensive dynamic model of a boiler comprising drum down-comer riser and superheater sections was proposed by Chien (36). His analysis was based on an oiled fired naval unit and from the twenty-one linear differential system equations which he developed six transfer functions, relating the input variables of steam flow, feed flow and heat, to the output variables of water level and drum pressure, were derived. The method of analysis used in this work which was later supplemented (37) has formed the basis of much subsequent work on boiler dynamics.

4.5.1. The Chien Model.

The boiler was divided into four sections (a) the gas path (b) riser down-comer loop (c) drum and (d) superheater. The time lag

associated with the economiser was considered to be of sufficient magnitude to justify its exclusion from the dynamic analysis. An outline of the flow process is shown in Figure 4.6.

The system equations of flow, heat transfer and state can generally be described by sets of nonlinear partial differential equations, the solution of which can be obtained either by numerical methods of by linearising about a steady operating point in the state space. To avoid prohibitive computational difficulties Chien opted for the latter approach. While introducing essential mathematical simplicity, linearisation also produces errors which are dependent not only on the incremental deviation from the operating point but also on the degree of nonlinearity involved and are thus particularly manifest in the high order nonlinear relationships associated with heat transfer.

Continuity momentum and energy equations were derived for the various sections and, where necessary, empirical relationships utilised. A summary of the assumptions made and of the general method of approach in the various sections will now be given.

(a) Down-comer Riser Loop.

Simple incompressible fluid flow was assumed to exist in the down-comer with no heat transfer, temperature everywhere being equal to drum temperature. Entry and head losses were accounted for and down-comer liquid kinetic energy was assumed completely dissipated in a mud drum which terminated the down-comer. This part of the loop was thus represented by a simple dead time.

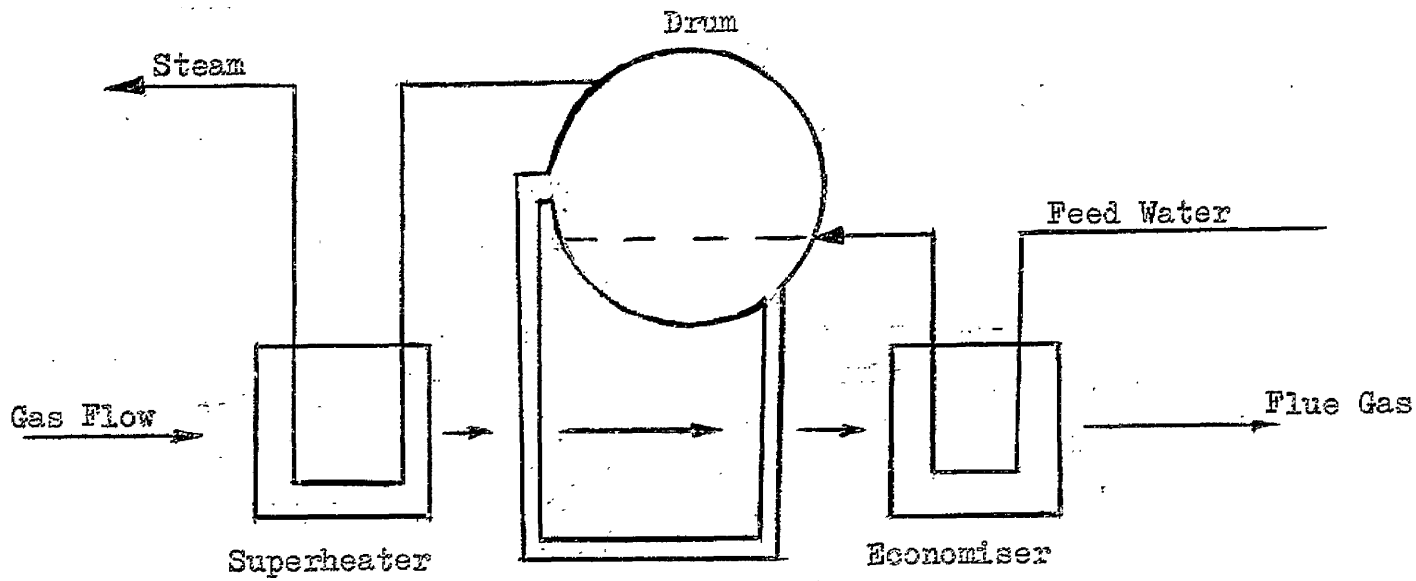

Figure 4.6. The CHIEN Model.

The riser dynamics were described by continuity, momentum and energy equations. Entrance loss, frictional, gravitational and inertial terms were included though the rate of change of kinetic energy of the riser fluid was assumed negligible in comparison with the heat energy involved. The liquid vapour mixture was assumed to be at the drum liquid temperature, steam slip to be zero and steam quality constant throughout the riser length. Heat transfer from the walls to the boiling mixture was based on the empirical relationship developed by Jens modified by the assumption that of the total heat transferred one quarter is used to bring the water to saturation temperature and the remainder used in evaporation. The modified boiling heat transfer equation used was

$$\text{Heat transferred} = K_g \, (t_x)^3$$

where t_x is the difference between wall and drum saturation temperatures and K_g the heat transfer coefficient which is derived from steady state conditions.

(b) Drum

Heat and mass balance equations were set up to describe the drum dynamics. The vapour phase is assumed to be at the saturation temperature and the liquid temperature to be uniform except for a thin surface layer where a temperature gradient existed due to turbulence. It was postulated that the inter-phase mass transfer rate was proportional to this liquid/vapour temperature differential which could be experimentally derived from boiler measurements and was of the order of $10^{\circ}F$.

(c) Gas Path

Gas temperature was taken as proportional to fuel flow and the heat transfer mechanism was assumed to be purely convective. In a modern boiler a fair proportion of the heat transfer is radiative and this latter assumption is not quite accurate, a point which has been made by Markson (38).

As the gas flow path was from the superheater to the riser banks, the heat transferred to the superheater was first calculated to obtain correct values for the gas temperature at the entrance to the riser section.

System equations.

The relevant system equations will now be listed for the various boiler sections. A nomenclature is included at the end of this chapter.

Down Comer.

Momentum equation

$$-(P_w - P_B) = f_r \frac{L_r}{gA_D^2 D_D} \frac{(W_w^2)}{\rho_w} - \rho_w L_r + \frac{W_w^2}{2g\rho_w A_D^2}$$

$$+ \frac{L_r}{gA_D} \frac{dW_w}{dt} .$$

On the RHS of this equation the first term represents friction, the second gravitational head, the third entrance losses and the fourth inertia. P_B is the drum pressure and P_w the pressure in the mud drum at the bottom of the down comer.

Riser.

state equation

$$\frac{1}{\rho} = \frac{x}{\rho_B} + \frac{(1-x)}{\rho_w}$$

continuity equation

$$W_w - W = L_r A_r \frac{d\rho}{dt}$$

momentum equation

$$(P_w - P_B) = \frac{L_r}{gA_r}\frac{dW}{dt} + f_r \frac{L_r}{g}\frac{W^2}{\rho A_r^2 D_r} + L_r \rho + \frac{1}{2gA_r^2}\frac{W^2}{\rho}$$

$$+\left\{\frac{W^2}{\rho A_r^2 g} - \frac{W_w^2}{\rho_w A_r^2 g}\right\}$$

Energy.

$$Q_B + W_w h_{wb} - x h_{fg} - (1-x)h_{wb}$$

$$= \frac{d}{dt} A_r L_r h \rho.$$

where h_{fg} is the enthalpy of evaporation and h is the enthalpy of the mixture.

Heat Input to Riser Tubes.

Heat transfer from riser tube wall into boiling liquid is given by

$$Q_B = K_g (T_{WB} - T_B)^3$$

Thus heat input to riser tubes

$$Q_{gB} - Q_B = M_B C_B \frac{dT_{WB}}{dt}$$

where M_B and C_B are respectively the mass and heat capacitance of the riser tube bank.

Drum.

Liquid heat balance.

$$(1 - x)W\,T_B + W_i\,T_i - W_w\,T_w - W_e - h_B = \frac{d}{dt}\,(M\,T_w).$$

where W_e is the rate of evaporation from the drum liquid and M is the mass of the liquid phase.

Liquid mass balance

$$W_i + (1 - x)W - W_w - W_e = \frac{dM}{dt}.$$

Steam mass balance.

$$W_e + xW - W_B = \frac{d}{dt}\left\{ V_B \rho_B \right\}$$

where V_B is the Volume of the steam phase,

also

$$\delta V_B = -A\,\delta y$$
$$\delta M = A \rho_w \delta y$$

where A is the liquid surface area and y the water level.

State equations.

The following state equations are assumed.

$$W_e = K_e (T_w - T_B)$$

$$\delta T_B = K_T \delta P_B$$

$$\delta \rho_B = K_B \delta P_B$$

where K_T and K_B are derived from steam tables for the range of steady state values considered.

Gas Path.

$$\delta T_c = K_f \delta W_f$$

where T_c is the combustion gas temperature entering the super heater banks, (see Figure 4.6.), and W_f the fuel flow rate.

Average gas temperature at superheater bank is given by

$$T_{gs} = T_c - \frac{1}{2} \frac{Q_{gs}}{C_g W_f}$$

where Q_{gs} is the heat input into the superheater walls and C_g is related to the heat capacitance of the combustion gases

$$C_g = C_c \left\{ 1 + \frac{W_A}{W_f} \right\}$$

Here the function $\frac{W_A}{W_f}$ represents the air fuel ratio and C_c is the heat capacitance of the combustion gases which is assumed to be constant.

Heat transfer rate from the hot gases to the superheater wall is assumed

given by

$$Q_{gs} = K_{gs} (W_f)^{0.6} (T_{gs} - T_{ws}).$$

K_{gs} being determined from steady state conditions.

Gas temperature at entrance to riser is thus

$$T_{CB} = T_c - \frac{Q_{gs}}{C_g W_f}$$

Average gas temperature at riser banks.

$$T_{gB} = T_{CB} - \frac{1}{2} \frac{Q_{gB}}{C_g W_f} = T_c - \frac{Q_{gs}}{C_g W_f} - \frac{1}{2} \frac{Q_{gB}}{C_g W_f}$$

Heat transfer rate to riser bank

$$Q_{gB} = 0.6 K_{gB} (W_f)^{0.6} (T_{gB} - T_{wB})$$

4.5.2. The Stafford Simulation.

In 1962 Stafford (9) programmed the Chien equations on a digital computer using physical data obtained from a natural circulation power station boiler. The boiler physical parameters are listed in APPENDIX 2 and the simulated transient responses obtained are shown in Figure 4.7., 4.8. and 4.9. The responses are seen to be of a quite simple nature and correspond closely to the earlier published results of Chien for a naval boiler.

These transient responses can be approximated closely by a series

Time Response of Pressure and Water Level to a Step Increase in Fuelling Rate

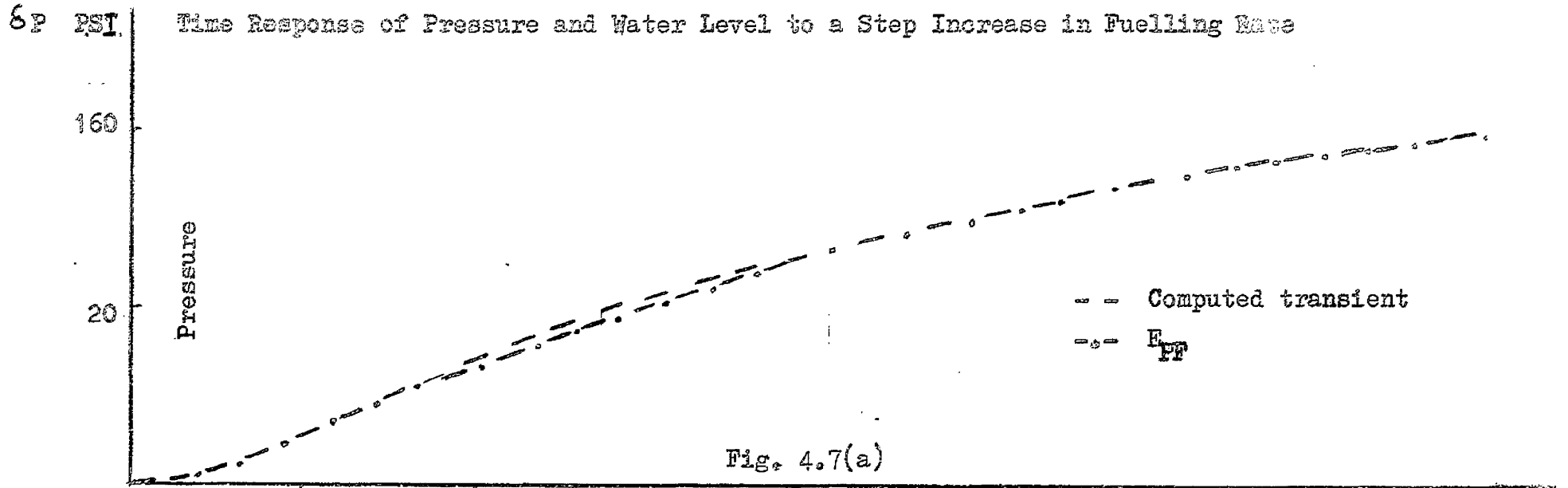

Fig. 4.7(a)

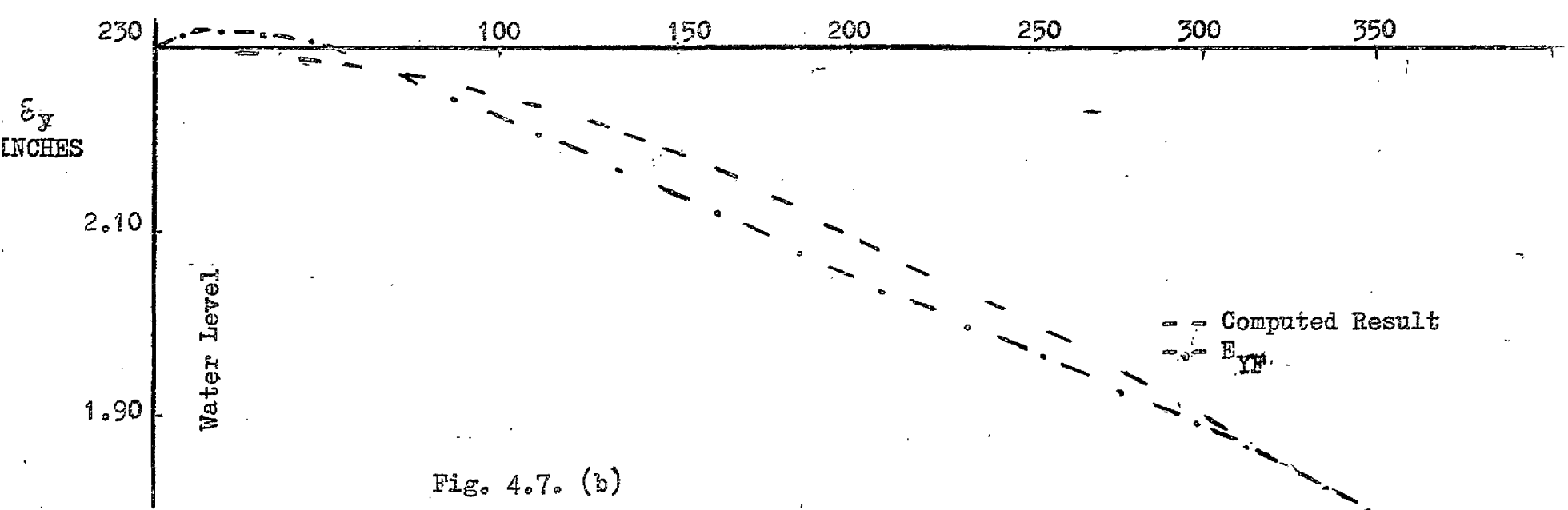

Fig. 4.7. (b)

Time response of pressure and water level to a step change in throttle position.

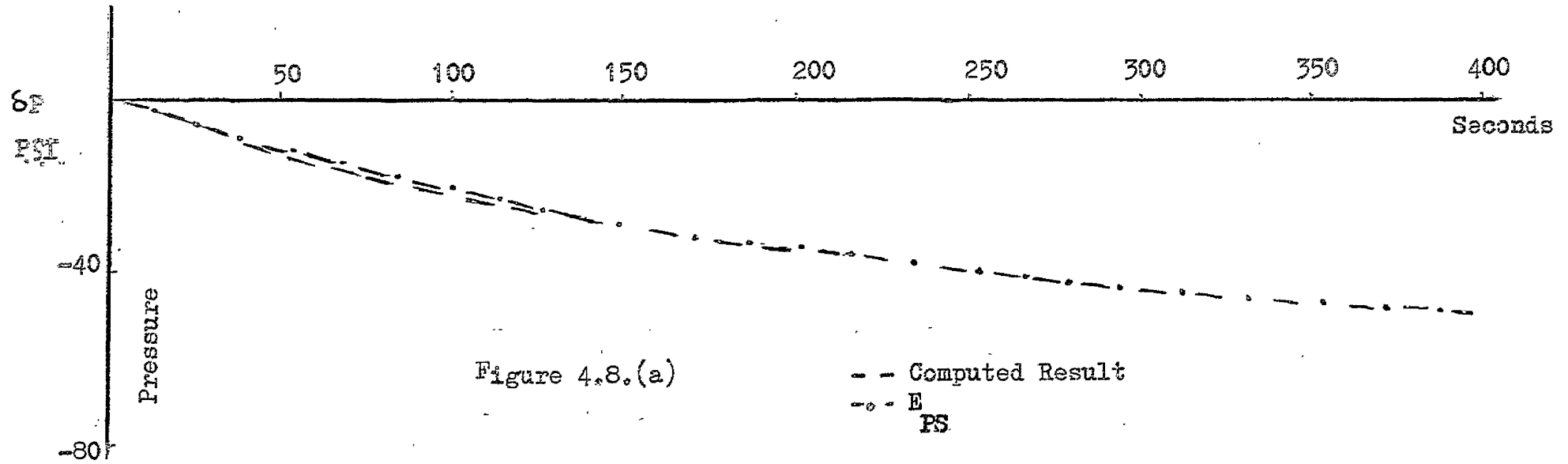

Figure 4.8.(a)

- - Computed Result
-∘- E_{PS}

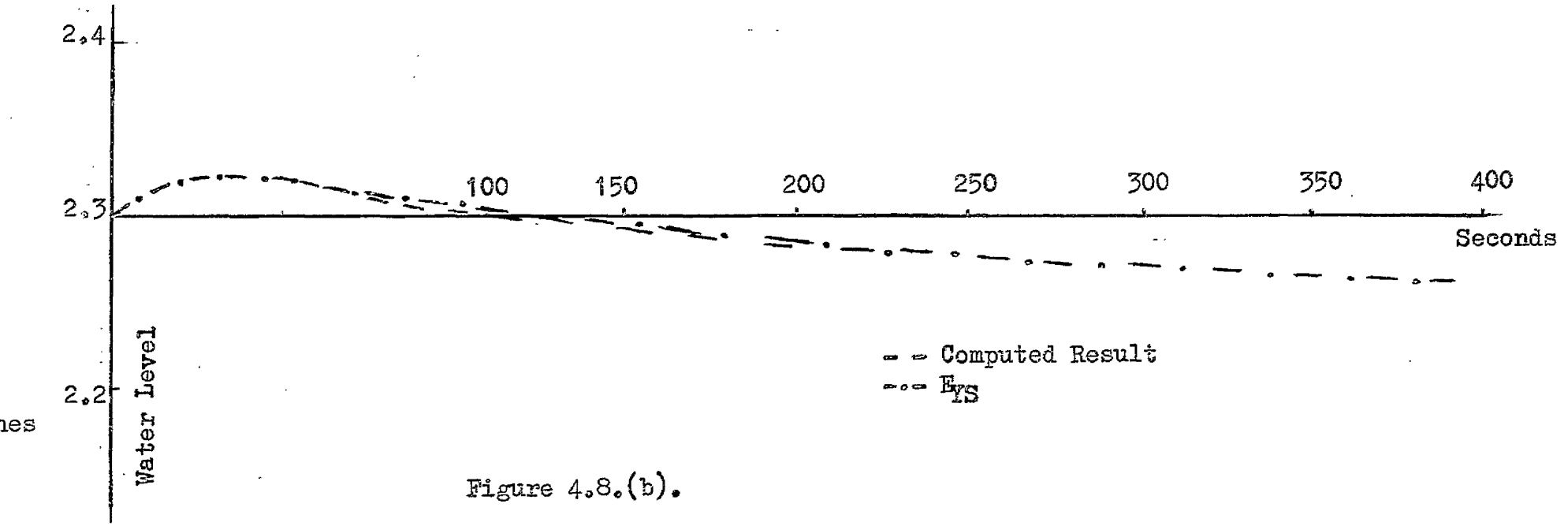

- - Computed Result
-∘- E_{YS}

Figure 4.8.(b).

Time response of pressure and water level to a step change in feed water flow rate

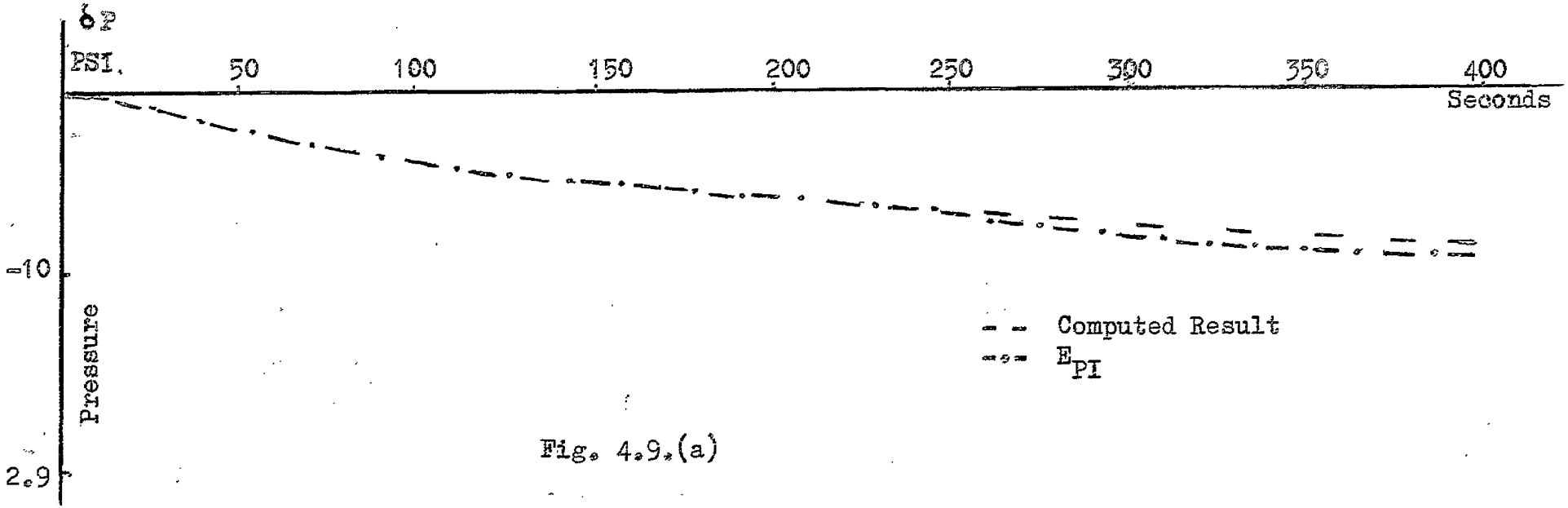

Fig. 4.9.(a)

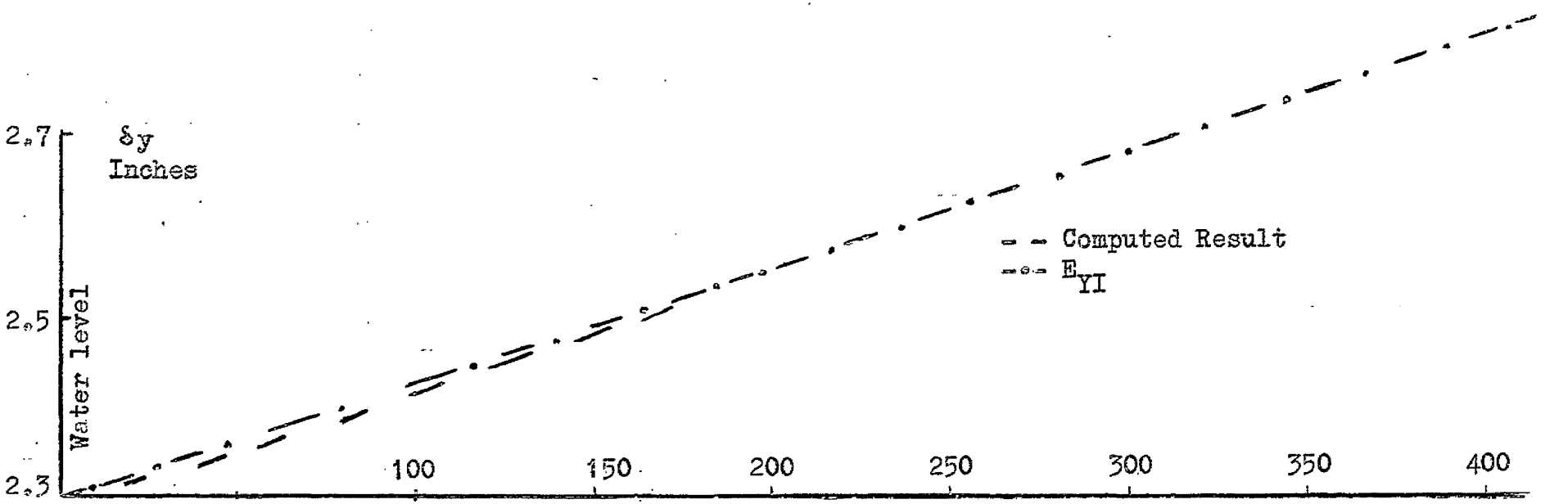

Fig. 4.9.(b)

of linear transfer functions. If E_{PF}, E_{PS}, E_{PI}, E_{YF}, E_{YS} and E_{YI} represent the boiler transfer functions relating pressure and water level variations to changes in the heat input rate from the furnace, steam flow rate and water flow rate we have

$$E_{PF} = \frac{K_1}{(1 + 25S)(1 + 250S)}$$

$$E_{PS} = \frac{-K_2}{(1 + 250S)}$$

$$E_{PI} = \frac{-K_3}{(1 + 250S)}$$

$$E_{YF} = \frac{K_4}{(1 + 20S)} - \frac{K_5}{S}$$

$$E_{YS} = \frac{K_6}{(1 + 20S)} - \frac{K_7}{(250S + 1)}$$

$$E_{YI} = \frac{K8}{S}$$

where

$$\frac{K_1}{K_2} = 4.62; \qquad \frac{K_4}{K_5} = 0.545; \qquad \frac{K_6}{K_7} = 0.404;$$

and $K_8 = 0.000093$.

The time responses of the above transfer functions are shown for comparison in Figures 4.7., 4.8 and 4.9. and can be seen to approximate closely to the computed responses. Thus in this operating range the steam generation section can be represented by the linear block diagram

of Figure 4.10. The complete block diagram relating pressure with steam flow and fuel demand is shown in Figure 4.11. This diagram, which is derived directly from Figures 4.10 and the equation derived in paragraph 4.2.6, represents the model structure which will form the basis of this study.

4.5.3. Parameter Variation.

The behaviour of the parameters K_c, T_f and T_m of Figure 4.11. have already been discussed in section 4.2. and we will deal here exclusively with the behaviour of the parameters K_1, K_2 T_1 and T_2. These parameters have been derived from a small signal linear analysis of a complex nonlinear system about a fixed operating point in the state space and their variation at different operating points must now be examined.

If T_2 is regarded as being associated entirely with the steam capacitance of the boiler a clearer insight may be obtained by redrawing the steam generation section of Figure 4.11. in the form shown in Figure 4.12. Here K is the factor of proportionality relating pressure to the evaporation rate F_G

and (a) $T_2' = T_2K.$ (b) $K_2 = {}^1/K.$

(c) $K_1' = K_1 K.$

The transfer function relating heat flow into the walls of the riser and boiling section and the evaporation rate is thus of the form

$$\frac{K_1'}{1 + ST_1}$$

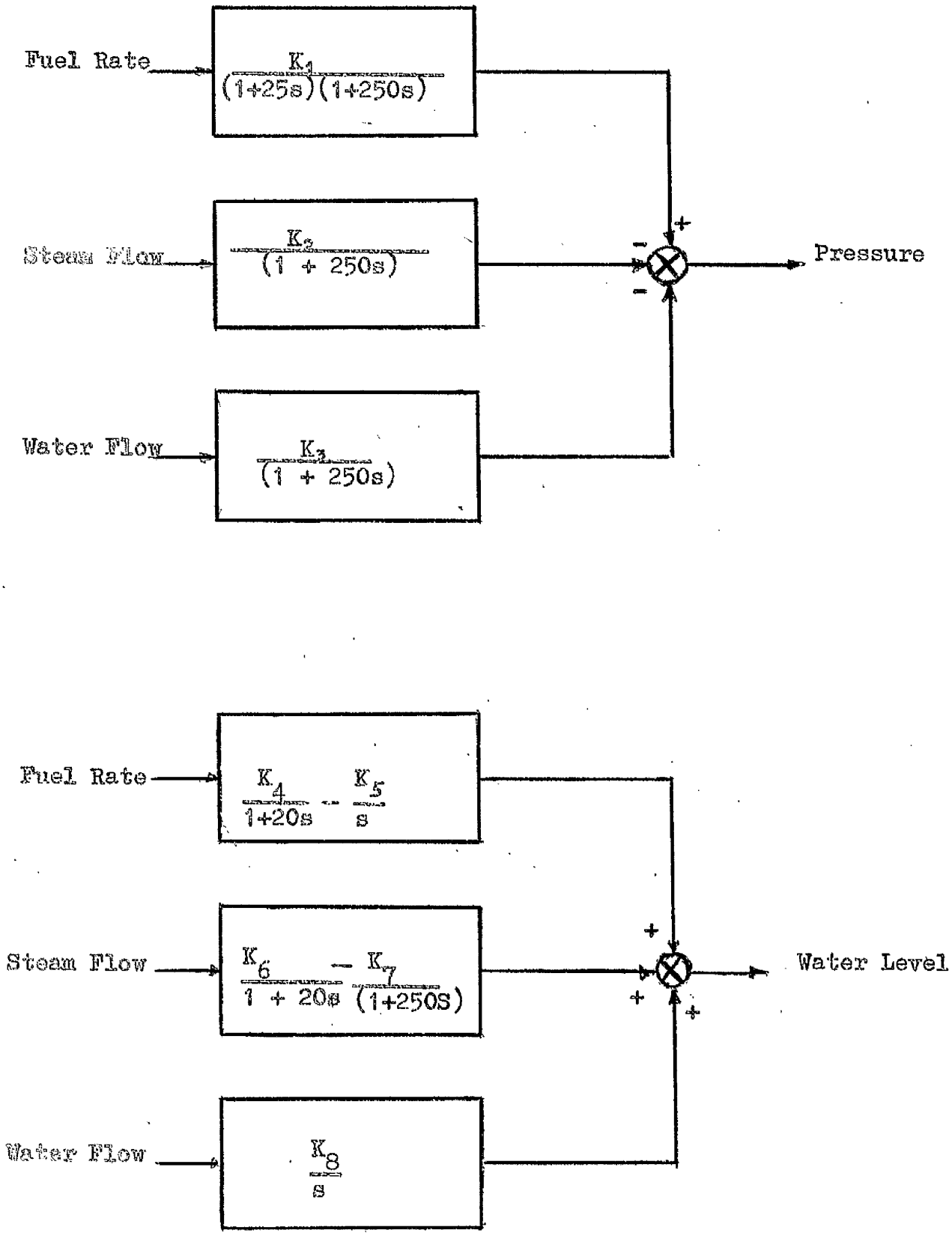

Block Diagram of Steam. Generation Section.

Figure 4.10.

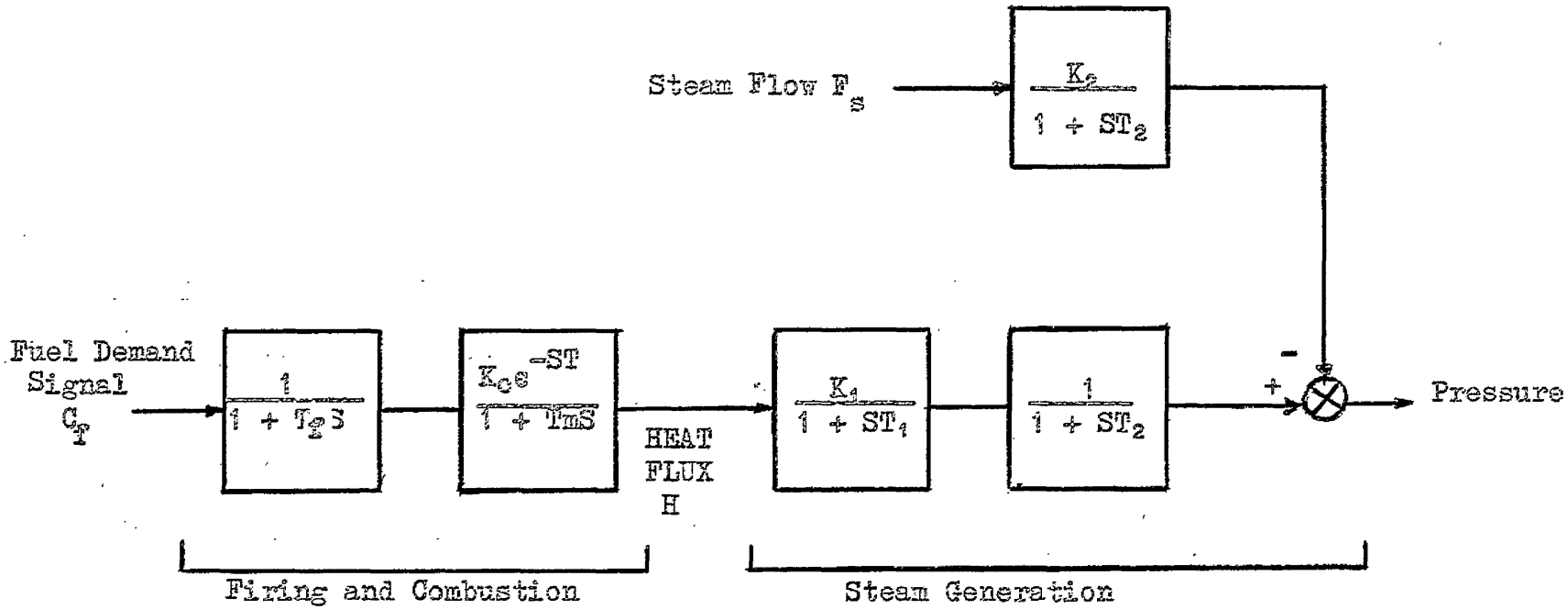

T_1 = 25 seconds

T_2 = 250 seconds.

Boiler Model

Figure 4.11.

The lag T_1 is related to the time required to establish the new wall temperature conditions which determine the heat transfer rate to the boiling water mixtures and to the time required to establish the new steaming conditions.

The first time interval is related to the thermal inertia of the heated water wall iron mass and is constant for any configuration. As we have seen earlier (paragraph 4.3.2.) the process of nucleate boiling tends to dominate the mixing and heat transfer rates in the boiling zone and thus little error seems to be incurred in assuming that the second time interval is also constant. T_1 can therefore be regarded as invariant.

K_1' is proportional to the heat transfer coefficients existing at the various sections of the riser tube walls corresponding to the different boiling regimes and is thus dependent on the evaporation rate. In the boiler model K_1' and hence K_1 will be regarded as a variable and its variation must be taken into account in the adaptive control process.

For any heat input rate the evaporation rate F_G is proportional to the drum pressure. The factor of proportionality K is a function of the boiler physical constants and steam tables indicate that it is invariant over a fairly wide range of pressure variation.

Morton has derived a value of K for a naval boiler which indicates the order of magnitude of this constant.

$$K = 5.31 \text{ lbs of steam per sec. per } lb/\square".$$

After leaving the riser steam enters the separator and a mass balance may be performed between entrance and exit steam flow. Any imbalance has a direct effect on the drum pressure via the boiler incremental capacity. T_2' which is a function of pressure and the boiler steam volume.

Thus, for a steam space of volume V cubic feet containing w llb of steam, the steam specific volume is given by

$$V_s = \frac{V}{w}$$

If a further mass δw is accumulated in the steam space the change in specific volume is given by

$$V_s + \delta V_s = \frac{V}{w + \delta w}$$

$$\therefore \quad w V_s + \delta w \; V_s + w \, \delta V_s + \delta w \, \delta V_s = V = V_s w$$

$$\delta w \, V_s + w \, \delta V_s = 0$$

$$\therefore \quad \frac{\delta V_s}{V_s} = - \frac{\delta w}{w}$$

Now for steam at pressure P

$$P V^N = \text{constant} = K_v$$

$$\frac{\delta P}{P} + N \frac{\delta V_s}{V_s} = 0$$

$$\therefore \quad \delta P = N P \frac{\delta w}{w} = \frac{NP}{w} \int (F_G - F_S) \, dt.$$

where F_G = generation rate of steam

F_S = steam flow rate.

so $$P = \frac{N\,P\,V_s}{V} \int (F_G - F_S)\ dt$$

$$= \frac{N\,P\,K_V\,P^{-N}}{V} \int (F_G - F_S)\ dt$$

$$= \frac{1.13\,K_V}{V\,P^{0.13}} \int (F_G - F_S)\ dt \qquad \text{for } N = 1.13 \text{ (Lewitt (41))}$$

$$\therefore T_2' = \frac{V\,P^{0.13}}{1.13\,K_V}$$

It is thus seen that T_2 is relatively independent of moderate pressure changes and can thus be regarded as constant.

Of the four parameters K_1, K_2, T_1 and T_2 considered therefore only K_1 need by regarded as variable and hence appropriate changes in its magnitude will render the steam generation section of Figure 4.11 valid over a wide range of steaming conditions.

4.6. Water Circuit.

If the drum is assumed to be a pure capacitance then water level is dependent on a mass balance of down comer, feed and separator mass flows. Following Estrada (32) we can thus perform a steady state mass balance at the drum end separator.

Drum mass balance.

$$\frac{d\,M_L}{dt} = F_F + F_D - F_X$$

Separator mass balance.

$$F_D + F_S = F_R$$

$$F_S = F_G,$$

where

M_L = drum water mass

F_F = feed liquid flow lb/sec

F_X = down comer liquid flow lb/sec

F_D = liquid flow out of separator lb/sec

F_R = riser mass mass flow into separator lb/sec.

It has been shown by Laird (paragraph 4.4.) that large pressure variations have little effect on the down comer and hence riser steady state mass flow rates and, at a given value of heat input, F_R can be taken as constant and virtually independent of pressure. A transient change in F_S which alters drum pressure and subsequently F_G has no effect therefore on F_R and any transient change in F_D will depend solely on a change in the generated steam rate.

Thus

$$\delta F_D = -\delta F_G.$$

and

$$y(t) = \frac{1}{L_1} \int \delta F_G(t) \, dt,$$

where y is the water level and L_1 a time constant related to the drum physical constants.

A complete transient relationship between steam flow rate and drum water level must include one other factor and this will now be discussed.

The quantity of water in the entire heat addition section is dependent on the evaporation rate, being less at high values than at low. A change in steam evaporation rate therefore results in a mass transfer of water between the down comer drum section and the heat addition section which is accomplished in the transient by a change in down comer mass flow rate. The magnitude of this phenomenon, which is directly responsible for the experienced non minimum phase response of boiler water level, is proportional to the relative water mass stored in the heat addition section at high and low rates of evaporation.

An empirical relationship has been derived by Morton (33) for a naval boiler and shown in Figure 4.13. Unless adequately controlled this effect sets an upper limit to the maximum rate of change of steam generation obtainable. Mortons relationship $f(F_G)$ which can easily be obtained experimentally for any boiler system, is valid only at constant pressure and during transient conditions a pressure connection factor must be added.

As the mass transfer of water is equal to the change in void fraction of the heat addition section we have the pressure volume relationship

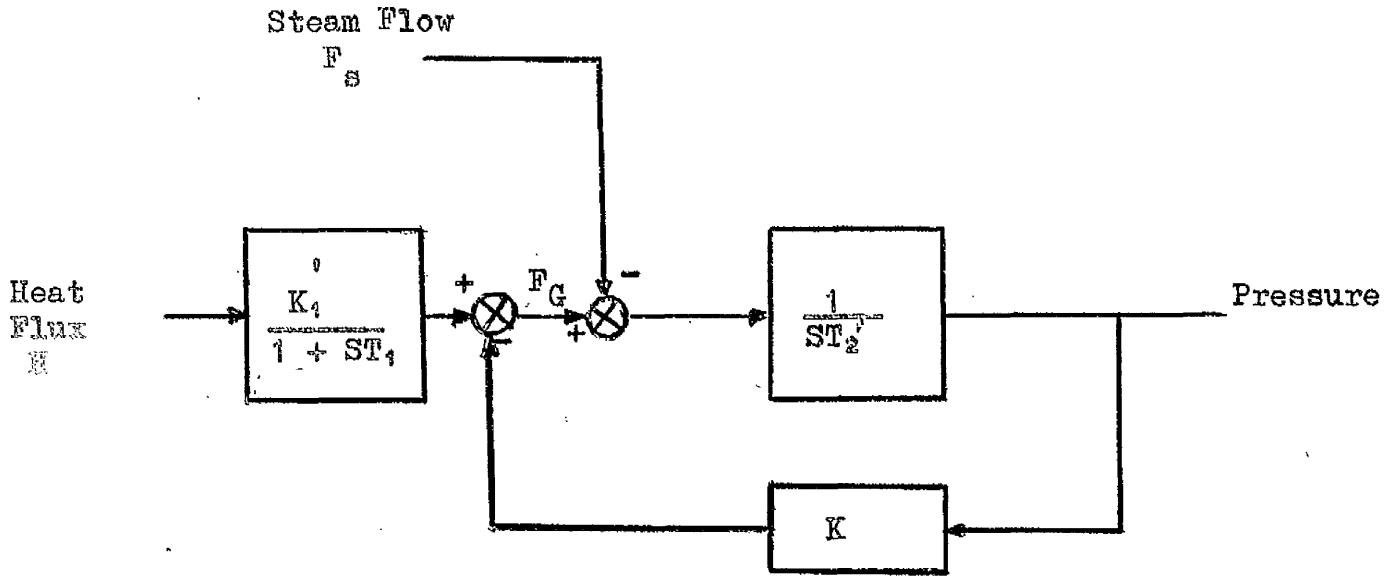

F_G = Steam Generation Rate.

Block Diagram Relating Heat Flux and Pressure.

Figure 4.12.

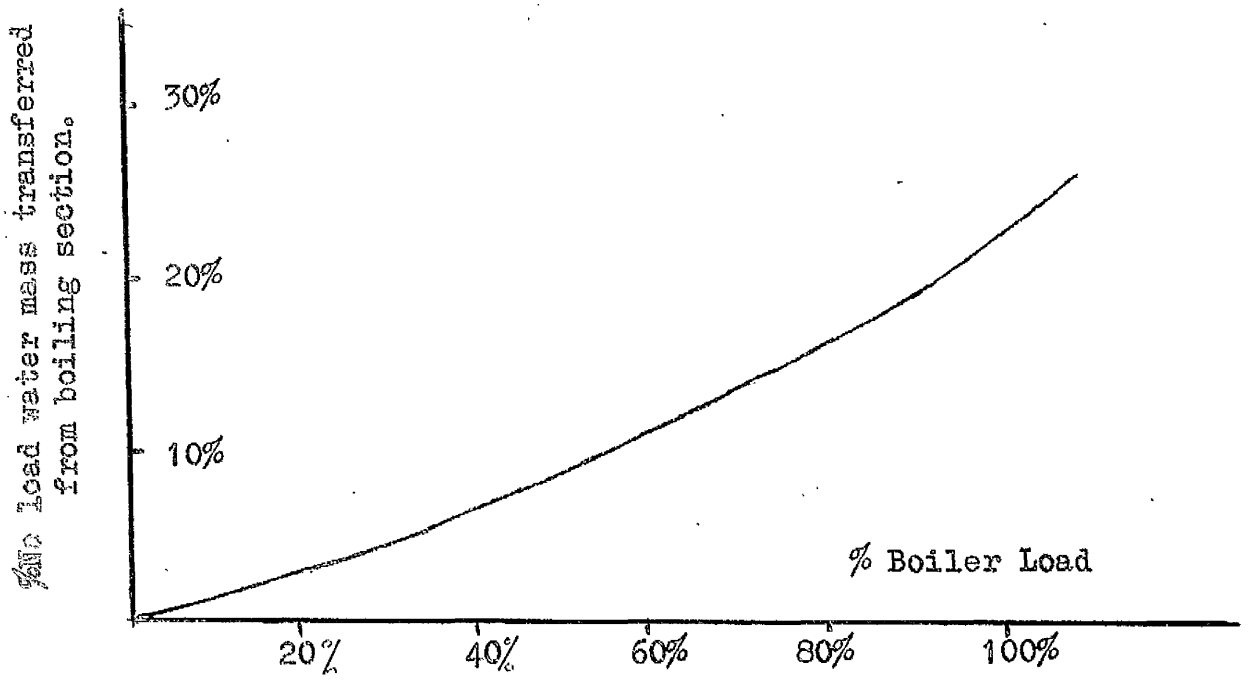

Figure 4.13. Water Mass Transfer in a Naval Boiler (After Morton).

$$P\,V^{1.13} = K_V = \text{constant}$$

$$\therefore \quad \text{LOG } V = 0.885 \text{ Log } \frac{K_V}{P}$$

$$V = \text{Antilog} \left\{ 0.885 \log \frac{K_V}{P} \right\}$$

If W = mass of water transferred then

$$W = F_G \; f(F_G) \; f_1(P)$$

where

$$f_1(P) = \text{Antilog} \left\{ 0.885 \log \frac{K_V}{P} \right\}$$

As W is proportional to F_G then W(s) must be proportional to $F_G(s)$ and thus the transient nature of this phenomenon can easily be estimated.

A block diagram showing the complete transient relationship between steam flow and water level is illustrated in Figure 4.14. In this diagram L_2 is a constant relating the inch change in water level per pound of water transferred from the boiling section into the down comer loop.

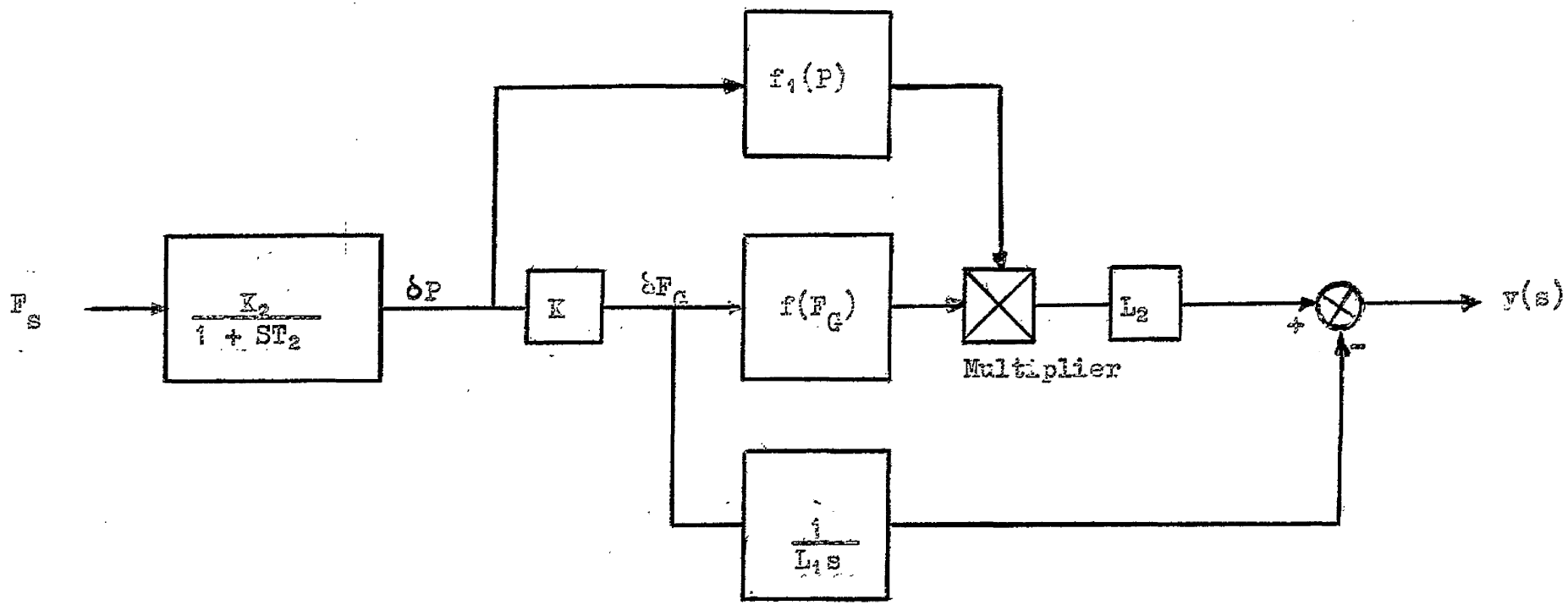

Block Diagram showing transient relationship between steam flow and water level.

Figure 4.14.

Chien Equations - Nomenclature

P_B = drum pressure

P_W = mud drum pressure

ρ_B = saturated vapour density corresponding to P_B

ρ_w = saturated liquid density corresponding to P_B

x = quality of mixture leaving riser

ρ = density of liquid vapour mixture leaving riser

T_i = feed water temperature

T_B = saturation temperature corresponding to P_B.

T_w = drum and down comer liquid temperature

T_{wS} = superheater tube wall temperature

T_{wB} = riser tube wall temperature

T_{gs} = average gas temperature of superheater banks

T_{gB} = average gas temperature at riser banks

T_c = combustion gas temperature entering super heater banks

h = enthalpy of riser mixture

h_B = enthalpy of saturated vapour corresponding to P_B

h_{WB} = enthalpy of saturated liquid corresponding to P_B

h_w = enthalpy of drum and down comer liquid

h_{fg} = enthalpy of evaporation corresponding to P_B

Q_{gs} = heat input rate from hot gases to into super heater tube walls.

Q_B = heat input rate from riser tube walls into boiling liquid

Q_{g3} = heat input rate from hot gases into riser tube walls

W_f = fuel mass flow rate

W_A = air mass flow rate

W_i = feed water mass flow rate

W_w = down comer mass flow rate

W = riser mass flow rate

W_e = mass evaporation rate from drum liquid surface

W_B = steam mass flow rate from drum into super heater

M = mass of drum liquid

M_B = mass of riser tubes

V_B = volume of vapour phase in drum

y = drum liquid level

I_r = riser tube length

A_D, A_r = down comer and riser cross sectional areas respectively

D_D, D_r = down comer and riser diameter respectively

C_B = heat capacitance of riser tubes

C_c = heat capacitance of combustion gases

K_{gs} = heat transfer coefficient from hot gases to super heater wall

K_{gB}, K_g = heat transfer coefficients from combustion to riser tubes and from riser tubes to boiling liquid respectively.

K_e = evaporation rate constant of drum liquid

f_r = friction coefficient of riser and down comer tubes

K_T, K_B = constants for state equations of saturated steam.

CHAPTER 5

CONTROLLER APPLICATION

5.1. Introduction.

The normal form of boiler combustion control is shown in Figure 5.1. where the three term controller can be realized either pneumatically or electronically (1). In practice controller set up is generally a purely empirical exercise though, when properly adjusted, such a control system produces satisfactory control characteristics for steady state operation. Three term control is, however, less than ideal for large transient load changes due mainly to the large thermal lags associated with the combustion and boiling processes.

A decrease in boiler response time would obviously be desirable as it would enhance the stability of the overall system during load transient conditions. Dual mode operation of a boiler thus seems attractive; the normal control terms being operative under steady steaming conditions and, at the onset of a transient, the system control being switched to a dynamic mode. The object of the dynamic controller would be to restore the boiler pressure in the minimum possible time in a manner compatible with the normal system constraints.

5.2. Dynamic Optimization.

The relatively simple monotonic time function relating fuel demand input and steam pressure which was derived in chapter 4 permits the realization of the dynamic optimization scheme of chapter 1 in

analogue rather than digital form. The general outline of such a control scheme will now be given.

A schematic diagram of a boiler dual mode control system is shown in Figure 5.2. the control computer performing the four distinct functions of

(a) mode switching

(b) switching function generation

(c) parameter estimation

(d) model adaptation

In the proposed boiler adaptive control system parameter estimation will take place only after the initiation of a transient with model formulation and switching function generation being completed before the end of the first possible switching interval. The elements of the control computer are shown schematically in Figure 5.3.

5.2.1. Mode Switching.

In a dual mode control scheme mode switching is initiated by a sudden load change of either polarity which is greater than a specified minimum value. In a boiler the load change F_s can be ascertained at any load value by measuring the resulting deviation of the boiler pressure P. from its set point condition.

$$\delta P(s) = \frac{-K_2}{1 + ST_2} \delta F_s(s).$$

$$\delta F_s(s) = -\frac{1}{K_2}\left\{\delta P(s) + sT_2 \delta P(s)\right\}$$

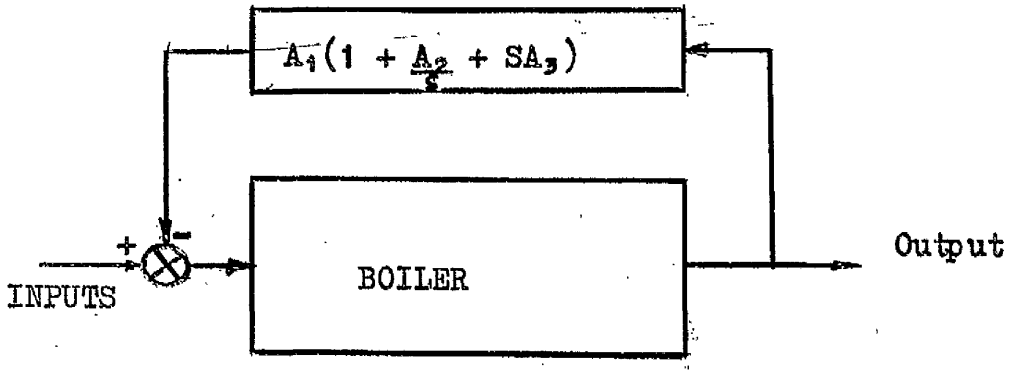

Figure 5.1. Three Term Boiler Control.

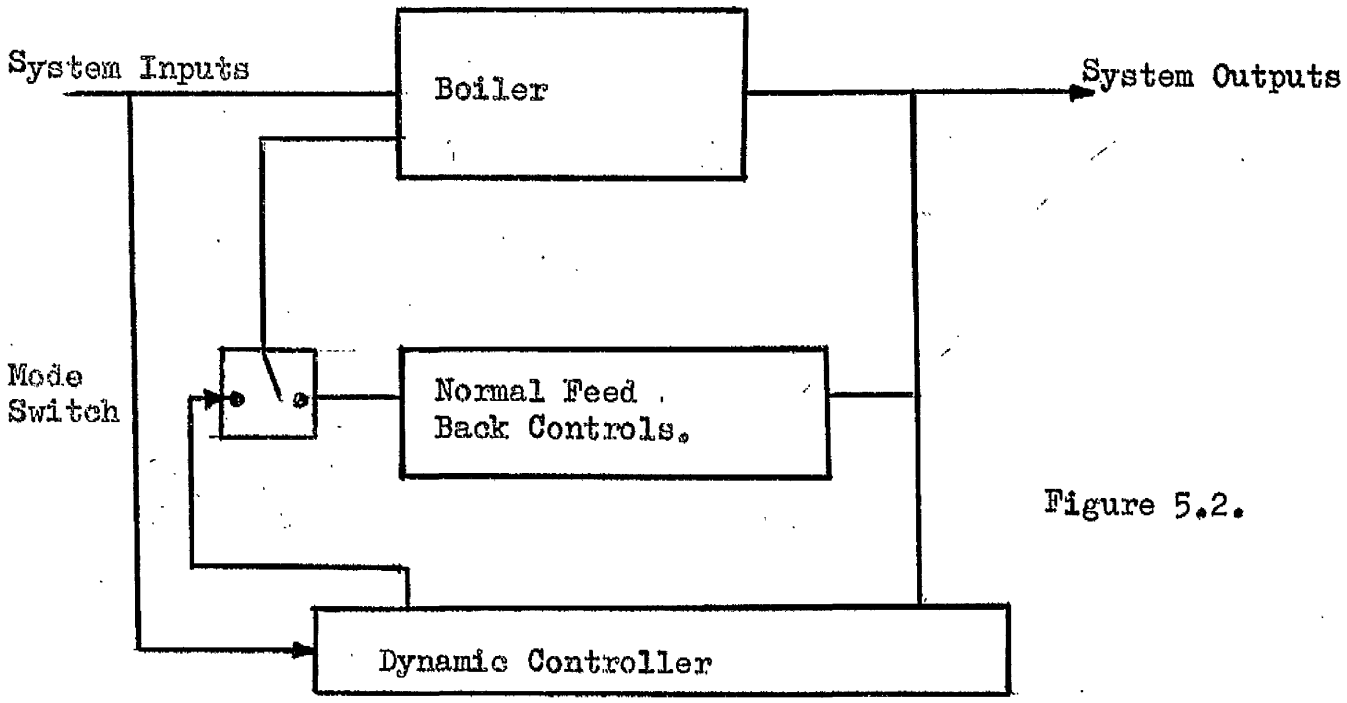

Figure 5.2.

Dual Mode Operation.

The arrangement is shown in Figure 5.4. the realizability of the differential term being due to the extremely low noise level associated with drum pressure measurement. As the load change can either be positive or negative two comparators are necessary to indicate the correct polarity to subsequent switching logic. Mode switching is effected by an output from either comparator.

The minimum value of load change over which the dynamic controller can exercise adequate control is a function of the combined boiler and controller characteristics and will be discussed in chaper 6. To avoid instability at the mode switching boundary the computer must be arranged to revert to normal feedback controls only on the completion of the full switching program.

5.2.2. Switching Function Generation.

Using the simplified boiler model derived from chapter 4 we can relate the incremental fuel flow signal to the boiler pressure change by the block diagram shown in Figure 5.5. If, due to an incremental change δF_s, which has occurred in the steam flow, an error δP exists between the set point boiler pressure P_{SP} and the measured boiler pressure, then the desired equilibrium value can be regained in minimum time by applying the maximum control effort available in the fuel supply mechanism in a manner determined by a previously derived switching function.

In Figure 5.5. M is the maximum turn up available at the

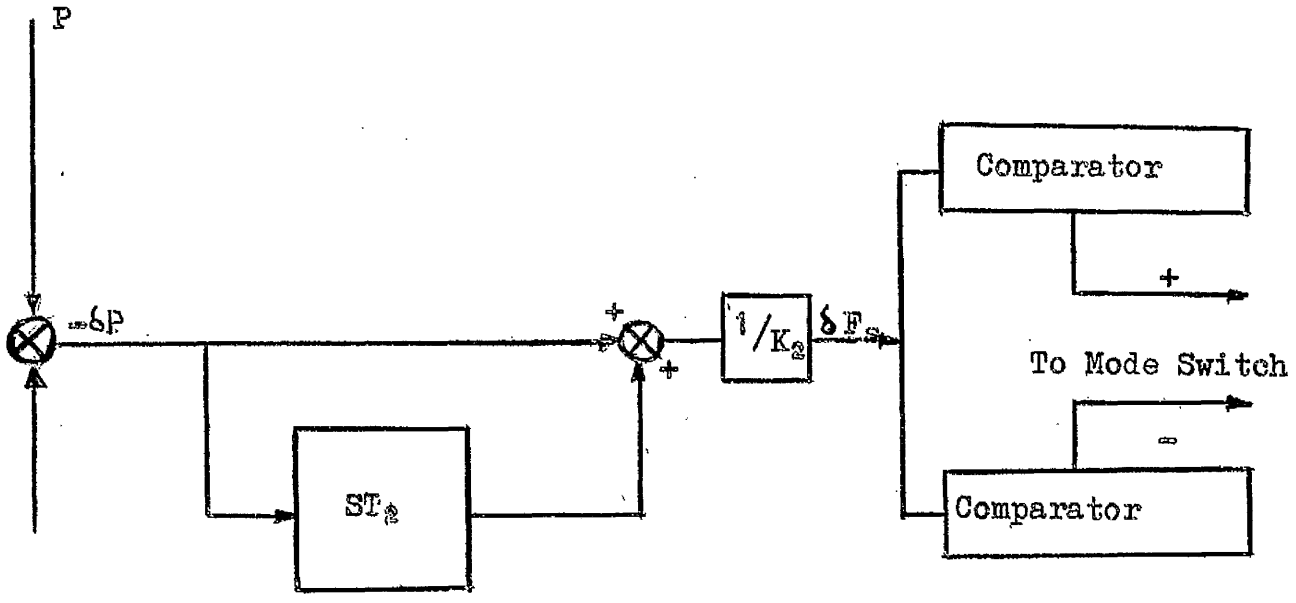

Mode Switching Figure 5.4.

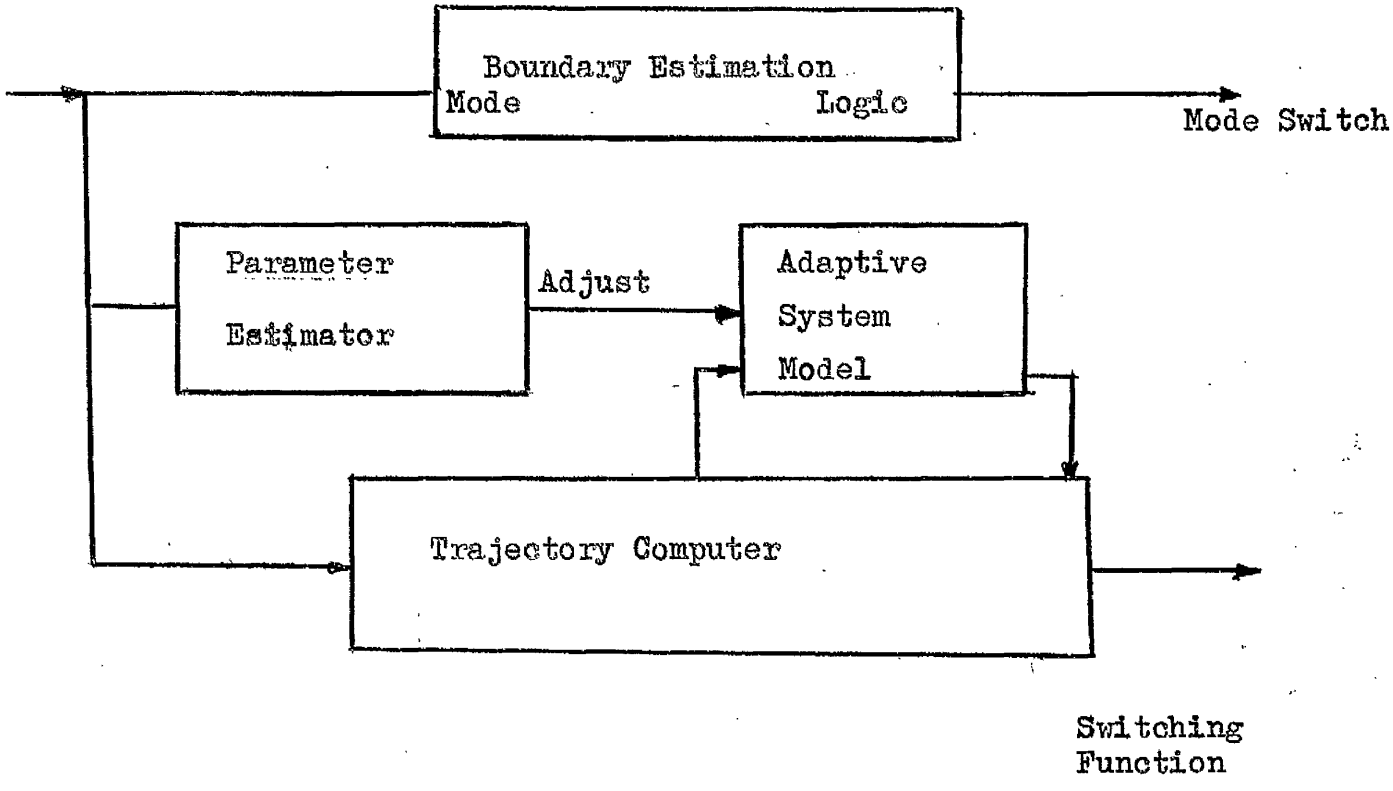

Figure 5.3. Dynamic Controller.

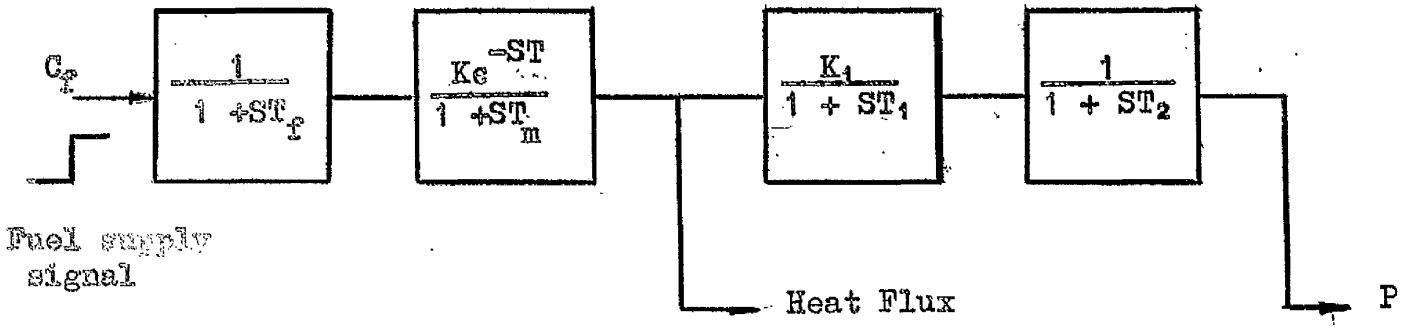

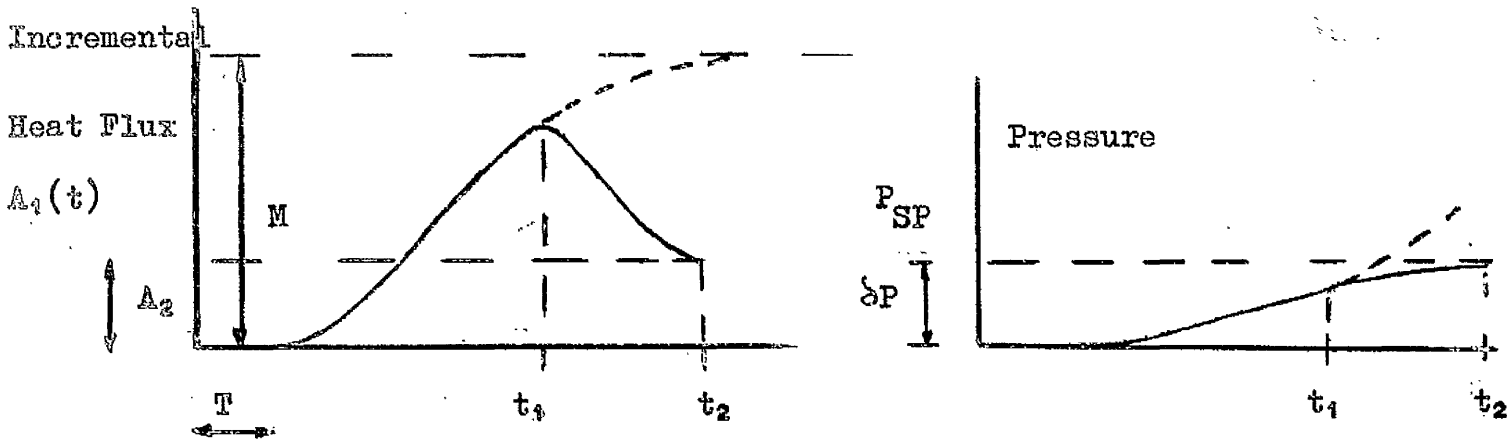

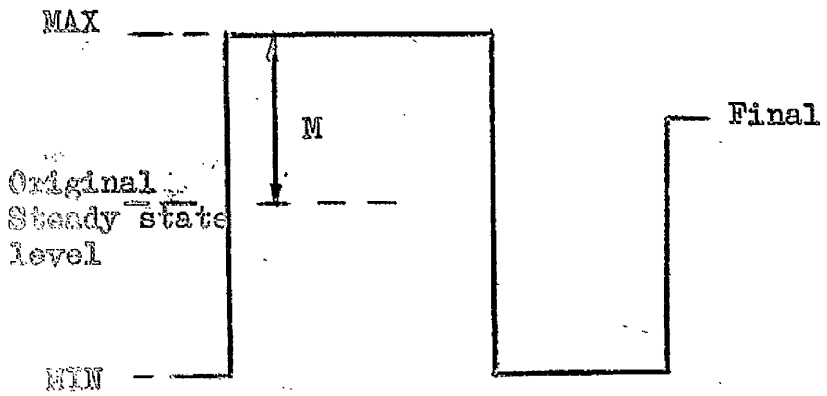

Heat Demand Switching Function.

Figure 5.5.

Figure 5.5. Optimum Switching.

original load level, A_2 is the final incremental position of the fuel supply actuator and t_1 and t_2 are the calculated switching times for minimum time response of the boiler pressure with no overshoot. If the plant parameters were time invariant the switching function could be derived for an incremental step in steam flow demand by the manner shown in Figure 5.6.(c).

Firstly the mode switching logic will determine the instant of operation of the controller and whether δF_s is positive or negative. For correct operation the computer must know the incremental value of F_s, and hence δP, and the value of M available at the current operating level. Incremental values of the system variables can only be measured if the initial zero time values are known. This requires memory elements which are formulated in an analogue system by track and hold amplifiers. Hence if we regard $F_s(t)$ in Figure 5.6.(a) as a time varying parameter, its value at any time is given by the output of the amplifier 1 where RC is small in comparison with any possible rate of $F_s(t)$. Amplifier 1 is said to track $F_s(t)$. If at any time the switch is open circuited the amplifier will hold the value of $F_s(t)$ at the instant of switching and the incremental value of δF_s will appear at the output of amplifier 2. M can also be determined by a track and hold amplifier monitoring the fuel actuator position as shown in Figure 5.6.(b).

In Figure 5.6.(c) we have assumed that δF_s determines δP and A_2 directly. As a direct relationship exists between the fuel

actuator position and the new load value determined by δF_s, the latter assumption is obviously true. The value of δP determined by δF_s is the final steady state value of the pressure error, it being assumed initially, for ease of presentation, that the incremental pressure change due to δF_s alone will have reached a steady state value before interval t_2. The relationship between δF_s and δP and its effect on the computation are discussed in chapter 6.

If the transient characteristics of the boiler are not constant and if any variation can be represented by parameter variations within a rigid model structure, then optimum switching can be performed by the method illustrated in Figure 5.6.(c). where the parameters of the plant analogue model are adapted to force a best fit between the model and the system. Model parameter adjustment will be based on the estimated values of the corresponding plant variable coefficients, which in accordance with chapter 4, are assumed to be K_c (a function of the fuel calorific value and throughput), T_m (a function of coal hardness, dampness and general mill response) and K_t which is a function of boiler load.

The actual switching function is produced by the trajectory computer for specific values of δP, A_2 and model output time functions. In this study the trajectory computer has been formulated in electronic analogue terms and a full description of its realization is given in chapter 6.

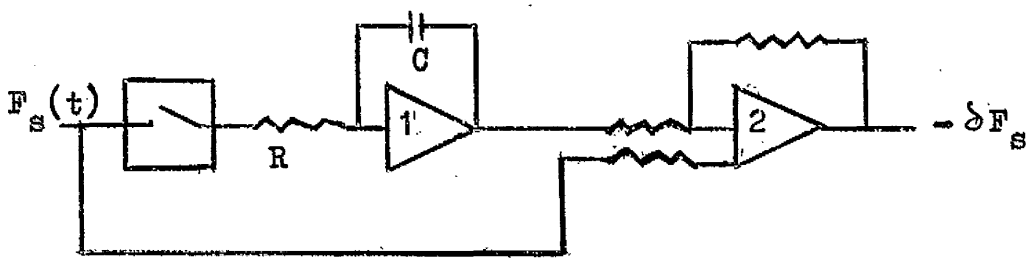

5.6(a)

Figure 5.6(a) Track and Hold Amplifier.

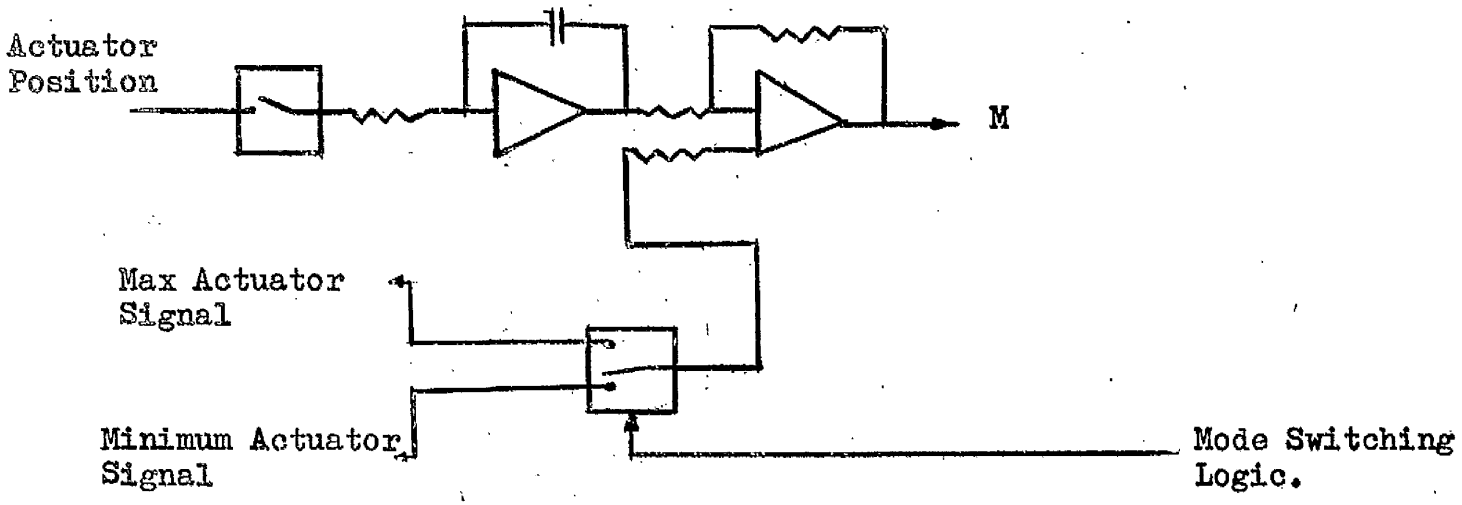

Fig. 5.6(b). Determination of M.

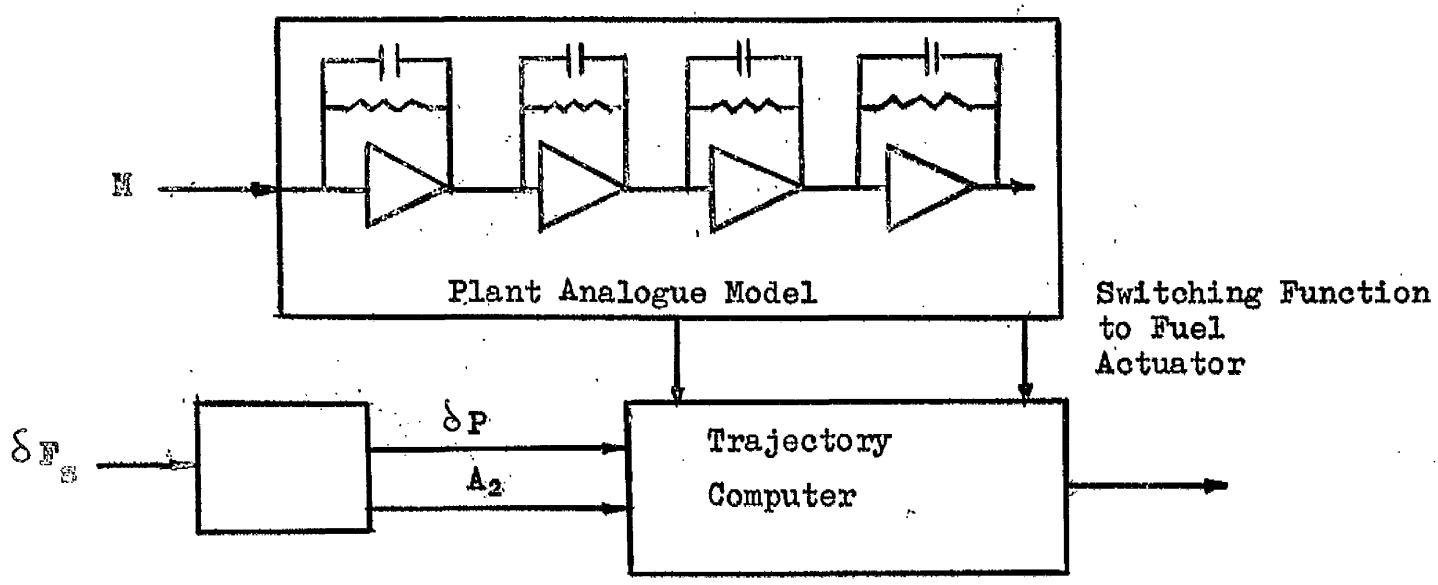

Figure 5.6(c). Switching Function Computation.

5.2.3. Parameter Estimation.

System parameter estimation can be carried out by direct measurements of the system outputs of heat flux and pressure, knowing the magnitudes of the incremental steam flow and fuel demand signals. Dividing the system into two parts we have

(a) The relationship between incremental fuel demand and incremental heat flux.

(b) The relationship between incremental change in heat flux and the resulting incremental change in boiler pressure.

From (a) we can determine the values of K_c and T_m and from (b) the value of K_s. The general outline of the parameter estimators is shown in Figure 5.7.

$\delta P'$ represents the total measured variation in the drum pressure due to the combined effect of variations in heat flux, steam flow and water flow. The incremental pressure change due to heat flux alone can be determined by subtracting the added effect of the other two factors from the total pressure variation. E_{PS} and E_{PI} represent the relevant transfer functions which have been defined in chapter 4. E_{PI} is load variant but as its effect in this case is second order it can be regarded as constant.

The realization of suitable logic controlled parameter estimators has already been described in chapter 3.

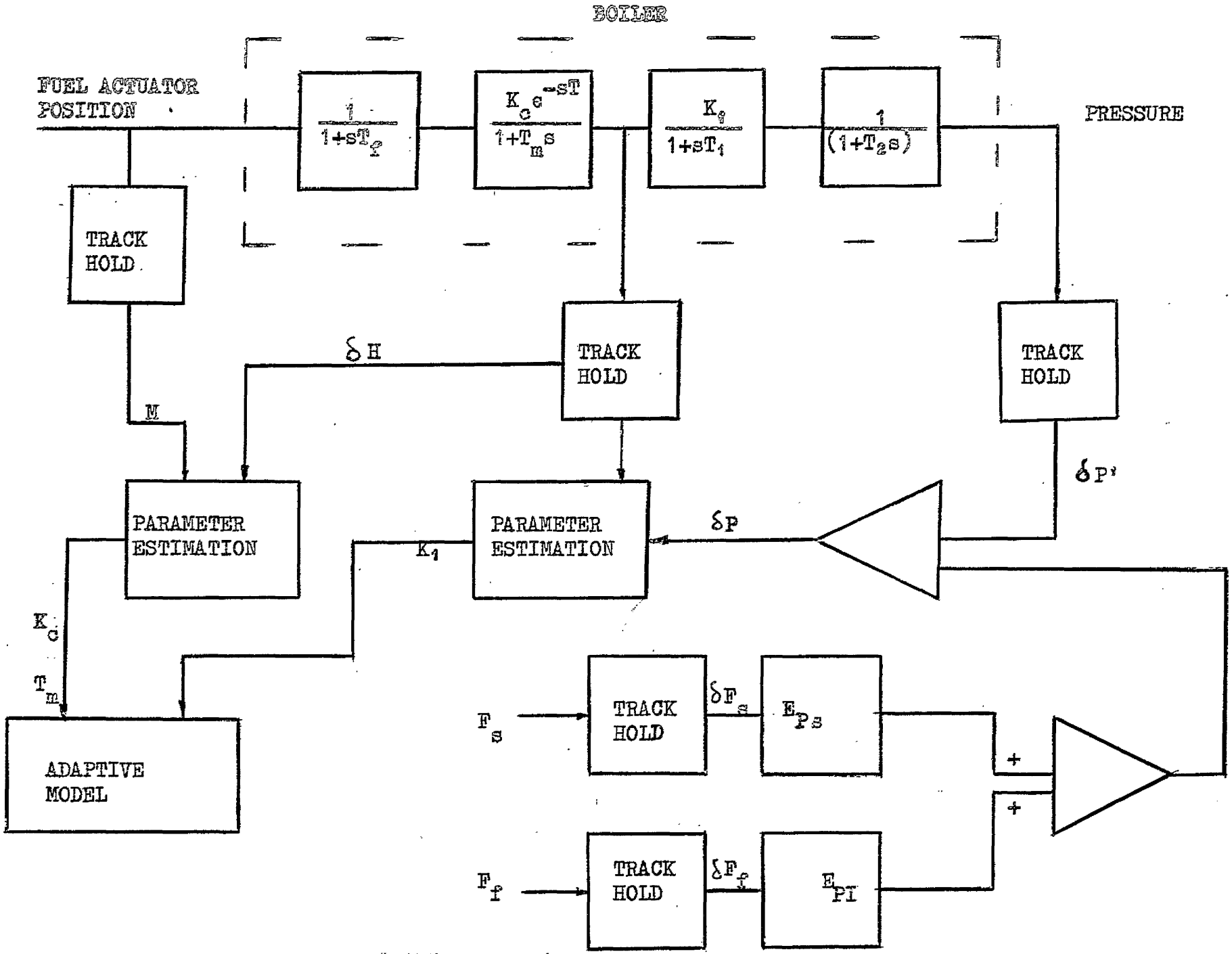

Figure 5.7. Parameter Estimation

5.2.4. Model Adaption.

If the plant model is formulated by analogue computer elements adaption can easily be performed by one of the adaptive elements described in chapter 2. The model has two modes, namely an adaptive mode and a computation mode; it being switched to the former in sequence with the outputs of the parameter estimators to obtain the correct degree of model up dating. After a brief interval of time to allow the solid state control circuitry to settle at the new steady state value the model is switched to the compute mode, enabling the trajectory computer to compute the correct switching function. The time response of the Luxistor adaptive mechanism is more than adequate to ensure compatability with the logic controlled parameter estimators.

The operations of parameter estimation, model adaptation and computation can be carried out repeatedly using the latest measured values of δF_s and δF_f until just before the end of the first switching interval at $t = t_1$ as shown in Figure 5.5.

5.3. Water Level Controller.

A major constraint on the controlled performance of a boiler in the transient mode is the behaviour of the drum water level. Drum water shrink or swell initiated by rapid variations of steam flow or heat addition can drive the water level outside the boundaries of safety and necessitate complete plant shut-down. Non-minimum phase characteristics

hinder the correct performance of the normally used two or three term controllers. Anticipatory proportional signals from the steam flow meter frequently used, though indicative of the ultimate feed flow necessary, conflict with the short term or transient requirements. Horton (3) has compared the transient performance of the common water level controllers and his results indicate the obvious advantages obtained by using a negative derivative function of steam flow.

The application of optimum switching techniques to water level control would make the best use of the installed pump capacity to suppress drum level surge. Anticipatory signals derived from a fast time adaptive model could be used to determine the switching function for the feed flow controls in the manner already outlined for fuel flow.

In Figure 5.8(a) the swell resulting from an increase in steam flow is shown. This swell can be suppressed in the minimum possible time by using the maximum possible control effort N, which represents the maximum turn down available in the feed pump controller at this load level, for a predetermined time t_q and then establishing the new steady state feed flow level. The improvement brought about by this method of control enables the boiler to be subjected to larger load transients without danger of exceeding the safety limits on the water level excursion.

Obviously the degree of control exercised by the pump is dependent on the initial steady state value, greater turn down being possible at half load than, say, at fifth load, and the worst case

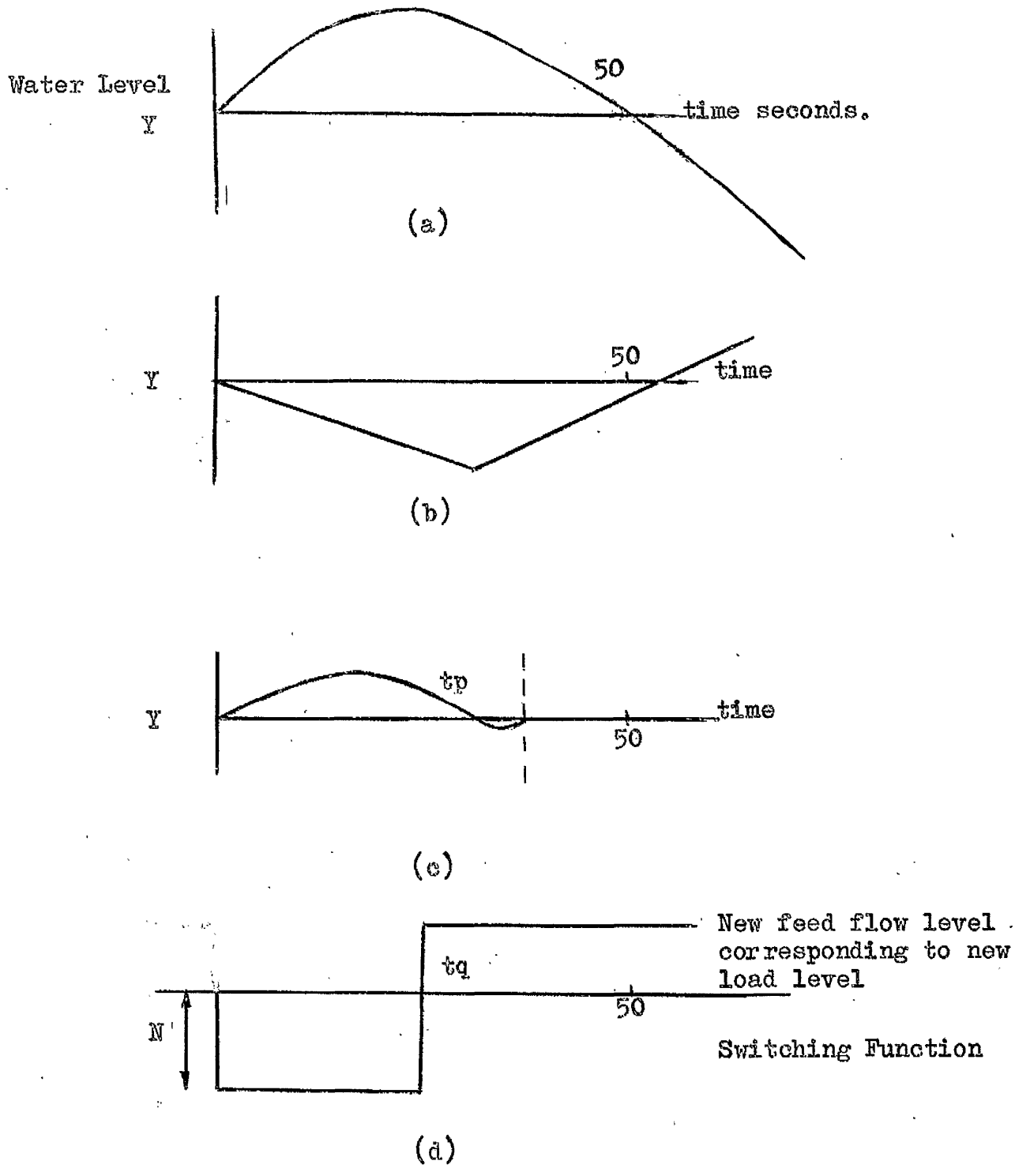

Figure 5.8. Switching function for feed water controller.

occurring at the two conditions of maximum and minimum load. If we assume that the latter is 10% full load, then a fair degree of turn down is possible, the limit being the danger of down comer ebullition due to increased downcomer enthalpy under the conditions of falling pressure as discussed in chapter 4. If the possibility of downcomer ebullition can be avoided by correct boiler design then the total turn down available can be used and the transient performance enhanced.

To cope with drum shrink due to a sudden drop in steam output at the maximum rated load some pump overload capacity must be available and it is reasonable to assume that this is of the order 10→20% of rated capacity.

Control at the two limiting conditions mentioned above could perhaps be improved by the provision of a small (of the order of 10% main pump capacity) high speed reversible pump activated and supervised by the transient controller.

In Figure 5.8(b) is shown the effect of the control effort N acting alone on the water level and in Figure 5.8.(c) the effect of the simultaneous application of N on the initiation of a transient. The water level should return to its original value in a time equal to t_p where $t_p > t_q$ due to the lags associated with the water pump.

A diagram of a possible computer configuration suitable for the predictive computation of the switching function is shown in

Figure 5.9. t_p is estimated by summing the combined effects of the incremental steam flow and the maximum pump response. A comparator will trigger when zero level is reached and its output, by switching an integrator which had been supplied with an input d.c. level from SOMETHING to HOLD, can generate an analogue value of t_p. Compensation for the pump transfer function can subsequently be determined.

The computer is basically a fast time model of the actual system, the model being rendered adaptive by the formulation of the function $f(F_G)\, f_1(P)$ (see Paragraph 4.6. and Figure 4.) for all load values. In the diagram $F_S(0)$ represents the initial steady state value of the steam flow determined by the track and hold amplifier from which the incremental change in $f(F_G)$ can be determined. The incremental pressure change δP due to δF_s has been generated to obtain $f_1(P)$ and also to represent the effect of pressure on the pump transfer function. This latter effect has been discussed by several authors (2), (4).

The final time response of the water level $y(t)$ is the sum of $y_1(t)$, the inherent boiler water level response to δF_s, and $y_2(t)$ which represents the water level response to the controlled feed water flow. As with the derivation of M is Figure 5.6.(b) the maximum or minimum actuation signal will be determined by the mode switching logic.

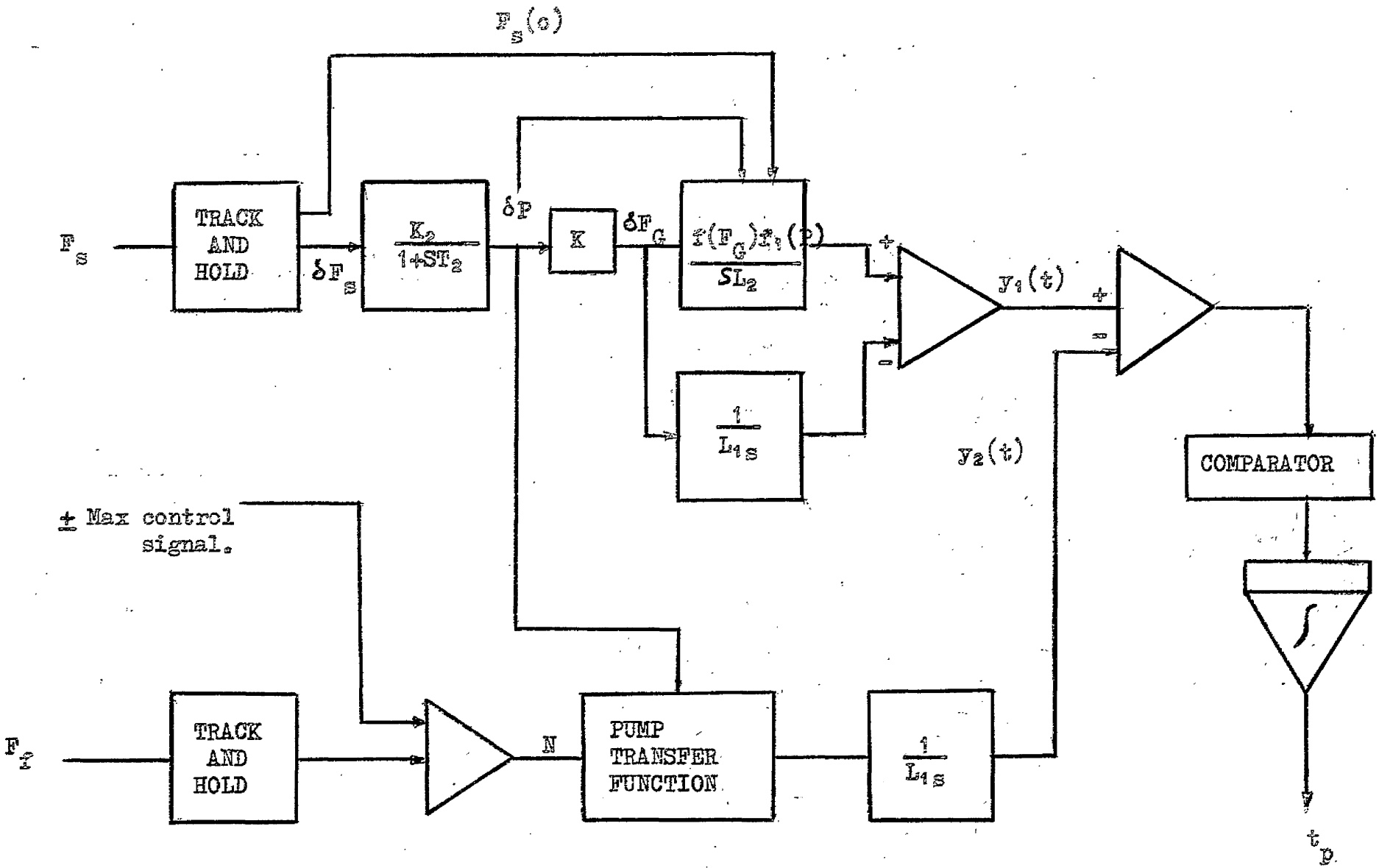

Generation of feed water switching function. Figure 5.9.

CHAPTER 6

GENERATION OF THE SWITCHING FUNCTION

6.1. Introduction.

In the proposed dynamic controller of Chapter 5 the controlled switching function is derived on a predictive basis by the trajectory computer using signals from both the process and the fast time adaptive model. Our concern here will be with the realization of a suitable configuration for this computer and to study the simulated behaviour of the plant under the influence of the derived switching function.

Control switching functions for on-off control systems have been developed by several authors (1), (2), (3), the formulation being more or less complex depending on the nature of the plant and the performance index chosen. It will be shown that the form of the boiler plant lends itself to a radical reduction in the computation process allowing the switching function to be derived by a simple electronic analogue configuration.

6.2. Statement of the Problem.

The relationship between steam flow, actuator position and boiler pressure is shown in Figure 6.1. On the occurrence of a transient change in F_s the trajectory computer must develop a switching function to control C_f, returning the boiler pressure to the set point condition in minimum time. Some degree of pressure overshoot is obviously possible, but this will be

kept to a minimum consistent with a fast time of response. Because of the complexity of the problem the solution was derived in two stages.

Initially a computer configuration was developed which, for any value of M - the maximum initial incremental value of C_f - and pressure error δP computed the zero overshoot time optimal switching function for the fourth order system of Figure 5.5. If the δP used in this computation is related to the incremental steam flow change by the relationship

$$\delta P = K_2 \delta F_s$$

and the lag T_2 is ignored then a large degree of pressure overshoot will result due to this lag unless the initially derived switching function is suitably modified. An iterative computation procedure has thus subsequently been developed which reduces overshoot to a negligible value.

The development of a time optimal switching function for a fourth order system though not difficult in theory results in the use of a large quantity of analogue equipment (4) and in order to reduce the system complexity some simplifying assumption must be made. Because of the relative magnitudes of the lags involved it was postulated that the fourth order system could be approximated to second order for the purposes of switching function computation. The appropriate second order function was thus developed and its performance checked on a second order system before being applied directly to the fourth order system.

6.3. Development of a Switching Function for a Second Order System.

For the second order system shown in Figure 6.2. it is required

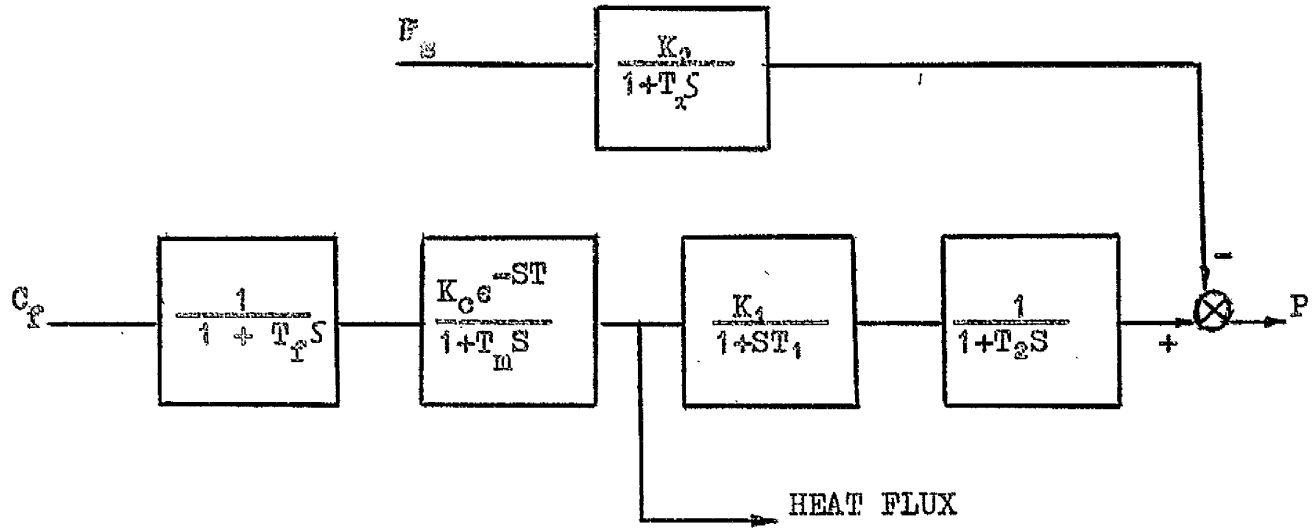

Figure 6.1. Boiler Model

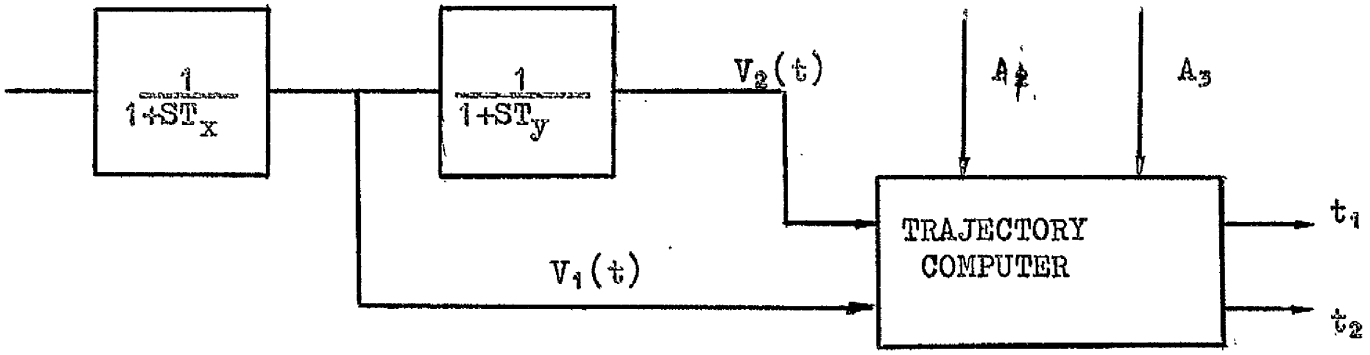

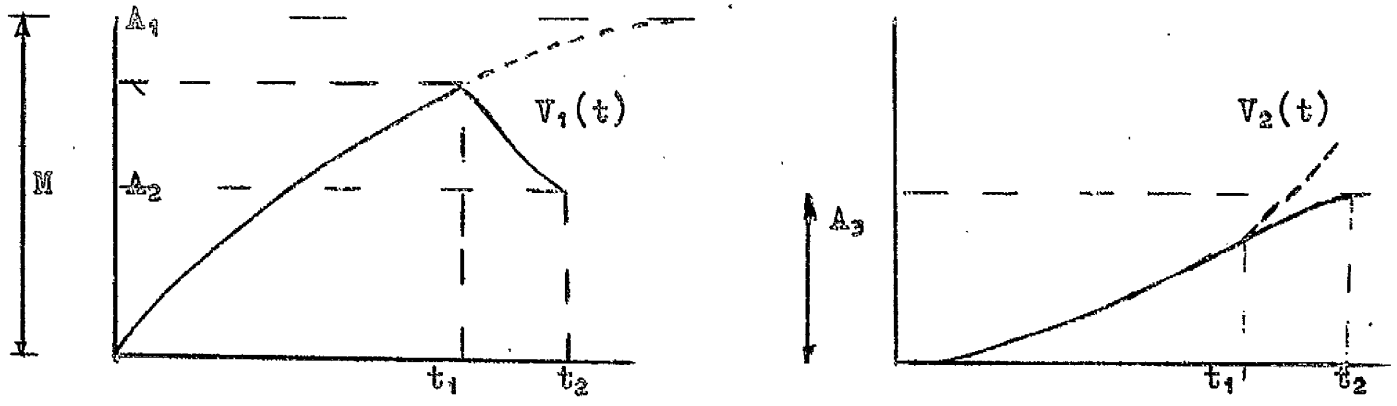

Switching function.

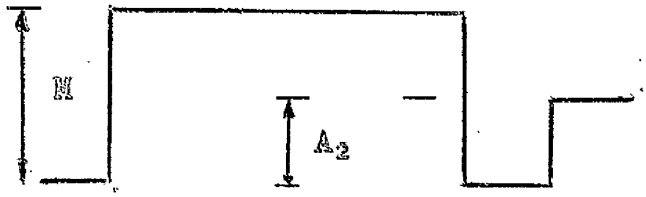

Figure 6.2.
2nd Order Approximation

to develop a computer configuration for the zero overshoot time optimal switching values t_1 and t_2 in terms of the maximum control effort M, the final input incremental A_2 and the final output incremental A_3. To illustrate the method of approach a unity gain system has been considered and hence in this instance $A_2 = A_3$.

It can be shown (5) that for $t > t_1$

$$V_2(t) = \frac{A_1}{1-\frac{T_y}{T_x}}\left\{ e^{-\frac{t-t_1}{T_x}} - e^{-\frac{t-t_1}{T_y}} \right\} + V_2(t_1)\, e^{-\frac{t-t_1}{T_y}}$$

where $A_1 = V_1(t_1)$

at $t = t_2$

$$V_2(t_2) = \frac{A_1}{(1-\frac{T_y}{T_x})}\left\{ e^{-\frac{t_2-t_1}{T_x}} - e^{-\frac{t_2-t_1}{T_y}} \right\} + V_2(t_1)\, e^{-\frac{t_2-t_1}{T_y}}$$

$\therefore$

$$A_3 = \frac{A_1}{(1-\frac{T_y}{T_x})}\left\{ e^{-\frac{T'}{T_x}} - e^{-\frac{T'}{T_y}} \right\} + V_2(t_1) e^{-T'/T_y}$$

where $A_3 = V_2(t_2)$ and $T' = t_2 - t_1$.

$\therefore$

$$A_3 = V_2(t_1)\, e^{-T'/T_y} = \frac{A_1}{(1-\frac{T_y}{T_x})}\left\{ \frac{A_2}{A_1} - e^{-T'/T_y} \right\}$$

writing $e^{-T'/T_y} = \left(\frac{A_2}{A_1}\right)^{T_x/T_y}$ we have

$$A_3 - V_2(t_1)\left(\frac{A_2}{A_1}\right)^{T_x/T_y} = \frac{A_1}{(1-\frac{T_y}{T_x})}\left\{ \frac{A_2}{A_1} - \frac{A_2}{A_1}^{T_x/T_y} \right\}$$

As $A_1 = V_1(t_1)$ and A_2 and A_3 are known this equation can be solved for t_1 if the functions $V_2(t)$ and $V_1(t)$ are available.

Rearranging the above equation in a manner more suitable for computer application we have

$$\left\{ A_3 - \text{ANTILOG} \left(\text{Log } V_2(t) + \frac{T_x}{T_y} \text{ Log } \frac{A_2}{A_1} \right) \right\} \left(1 - \frac{T_y}{T_x}\right)$$
$$= A_2 - \text{ANTILOG} \left(\text{Log } A_1 + \frac{T_x}{T_y} \text{ Log } \frac{A_2}{A_1} \right)$$

A suitable computer configuration for the solution of this equation is shown in Figure 6.3.

The second order system of Figure 6.2. and the switching function computer were set up on a Solartron 272 machine. The inputs to the switching function or trajectory computer are determined as follows. $V_1(t)$ and $V_2(t)$ are obtained directly from the second order model outputs. A_3 represents the initial error existing at the output of the second order system and A_2 the final value of the input to be applied at t_2. As a unity gain system has been assumed for ease of scaling $A_2 = A_3$. It should be noted that the switching function computer configuration can be rendered valid for all values of T_x, if this should be a variable, by incorporating suitable adaptive elements in the amplifiers D and E.

6.3.1. Method of Operation.

When the outputs of amplifiers A and B are equal the comparator triggers switching the computer to the HOLD mode. The output of

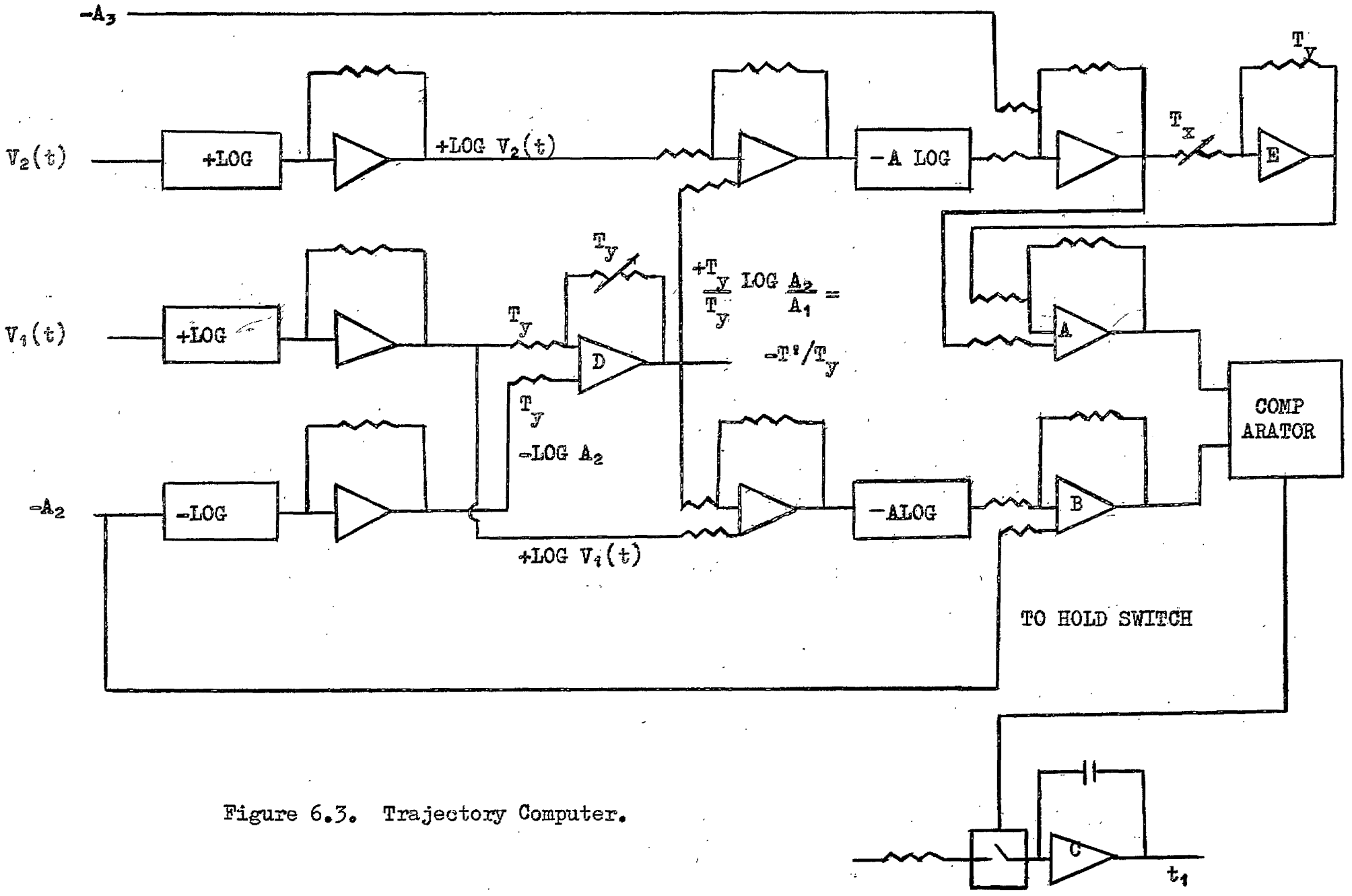

Figure 6.3. Trajectory Computer.

integrator C then gives the analogue value of t_1 for any value of A_3 or M. T' can be obtained as follows

$$A_2 = A_1 e^{-T'/T_x}$$

$$\frac{A_2}{A_1} = e^{-T'/T_x}$$

$$\therefore \text{Log} \frac{A_2}{A_1} = -\frac{T'}{T_x}$$

$$\therefore \quad T' = -T_x \log \frac{A_2}{A_1}$$

Therefore in the HOLD mode the output of amplifier D is equal to $-\frac{T'}{T_y}$ from which T' can easily be obtained if T_y is assumed constant. The time of the second switching function t_2 can thus be obtained as

$$t_2 = t_1 + T'$$

6.3.2. Computer Results.

As the computer configuration was to be used finally to control the full boiler model T_y and T_x were arranged in the ratio 5:1 to correspond to the relationship established in Chapter 4 between T_2 and T_m. The maximum control signal applied to the fuel supply actuator is limited in practice in the positive sense by the overload capabilities of the furnace and in the negative sense by the maximum turn down possible while still maintaining adequate flame stability. To comply with the

latter restriction the minimum value of C_2 was fixed at 10% full load rating.

Figure 6.4. shows the computed values of t_1 for three values of the overload rating L namely (a) L = 10% (b) L = 20% and (c) L = 30%. The initial steady state value of the plant was taken as 30% of full load (100%) rating, with t_1, as read along the abcissa, being the first switching time to achieve any load value indicated on the ordinate. The corresponding values of T' are shown in Figure 6.5.

As the equations governing the switching function for a negative load change are similar to those for a positive load change due to the symmetry of the system the computer configuration of Figure 6.3. will also compute the negative switching function provided that the correct values are used for the terms A_3, A_2 and M. The minimum load variation controllable by the controller is a direct function of the combined deadtime T and the time required for parameter estimation. This combined time must be less than the first switching time interval derived in Figure 6.4.

6.4. Application of the Switching Function to a Second Order System.

The response of the second order system of Figure 6.2. under the influence of the switching function was now studied using a 17" display oscilloscope. Oscillograms were obtained using a 5" Cossor oscilloscope and are shown in the following series of plates. The necessary

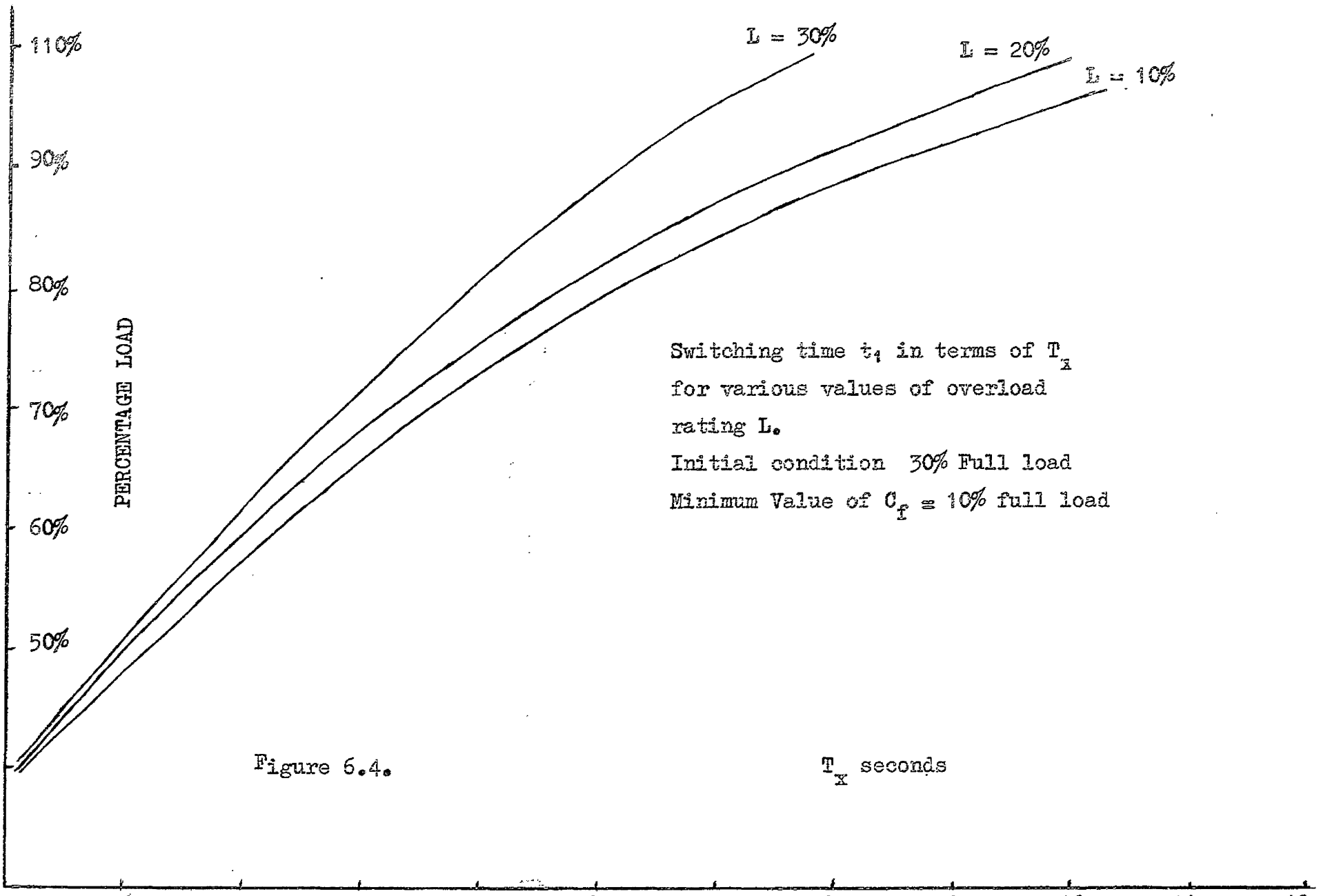
110%
90%
80%
70%
60%
50%
PERCENTAGE LOAD
L = 30%
L = 20%
L = 10%
Switching time t_1 in terms of T_i
for various values of overload
rating L.
Initial condition 30% Full load
Minimum Value of C_f = 10% full load
1
2
3
4
5
6
7
8
9
10
11
12
T_x seconds

Figure 6.4.

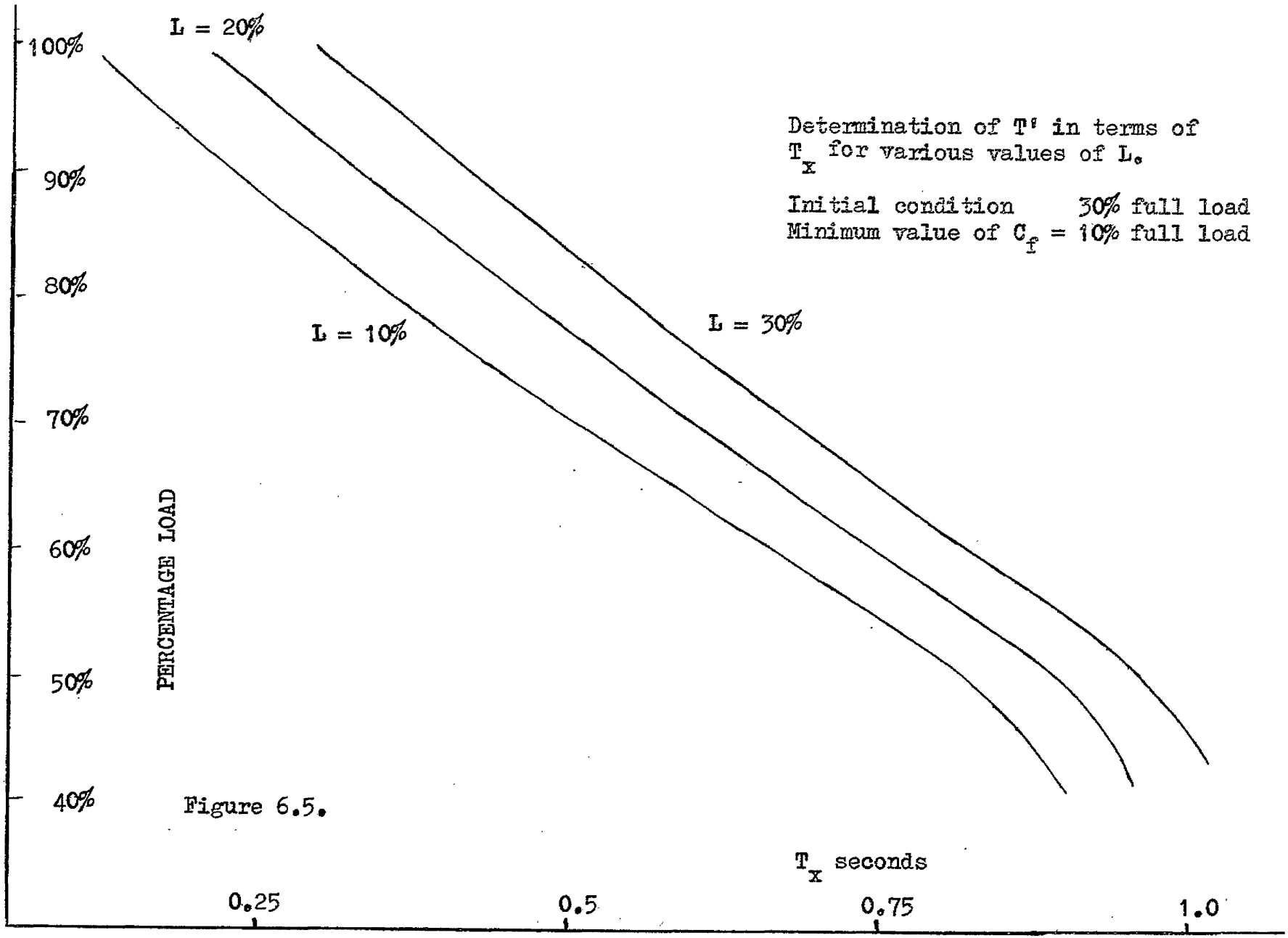
L = 20%
100%
90%
80%
70%
60%
50%
40%
L = 10%
L = 30%
PERCENTAGE LOAD
Determination of T' in terms of
T_x for various values of L.
Initial condition 30% full load
Minimum value of C_f = 10% full load
T_x seconds
0.25
0.5
0.75
1.0

Figure 6.5.

reduction in oscillogram size necessitated by the photographic reproduction process has resulted in some loss of clarity but sufficient remains to indicate the general nature of the responses. The output voltage of the system $V_2(t)$ has been taken as directly proportional to the load.

All percentage load changes mentioned below refer to load changes as a percentage of full load value above an initial operating point of 30% full load value. T_x was made equal to 4 seconds and T_y 20 seconds. In all cases the upper trace represents $V_1(t)$ and the lower trace $V_2(t)$.

PLATE 1

This plate shows the response of the system to a 60% load change in the absence of any switching function. The settling time is of the order of 100 seconds.

PLATE 2

The optimum switching function has now been applied. Load increase is 60% and the overload rating L = 10%.

PLATE 3

As PLATE 2 with L = 20%.

PLATE 4

As PLATE 2 with L = 30%.

As can be seen these results are quite satisfactory and the improvement in the response is quite marked. Exact switching times for

PLATE 1

PLATE 2

PLATE 3

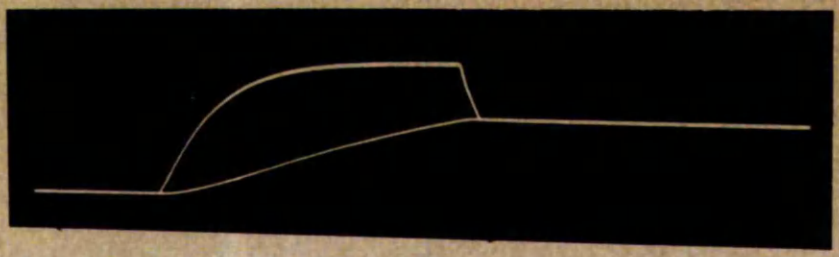

PLATE 4

PLATE 5

the last three plates can be obtained directly from Figures 6.4. and 6.5.

6.5. Application of Second Order Switching Function to Fourth Order System.

The fourth order system of Figure 6.6. was now simulated with the various constants taking the following values.

T_m = 4 seconds

T_f = 0.4 seconds

T_1 = 2.0 seconds

T_2 = 20 seconds

$K_C = K_1 = K_2 = 1.$

Application of the second order switching function resulted in an undershoot at all levels of input signal with $V_2(t)$ reaching its steady state value a period of between T_m and 2 T_m seconds after the second switching time t_2. The results indicated that an improved response could be obtained by increasing t_1 by an interval equal to $T_m/4$. With this modification the output reached steady state value within $T_m/2$ second after the first switching time t_2. For an initial input level of 30% no perceptible overshoot was noticed for load changes greater than 40%, but overshoot now did occur for smaller load changes, the maximum being 5% for a 10% change. As with the second order system the output voltage $V_2(t)$ has been taken as directly proportional to the load.

PLATE 5

Shows the response of the fourth order system for a 60% load change with L = 10%. The unmodified second order switching function

was used in this case.

Application of Switching Function to Complete Boiler Model.

The boiler model of Figure 6.1. was now simulated with the same scaling as indicated in Paragraph 6.5. The dead time T was included and made equal in magnitude to T_m. Steam flow F_s now constitutes the load and hence the output voltage $V_2(t)$ of the fourth order system, which can now represent the output pressure, is no longer directly proportional to load but lags it by T_2 seconds.

In reply to a step change in F_s the second order switching function was applied directly to control the pressure signal $V_2(t)$. The response of the pressure signal is shown in the following plates for various load changes from an initial steady state value of 30% maximum load. For comparison the system responses in the absence of the switching function are first given.

PLATE 6

No switching function used. Final steady state value of the input applied instantaneously at onset of load change. The load change here is 20%.

PLATE 7

As PLATE 6 but with load change of 40%.

PLATE 8

As PLATE 6 but with load change of 60%.

PLATE 9

Load change of 20%. Second order switching function applied with L = 10%.

PLATE 10

Load change of 40% second order switching function now applied L = 10%.

PLATE 11

Load change of 60% second order switching function now applied L = 10%.

A high degree of overshoot is evident in the last three responses and in order to correct this the following iterative procedure was developed.

6.6. The Iterative Computation.

If the final uncorrected pressure error due to a change in load F_s can be represented by A_3 where

$$A_3 = K_2 \delta F_s$$

and A_3 is used as the basis of computation of the switching function then an overshoot will occur when this function is applied to the system because at the final switch point t_2 the actual pressure error is not A_3 but $A_3 - Z$ where Z is defined in Figure 6.7(a).

For any load change δF_s Z will be known at the end of the computation

PLATE 6

PLATE 7

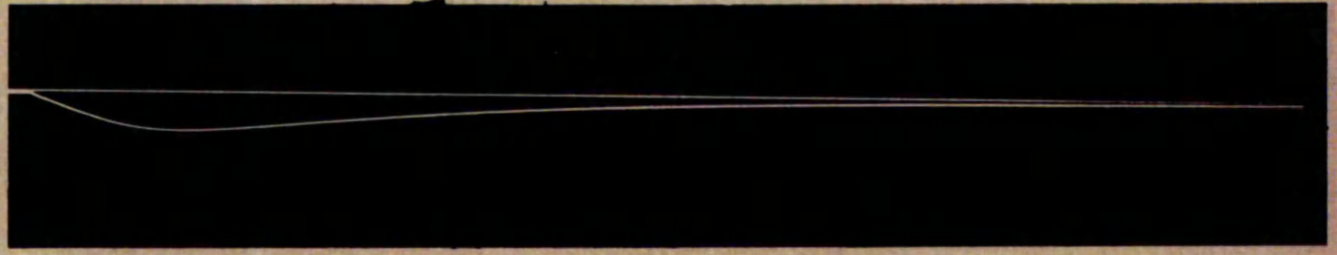

PLATE 8

PLATE 9

PLATE 10

PLATE 11

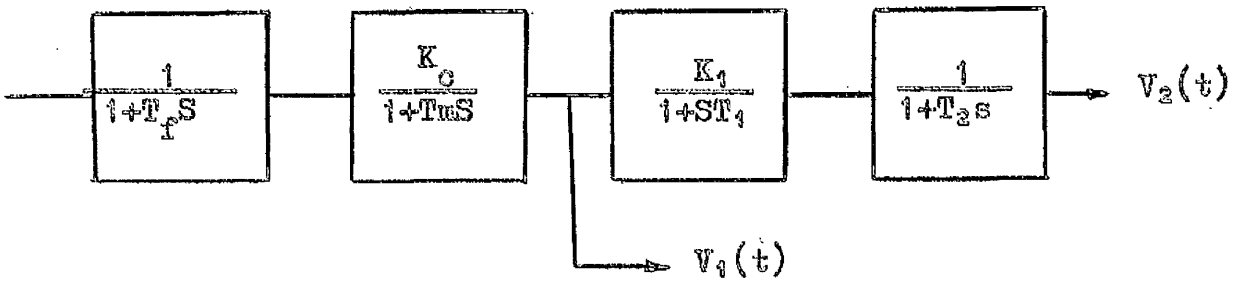

Figure 6.6. 4th order system with dead time.

Iterative Procedure

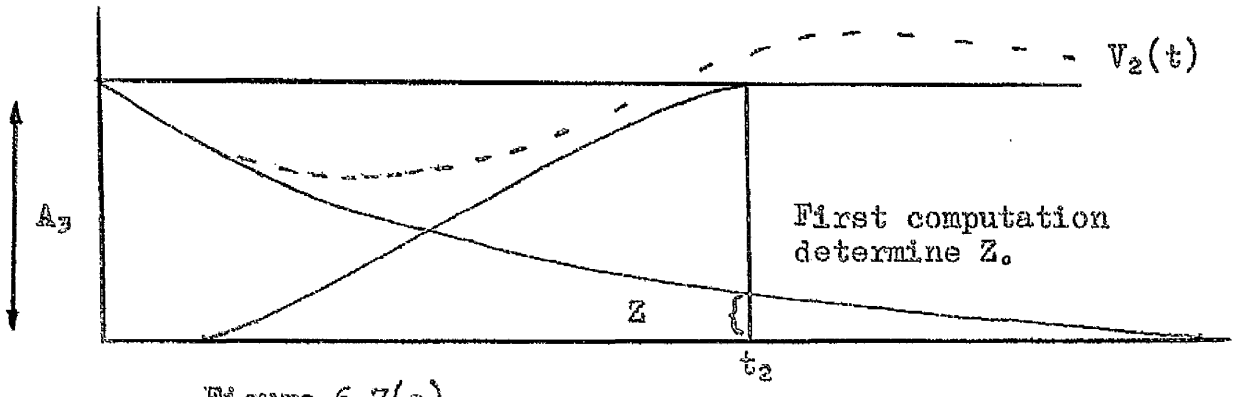

Figure 6.7(a)

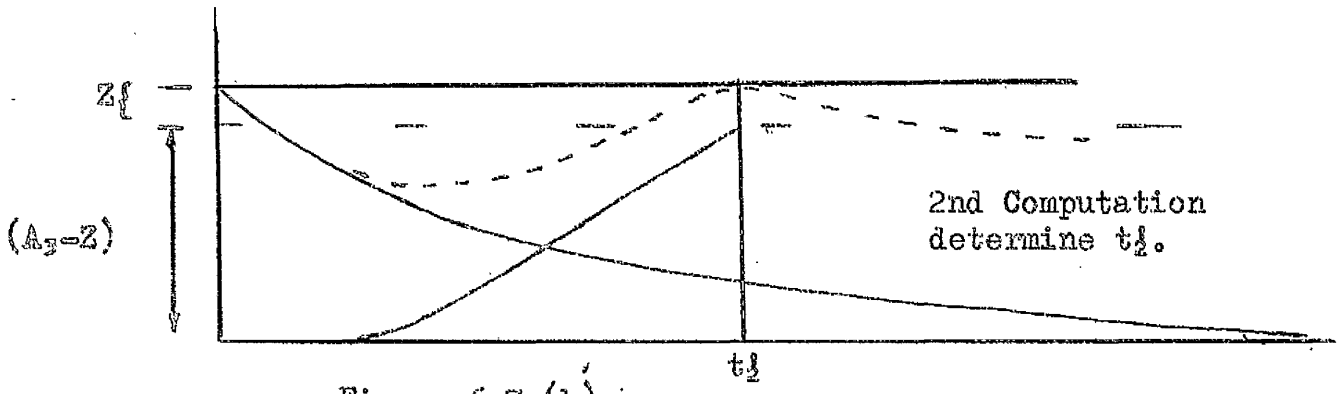

Figure 6.7.(b)

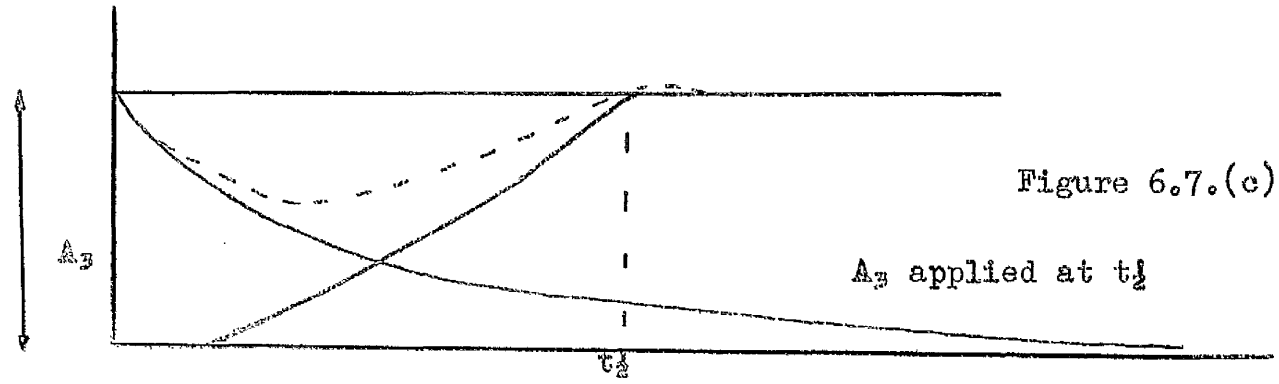

Figure 6.7.(c)

and its value can be held in a track and hold amplifier. If a second computation is now undertaken with a pressure error of (A_3-Z) as the initial condition then a new value for t_2, say t_2', will be derived as shown in Figure 6.7.(b) and the overshoot will be quite small if at t_2' the input level is fixed at a value proportional to (A_3-Z).

Due to the uncorrected error Z, however, the output function $V_2(t)$ will not stay at the correct level but will decay gradually to a final steady state error Z. This effect is shown in the following two plates.

PLATE 12

First iteration with an input signal equal to (A_3-Z) applied at time t_2' 20% load change L = 10%.

PLATE 13

As PLATE 12 but with a load change of 60%.

The final droop in the response characteristic could be removed by applying the full correction A_3 at t_2'. Some degree of overshoot was now to be expected due to inexact cancellation of the droop but it was thought that this would be minimal. The computation thus proceeds as follows.

(a) t_2 is first determined on the basis of the error A_3 where $A_3 = k_2 \delta F_s$.

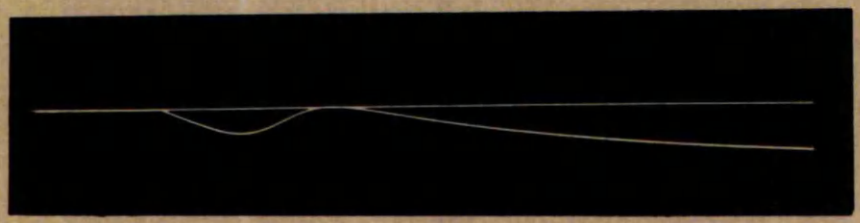

PLATE 12

PLATE 13

(b) The value of Z is determined.

(c) A second computation is performed on the basis of an error (A_3-Z).

(d) A final input level equal to A_3 is now applied to the system at t'_2.

It can be seen that one iteration only is required.

The system response for two values of load increase is illustrated in the following plates.

PLATE 14

First iteration with input signal equal to A_3 applied at t'_2. 20% Load change L = 10%.

PLATE 15

As PLATE 14 but with a load change of 60%.

No overshoot is evident in PLATE 14 and the maximum overshoot shown in PLATE 15 represents 3% of the applied load change.

6.7. Summary.

A suitable iterative computation procedure has been derived to produce a switching function capable of controlling the boiler model developed in Chapter 4 in a time optimal fashion with little overshoot over a wide range of boiler loads. The relative simplicity of the computation is due, in the main, to the relative magnitudes of the boiler time constants which enable a switching function derived for a second order system to be applied successfully to the higher order model.

PLATE 14

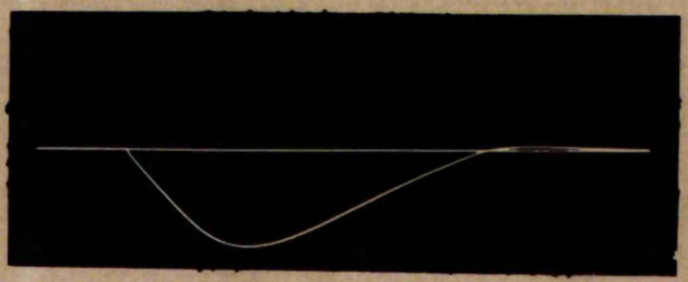

PLATE 15

CHAPTER 7

CONCLUSIONS

The initial part of the thesis has dealt with the solution of the actuation and identification problem in a model adaptive control scheme for a particular type of plant and structure. The plant structure chosen was of a form which was very suitable for analogue simulation and the actuation and identification elements have thus been formulated in analogue computer terms. The fuel supply pressure loop of a pulverised coal fired power station boiler model was subsequently taken as an example of the application of the model adaptive system and the formulation of a suitable decision computer to generate a sub optimal control forcing function for this model has been described.

The actuation or adaptive element based on the Luxistor was shown to be simple in configuration, fast acting, accurate and linear with the potential to be produced ultimately as a fully solid state unit. In the adjustment of adaptive model lag parameters it has several advantages over the conventional servo potentiometer:

(1) The adaptive mechanism has no mechanical moving parts and the only high quality component required in its construction is a high performance operational integrator.

(2) Noise-free resistance variation with a settling time approximately six times shorter than the best available servo potentiometer. This latter property greatly

increases the repitition rate obtainable in the subsequent exploration of the system performance contours.

(3) The present circuit is relatively insensitive to temperature variation and in its ultimate developed form it will be of very small physical dimensions and capable of correct operation in extreme environmental conditions.

The Luxistor control system should find a wide range of use not only in the analogue and hybrid computer field but also in many other applications where the adaptive function is at present being performed by slow acting servo potentiometers.

The final settling time of the Luxistor control circuit was determined by the relatively large lags associated with the filament lamp and cadmium sulphide current rise timeof the Luxistor unit. Complete elimination of these lags, though obviously not possible, would result in a speed of adaptation limited only by operational amplifier capabilities. In an effort to approach this ideal condition the Luxistor was replaced by a new solid state lamp detector unit. This new combination had a response time of several orders of magnitude less than the Luxistor and, utilising the same circuit philosophy,

the settling time of the complete adaptive system was reduced to approximately 160 microseconds with no loss of linearity. This settling time was less than the settling time of the Luxistor system by a factor of 1500.

Besides decreasing the system response time, two other advantages result from the use of the gallium arsenide - duo diode combination. Firstly, the crystal lamp has a very long life time and is completely immune from the danger of filament failure and secondly, the physical size of the new combination is much less than that of the Luxistor, rendering even smaller unit packaging possible.

So far as is known to the author this is the first time that an adaptive mechanism has been devised for adaptive model lag parameter adjustment which has a speed of response compatible with the limit speed of parallel analogue computation. The adaptive mechanism can also be used for changing adaptive model gain parameters provided that the maximum parameter variation is less than one order. While possessing a bandwidth compatible with the best available electronic multiplier which could be used for such an application the adaptive mechanism has the added advantages of constructional simplicity and the flexibility inherent in its ability to perform the dual role of adjusting both types of parameter.

Proposed further development work here will involve replacing the computer operational amplifiers in the circuit by solid state integrated amplifiers and relays by field effect transistor switching units with a view to producing a compact, inexpensive completely solid state adaptive mechanism which would be suitable for use in a modern high speed hybrid computing system. Due to the simplicity of the circuit construction the cost of the finally developed adaptive unit should be less than 20% the cost of a standard computer multiplier.

For the particular plant model structure chosen the logic controlled parameter estimation system discussed in Chapter 3 provides a fast and accurate method for the simultaneous on-line identification of two unknown parameters with the minimum of computation capacity. The output of the parameter estimator was compatible with the input signal requirements of the adaptive mechanism and, like this device, is capable of being developed as a completely reliable solid state unit. This combination of actuation and identification elements should constitute a useful contribution to adaptive control technology especially in those applications where the plant can be structured by a series of lag elements.

The application of Corbin's method to the identification problem found in the boiler combustion-pressure loop has also been discussed in Chapter 3 and the accuracy of the method demonstrated in

a computer simulation where compensation was provided for the second order nature of the pressure output time function. It will be seen that the advantage of Corbin's method lies in the simplicity of the identification configuration and that its application is particularly relevant to the plant structure discussed in this thesis.

In Chapter 4 Stafford's simulation of Chien's boiler model demonstrated thatthough boiler physical processes are governed by complex hydrodynamic and thermodynamic phenomena the overall plant characteristics, while being time varying, were of relatively simple form and can be closely represented by the type of generalised model chosen in Chapter 1 for the model adaptive control scheme. The boiler model derived here can thus be regarded as a suitable example of the utilization of theactuation and identification technique developed earlier.

A discussion of the physical behaviour of the boiler plant isolates the time varying parameters which were found to be three in number. Two were gain factors one of these being associated with the combustion section and the other with the heat transfer coefficient in the riser section. The third variable parameter was the lag coefficient of the coal grinding mill transfer function which was a function of fuel condition.

Direct application of the model adaptive control scheme to the

boiler combustion pressure loop depended on the availability of the heat flux time function for a plant identification. A suitable heat flux measuring instrument possessing the correct dynamic characteristics has only recently been developed and it is thought that this is the first time that such an instrument has been proposed as an integral part of a boiler control loop. In this instance it was shown that adaptive controller application requires only the use of standard operational elements and procedure and the feasibility of extending feed forward predictive control techniques to achieve improved boiler water transient behaviour has also been discussed.

The generation of an optimal switching function for a fourth order system can result in a quite complex computation procedure. Due to the relative magnitudes of the derived boiler lag parameters it seemed reasonable to assume that a switching function derived for a second order system could be applied successfully to the fourth order boiler model. The validity of this assumption has been demonstrated in Chapter 6 and a simple iterative computation procedure outlined which deals with the added complexity of the steam flow pressure transfer function.

APPENDIX 1

FURNACE EFFICIENCY

The heat balance equation for a furnace is given below:

$$Q\,C_V = \underbrace{H \times A\,(t_f - t_w)}_{\text{Heat transferred}} + \underbrace{Q\,Y\,I_f}_{\text{Heat in combustion products}}$$

where

Q = fuel flow

C_V = calorific value of fuel

H = heat transfer coefficient coefficient

A = heated surface area

Y = lbs of combustion products PER lb of fuel

t_f = gas temperature $= K_1 Q^N$ where K_1 is a constant and N a +ve constant.

I_f = enthalpy of flue gas $\propto K_2 t_f$ where K_2 is a constant

For turbulent flow

$$H = K_0 Q^{0.6} \quad \text{(McAdams 43))}$$

K is a proportionality factor

$$\therefore\ Q\,C_V = K\,Q^{0.6} \times A \times K_1\,Q^N + Q \times Y \times K_2 t_f$$

assuming that $t_f \gg t_w$.

$$\therefore \quad Q\,C_v = K\,K_1\,Q^{N+0.b}\,A + Q^{N+1}K_2\,Y\,K_1$$

Heat transferred — Heat in combustion products

effective heat transferred is proportional to $(Q)^{N+0.b}$

heat lost in combustion products is proportional to Q^{N+1}.

Thus furnace efficiency, which depends on the ratio of flue gas loss to useful heat transferred, decreases as fuel throughput increases.

APPENDIX 2

POWER STATION BOILER

The general specifications of the plant was delivery of 860,000 lb/h_r of steam at a throttle temperature of 1010°F and 1100 P.S.I. with reheat at a temperature of 1005°F.

Boiler data

Drum 66" dia 48' long circular section with a volume of 1228 ft^3.

Downcomer 5 off $14\frac{3}{8}$" I.D. 133' long 1" M.S. Liquid Velocity 12'/second.

Risers 524 off 3" O.D. Fluid Velocities 4-5'/sec.

Radiant Primary Superheater — Effective Surface area 1443 ft^2. water Equivalent 3530 lbs.

Radiant Secondary Superheater — Effective Surface area 235 ft. Water equivalent 7760 lbs.

Convection Primary Superheater — Effective Surface area 752 ft^2. Water Equivalent 25000 lbs.

Fuel 124500 lbs/hr of gross C.V. 9600 BTU/lb. moisture content 14%.

Air. 1,038,000 lbs/h_r.

Air Temperature 502°F at entry. 355°F at mills 90° F at inlet

Gas Temperature	At Furnace exit	2030°F
	At entrance to reheater	1575°F
	At entrance to economiser	820°F
	At entrance to air heater	550°F
	At exit to stack	255°F

Drum water inlet temperature 520°F.

Steam Temperature

Outlet primary S/H radiant	830°F
Outlet primary S/H convective	745°F
Outlet secondary S/H radiant	905°F
Outlet secondary S/H convective	1010°F.

Tube Metal Temperatures

Furnace riser wall	920°F
Primary S/H radiant	920°F
Secondary S/H radiant	985°F
Secondary S/H convective	1050°F
Primary S/H convective	790°F
Reheater	1050°F
Economiser	590°F

Reheater

8% wet on low pressure	
Inlet temperature	697°F
Outlet temperature	1005°F
Outlet pressure	391 P.S.I.
Exhaust low pressure	0.75 P.S.I.

REFERENCES

Chapter 1

1. Draper, C.S. Li, Y.T. — Principles of Optimalizing Controls and an application to the internal combustion engine. Proc. A.S.M.E. Sept. 1951.

2. Li, Y.T. — The Philosophy of Adaptive Control. Proceedings I.F.A.C. 1960 Moscow.

3. Gregory, F.C. — Proceedings of the Self Adaptive Flight Control Systems Symposium. W.A.D.C. Tech. Rept. 59.49. March 1959.

4. Foody, J.J. — Control October 1960 page 105

5. Mishkin, E. Braun, L. — Adaptive Control Systems McGraw-Hill 1961.

6. MacDonald, D. — Multiple Mode Operation of Servomechanisms. Review of Sci. Inst. 23. 1952.

7. Taylor, C. Flugge-Lotze, I. — Synthesis of a Non Linear Control System. Trans. I.R.E. P.G.A.C. May 1956.

8. Kirshmeyer, L.K. — Optimalizing Control in the Electric Utility Industry. Proc. I.F.AC. Moscow 1960.

9. Kalman, R.E. — Design of Self-Optimizing Control Systems. Trans. A.S.M.E. 80. 1958.

10. Bellman, R.E. — Dynamic Programming. Princeton Univ. Press. 1957.

11. Kalman, R.E. Lapidus, L. Shapiro, E. — The Optimal Control of Chemical and Petroleum Products. Joint Symp. Inst. and Comp. Inst. Chem. Eng. London 1959.

12. Nicholson, H. — Dual Mode Control of a Time Varying Boiler Model with Parameter and State Estimation. Proc. I.E.E. February 1966.

13. Tomlinson, N.R. — Discussion on Dynamic Optimization of a Boiler. Proc. I.E.E. October 1965.

14. Gibson, J.E. — Self Optimizing or Adaptive Control Systems. Proceedings I.F.A.C. Moscow 1960.

15. Eckman, D.P. Lefkowitz, I. — Principles of Model Techniques in Optimizing Control. Proc. I.F.A.C. Moscow 1960.

16. Lefkowitz, I. Barnard, D. — Optimizing Control Based on a Generalized Dynamic Model. Joint Automatic Control Conference June 1962.

17. Whitaker, H.P. Yamron, J. — Design of a Model Reference Adaptive Control System for Aircraft. M.I.T. Inst. Lab. Rept. R.164 Sept. 1958.

18. Horrocks, T. — Investigation into Model Reference Adaptive Control Systems. Proc. I.E.E. Nov. 1964.

19. Truxal, J.G. — Adaptive Control. Proc. I.F.A.C. Basle 1963.

20. Desoer, C.A. — The Bang Bang Servo Problem Treated by Variational Techniques. Information and Control.2. 1959.

21. Coales, J.F. Noton, A.R. — An On Off Servomechanism with Predicted Change Over. Proc. I.E.E. August 1955.

Chapter 2

1. Douce, J.L. Ng, K.C. — Six Channel Adaptive Computer. Proc. I.E.E. October 1964.

2. Leondes, C.T. — A Parameter Tracking Computer for Adaptive Control. Trans. I.R.E. R.G.A.C.4. Nov. 1959.

3. Hunter, L.P. — Introduction to Semiconductor Phenomena and Devices. Addison Wesley 1966 Page 43.

4. — Mullard Technical Hand Book Photo Electric Devices.

5. Bube, R.H. — Photo Conductivity of Solids. Wiley 1960 p.280

6. Del.Toro, V. Parker, S. — Principles of Control Systems Engineering. McGraw-Hill 1960 p.109.

7. Lo. Endres. — Transistor Electronics. Macmillan 1958. Page 137

8. — Reed Switches Application Report Flight Refuelling Ltd. Wimborne Dorset England.

9. — The Application of Linear Microcircuits. S.G.S. Fairchild.

10. Haynes, J.R. Lox, M. — Journal Physics. Chem. Solids Vol. 8, 392. 1959.

11. Guillaume, E. Parodi, O. — Proceedings International Conference on Semiconductor Physics. Prague 1960.

12. Choyke, W.J.
Patrick, L.
Bulletin American Physical Society
7. 77. 1962.

13. Keys, R.J.
Quist, T.M.
Proc. I.R.E. Vol. 50, 1822, 1962.

14. Burns, G.
Nathan, M.I.
P.N. Junction Lasers
Proc. I.E.E.E. July 1964.

15. Effer, D.
Semiconductor Crystal Lamps
New Techniques A.6. 1965.

16.
Semiconductor Device Manual
Ferranti Ltd. Oldham Lancs.

17.
Semiconductor Device Manual
Texas Instruments Ltd., Bedford.

18. Lynch, W.T.
Melchior, H.
Avalanche Photo Diodes.
Bell Laboratory Report
Scientific American, February 1967.

CHAPTER 3

1. Lee, Y.W. — Applications of Statistical Methods to Communications Problem. M.I.T. Electronics Research Report No. 181 Sept. 1951.

2. Anderson, G.W. Buland, R.N. — Use of Cross-correlation in an Adaptive Control System. Proc. N.E.C. Vol. 15, October 1959.

3. Kalman, R.E. — Design of a Self Optimizing Control System. Trans. A.S.M.E. Vol. 80 1958.

4. Margolis, M. Leondes, C.T. — A Parameter Tracking Servo for Adaptive Control Systems. I.R.E. Trans. on Automatic Control Vol. A.C.4. No. 2. Nov. 1959.

5. Corbin, R.M. Mishkin, E. — On the Measurement Problem in Adaptive Systems Utilizing Analogue Computer Techniques. Research Report R.699 Brooklyn Poly. 1958.

6. Lefkowitz, I. Bernard, J.W. — An approach to optimizing control based on a generalised dynamic model. I.S.A. Transactions Vol. 2, No. 1, 1963.

7. Chaussard, R. — Use of methods of transient analysis and the criterion of Naslin for the regulation of thermal power station boilers. Advances in Automatic Control. Joint Inst.E.E. I.Chem.E., Nottingham June 1965.

8. Paul, R. — An analogue computer with iterative computing facilities. Cranfield Technical Report No. E and C_2 May 1964.

9. Korn, G.A.
Korn, T.A.
Electronic analogue and hybrid computers.
McGraw-Hill.

10. Pace. T.R.10 Manual Electronic Associates Inc.
Long Branch New Jersey.

11. Hurley, R.B. Junction Transistor Electronics.
Wiley 1960 p.425.

12. Griffin, D.J. Design techniques for low drift D.C. amplifiers using silicon transistors.
Texas Instruments Application Report No. 5. Vol. 1.

13. Hamer, H. Optimum linear-segment function generation.
A.I.E.E. Trans. Nov. 1956.

14. Tables of exponential functions A.M.S. 14
National Bureau of Standards, U.S.A.

15. Solartron random signal generator
Type B.O. 1227 manual.
Solartron Electronics Farnborough, Hants.

CHAPTER 4.

1. Ergin, E.I.
Ling, C.
Development of a non-interacting Controller for Boilers.
Proc. I.F.A.C. Moscow 1960.

2. Ferrier, J.I.
Naval Experience in the design and operation of machinery control systems.
Inst. Mar. Eng. Student Transactions April 1965.

3. Hazard, H.R.
Buckley, F.D.
Experimental Combustion of Pulverized Coal at Atmospheric and Elevated Pressures.
Trans. A.S.M.E. 1948.

4. Frensch, J.
Klefenz, G.
1961 Brennstoff - Warme Kraft 13, 532-537.

5. Schneider, A.
Das Regeldynamische verhalten von kohlenstaubfeuerungen
Ph.D. Thesis 1959, Stuttgart Technische Hoschschule.

6. Profos, P.
Dynamics of Pressure and Combustion in Steam Generators.
Sulzer Tech. Review, No. 4. 1955.

7. Loveridge, D.J.
Some studies of the dynamic behaviour of steam generators.
B.C.U.R.A. Bulletin No. 5 1964.

8. Quack, R.
Schneider, A.
Measurement of Control Behaviour of steam generators
Proc. I.F.A.C. Moscow, 1960.

9. Stafford, T.J.
The simulation and control of power generating plant.
M.Sc.Tech.Thesis, Manchester 1962.

10. Morris, F.J.
Operational Data on a Ring Ball Pulverizer.
Journ. Inst.Fuel. October 1959.

11. Bishop, D.M. — I.C.I. Middlesborough, Private Communication, 1965.

12. Northover, E.W. Hitchock, J.A. — The development of a disc type flux meter for measuring boiler heat flux. Thermodynamics and Fluid Mechanics Convention, Liverpool, May 1965.

13. Rohsenow, W.M. — Heat transfer associated with nucleate boiling, Journ. Heat Transfer and Fluid Mechanics Institute, 1953, p.123.

14. Jakob, M. Fritz, W. — Forschung a.d. Gebiet.d. Ingenieurwes, 2.4.35. 1931.

15. Rohsenow, W.M. — Heat transfer with evaporation Symposium on Heat Transfer, Univ. Michigan, 1952.

16. Jens, W.H. Lottes, P.A. — Argonne Natl. Lan. Newport, ANL - 4627, 1951.

17. Dengler, C.E. Addoms, J.N. — Heat transfer mechanism for Vaporization in a vertical tube, A.I.Chem.E.Symps.18 Vol. 52, 1956.

18. Laird, A.M. Scott, A.W. Thompson, A.S. — Natural Circulation Investigation on an experimental two tube boiler Trans. N.E. Const. Inst. Engrs., Shipbld. Vol. 74, 1958.

19. Haywood, R.W. Knights, G.A. Middleton, G.E. — Experimental study of the flow conditions and pressure drop of steam-water mixtures at high pressures in heated and unheated tubes, Proc.Inst.Mech.Eng.Vol.175S, No. 13, 1961.

20. Gunther, F. — A study of surface boiling heat transfer to water with forced convenction. A.S.M.E. Trans. Vol. 73, 19. 1.

21. Tippets, F.F. — Critical heat fluxes and flow patterns in high pressure boiling water flows. A.S.M.E. Trans. Feb. 1964.

22. Zahn, W.R. — A visual study of two phase flow while evaporating in horizontal tubes. A.S.M.E. Trans. Aug. 1964.

23. Becker, K.M. Hernborg, G. — Measurement of burnout conditions for flow of boiling water in a vertical annulus. A.S.M.E. Trans. Aug. 1964.

24. Swenson, H.S. Carver, J.R. — The effects of nucleate boiling versus film boiling on heat transfer in power boiler tubes Trans.A.S.M.E. October, 1962.

25. Martinelli, G.C. — Prediction of pressure drop during forced circulation boiling of water. Trans.A.S.M.E.70 August, 1948.

26. Levy, S. — Steam slip - Theoretical prediction from Momentum Model. Trans.A.S.M.E. May, 1960.

27. Hillier, M.J. — Dynamics and Thermodynamics of Transient States in Engineering Liquid-Vapour Systems. Journal Mech.Eng.Sci. Vol.4, No.4, 1962.

28. Chisholm, D. Laird, A.M. — Natural circulation in water tube boilers. B.S.R.A. Report No. 124, 1954.

29. Bankoff, S.G. — A variable density single fluid model for two phase flow with particular reference to steam water flow. Trans. A.S.M.E. November, 1960.

30. Haywood, R.W. — Research into the fundamentals of Boiler Circulation Theory. Joint. Instn. Mech.Engrs.A.S.M.E. Discussion on heat transfer 1951.

31. Anderson, R.P. Bryant, L.T. — An analogue simulation of the transient behaviour of two phase natural circulation systems. A.I.Chem.E. Symposium No. 41, Vol. 59, 1963.

32. Estrada, H. Leeds, J.V. — Transient response of water level in recirculating boilers and steam generators. A.S.M.E. W.A.M. Dec. 1964.

33. Morton, A.J. — Control of water level in marine boilers during rapid changes of load. Proc.Inst.Mech,Engrs. Vol.175,1961.

34. Brown, J.P. — Communications on control of water level in marine boilers during rapid changes of load. Proc.Instn.Mech.Eng. Vol. 175 1961.

35. Thomas, R.V. — Private document No. R.1/6/10 B.C.U.R.A. 1963.

36. Chien, K.L. Ergin, E.I. Ling, C. — Dynamic Analysis of a boiler Transactions A.S.M.E. 1958.

37. Chien, K.L. Ergin, E.I. Ling, C. — The non interacting controller for a steam generating system. Control Engineering, October 1958.

38. Markson, A.A. — Discussion on the dynamic analysis of a boiler. Trans.A.S.M.E. 1958.

39. Daniels, J.H. Hottenstine, R.D. Enns, M. — Dynamic representation of a Large boiler turbine unit. Transactions A.S.M.E. S.A.M. 1961.

40. Dallas, H.G. Sauter, D.M. — Field Testing for Verification of a dynamic Model, Transactions A.S.M.E. S.A.M. 1961.

41. Lewitt, E.H. — Thermodynamics Applied to Heat Engineers, p.124 Pitman.

42. Northover, E.W. — C.E.G.B. Laboratories, Leatherhead, Private communication February, 1966.

43. McAdams, W.H. — Heat transmission - 3rd edition McGraw Hill 1954 p.272.

CHAPTER 5.

1. Barnard, C.H.
Vollmer, H.D.
Analogue Computer techniques for optimizing power plant operation
I.S.A. Transactions July 1963.

2. Daniels, J.H.
Buttenstine, R.V.
Emms, M.
Dynamic Representation of a large boiler turbine unit.
Trans. A.S.M.E. S.A.M. 1961.

3. Morton, A.J.
Control of water level in marine boilers during rapid changes of load.
Proc. Instn.Mech.Engs. Vol. 175, 1961.

4. Morton, A.J.
Boiler feed discharge systems under changing load.
Control. Nov. 1960.

CHAPTER 6

1. Cooles, J.F. — An On Off servomechanism with predicted change over. Proc.I.E.E. August 1955.

2. Maxwell, D.J. — Time optimal control of second order systems. Joint Automatic Control Conference. Minnesota 1963.

3. Horing, S. — On the design of predictor control systems. Proceedings I.F.A.C., Basle 1963.

4. Gulko, F.B. Kogan, B.Y. — A method of optimal control prediction Proceedings I.F.A.C. Basle 1963.

5. Brenner, E. Javid, M. — Analysis of Electric Circuits McGraw Hill 1960 p.165.